

***Grassy Mountain Gold and Silver Project,
Numerical Hydrogeologic Assessment***

***Prepared for:
SLR International Corporation***

***On behalf of:
Paramount Gold Nevada Corp.***

***Prepared by:
Lorax Environmental Services
2289 Burrard St.
Vancouver, B.C., V6J 3H9***

***Project No. A651-1
October 21, 2022***



Executive Summary

Executive Summary

A numerical groundwater model was developed using FEFLOW 7.4. The primary objectives of the modeling are to refine estimates of groundwater inflows to the underground mine, to characterize changes to groundwater flow during mining and after closure, and to characterize drawdown at springs in the mine vicinity that result from mine dewatering and groundwater production for mineral processing. The model was calibrated to steady state heads at wells springs in the mine area. Secondary calibration targets included the baseflow to the springs and the drawdown response at four pumping wells—PW-4, Prod-1, PW-1, and GMW17-33.

The calibrated model simulates the observed hydraulic compartmentalization with a combination of stratigraphic units as well as 19 fault zones, of which 11 are barrier faults, and 8 are transmissive features.

The normalized root mean squared error for the steady state calibration was 4.1% for all piezometers and springs and 5.8% in the mine area.

The base case simulation predicts groundwater inflows to the underground mine ranging from 15 gpm during the mine-construction Year -1 to 115 gpm in Year 1. The average annual mine inflow is predicted to be 60 gpm. Therefore, there are opportunities to reduce the pumping from the proposed production wellfield as the mine develops.

The drawdown predicted due to the underground mine is relatively limited to the area in the immediate vicinity of the mine due to the compartmentalization evident in the field data. Much greater drawdown is predicted from the 10-year duration operation of the proposed production wellfield at a constant average extraction rate of 72 gpm. Reducing the pumping rate as the underground mine develops will significantly reduce the simulated drawdown impacts.

The numerical modeling predicts that the water table in the wellfield area will recover rapidly after the end of mining. The residual drawdown 20 years after the end of mining in the wellfield area is predicted to be less than approximately 2 feet. The majority of springs included in the numerical model are not predicted to experience noticeable declines in water level as a result of mine dewatering.

A series of eight sensitivity runs were completed for the calibration and prediction phases of the model. In each of the eight runs, one or more individual parameters were adjusted with the objective of producing a greater zone of drawdown. Recharge, hydraulic conductivity and storage properties were adjusted in the sensitivity analysis. Within the runs, the annual average mine groundwater inflows, including all of the sensitivity runs,

ranges from 38 gpm to 100 gpm. The simulated drawdown in about half of the sensitivity runs was noticeably greater than the base case drawdown zone. However, only four or five regional springs are predicted to experience a drawdown of greater than 0.5 ft due to the operation of the production well. These are Red Tank #3, Lowe Spring, Sagebrush Spring, the Spring North of Lowe Reservoir and Government Corral.

Table of Contents

Table of Contents

EXECUTIVE SUMMARY	I
TABLE OF CONTENTS	III
1 INTRODUCTION	
1.1 PROJECT BACKGROUND	1-2
1.2 OBJECTIVES AND SCOPE OF WORK	1-2
1.3 SOURCES OF INFORMATION.....	1-3
2 PROPOSED MINING METHOD, LAYOUT AND SCHEDULE	
3 CONCEPTUAL HYDROGEOLOGIC MODEL	
3.1 HYDROLOGIC AND GEOLOGIC SETTING	3-1
3.1.1 TOPOGRAPHY AND CLIMATE	3-1
3.1.2 GEOLOGIC SETTING	3-1
3.2 GROUNDWATER RECHARGE.....	3-3
3.3 GROUNDWATER DISCHARGE.....	3-3
3.4 GROUNDWATER LEVELS AND FLOW DIRECTIONS	3-8
3.5 HYDRAULIC PARAMETERS	3-16
3.5.1 HYDRAULIC CONDUCTIVITY AND SILICIFICATION	3-16
3.5.2 PUMPING TESTS	3-17
3.6 CONCEPTUAL MODEL	3-21
4 NUMERICAL MODEL CONFIGURATION	
4.1 SOFTWARE	4-1
4.2 MODEL DOMAIN	4-1
4.3 REGIONAL BOUNDARY CONDITIONS.....	4-4
4.4 PUMPING TEST CALIBRATION BOUNDARY CONDITIONS	4-8
4.5 MINE BOUNDARY CONDITIONS.....	4-10
4.6 MODEL STRATIGRAPHY	4-17
4.7 STRUCTURES.....	4-25
4.8 SECTIONS THROUGH NUMERICAL MODE	4-30
4.8.1 REGIONAL SECTIONS	4-31
4.8.2 INTERMEDIATE SCALE SECTIONS.....	4-36
4.8.3 MINE AREA SECTIONS	4-44
4.8.4 SUMMARY OF MODEL STRATIGRAPHY	4-48
4.9 STORAGE AND UNSATURATED FUNCTIONS	4-49
4.10 CALIBRATION METHODOLOGY	4-52
4.11 CALIBRATION RESULTS	4-52
4.11.1 STEADY STATE HEADS	4-52
4.11.2 WATER BALANCE AND STEADY STATE SPRING FLOW RATES	4-59
4.11.3 PUMPING TEST CALIBRATION.....	4-63
4.11.4 CALIBRATED PARAMETERS.....	4-65
4.12 SENSITIVITY ANALYSIS.....	4-70
4.12.1 INTRODUCTION	4-70
4.12.2 STEADY STATE CALIBRATION	4-70
4.12.3 TRANSIENT CALIBRATION	4-76
5 MODEL PREDICTIONS	
5.1 BASE CASE PREDICTIONS.....	5-1
5.2 SENSITIVITY ANALYSIS.....	5-10
5.3 DISCUSSION	5-22
6 SUMMARY AND CONCLUSIONS	

7	LIMITATIONS	
7.1	LIMITATIONS.....	7-1
8	CLOSURE	
	REFERENCES.....	R-1

APPENDIX I: SENSITIVITY ANALYSIS PARAMETER TABLES

APPENDIX II: SENSITIVITY ANALYSIS INDIVIDUAL DRAWDOWN MAPS

LIST OF FIGURES

FIGURE 1-1	LOCATION PLAN (AFTER CALICO, 2021).....	1-1
FIGURE 1-2	SITE PLAN (AFTER CALICO, 2021).	1-2
FIGURE 2-1	PLAN VIEW OF GRASSY MOUNTAIN MINE UNDERGROUND WORKINGS (FROM CALICO, 2021).....	2-1
FIGURE 2-2	CROSS-SECTIONAL VIEW OF GRASSY MOUNTAIN MINE LOOKING NORTH (FROM CALICO, 2021).....	2-2
FIGURE 3-1	SPRING FLOW DATA – BASELINE SPRINGS.	3-4
FIGURE 3-2	SPRING FLOW DATA – BACKGROUND SPRINGS WITH MEASURABLE FLOWS.	3-5
FIGURE 3-3	SPRING FLOW DATA – ARTESIAN WELLS.	3-5
FIGURE 3-4	SPRING AND ARTESIAN WELL LOCATIONS (FROM SPF, 2021A).	3-7
FIGURE 3-5	INTERPRETED PIEZOMETRIC HEAD MAP.....	3-9
FIGURE 3-6	PIEZOMETRIC HEAD HYDROGRAPHS, REGIONAL WELLS.....	3-11
FIGURE 3-7	PIEZOMETRIC HEAD HYDROGRAPHS, MINE VICINITY WELLS.	3-12
FIGURE 3-8	MINE AREA PIEZOMETRIC HEADS, INCLUDING VWPs.	3-15
FIGURE 3-9	PUMPING TEST LOCATIONS.	3-17
FIGURE 3-10	PW-4 PUMPING TEST DATA.	3-18
FIGURE 3-11	PROD-1 PUMPING TEST DATA.	3-18
FIGURE 3-12	PW-1 PUMPING TEST DATA.	3-19
FIGURE 3-13	GMW17-33 PUMPING TEST DATA.	3-20
FIGURE 3-14	GMW17-32 PUMPING TEST DATA.	3-20
FIGURE 3-15	59762 PUMPING TEST DATA.....	3-21
FIGURE 3-16	MAIN FEATURES OF CONCEPTUAL MODEL.....	3-24
FIGURE 4-1	MODEL DOMAIN.....	4-2
FIGURE 4-2	MODEL MESH.....	4-3
FIGURE 4-3	OBLIQUE VIEW OF MODEL DOMAIN, SHOWING ELEMENT DIAMETERS.	4-3
FIGURE 4-4	BOUNDARY CONDITIONS – GENERAL.....	4-5
FIGURE 4-5	BOUNDARY CONDITIONS – RECHARGE.....	4-6
FIGURE 4-6	BOUNDARY CONDITIONS – SPRINGS.....	4-7
FIGURE 4-7	BOUNDARY CONDITIONS – CATCHMENTS FOR RECHARGE.....	4-8
FIGURE 4-8	PW-1 AND PW-4 PUMPING RATES IN TRANSIENT CALIBRATION RUN 1.....	4-9
FIGURE 4-9	PROD-1 AND GMW17-33 PUMPING RATES IN TRANSIENT CALIBRATION RUN 2.	4-9
FIGURE 4-10	LOCATION OF PRODUCTION WELL.	4-11
FIGURE 4-11	MINE BOUNDARY CONDITIONS, MINE YEAR -1.....	4-12
FIGURE 4-12	MINE BOUNDARY CONDITIONS, MINE YEAR 1 TO 3.	4-13
FIGURE 4-13	MINE BOUNDARY CONDITIONS AND HYDRAULIC CONDUCTIVITY CHANGES, MINE YEAR 4 TO 6.	4-14

FIGURE 4-14	MINE BOUNDARY CONDITIONS AND HYDRAULIC CONDUCTIVITY CHANGES, MINE YEAR 7 TO 9.	4-15
FIGURE 4-15	MINE HYDRAULIC CONDUCTIVITY CHANGES, POST-CLOSURE PERIOD.....	4-16
FIGURE 4-16	MODEL STRATIGRAPHY – OVERVIEW.....	4-19
FIGURE 4-17	TIS (CONGLOMERATE AND SANDSTONE) ZONE.	4-20
FIGURE 4-18	HYDRAULIC CONDUCTIVITY ZONES, LAYERS 1 TO 3.....	4-22
FIGURE 4-19	HYDRAULIC CONDUCTIVITY ZONES, LAYERS 4 TO 6.....	4-23
FIGURE 4-20	HYDRAULIC CONDUCTIVITY ZONES, LAYERS 7 TO 9.....	4-24
FIGURE 4-21	HYDRAULIC CONDUCTIVITY ZONES, LAYERS 10 AND 11.	4-25
FIGURE 4-22	REGIONAL FAULTS.	4-27
FIGURE 4-23	MINE AREA FAULTS.	4-28
FIGURE 4-24	INTERACTION BETWEEN FAULTS AND DEEP HIGH-K ZONES.	4-29
FIGURE 4-25	WEST-EAST SECTION 1992A (AFTER ADRIAN BROWN, 1992).....	4-32
FIGURE 4-26	NORTH-SOUTH SECTION 1992B (AFTER ADRIAN BROWN, 1992).	4-33
FIGURE 4-27	WEST-EAST SECTION 2021 (AFTER SPF, 2021C).....	4-34
FIGURE 4-28	SOUTH-NORTH SECTION 2021 (AFTER SPF, 2021C).	4-35
FIGURE 4-29	SECTION H (AFTER SPF, 2021C).....	4-37
FIGURE 4-30	SECTION I (AFTER SPF, 2021C).	4-38
FIGURE 4-31	SECTION J (AFTER SPF, 2021C).	4-40
FIGURE 4-32	SECTION K (AFTER SPF, 2021C).....	4-41
FIGURE 4-33	SECTION B (AFTER SPF, 2021C).	4-42
FIGURE 4-34	SECTION C (AFTER SPF, 2021C).	4-43
FIGURE 4-35	SECTION D (AFTER SPF, 2021C).....	4-45
FIGURE 4-36	SECTION E (AFTER SPF, 2021C).	4-46
FIGURE 4-37	SECTION F (AFTER SPF, 2021C).	4-47
FIGURE 4-38	SECTION G (AFTER SPF, 2021C).....	4-48
FIGURE 4-39	UNSATURATED FUNCTIONS.	4-51
FIGURE 4-40	SIMULATED VERSUS OBSERVED HEADS.	4-53
FIGURE 4-41	RESIDUAL VERSUS OBSERVED HEADS.....	4-53
FIGURE 4-42	CALIBRATED PIEZOMETRIC HEAD, TOP OF LAYER 2, AT APPROXIMATE WATER TABLE ELEVATION.....	4-56
FIGURE 4-43	CALIBRATED PIEZOMETRIC HEAD, TOP OF LAYER 2, IN MINE AREA.....	4-57
FIGURE 4-44	CALIBRATED PIEZOMETRIC HEAD, SLICES 1, 3, 5, 7, 9, 10 AND 12.	4-58
FIGURE 4-45	MEASURED AND SIMULATED SPRING AND ARTESIAN WELL DISCHARGE.....	4-61
FIGURE 4-46	TIS ZONE PUMPING TEST CALIBRATION – PW-4 AND PROD-1.....	4-64
FIGURE 4-47	MINE-AREA SANDSTONE PUMPING TEST CALIBRATION – PW-1 AND GMW17-33.....	4-65
FIGURE 4-48	CALIBRATED HYDRAULIC CONDUCTIVITY AND SPECIFIC STORAGE OF HYDROGEOLOGICAL UNITS.	4-67

FIGURE 4-49	CALIBRATED HYDRAULIC CONDUCTIVITY OF FAULT ZONES.	4-69
FIGURE 4-50	SENSITIVITY RUN STEADY STATE NRMSE AND RESIDUAL MEAN.	4-72
FIGURE 4-51	SENSITIVITY RUN STEADY STATE CALIBRATION STATISTICS.....	4-74
FIGURE 4-52	BASELINE SPRING AND WELL FLOW – SENSITIVITY RUNS	4-75
FIGURE 4-53	BACKGROUND SPRING AND WELL FLOW – SENSITIVITY RUNS	4-76
FIGURE 4-54	TIS ZONE PUMPING TEST CALIBRATION – SENSITIVITY RUNS	4-78
FIGURE 4-55	PW-1 PUMPING TEST CALIBRATION – SENSITIVITY RUNS	4-79
FIGURE 4-56	GMW17-33 PUMPING TEST CALIBRATION – SENSITIVITY RUNS	4-80
FIGURE 5-1	PREDICTED GROUNDWATER INFLOWS, BASE CASE MODEL.	5-1
FIGURE 5-2	PREDICTED DRAWDOWN, MODEL SLICES 1 AND 5, END OF MINE YEARS 2, 5 AND 9.	5-4
FIGURE 5-3	PREDICTED DRAWDOWN, MODEL SLICES 1 AND 5, 10, 20 AND 50 YEARS AFTER END OF MINING.....	5-5
FIGURE 5-4	PREDICTED DRAWDOWN, MODEL SLICES 1 AND 5, 80 AND 100 YEARS AFTER END OF MINING.....	5-6
FIGURE 5-5	TIME-SERIES OF SIMULATED DRAWDOWN, HIGHER DRAWDOWN WELLS.....	5-7
FIGURE 5-6	TIME-SERIES OF SIMULATED DRAWDOWN, LOWER DRAWDOWN WELLS.....	5-8
FIGURE 5-7	TIME-SERIES OF SIMULATED DRAWDOWN, SPRINGS.	5-9
FIGURE 5-8	PREDICTED UNDERGROUND MINE INFLOWS, SENSITIVITY RUNS.	5-10
FIGURE 5-9	COMPARISON OF 1-FT DRAWDOWN CONTOURS, SENSITIVITY RUNS, AT END OF MINING.....	5-12
FIGURE 5-10	COMPARISON OF 1-FT DRAWDOWN CONTOURS ON SLICE 1, END OF MINING.....	5-13
FIGURE 5-11	COMPARISON OF 1-FT DRAWDOWN CONTOURS ON SLICE 5, END OF MINING.....	5-14
FIGURE 5-12	COMPARISON OF 1-FT DRAWDOWN CONTOURS, SENSITIVITY RUNS, 20 YEARS AFTER END OF MINING.	5-16
FIGURE 5-13	COMPARISON OF 1-FT DRAWDOWN CONTOURS ON SLICE 1, 20 YEARS END OF MINING..	5-17
FIGURE 5-14	COMPARISON OF 1-FT DRAWDOWN CONTOURS ON SLICE 5, 20 YEARS END OF MINING..	5-18
FIGURE 5-15	COMPARISON OF 1-FT DRAWDOWN CONTOURS, SENSITIVITY RUNS, 100 YEARS AFTER END OF MINING.	5-19
FIGURE 5-16	COMPARISON OF 1-FT DRAWDOWN CONTOURS ON SLICE 1, 20 YEARS END OF MINING..	5-20
FIGURE 5-17	COMPARISON OF 1-FT DRAWDOWN CONTOURS ON SLICE 5, 100 YEARS END OF MINING.....	5-21
FIGURE II-1	PREDICTED DRAWDOWN, MODEL SLICES 1 AND 5, END OF MINE YEARS 2, 5 AND 9, SENSITIVITY RUN S1.	1
FIGURE II-2	PREDICTED DRAWDOWN, MODEL SLICES 1 AND 5, 10, 20 AND 50 YEARS AFTER END OF MINING, SENSITIVITY RUN S1.....	2
FIGURE II-3	PREDICTED DRAWDOWN, MODEL SLICES 1 AND 5, 80 AND 100 YEARS AFTER END OF MINING, SENSITIVITY RUN S1.....	3
FIGURE II-4	TIME-SERIES OF SIMULATED DRAWDOWN, HIGHER DRAWDOWN WELLS, SENSITIVITY RUN S1.....	4
FIGURE II-5	TIME-SERIES OF SIMULATED DRAWDOWN, LOWER DRAWDOWN WELLS, SENSITIVITY RUN S1.....	5
FIGURE II-6	TIME-SERIES OF SIMULATED DRAWDOWN, SPRINGS, SENSITIVITY RUN S1.	6

FIGURE II-7	PREDICTED DRAWDOWN, MODEL SLICES 1 AND 5, END OF MINE YEARS 2, 5 AND 9, SENSITIVITY RUN S2.	7
FIGURE II-8	PREDICTED DRAWDOWN, MODEL SLICES 1 AND 5, 10, 20 AND 50 YEARS AFTER END OF MINING, SENSITIVITY RUN S2.	8
FIGURE II-9	PREDICTED DRAWDOWN, MODEL SLICES 1 AND 5, 80 AND 100 YEARS AFTER END OF MINING, SENSITIVITY RUN S2.	9
FIGURE II-10	TIME-SERIES OF SIMULATED DRAWDOWN, HIGHER DRAWDOWN WELLS, SENSITIVITY RUN S2.	10
FIGURE II-11	TIME-SERIES OF SIMULATED DRAWDOWN, LOWER DRAWDOWN WELLS, SENSITIVITY RUN S2.	11
FIGURE II-12	TIME-SERIES OF SIMULATED DRAWDOWN, SPRINGS, SENSITIVITY RUN S2.	12
FIGURE II-13	PREDICTED DRAWDOWN, MODEL SLICES 1 AND 5, END OF MINE YEARS 2, 5 AND 9, SENSITIVITY RUN S3A.	13
FIGURE II-14	PREDICTED DRAWDOWN, MODEL SLICES 1 AND 5, 10, 20 AND 50 YEARS AFTER END OF MINING, SENSITIVITY RUN S3A.	14
FIGURE II-15	PREDICTED DRAWDOWN, MODEL SLICES 1 AND 5, 80 AND 100 YEARS AFTER END OF MINING, SENSITIVITY RUN S3A.	15
FIGURE II-16	TIME-SERIES OF SIMULATED DRAWDOWN, HIGHER DRAWDOWN WELLS, SENSITIVITY RUN S3A.	16
FIGURE II-17	TIME-SERIES OF SIMULATED DRAWDOWN, LOWER DRAWDOWN WELLS, SENSITIVITY RUN S3A.	17
FIGURE II-18	TIME-SERIES OF SIMULATED DRAWDOWN, SPRINGS, SENSITIVITY RUN S3A.	18
FIGURE II-19	PREDICTED DRAWDOWN, MODEL SLICES 1 AND 5, END OF MINE YEARS 2, 5 AND 9, SENSITIVITY RUN S3B.	19
FIGURE II-20	PREDICTED DRAWDOWN, MODEL SLICES 1 AND 5, 10, 20 AND 50 YEARS AFTER END OF MINING, SENSITIVITY RUN S3B.	20
FIGURE II-21	PREDICTED DRAWDOWN, MODEL SLICES 1 AND 5, 80 AND 100 YEARS AFTER END OF MINING, SENSITIVITY RUN S3B.	21
FIGURE II-22	TIME-SERIES OF SIMULATED DRAWDOWN, HIGHER DRAWDOWN WELLS, SENSITIVITY RUN S3B.	22
FIGURE II-23	TIME-SERIES OF SIMULATED DRAWDOWN, LOWER DRAWDOWN WELLS, SENSITIVITY RUN S3B.	23
FIGURE II-24	TIME-SERIES OF SIMULATED DRAWDOWN, SPRINGS, SENSITIVITY RUN S3B.	24
FIGURE II-25	PREDICTED DRAWDOWN, MODEL SLICES 1 AND 5, END OF MINE YEARS 2, 5 AND 9, SENSITIVITY RUN S4.	25
FIGURE II-26	PREDICTED DRAWDOWN, MODEL SLICES 1 AND 5, 10, 20 AND 50 YEARS AFTER END OF MINING, SENSITIVITY RUN S4.	26
FIGURE II-27	PREDICTED DRAWDOWN, MODEL SLICES 1 AND 5, 80 AND 100 YEARS AFTER END OF MINING, SENSITIVITY RUN S4.	27
FIGURE II-28	TIME-SERIES OF SIMULATED DRAWDOWN, HIGHER DRAWDOWN WELLS, SENSITIVITY RUN S4.	28
FIGURE II-29	TIME-SERIES OF SIMULATED DRAWDOWN, LOWER DRAWDOWN WELLS, SENSITIVITY RUN S4B.	29
FIGURE II-30	TIME-SERIES OF SIMULATED DRAWDOWN, SPRINGS, SENSITIVITY RUN S4.	30

FIGURE II-31	PREDICTED DRAWDOWN, MODEL SLICES 1 AND 5, END OF MINE YEARS 2, 5 AND 9, SENSITIVITY RUN S5.	31
FIGURE II-32	PREDICTED DRAWDOWN, MODEL SLICES 1 AND 5, 10, 20 AND 50 YEARS AFTER END OF MINING, SENSITIVITY RUN S5.	32
FIGURE II-33	PREDICTED DRAWDOWN, MODEL SLICES 1 AND 5, 80 AND 100 YEARS AFTER END OF MINING, SENSITIVITY RUN S5.	33
FIGURE II-34	TIME-SERIES OF SIMULATED DRAWDOWN, HIGHER DRAWDOWN WELLS, SENSITIVITY RUN S5.	34
FIGURE II-35	TIME-SERIES OF SIMULATED DRAWDOWN, LOWER DRAWDOWN WELLS, SENSITIVITY RUN S5.	35
FIGURE II-36	TIME-SERIES OF SIMULATED DRAWDOWN, SPRINGS, SENSITIVITY RUN S5.	36
FIGURE II-37	PREDICTED DRAWDOWN, MODEL SLICES 1 AND 5, END OF MINE YEARS 2, 5 AND 9, SENSITIVITY RUN S6.	37
FIGURE II-38	PREDICTED DRAWDOWN, MODEL SLICES 1 AND 5, 10, 20 AND 50 YEARS AFTER END OF MINING, SENSITIVITY RUN S6.	38
FIGURE II-39	PREDICTED DRAWDOWN, MODEL SLICES 1 AND 5, 80 AND 100 YEARS AFTER END OF MINING, SENSITIVITY RUN S6.	39
FIGURE II-40	TIME-SERIES OF SIMULATED DRAWDOWN, HIGHER DRAWDOWN WELLS, SENSITIVITY RUN S6.	40
FIGURE II-41	TIME-SERIES OF SIMULATED DRAWDOWN, LOWER DRAWDOWN WELLS, SENSITIVITY RUN S6.	41
FIGURE II-42	TIME-SERIES OF SIMULATED DRAWDOWN, SPRINGS, SENSITIVITY RUN S6.	42
FIGURE II-43	PREDICTED DRAWDOWN, MODEL SLICES 1 AND 5, END OF MINE YEARS 2, 5 AND 9, SENSITIVITY RUN S7.	43
FIGURE II-44	PREDICTED DRAWDOWN, MODEL SLICES 1 AND 5, 10, 20 AND 50 YEARS AFTER END OF MINING, SENSITIVITY RUN S7.	44
FIGURE II-45	PREDICTED DRAWDOWN, MODEL SLICES 1 AND 5, 80 AND 100 YEARS AFTER END OF MINING, SENSITIVITY RUN S7.	45
FIGURE II-46	TIME-SERIES OF SIMULATED DRAWDOWN, HIGHER DRAWDOWN WELLS, SENSITIVITY RUN S7.	46
FIGURE II-47	TIME-SERIES OF SIMULATED DRAWDOWN, LOWER DRAWDOWN WELLS, SENSITIVITY RUN S7.	47
FIGURE II-48	TIME-SERIES OF SIMULATED DRAWDOWN, SPRINGS, SENSITIVITY RUN S7.	48

LIST OF TABLES

TABLE 3-1	AVERAGE SPRING FLOW TARGETS	3-6
TABLE 3-2	AVERAGE GROUNDWATER HEAD TARGETS – MONITORING WELLS.....	3-13
TABLE 3-3	AVERAGE GROUNDWATER HEAD TARGETS – ARTESIAN WELLS AND SPRINGS	3-14
TABLE 4-1	PUMPING WELL CONFIGURATION.....	4-9
TABLE 4-2	MINE PREDICTION TRANSIENT MODEL STAGES	4-10
TABLE 4-3	MODEL LAYERING.....	4-20
TABLE 4-4	STRATIGRAPHIC UNITS	4-21
TABLE 4-5	LIST OF MODEL FAULTS	4-30
TABLE 4-6	UNSATURATED PARAMETERS	4-50
TABLE 4-7	SIMULATED AND PREDICTED HEAD, MONITORING WELLS.....	4-54
TABLE 4-8	SIMULATED AND PREDICTED HEAD, SPRINGS AND REGIONAL ARTESIAN WELLS	4-55
TABLE 4-9	MODEL-WIDE WATER BALANCE.....	4-59
TABLE 4-10	SIMULATED AND PREDICTED FLOW, BASELINE SPRINGS AND ARTESIAN WELLS	4-62
TABLE 4-11	SIMULATED AND PREDICTED FLOW, BACKGROUND SPRINGS AND ARTESIAN WELLS	4-62
TABLE 4-12	CALIBRATED HYDRAULIC CONDUCTIVITY OF HYDROGEOLOGICAL UNITS	4-66
TABLE 4-13	CALIBRATED HYDRAULIC CONDUCTIVITY OF FAULT ZONES	4-68
TABLE 4-14	SENSITIVITY RUNS	4-70
TABLE 4-15	SENSITIVITY RUN CALIBRATION STATISTICS.....	4-73
TABLE 5-1	PREDICTED UNDERGROUND MINE INFLOW, SENSITIVITY RUN PREDICTION.....	5-11
TABLE I-1	SENSITIVITY RUNS ON HYDRAULIC CONDUCTIVITY	1
TABLE I-2	SENSITIVITY RUNS ON STORAGE AND POROSITY	2
TABLE I-3	SENSITIVITY RUNS ON OTHER PARAMETERS	2

1. Introduction

1 Introduction

On behalf of Paramount Gold Nevada Corp. (Paramount), Lorax Environmental Services Ltd. (Lorax) has completed a numerical modeling assessment of the Grassy Mountain Gold and Silver Project (Project), a proposed underground gold-silver mining operation located in the high desert region of the far western Snake River Plain in Oregon, USA. The Grassy Mountain property encompasses approximately 9,300 acres in Malheur County, Oregon about 70 miles west of Boise, Idaho (Figure 1-1).

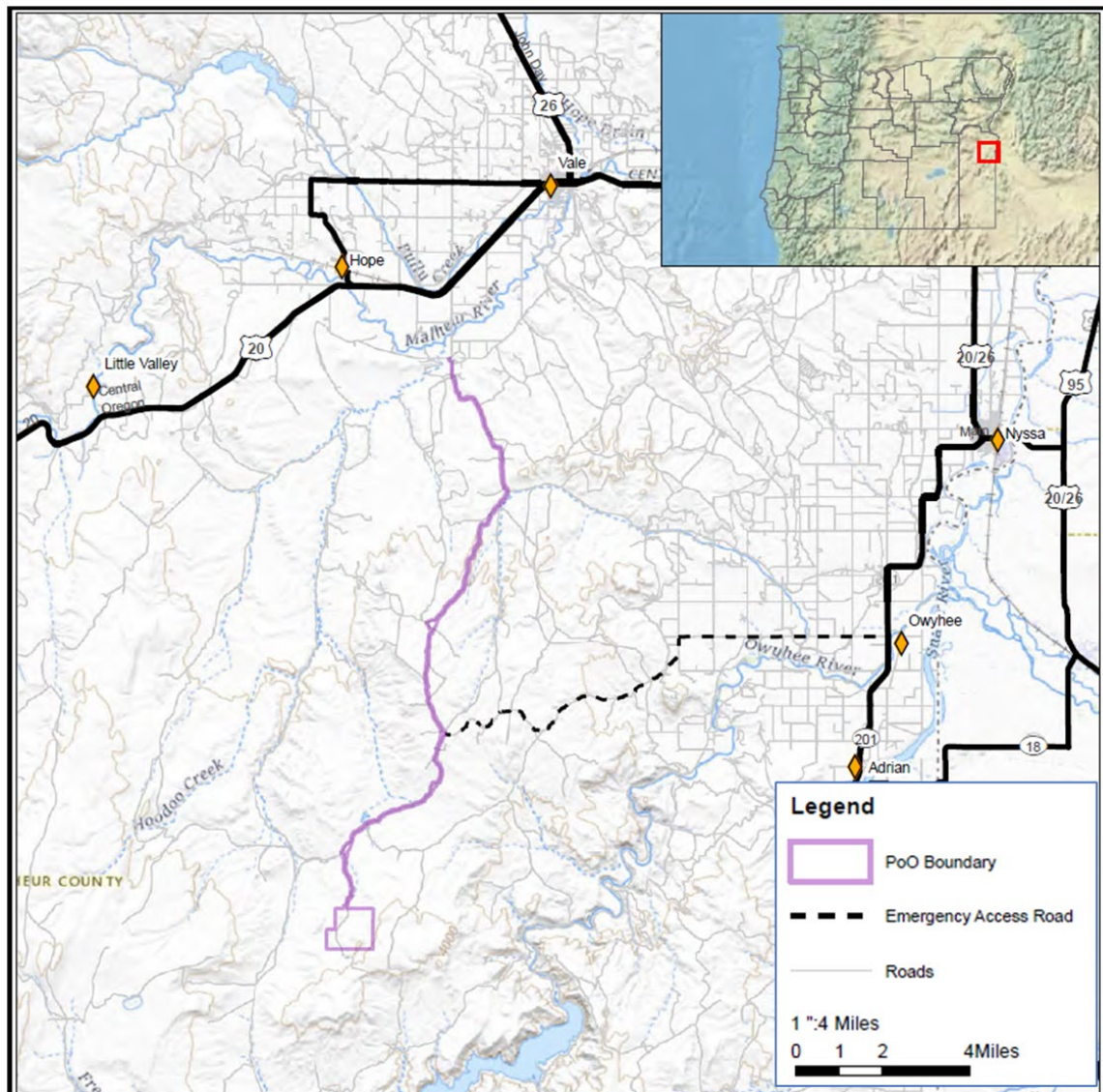


Figure 1-1: Location Plan (after Calico, 2021)

1.1 Project Background

The Project facilities are shown in Figure 1-2. The key facilities with respect to the current groundwater model are the underground excavations (shown in yellow) and water supply wells located to the north and not shown in Figure 1-2.

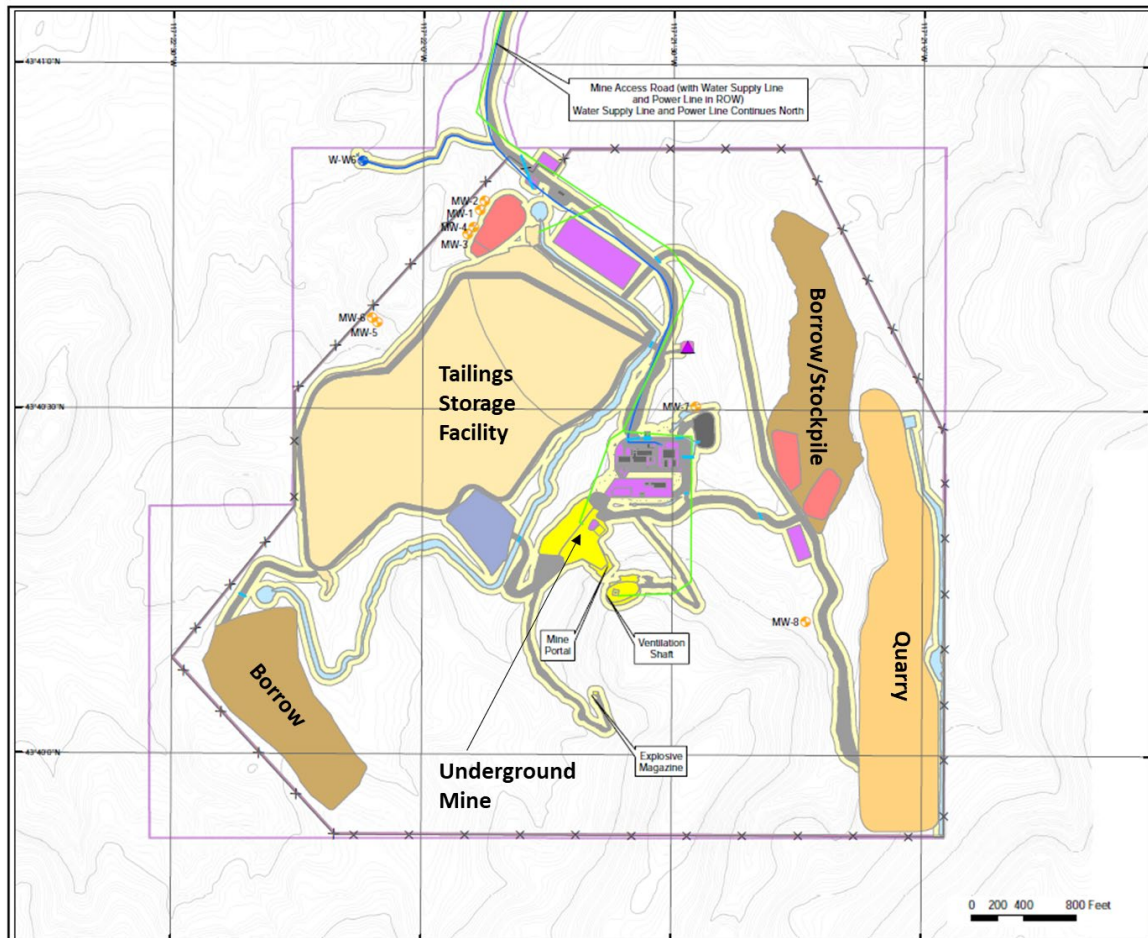


Figure 1-2: Site Plan (after Calico, 2021).

1.2 Objectives and Scope of Work

The groundwater flow model described in this report was developed to more completely reflect the site hydrogeologic conceptual site model described in the Grassy Mountain Gold Project Groundwater Baseline Report (SPF, 2021a-c) and uses the most recent and complete site data. Therefore, this model supercedes and replaces the existing models previously created by SPF (2021c) and Lorax (2021).

The current model was designed to encompass the larger model domain of the SPF (2021c) model while including the numerical mesh refinements in the mine area of the Lorax (2021)

model. In this manner, the new model presented in this report has the ability to simulate local groundwater flow processes in the mine area as well as to project future groundwater drawdown impacts from the Grassy Mountain project.

The primary objectives of the modeling are to refine estimates of groundwater inflows to the underground mine, to characterize changes to groundwater flow during mining and after closure, and to characterize drawdown at springs in the mine vicinity that result from mine dewatering and groundwater production for mineral processing.

1.3 Sources of Information

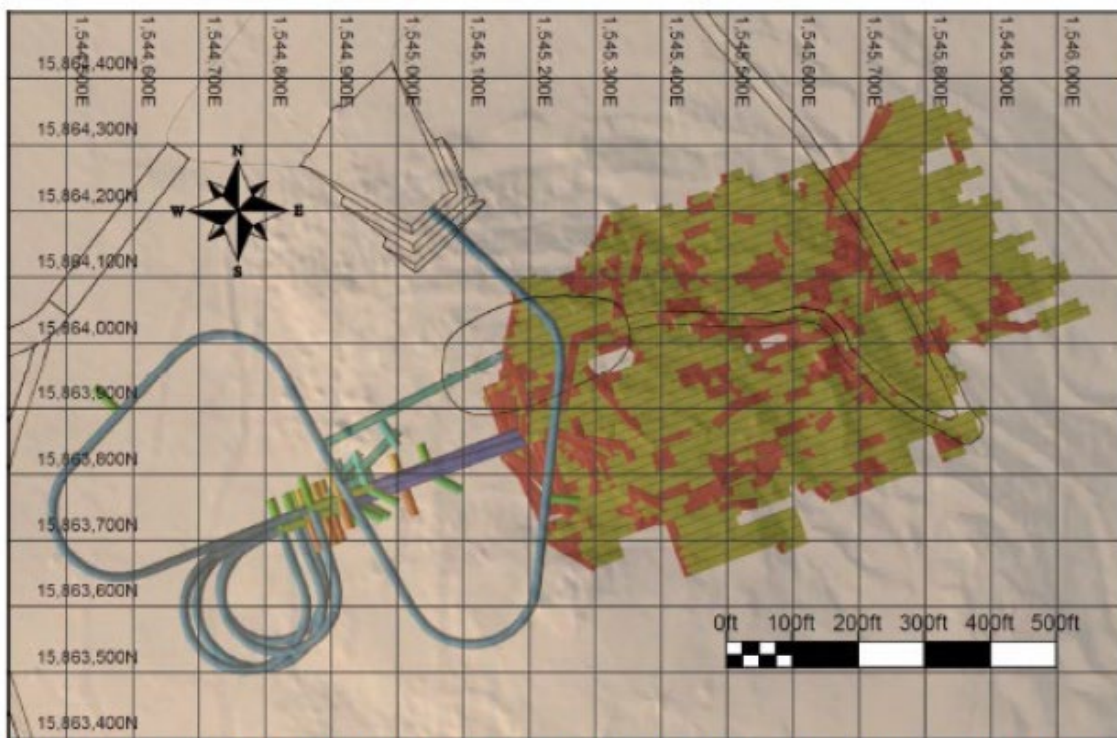
The following reports were reviewed in support of the current groundwater model development:

- *Grassy Mountain Mine Project, Mine Plan of Operations* (Calico Resources, 2021);
- *Grassy Mountain Gold Project Groundwater Vol. I, Groundwater Baseline Data Report* (SPF, 2021a);
- *Grassy Mountain Gold Project Groundwater Vol. II, Groundwater Characterization Report* (SPF, 2021b); and
- *Grassy Mountain Gold Project Groundwater Vol. III, Dewatering Projections and Evaluation of Potential Pumping Impacts* (SPF, 2021c).

2. Proposed Mining Method, Layout and Schedule

2 Proposed Mining Method, Layout and Schedule

Extraction of the Grassy Mountain estimated mineral reserves is planned via a proposed underground mine that will be accessed via one decline and a system of internal ramps as shown in Figure 2-1 and Figure 2-2. One shaft is planned for exhaust ventilation and secondary egress. The planned mining method is drift-and-fill (D&F) using diesel-powered mining equipment. Cemented rock fill (CRF) will be used for back-fill of the production drifts and level access to prevent subsidence.



Note: Figure prepared by MDA, 2020. Mining activity types of workings shown by the same colors used in Figures 4 and 5.

Figure 2-1: Plan View of Grassy Mountain Mine Underground Workings (from Calico, 2021).

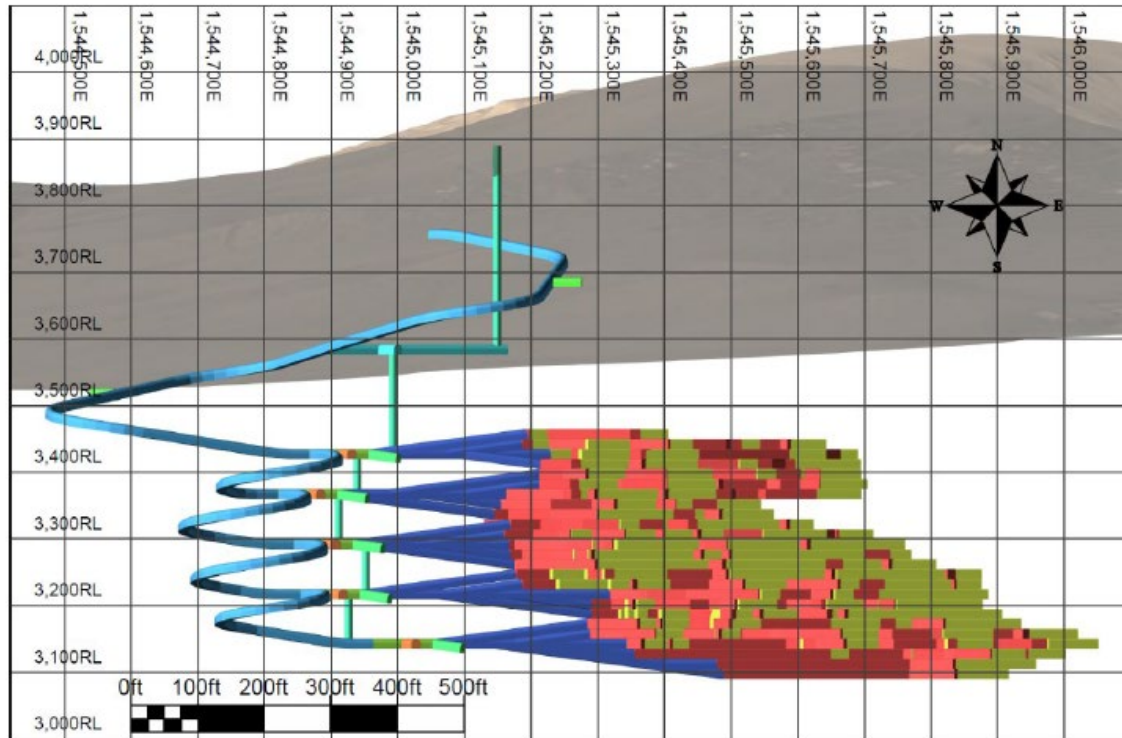


Figure 2-2: Cross-Sectional View of Grassy Mountain Mine looking North (from Calico, 2021).

Nominal development sizes of 15 ft (feet) wide by 15 ft high are planned for the main decline and 13 ft wide by 13 ft high for horizontal access to production areas. All production drifts will be 15 ft high and will have three different width sizes: 15 ft, 20 ft, and 30 ft wide. Production drifts will vary in width depending on ground conditions and ground support requirements.

The mining cycle involves drilling, blasting, and mucking for the development and production drifts. This will be followed by reinforcement and ground support for safe operation, and finally backfill of the production drifts.

3. Conceptual Hydrogeologic Model

3 Conceptual Hydrogeologic Model

3.1 Hydrologic and Geologic Setting

3.1.1 Topography and Climate

The project area is located in the plateau region of eastern Oregon. Terrain at the project area is mainly open steppe with mesas, broad valleys, and gently rolling hills to steeper uplands. Elevations range from 3,330 to 4,300 ft amsl (feet above mean sea level). Vegetation consists of sagebrush, weeds, and desert grasses tolerant of semi-arid conditions (Adrian Brown, 1992).

The climate can be described as the semi-arid, continental interior type, with average annual precipitation of about 10 inches, roughly half of which falls as snow between November and March. Local weather data indicate a mean annual temperature of 52° F, with daily temperatures ranging from an extreme low of -20°F in the winter to extreme highs of 100°F and higher in the summer (SPF, 2021c).

3.1.2 Geologic Setting

SPF (2021b) provides a detailed description of the regional and local geologic setting based on excerpts from *Calico Resources USA Corp, Grassy Mountain Gold Project, Malheur County, Oregon, Geology and Soils Baseline Report* (Abrams, 2018). The following is a summary based on that description, pertinent to the numerical hydrogeology assessment:

- Caldera volcanism occurred in response to large, silicic magma chambers emplaced in the shallow crust throughout the region. The volcanic field includes several caldera-sourced ash-flow sheets and rhyolite tuff cones.
- Subsidence of the Lake Owyhee volcanic field resulted in small volume, basalt-rhyolite deposits of limited extent.
- Regional extension and subsidence facilitated the formation of throughgoing fluvial systems and extensive lacustrine basins. Large volumes of fluvial sediments, sourced from the exhumed Idaho Batholith to the southeast, were deposited in conjunction with volcanism and hot spring activity during the waning stages of volcanic field development.
- The resulting regional stratigraphic section is a thick sequence of volcanic rocks and non-marine lacustrine, volcanoclastic, and fluvial sedimentary rocks.
- The Grassy Mountain gold-silver deposit is located beneath a prominent, 150-foot high, silicified and iron-stained hill. Bedding is horizontal at the hilltop, and dips at

10 to 25 degrees to the north-northeast on the northern and eastern flanks of the hill and steepens to 30 to 40 degrees on the west side of the hill.

SPF (2021b) describes the surficial geology as follows:

- In the general vicinity of the Project, there is geologic unit *Tsau*, described as upper arkosic sandstone, conglomerate, and tuffaceous siltstone. This unit is also referred to as the Grassy Mountain Formation.
- To the east of the Project, geologic unit *Tbcu*, described as upper calc-alkaline lava flows, occurs.
- Holocene-age alluvium (*Qal*) occurs within the Twin Springs drainage to the west of the Project and to a lesser extent in the minor drainage extending north from the deposit.
- The Grassy Mountain Formation generally strikes from east to west and dips towards the north with faulting, fractures, and folding that, in the vicinity of the Project site, create two graben or syncline features that extend down Negro Rock Canyon and Sourdough Gulch. Between these two basin features is a horst block or anticline where the Tuff of Kern Basin surfaces approximately 0.9 miles west of the proposed Grassy Mountain Mine.

SPF (2021b) describes the structural geology as follows, based on excerpts from Abrams (2018):

- The Grassy Mountain gold-silver deposit is located within an interpreted horst block that has been raised 50 to 200 ft in a region of complex block faulting and rotation.
- Faults at the Grassy Mountain deposit are mainly post-mineral 30 degrees west of north (N30°W) to ten degrees east of north (N10°E), striking normal faults developed during basin and range extension.
- At a local scale and within the immediate vicinity of the Grassy Mountain gold deposit, fault orientations can be grouped into two major sets: 20 degrees west of north to ten degrees east of north (N20°W to N10°E) striking faults, and 70 degrees east of north (N70°E) striking faults.

The project area stratigraphy was derived from the baseline study (SPF, 2021a, 2021b, 2021c) and borehole logs and sections contained in that report. A comparison of the numerical model to the geological model is presented in Section 4.8.

numerical model to the geological model is presented in Section 4.8.

3.2 Groundwater Recharge

Adrian Brown Consultants, Inc. (1992) estimated an annual recharge to groundwater (infiltration of precipitation) in the vicinity of Grassy Mountain in the range of 0.25 to 1 inch based on climatic and topographic conditions and a numerical groundwater model.

3.3 Groundwater Discharge

Discharge occurs to springs and surface channels at lower elevations. Regional groundwater flow is to the north towards the Malheur River (SPF, 2021c). The following additional points are summarized from SPF (2021c):

- Within the Grassy Mountain vicinity, numerous individual springs (some ephemeral) have been monitored for flow, with the majority of springs having flow rates of less than one gpm.
- The total maximum discharge from monitored springs located on the north side of the Grassy Mountain hydrologic divide is on the order of approximately 30 gpm based on flow measurements collected between 2013 and 2018.
- The total aggregate visible groundwater discharge is an indicator of the low annual recharge rate.

Spring flow measurements from 2013 to 2022 are plotted on Figure 3-1 for baseline springs and Figure 3-2 for background springs. Note that some of the background springs do not have measurable flows. These springs are listed in Table 3-1 but not shown in the charts.

In addition to these springs, there are three artesian wells in the project area. The flows measured at these artesian wells are plotted on Figure 3-3.

The location of the springs and two of the artesian wells is shown in Figure 3-4. Artesian well Prod-1 is shown in Figure 3-9. The average flows for the springs and artesian wells were used as calibration targets in the groundwater model and are listed in Table 3-1.

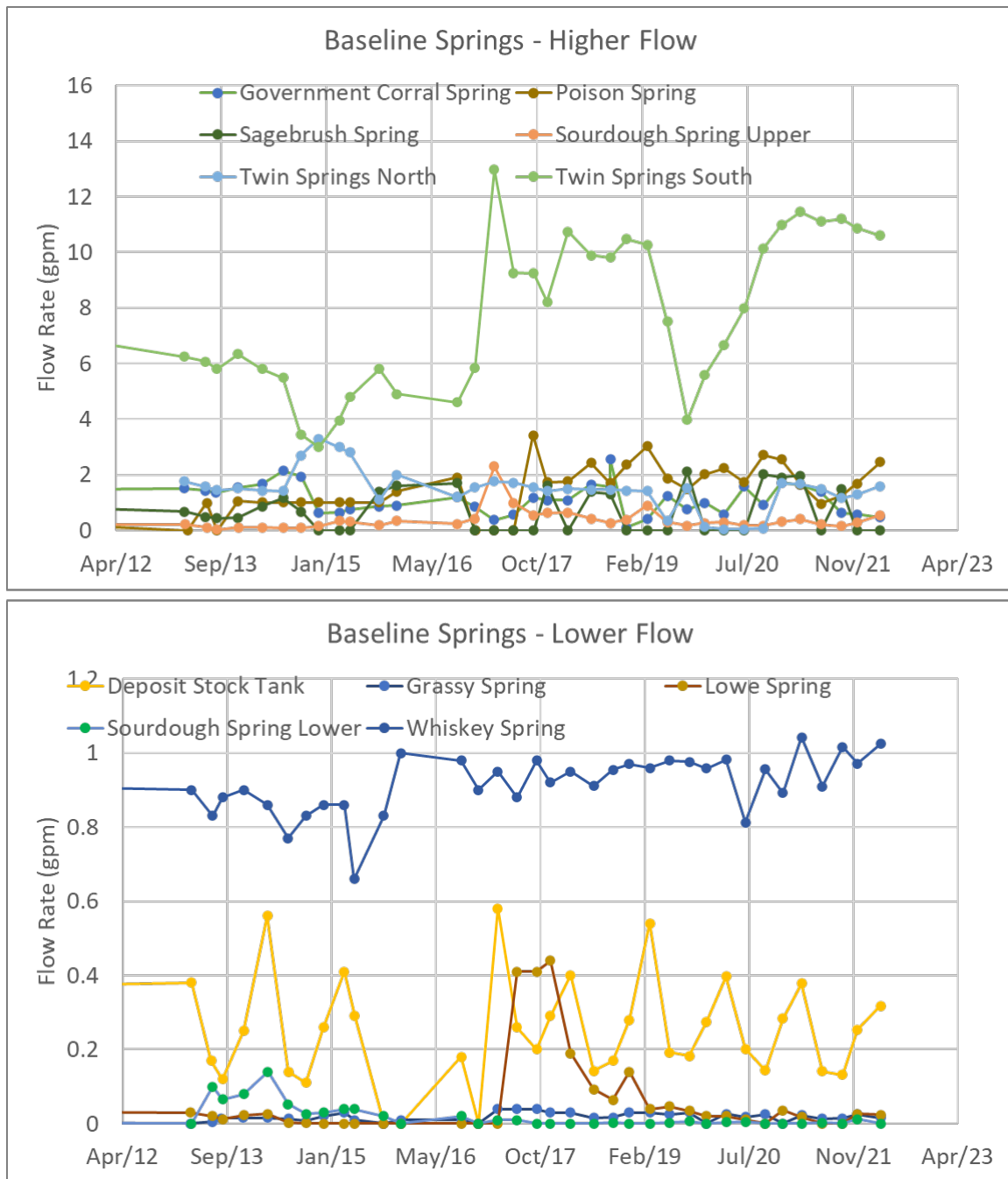


Figure 3-1: Spring Flow Data – Baseline Springs.

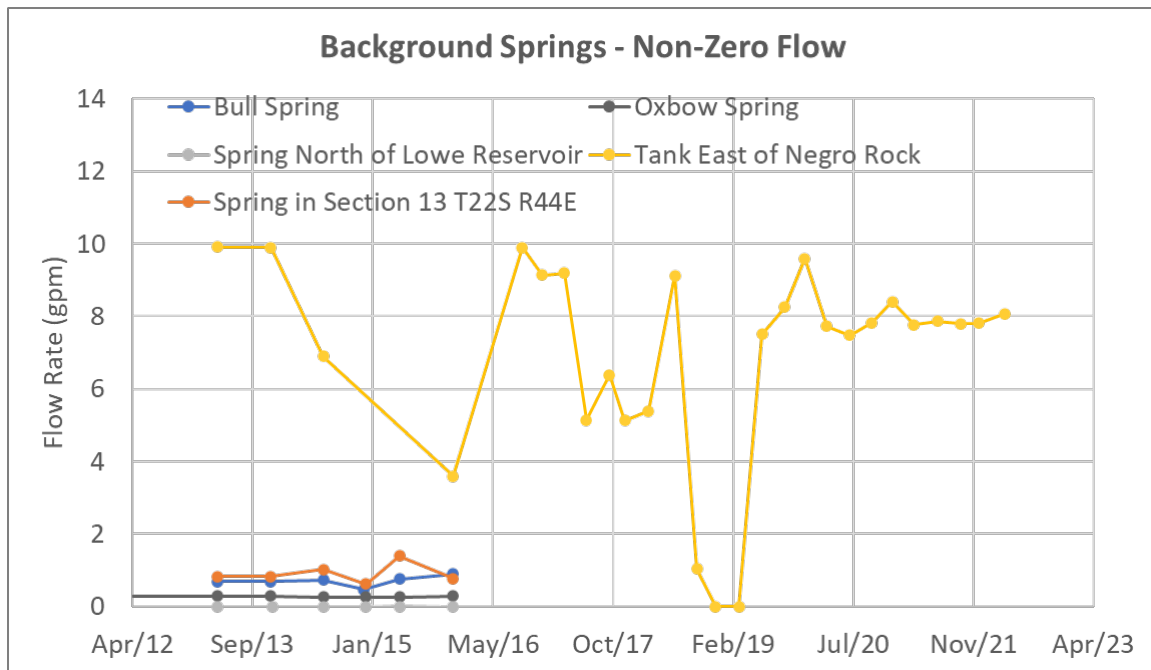


Figure 3-2: Spring Flow Data – Background Springs with Measurable Flows.

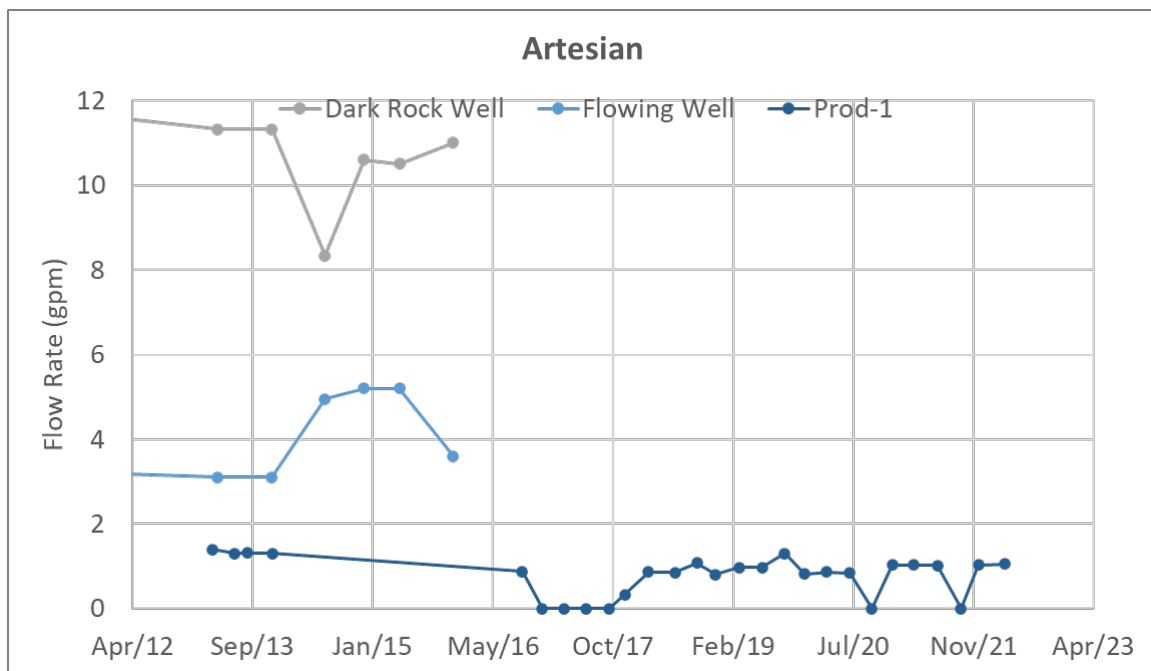


Figure 3-3: Spring Flow Data – Artesian Wells.

**Table 3-1:
Average Spring Flow Targets**

Spring or Well Name	Average Spring Flow Rate (gpm)	Easting (ft) ¹	Northing (ft) ¹
Bull Spring Tank	0.71	5753206.76	756212.71
Central Grassy Mountain Spring	-0-	5755880.22	738802.55
Darky Rock Well	10.5	5737016.70	726474.29
Deposit Stock Tank	0.27	5750879.69	748376.46
East Grassy Mountain Spring	-0-	5756563.61	729591.48
Flowing Well	4.4	5741317.08	758410.11
Government Corral Spring	1.1	5728058.73	737588.00
Grassy Spring	0.02	5746824.85	725895.95
Lowe Spring	0.07	5728513.41	757611.37
Negro Rock Canyon Spring	-0-	5740634.21	759368.75
Negro Rock Spring Tank	-0-	5732821.85	757839.97
Oxbow Spring Tank	0.29	5756588.35	737920.33
Oxyoke Spring Tank	0.00	5757094.64	726801.09
Poison Spring	1.8	5735633.31	767800.84
Prod-1	0.78	5751275.24	753540.87
Red Tank No. 3	0.20	5727332.01	761550.47
Sagebrush Spring	0.85	5730323.90	731798.68
Sourdough Spring Lower	0.02	5750275.77	741738.61
Sourdough Spring Upper	0.37	5752193.55	764826.92
Spring in Section 13 T22S R44E ²	0.91	5773378.13	739203.81
Spring in Section 23 T21S R43E	-0-	5732244.79	769162.95
Spring North of Lowe Reservoir	0.00	5731598.43	737582.25
Spring South of Poison Spring	-0-	5732296.36	756210.06
Tank East of Negro Rock	6.9	5732244.79	769162.95
Twin Springs North	1.5	5757863.85	756975.56
Twin Springs South	7.7	5761380.84	759029.76
West Grassy Mountain Spring	-0-	5753456.68	761799.48
West Whiskey Spring	-0-	5737632.84	725277.03
Whiskey Spring	0.92	5757538.71	738055.90
Wildcat Spring	0.21	5737277.02	754844.53

Notes:¹ Oregon State Plane South coordinate system. ²Spring is outside of groundwater model domain.

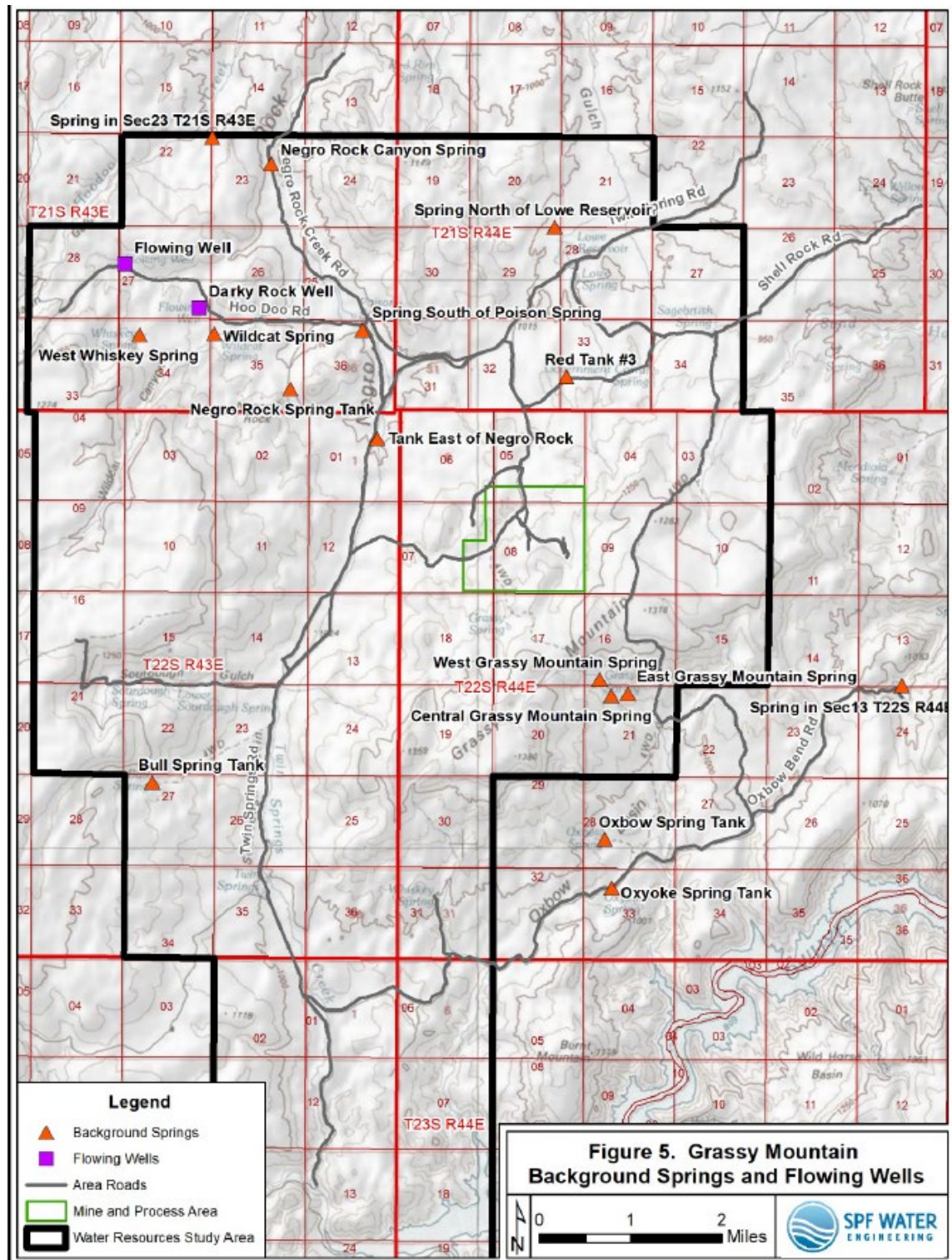


Figure 3-4: Spring and Artesian Well Locations (from SPF, 2021a).

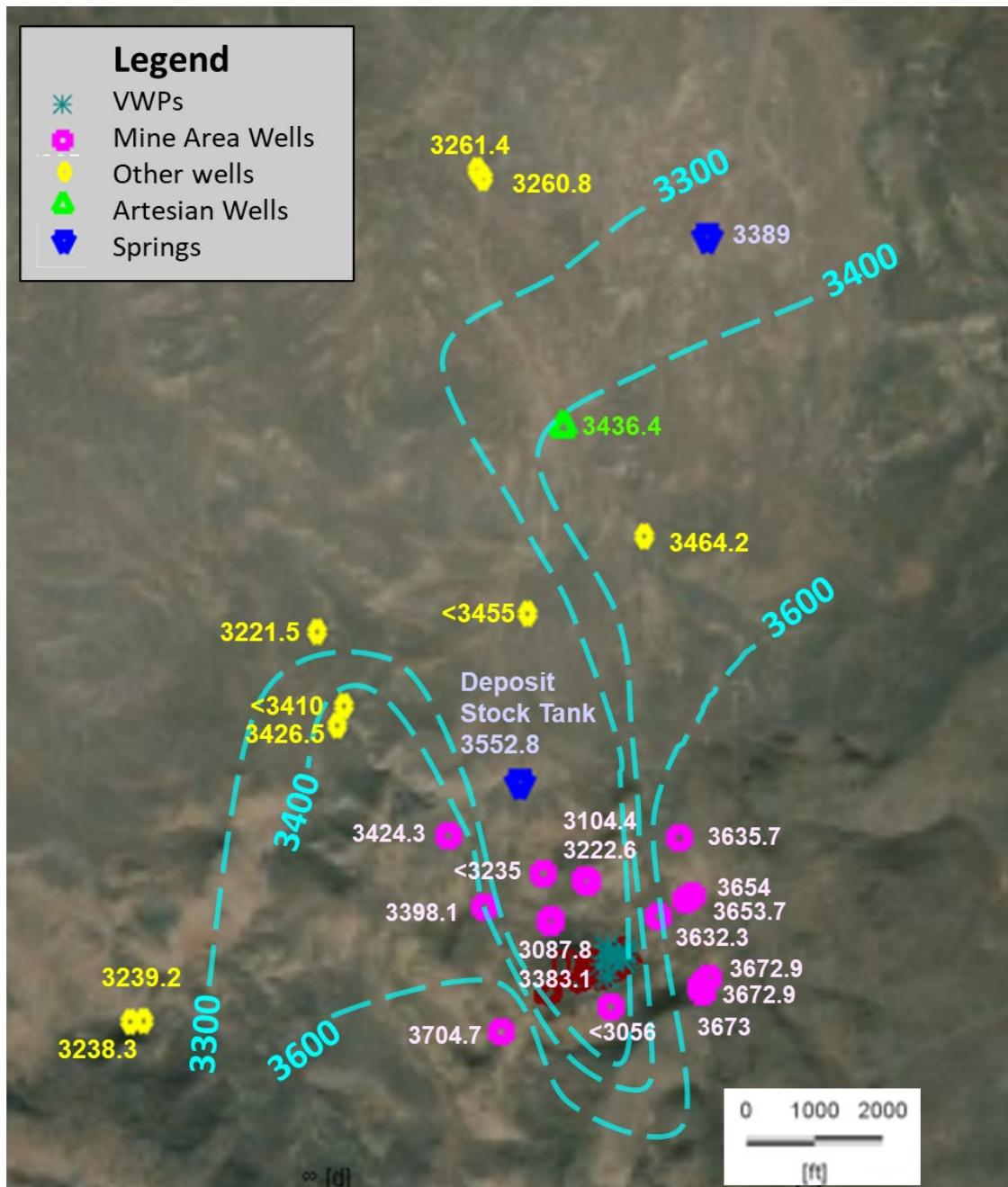
3.4 Groundwater Levels and Flow Directions

SPF (2021b) describes two groundwater flow systems based on a shallow potentiometric surface and a deep potentiometric surface. The potentiometric surface maps based on shallow wells support a consistent flow direction without seasonally influenced variations. Groundwater flow appears to follow the surface topography, generally to the northwest in the mine area. The pattern of groundwater flow shows local variations attributed to the presence of faults, fractures, lithologic facies changes, vertical gradients, or some combination of these influences (SPF, 2021b). A deep potentiometric surface was based on water levels measured from two deeper well completions (59762 and GMW17-32) and the average of six vibrating wire piezometers (VWPs) installed at deep and intermediate depths (GM17-16-I, GM17-16-D, GM17-20-I, GM17-20-D, GM17-21-I, and GM17-30-I). This potentiometric surface suggests the direction of groundwater flow in the deeper water-bearing intervals is also toward the northwest in the vicinity of the proposed Grassy Mountain Mine, from higher elevations along the base of Grassy Mountain to lower elevations along Negro Rock Canyon. These groundwater elevations range from approximately 3,150 ft amsl at the proposed Grassy Mountain Mine to approximately 3,100 ft amsl at the two monitoring wells just northwest of the proposed Grassy Mountain Mine.

SPF (2021b) further states:

- Only deep monitoring wells in the network are completed near the proposed Grassy Mountain Mine. Other monitoring wells completed at similar elevation (approximately 3,000 to 3,100 ft amsl) including PW-4, GW-4, GW-6, and 59770 all have static water elevations more than 100 ft higher than the deep wells.
- Large vertical gradients in the ore zone are due to significant compartmentalization of the aquifer resulting from the silicification, faulting, and steeply dipping sedimentary beds.

Figure 3-5 presents an interpreted piezometric head map in the project area. The data point to a zone of depressed groundwater head extending north-northwestward from the mine. There is also a strong downward hydraulic gradient, which will be discussed later. For this reason, the spring in the head trough (Deposit Stock Tank) has a significantly higher head—3552.8 ft amsl—than the groundwater measurements immediately south-southeast of this spring (see charts on Figure 3-7).



Note: Calibration head targets shown for wells. No values displayed for VWPs.

Figure 3-5: Interpreted Piezometric Head Map.

Figure 3-6 presents the hydrographs from wells within the numerical model domain that are relatively far from the mine property. All charts have the same vertical range (16 ft) of piezometric head. On the other hand, the magnitude of head varies significantly, from above 3660 ft amsl at GW-2 to approximately 3220 ft amsl at GW-5. The long-term head

values at the wells are generally stable. However, six wells—59763, 59764, 59766, 59770, 89-2, and GW-6—show a gradual long-term trend of declining heads. Conversely, four wells—BLM, GW-4, GW-5 and PW-4—have shown long-term gradual increases in head.

Figure 3-7 shows the long-term head trends in wells in the mine vicinity. The vertical range of heads in the charts on Figure 3-7 is approximately twice that of the previous charts, and the piezometric head in some of these wells shows greater temporal variability. For instance, the head at 57-1 has ranged from 3694 ft amsl to 3720 ft amsl during the period of record. Water levels in wells installed near the mine in 2017, such as GMW17-33 and GMW17-32 have shown long-term water level recoveries over the period of record.

The mine area wells in Figure 3-7 also show a larger range in absolute head values than the regional wells in Figure 3-6. The maximum heads measured in the mine-area wells shown in Figure 3-7 occurred at 57-1, where heads were generally above 3700 ft amsl. By comparison, the single measurement at GMW18-34, which is usually dry, was 3062 ft amsl, or more than 600 ft lower than at 57-1. Heads below 3120 ft amsl were also recorded at 59762 and GMW17-32.

Average piezometric head values used for the groundwater model calibration are shown in Table 3-2 for monitoring wells, and in Table 3-3 for artesian wells, including Prod-1, and springs. In both tables, Easting and Northing are presented in the Oregon State Plane South coordinate system. The average heads for monitoring wells listed in Table 3-2 were computed for the entire period of March 2013 to March 2022, unless otherwise noted in the table. The exceptions are as follows:

- For wells with a data record that begins before 2015 that show a temporal trend in head, the average heads from September 2018 were used. These wells are: 59766, 57-1, BLM, and GW-3
- For PW-1 and GW-1, which have a sharp decrease in head in late 2016 due to apparent pumping of this well, the period containing the lowest water levels was excluded. The dates excluded from the average calculation were the December 2016, March 2017 and June 2017 measurements.
- For wells GMW17-31 and GMW17-32, the head values starting in September 2020 were used for the head target. GMW17-32 exhibits a long-term trend that indicates the possibility that it is still recovering from drilling and testing activities.

Table 3-2 also includes approximate average heads from the vibrating-wire piezometers (VWPs) in the mine area.

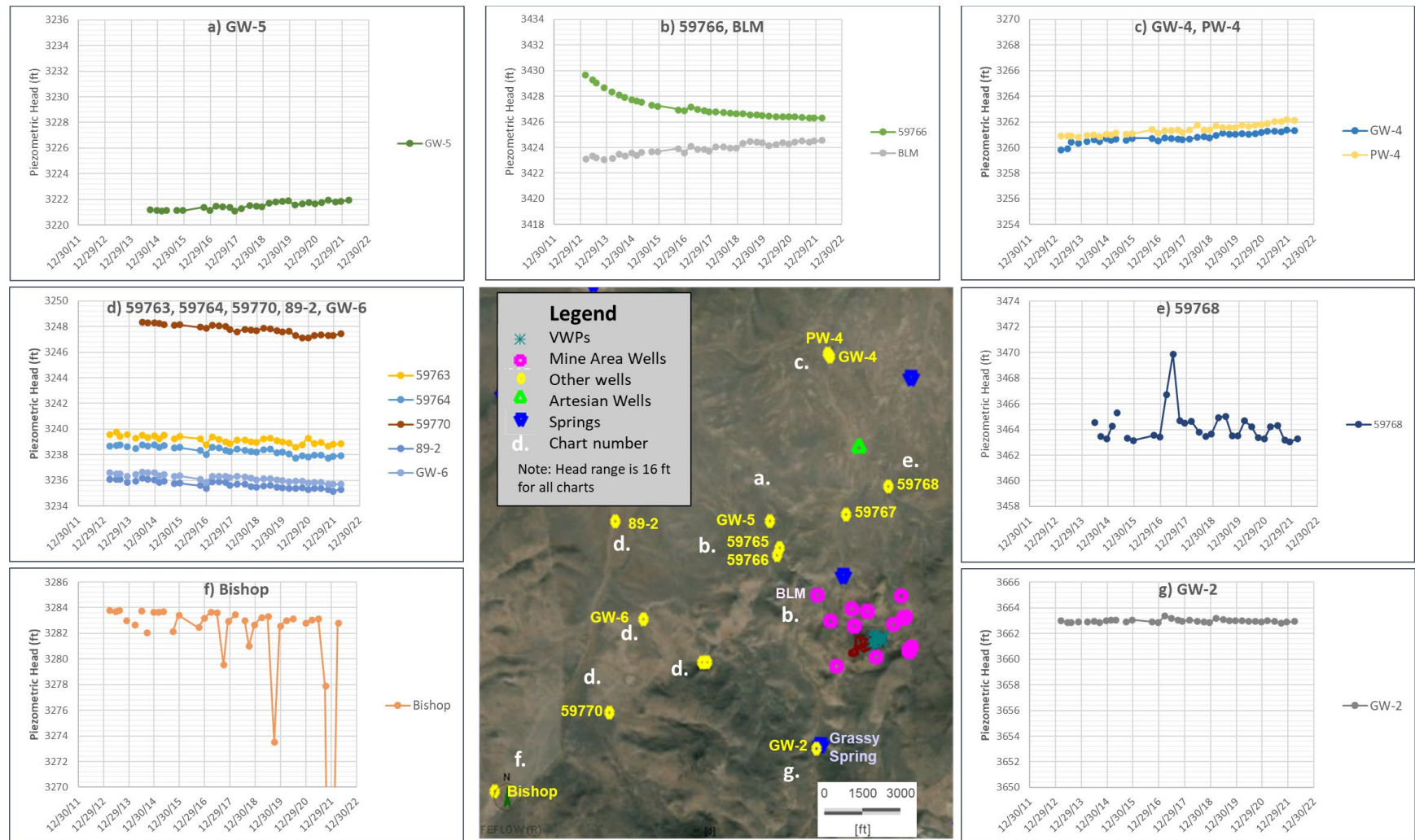


Figure 3-6: Piezometric Head Hydrographs, Regional Wells.

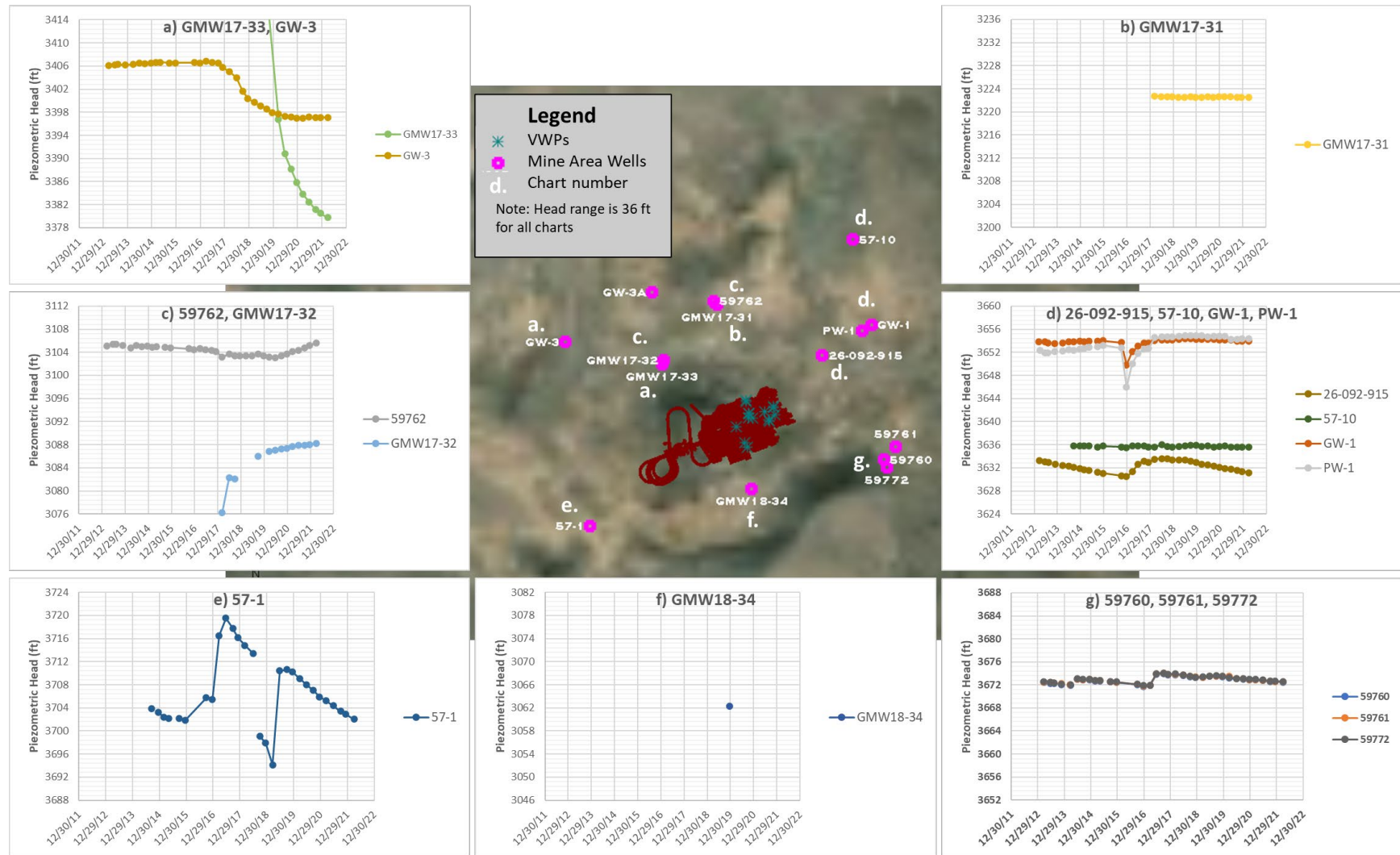


Figure 3-7: Piezometric Head Hydrographs, Mine Vicinity Wells.

**Table 3-2:
Average Groundwater Head Targets – Monitoring Wells**

ID	Easting (ft)	Northing (ft)	Midpoint (ft)	Measured Head (ft)	Comment
59760	5753551.5	745646.0	3579.0	3672.9	
59761	5753658.5	745772.8	3650.0	3672.9	
59762	5751855.0	747093.5	3084.8	3104.4	
59763	5745692.0	744833.3	3211.0	3239.2	
59764	5745502.5	744814.4	3223.0	3238.3	
59765	5748338.6	749408.5	3410.0	<3410	dry
59766	5748254.8	749128.4	3421.3	3426.5	From Sep 2018
59767	5750882.3	750823.4	3455.0	<3455	dry
59768	5752488.8	751987.9	3460.2	3464.2	
59770	5741955.4	742710.9	2990.0	3247.8	
59772	5753583.6	745572.4	3583.0	3673.0	
26-092-915	5752915.8	746617.8	3462.0	3632.3	
57-1	5750760.3	744890.8	3648.0	3704.7	From Sep 2018
57-10	5753164.9	747741.1	3540.0	3635.7	
89-2	5741874.8	750181.8	2897.0	3235.7	
Bishop	5737602.8	739450.4	3252.0	3281.4	
BLM	5749895.1	747633.6	3417.5	3424.3	From Sep 2018
GM17-16-D	5752204.2	746157.7	3081.1	3081.5	
GM17-16-I	5752206.5	746144.9	3108.3	3181.0	
GM17-16-S	5752234.9	745990.4	3443.6	<3444	dry
GM17-20-D	5752470.1	746109.9	3021.5	3156.0	
GM17-20-I	5752472.4	746099.2	3080.6	3159.0	
GM17-20-S	5752487.7	746029.8	3485.3	<3486	dry
GM17-21-D	5752437.3	745965.4	3059.1	<3060	dry
GM17-21-I	5752429.2	745980.3	3107.1	3107.0	
GM17-21-S	5752388.3	746056.0	3342.9	<3343	dry
GM17-28-D	5752235.4	745707.7	3173.8	<3174	dry
GM17-28-I	5752210.1	745750.9	3237.6	<3238	dry
GM17-28-S	5752122.5	745900.1	3459.1	<3460	dry
GM17-30-D	5752234.9	746035.7	3087.9	<3088	dry
GM17-30-I	5752239.7	746030.5	3118.1	3186.0	
GM17-30-S	5752276.1	745990.6	3352.9	<3353	dry
GMW17-31	5751890.4	747062.1	3222.0	3222.6	
GMW17-32	5751400.1	746507.8	3006.0	3087.8	From Sep 2020
GMW17-33	5751387.6	746468.9	3407.5	3383.1	From Sep 2020
GMW18-34	5752293.7	745311.5	3056.0	<3056	dry
GW-1	5753379.2	746929.7	3563.5	3654.0	Excludes pumping period
GW-2	5750108.4	741642.1	3522.0	3663.0	
GW-3	5750449.6	746644.7	3299.0	3398.1	From Sep 2018
GW-3A	5751260.8	747154.7	3235.0	<3235	dry
GW-4	5749996.5	756962.0	3028.0	3260.8	
GW-5	5747915.3	750443.4	3199.0	3221.5	
GW-6	5743134.9	746405.8	3057.0	3236.2	
PW-1	5753289.9	746870.0	3299.0	3653.7	Excludes pumping period
PW-4	5749908.3	757070.9	3021.0	3261.4	

**Table 3-3:
Average Groundwater Head Targets – Artesian Wells and Springs**

ID	Easting (ft)	Northing (ft)	Elevation of Screen Midpoint (ft)	Measured
Prod-1-Bot ¹	5751275.2	753540.9	3036.0	3436.4
Prod-1-Top ¹	5751275.2	753540.9	3186.0	3436.4
Bull Spring Tank	5730323.9	731798.7	3723.1	3727.0
Central Grassy Mtn Spring	5756588.3	737920.3	3480.4	3489.0
Darky Rock Well	5732296.4	756210.1	3391.0	3542.6
Deposit Stock Tank	5750879.7	748376.5	3552.5	3552.8
East Grassy Mtn Spring	5757538.7	738055.9	3482.2	3489.0
Flowing Well at Topo	5727332.0	761550.5	3528.5	3532.0
Government Corral	5757863.8	756975.6	3450.6	3456.0
Grassy Spring	5750275.8	741738.6	3822.8	3822.8
Lowe Spring	5753456.7	761799.5	3279.0	3279.0
Negro Rock Canyon Spring	5735633.3	767800.8	3108.8	3117.0
Negro Rock Spring Tank	5737277.0	754844.5	3315.5	3319.0
Oxbow Spring Tank	5756563.6	729591.5	3065.0	3065.0
Oxyoke Spring Tank	5757094.6	726801.1	3025.5	3029.0
Poison Spring	5740634.2	759368.8	3213.9	3213.9
Red Tank 3	5753206.8	756212.7	3384.0	3389.0
Sagebrush Spring	5761380.8	759029.8	3479.5	3481.9
Sourdough Lower	5731598.4	737582.3	3565.4	3565.4
Sourdough Upper	5728058.7	737588.0	3750.7	3754.1
Spring N of Lowe Reservoir	5752193.6	764826.9	3247.0	3247.0
Spring S of Poison Spring	5741317.1	758410.1	3232.0	3232.0
Spring Sec23 T21S R43E	5732244.8	769163.0	3291.8	3297.0
Tank E of Negro Rock	5742408.2	752204.3	3271.3	3273.0
Twin Springs North	5737016.7	726474.3	3235.6	3240.0
Twin Springs South	5737632.8	725277.0	3204.4	3210.3
West Grassy Mtn Spring	5755880.2	738802.6	3609.5	3619.0
West Whiskey Spring	5728513.4	757611.4	3547.0	3547.0
Whiskey Spring	5746824.8	725895.9	3230.0	3230.0
Wildcat Spring	5732821.8	757840.0	3359.9	3366.0

Notes:¹ Prod-1 has three screens. The top screen is simulated with Prod-1-Top, and the bottom two are simulated together as Prod-1-Bot. Both zones are monitored and assigned the same head target.

Vertical hydraulic gradients can be computed using the average head values. The location of the two standpipe couplets for vertical head calculation are shown in Figure 3-8. The computed vertical gradients at these locations are:

- **GMW17-33 and GMW17-32:** 0.74 ft/ft gradient, favoring downward groundwater flow
- **GMW17-31 and 59762:** 0.86 ft/ft gradient, favoring downward groundwater flow

Vertical gradients were also computed from VWP heads. Using the available data, the gradients are 3.7 ft/ft from GM17-16-I to GM17-16-D and 0.05 ft/ft from GM17-20-I to GM17-20-D.

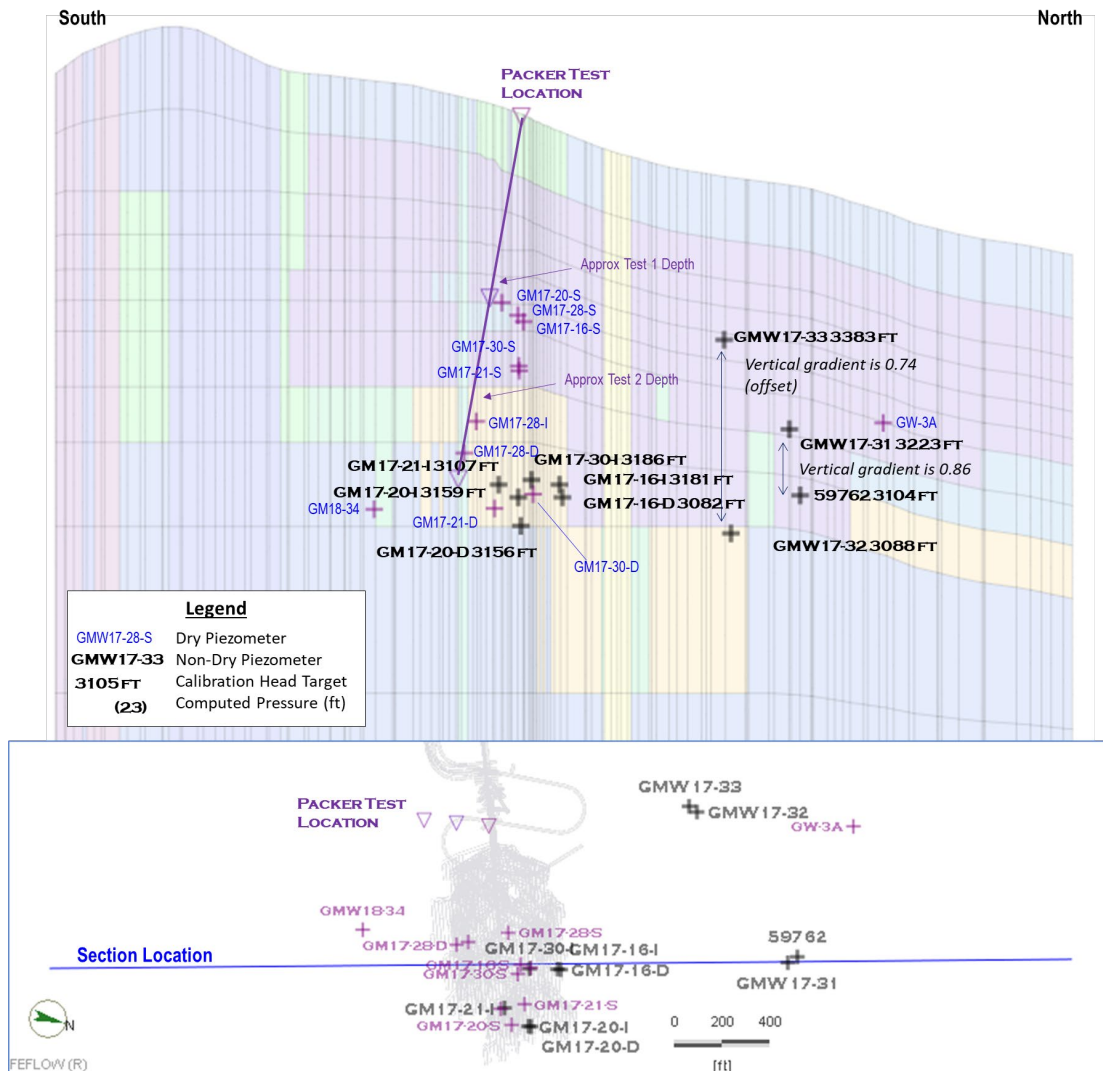


Figure 3-8: Mine Area Piezometric Heads, Including VWP.

3.5 Hydraulic Parameters

3.5.1 Hydraulic Conductivity and Silicification

Hydraulic conductivity in the Project area is closely related to silicification. The following discussion on silicification is summarized from SPF (2021b).

- In and near the proposed Grassy Mountain Mine, most of the sedimentary units are silicified and strongly indurated (Abrams 2018).
- In 2012, a controlled-source audio-frequency magnetotelluric (CSAMT) survey was conducted by Zonge Geosciences Inc. (SPF, 2021c). The CSAMT survey lines were oriented N20°W and located across the area of known mineralization to identify zones of high resistivity, indicative of highly silicified rocks that host the ore zone.
- An increase in resistivity/silicification was noted with depth.
- The CSAMT survey was completed at four different depth ranges where the degree of silicification is reflected by the productivity of wells:
 - 0 to 50 meters (0 to 164 ft) – Wells completed in non-silicified sediments, and basalt respectively, produce in excess of 50 gpm on a short-term basis. Drill holes generally encountered more water at this depth interval compared to the deeper intervals, with the degree of silicification appearing to have less of an impact on the presence of water;
 - 50 to 100 meters (164 to 328 ft) – monitoring wells completed in moderately-silicified sediments and basalt produce at least 10 gpm on a short-term basis. The wells completed in more silicified materials typically produce less than 5 gpm;
 - 100 to 200 meters (328 to 656 ft) – The drill holes that encountered water are typically on the periphery of the highly silicified deposit; and
 - 200 to 400 meters (656 to 1,312 ft) – where little or no water was encountered in boreholes.
- Values of high resistivity can be correlated to low porosity and low hydraulic conductivity. Hydraulic conductivity increases moving away from the proposed Grassy Mountain Mine.
- The large section of silicified formation upgradient and encompassing the proposed Grassy Mountain Mine is an impediment to groundwater flow through the proposed Grassy Mountain Mine.

3.5.2 Pumping Tests

Hydraulic conductivity measurements from pumping tests are available at six locations in the mine area. The locations of these tests are shown in Figure 3-9. They are discussed in detail in SPF (2021c). The following is a summary of the available data.

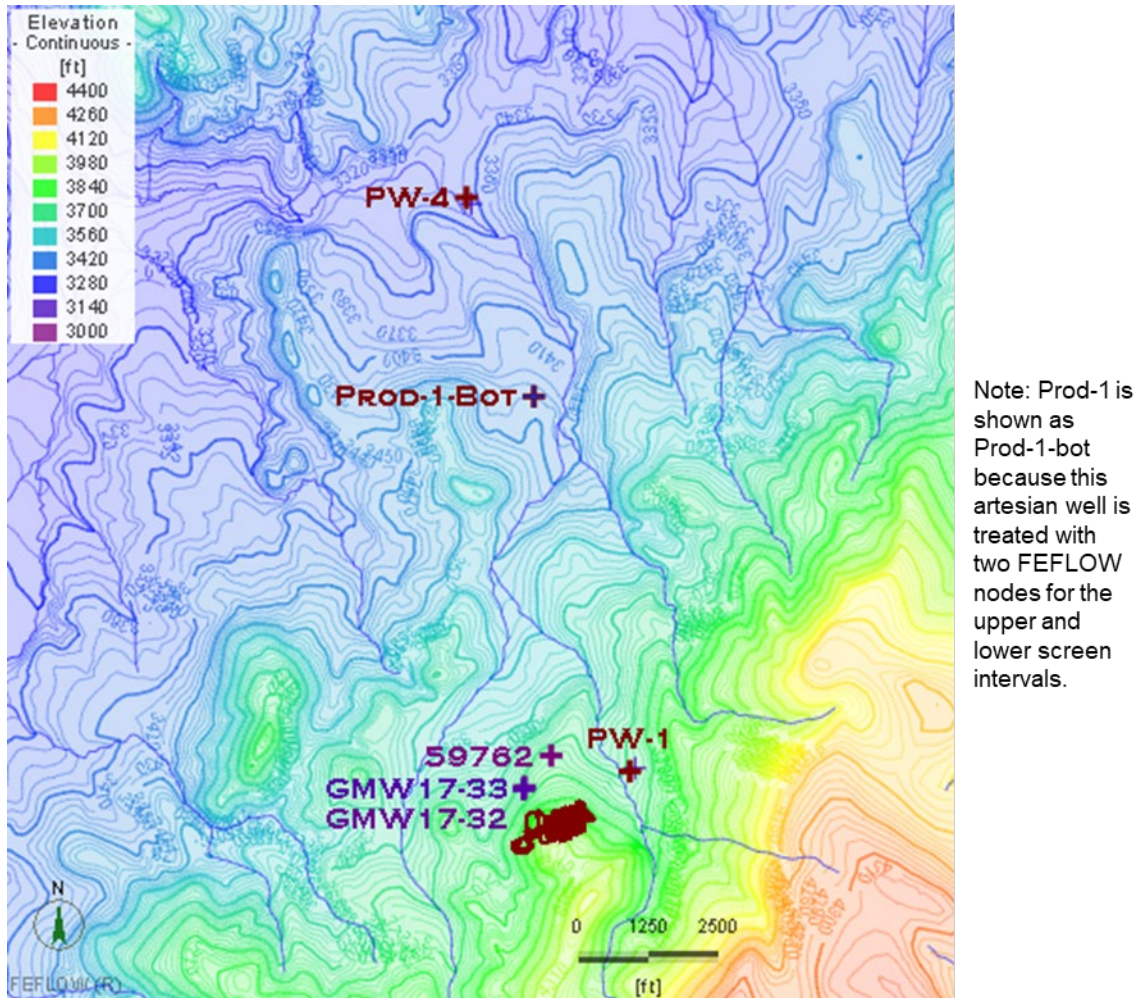


Figure 3-9: Pumping Test Locations.

In the proposed production well area, a three-day pumping test was conducted in PW-4 in 1989. The pumping rate during the test was 140 gpm, and the recorded drawdowns in the pumping well and in observation well GW-4 are shown in Figure 3-10. GW-4 is located 140 ft from PW-4, at approximately the same elevation as PW-4. As discussed by SPF (2021c), the drawdowns recorded in the PW-4 pumping test indicated that it was affected by a hydraulic barrier. Pumping well PW-4 is conceptualized to intersect a portion of the basin sediments interpreted as Unit TIS—interbedded conglomerate and sandstone (SPF, 2021c). This zone is shown in Figure 4-17 and discussed in Section 4.6.

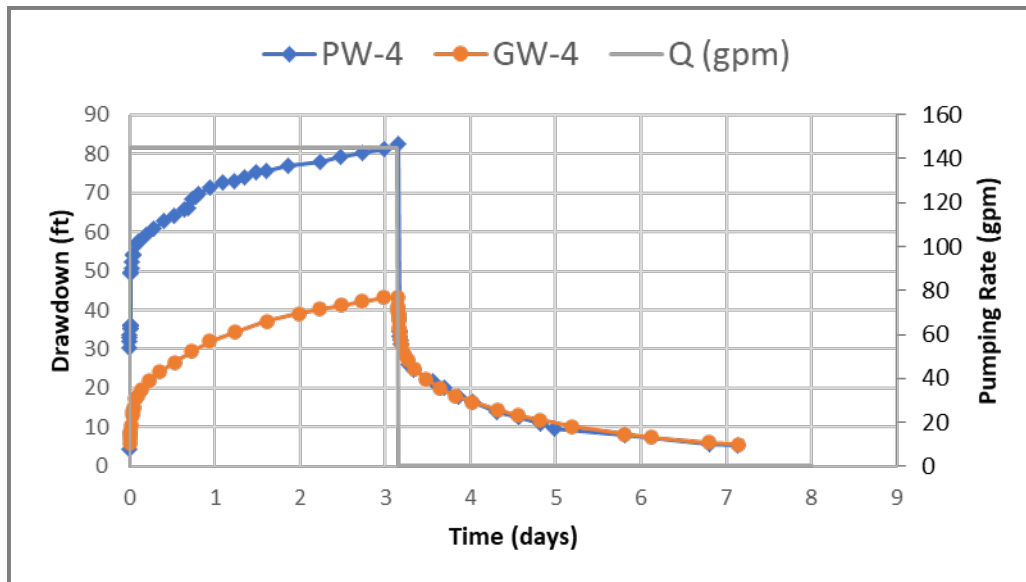


Figure 3-10: PW-4 Pumping Test Data.

In 1991, a pumping test was conducted on artesian well Prod-1. This well was pumped at a rate of 100 gpm for a period of 45 hours. Like PW-4 it exhibits drawdown behavior consistent with the presence of hydraulic barriers. The data for this test are presented in Figure 3-11. The Prod-1 pumping tests yielded a much more rapid drawdown than PW-4 and indicated more than one hydraulic barrier in the vicinity of the well. In the FEFLOW model, Prod-1 is located between two barrier faults, the Grassy Mountain East and Grassy Mountain West faults (see Section 4.7). A combination of these barrier faults and a hydraulic conductivity equal to that in the vicinity of the PW-4 pumping test was used in the calibration of this pumping test.

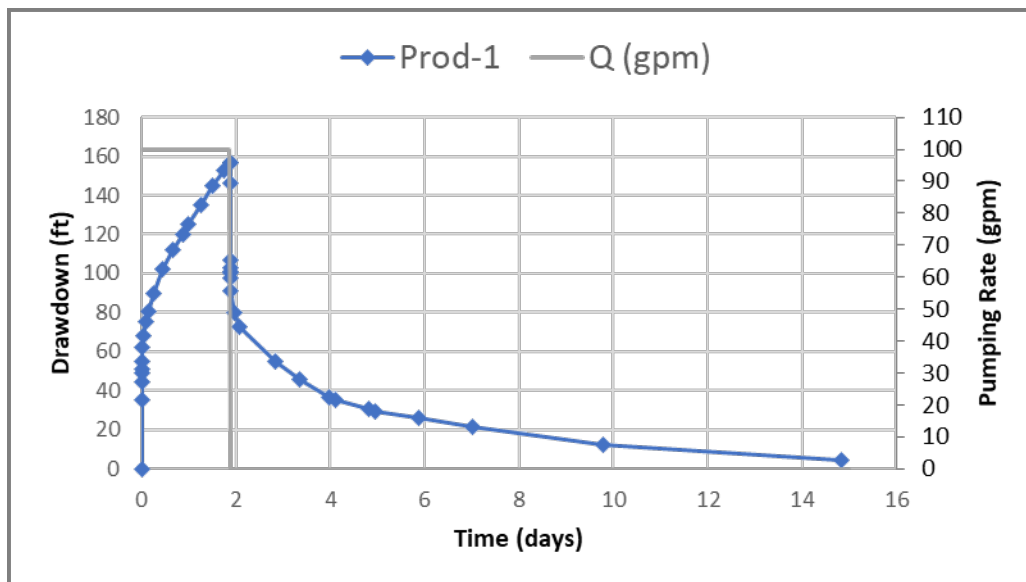


Figure 3-11: Prod-1 Pumping Test Data.

In 1989, a seven-day pumping was completed in PW-1, with a pumping rate of 30 gpm. Nearby observation well GW-1 was also monitored during this time. GW-1 is located 107 ft from PW-1 and has a screen midpoint that is 265 ft above the screen midpoint of PW-1. One important feature of the PW-1 pumping test is the contrast in the drawdown of 230 ft at PW-1 compared to maximum drawdown of 6 ft in GW-1. As in the PW-4 and Prod-1 pumping tests, barrier effects were observed during this test (SPF, 2021c). The drawdown and pumping data are shown in Figure 3-12.

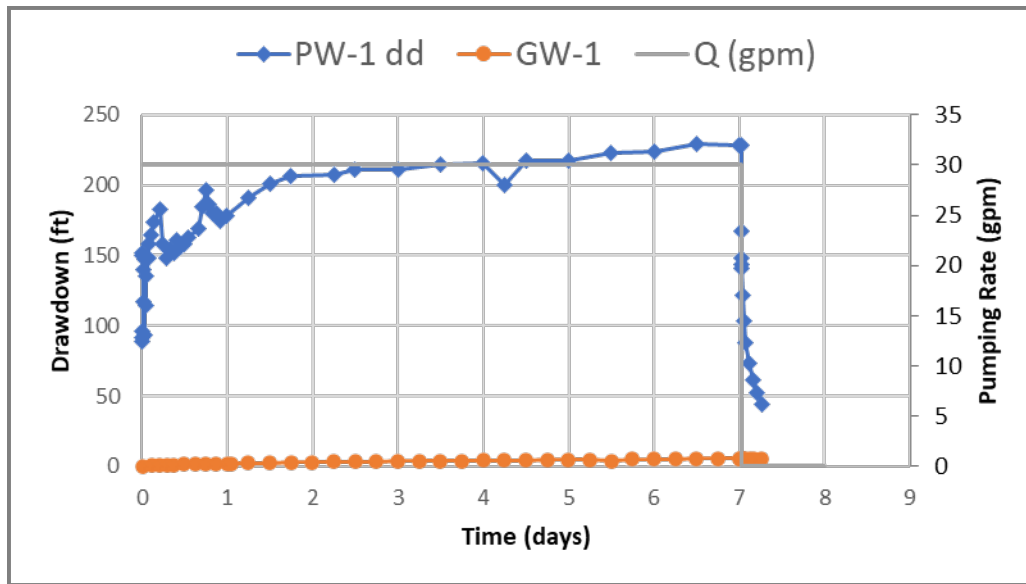


Figure 3-12: PW-1 Pumping Test Data.

As indicated in Figure 3-9, there were three pumping tests near the proposed mine, at GMW17-32, GMW17-33 and 59762. All of these tests were completed at the end of 2017, soon after the drilling program. The data from these tests are presented here using November 29, 2017 at 5:52 pm as the initial time, during the development of GMW17-32. Figure 3-13 shows the data for GMW17-33. The pumping test in this well began 15 days after the start of the development of GMW17-32 and was preceded by a step-drawdown test on Day 14. The pumping rate used for the test was 30 gpm, which was maintained for a period of approximately 2.5 days at the end of which the drawdown became excessive. As a consequence, the pumping rate was gradually decreased to 29 gpm, 27 gpm, 25 gpm, 24.5, 20 gpm, 17.5 gpm, and finally 17.2 gpm, before the test was shut down after 1.6 days.

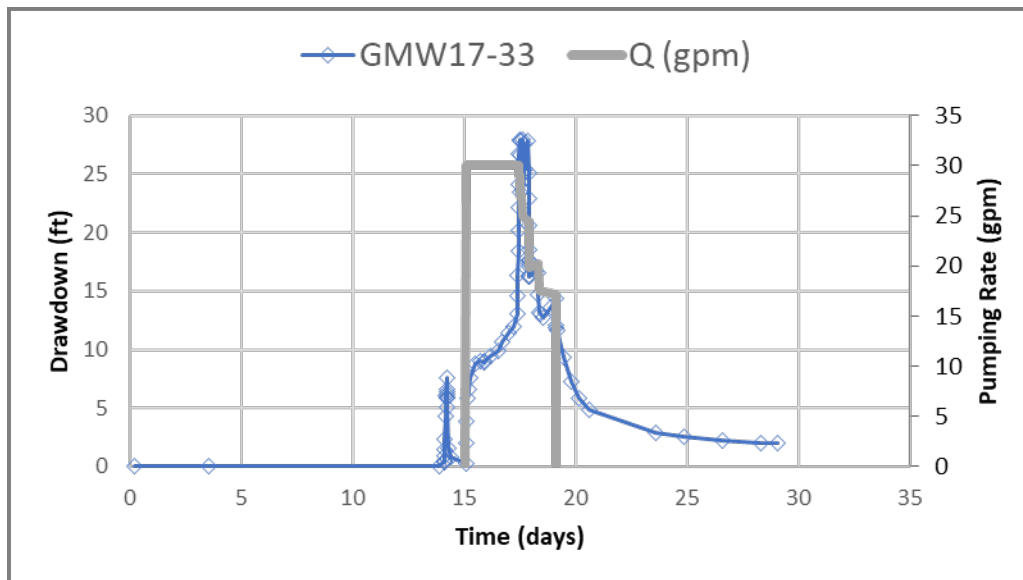


Figure 3-13: GMW17-33 Pumping Test Data.

The data for the pumping test at deep well GMW17-33 is presented in Figure 3-14. As mentioned above, the drawdown dataset begins during the development of GMW17-33. The long recovery period evident during and following well development indicates a low permeability in the units screened by this well. The initial static water level was unknown for this well, and an initial water level of 624.67 ft below the measurement point was used, as suggested by SPF in the dataset provided. The most important result of this pumping test is that it was not possible to maintain a pumping rate of 1 gpm for a period of 2 hours. Furthermore, the recovery period was significant, lasting over two weeks.

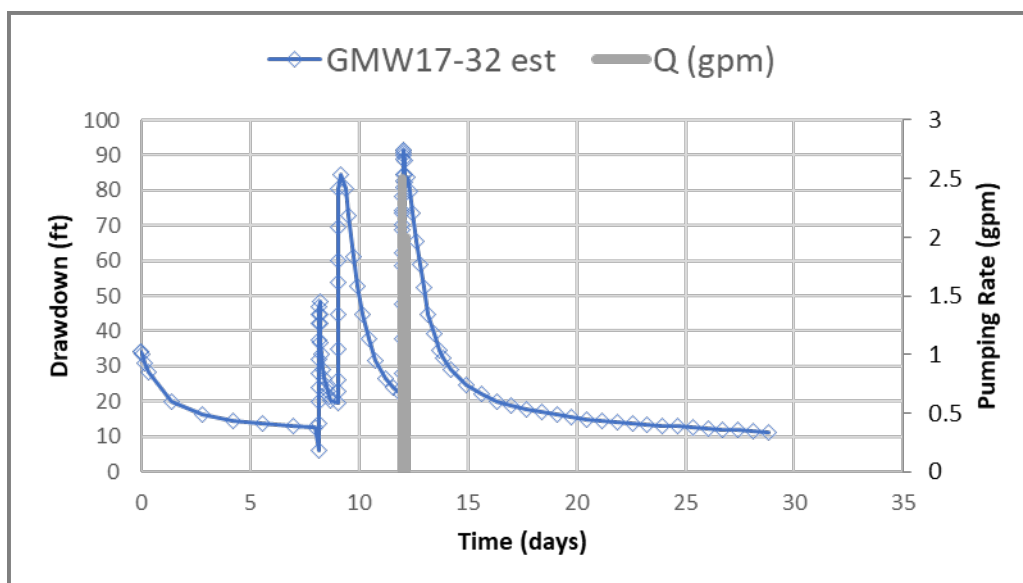


Figure 3-14: GMW17-32 Pumping Test Data.

A similar result was observed at 59762, as shown in Figure 3-15. Rapid drawdown was observed in this well, and a pumping rate of 1 gpm could not be maintained for two hours. The recovery period for this well was also long, as for GMW17-32. Because of the low hydraulic conductivity that is evident at GMW17-33 and 59762, these tests were not included in the transient calibration discussed below.

In addition to the pumping tests summarized above, Paramount Gold Nevada completed a geotechnical borehole in the area of the decline, and Lorax performed packer testing on the borehole to obtain estimates of the hydraulic conductivity. However, more recent water level measurements from the mine area (see Figure 3-8) indicate that the intervals of the borehole that was packer-tested were largely unsaturated. Therefore, high estimates of hydraulic conductivity from the packer tests are assumed to be due to unsaturated bedrock surrounding the borehole.

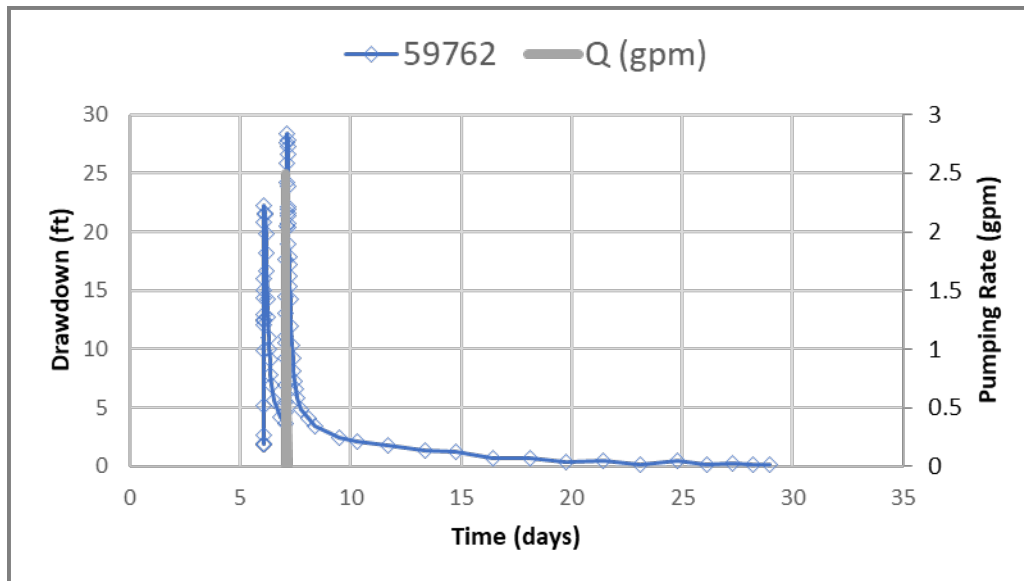


Figure 3-15: 59762 Pumping Test Data.

3.6 Conceptual Model

The groundwater system in the Grassy Mountain project areas is characterized by the following features:

- **Recharge** – The area is semi-arid, and groundwater recharge is estimated to be on the order of 0.5 inch per year to 1 inch per year.
- **Discharge** – Groundwater in the project area discharges to the Owyhee Reservoir in the south, toward the Malheur River in the north, and to a few dozen springs and artesian wells in the project area. Discharge also occurs to intermittent streams in

- the model domain. Figure 3-16 shows a south-to-north section from Owyhee Reservoir to the Malheur River, running through the proposed mine.
- **Geology** – The Grassy Mountain Formation is the host unit for the proposed Grassy Mountain Mine. It consists of arkosic sandstone, siltstone, and conglomerate and is underlain by the Kern Basin Tuff, a fine-grained lithic tuff. The geological database in the mine area suggests an increase in the incidence of arkosic sandstone with depth in the deposit, with a greater proportion of siltstone in shallower portions of the mine area.
 - **Hydraulic Conductivity** – The Grassy Mountain Formation in and near the proposed Grassy Mountain Mine is silicified and strongly indurated. Hydraulic conductivity and resultant groundwater flow appear to be severely restricted by silicification and/or faulting. In addition:
 - Testing of GMW17-32, completed in silicified sediments near the proposed Grassy Mountain Mine, suggests a very low hydraulic conductivity on the order of 10^{-8} to 10^{-9} m/s. The screen interval of this well is 3026 ft amsl to 2986 ft amsl.
 - Near the proposed Grassy Mountain, Mine there are isolated pockets of less-silicified material with higher conductivity, and faults in these areas may act as conduits for groundwater flow. One pocket of higher permeability rock was tested at GMW17-33, located adjacent to GMW17-32. GMW17-33 is screened between 3465 ft amsl and 3365 ft amsl, or approximately 400 ft above the screen zone of low-permeability GMW17-32.
 - The silicification and faulting seems to decrease the hydraulic conductivity of the arkosic sandstone but potentially increase the hydraulic conductivity of the underlying tuff. Hydraulic conductivity values downgradient of the proposed Grassy Mountain Mine derived from test pumping are on the order of 10^{-5} m/s to 10^{-7} m/s, representative of sandstone and conglomerate aquifers. The Grassy Mountain fault zone extending north of the proposed Grassy Mountain Mine acts like a barrier to groundwater flow based on testing of nearby wells.
 - **Water-bearing zones** – The water-bearing zones within the Grassy Mountain Formation are found within unconsolidated or weakly consolidated sandstone and conglomerate (TIS) units and interbedded sediments that appear to be compartmentalized due to faults, sedimentary facies changes, and silicification. The main water-bearing units were noted around wells PW-4 and Prod-1. Lower hydraulic conductivities were observed at PW-1 and GMW17-33. The TIS zone is discussed in SPF (2021c) and shown in Figure 3-16.

- **Groundwater Levels** –Based on available information, a saturated zone occurs within the proposed Grassy Mountain Mine at an elevation ranging from 3,080 to 3,200 ft amsl, which is above the expected maximum depth of the proposed mine (approximately 3,050 ft amsl). Water levels in the area are typically stable, with some seasonal variations evident in shallow wells or wells otherwise subject to more direct recharge.
- **Hydraulic Gradients** – Strong vertical and horizontal hydraulic gradients are evident in the project area, indicating significant compartmentalization. In particular, groundwater levels at and north of the proposed mine are significantly lower than those measured east and west of the mine. At all locations where vertical gradients were calculated, a gradient favoring downward flow was noted. Groundwater flow in the Project area is generally from the southeast to the northwest, from higher elevations along the base of Grassy Mountain to lower elevations along Negro Rock Canyon. This flow direction is evident in both the shallow and deep potentiometric surfaces. In the mine area, vertical gradients are on the order of 0.7 to 0.9 ft/ft.

As discussed below, the strong vertical gradient in the mine area is simulated using a structure at depth located north of the proposed mine. Figure 3-16 shows a conceptual section that places the Grassy Mountain FEFLOW model in the context of the regional groundwater flow system. The elevation of the surface of the Malheur River at Vale is approximately 2220 ft amsl, or approximately 900 ft below the piezometric head in the deep VWPs at the proposed mine property. As shown in Figure 3-16b, the vertical downward gradient in the mine area could be associated with a regional groundwater flow pathway from a recharge zone at Grassy Mountain to a discharge zone at the Malheur River. A larger model domain would likely be able to capture this flow path, provided the model included the Malheur River and was sufficiently deep.

As a general rule, the deep flowpath labeled “alternative groundwater flow direction” in Figure 3-16b would require that the hydraulic conductivity of the deep strata is not excessively low. Because the FEFLOW model does not extend to the Malheur River, due to computational and data constraints, the likely presence of the deep flow path associated with regional groundwater flow from Grassy Mountain to the Malheur River was simulated with a local high permeability zone to depress the water table and encourage downward flow in the northern half of the model domain, the area in which generally downward groundwater gradients are conceptualized in Figure 3-16b.

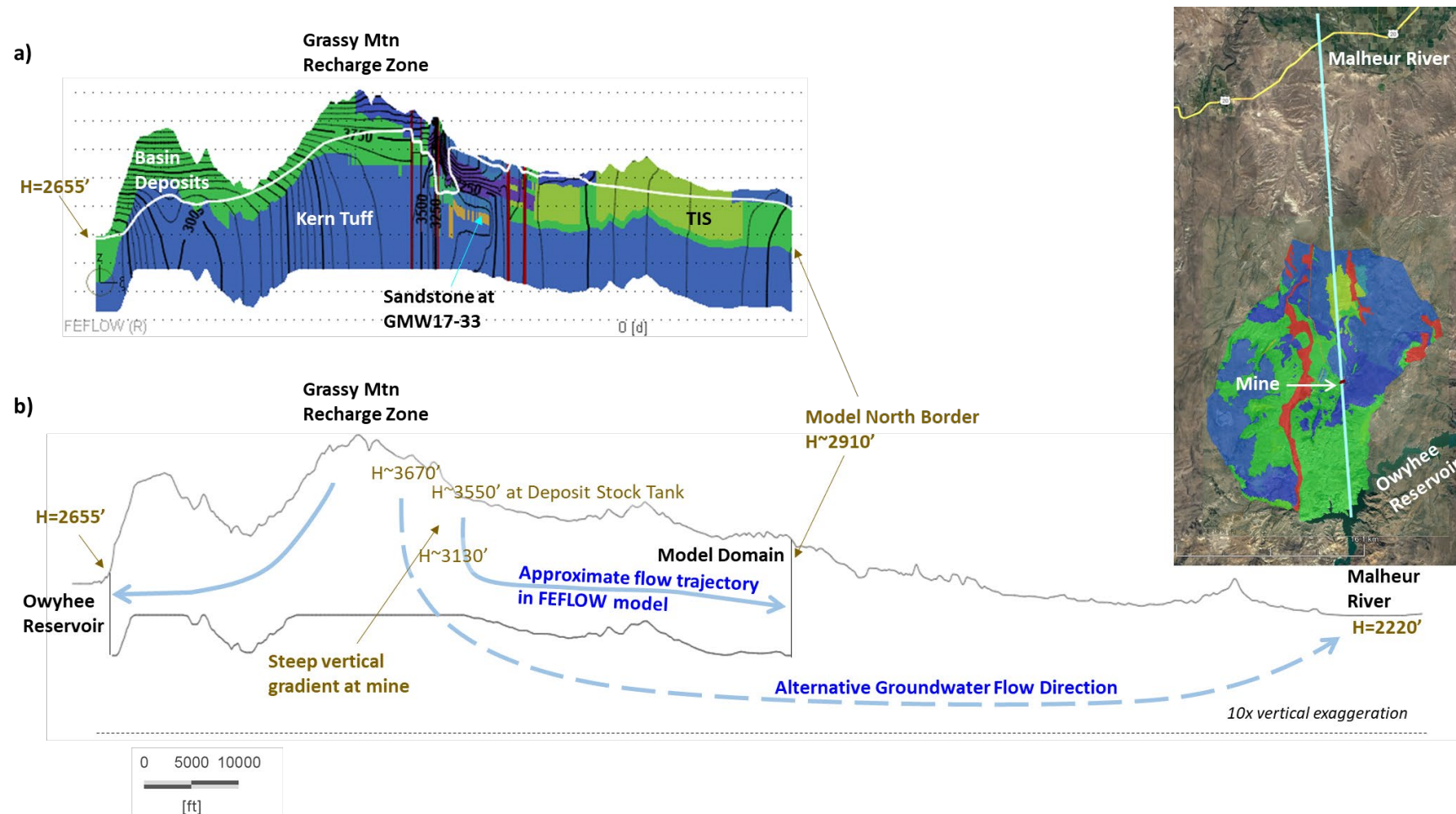


Figure 3-16: Main Features of Conceptual Model.

Because of the uncertainty in the dimensions and properties of the deep structure, the importance of the structure was evaluated in a sensitivity analysis (see Section 5.2). This analysis showed that the high-permeability zone at the bottom of the model domain does not significantly influence the predicted zone of drawdown from mine operations. Because the high permeability structure is not simulated to extend into the mine area, its presence is not expected to affect the predicted inflow to the underground mine.

To summarize, the numerical groundwater model was developed to simulate the groundwater flow processes observed at the site, with an emphasis on the steep hydraulic gradients. The approach used to model the downward gradient at the property made use of a deep high-permeability structure to lower the hydraulic heads in the mine area. This deep structure improves the head calibration, and a sensitivity analysis completed around the base case model showed that the structure did not significantly influence the inflow and impact predictions. The sensitivity analysis also evaluated the importance of other model assumptions on the calibration and predictions, including the degree of compartmentalization by both barrier faults and low-permeability aquitards, and the recharge rate (Section 5.2).

4. Numerical Model Configuration

4 Numerical Model Configuration

The numerical groundwater model builds on previous models by Adrian Brown (1992), SPF (2021c), and Lorax (2021). The current model incorporates features of previous models but differs from them primarily by both (1) including key mapped structures and (2) subjecting the model to a transient calibration phase. Like the Adrian Brown (1992) model, the current model includes consideration of barrier faults, including the Grassy Mountain Faults. Like the SPF (2021c) model, the current model has a sufficiently large domain to evaluate drawdown impacts and to include a simulation of the proposed production well(s) for mine process water. The model builds on the Lorax (2021) model, which incorporates greater detail in the underground mine than the Adrian Brown and SPF models. The current model also incorporates and is calibrated with the most up-to-date site data.

4.1 Software

The numerical model was developed using the finite element subsurface flow system (FEFLOW v. 7.4) developed by DHI. FEFLOW is well accepted and widely used in industry and academia for simulating groundwater flow and mass transfer in fractured bedrock systems. The finite element analysis of FEFLOW is ideal for solving the groundwater flow equation for systems with a complex geometry.

4.2 Model Domain

The model domain is shown in Figure 4-1. As much as practical, the model makes use of hydrological borders. In the southeast, the model abuts the Owyhee Reservoir. The east and west boundaries follow either drainage traces or ridgelines, both of which are often no-flow boundaries for groundwater. The dimensions of the model were defined to be sufficiently large that the boundaries do not have a significant influence on the predicted drawdown from mine operations. As noted below, the majority of the lateral borders are no-flow boundaries, so if the predicted impacts intersect a model border, the model will overestimate the magnitude of the drawdown at that border.

The model has 11 layers, 1.9 million nodes and 3.5 million triangular elements (Figure 4-2). The elemental diameters range from 49 ft to 3,200 ft (see Figure 4-3), with the smallest elements in the mine area, at significant drainages/creekbeds, and along geologic structures.

Structural features that appear to have a significant influence on groundwater flow paths are included as finite elements with anisotropy angles aligned with the fault trace, applying

the strike angle to the hydraulic conductivity orientation and assuming a vertical orientation for the faults. The location of finite element mesh refinement to accommodate potentially important faults can be seen in Figure 4-2.

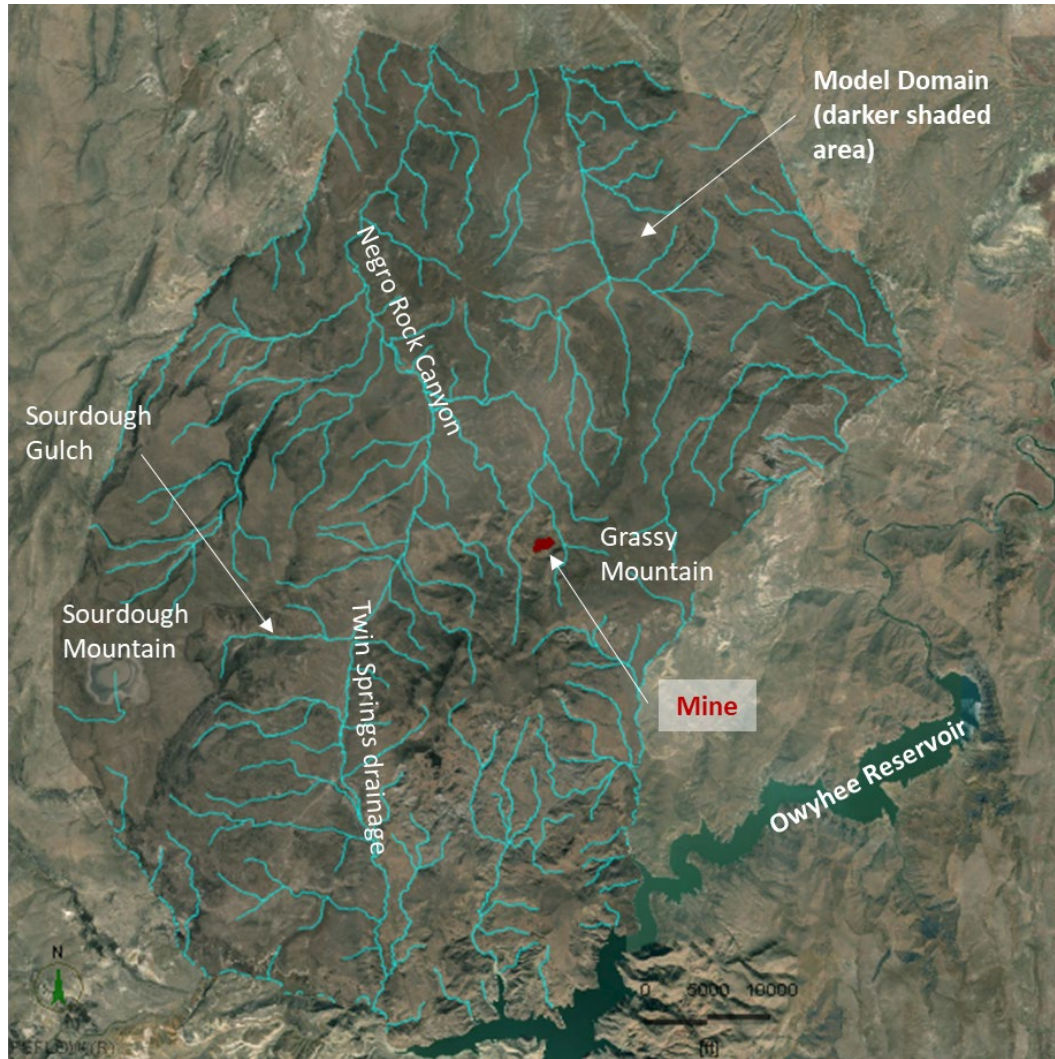


Figure 4-1: Model Domain.

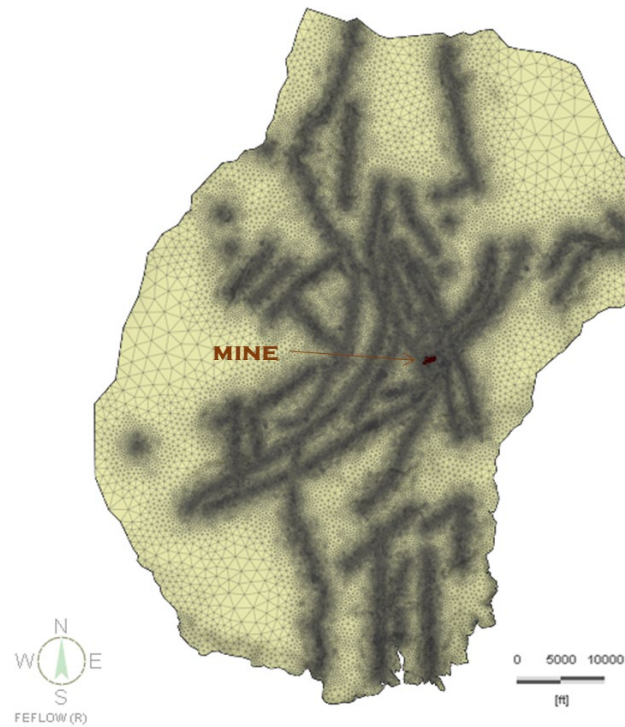


Figure 4-2: Model Mesh.

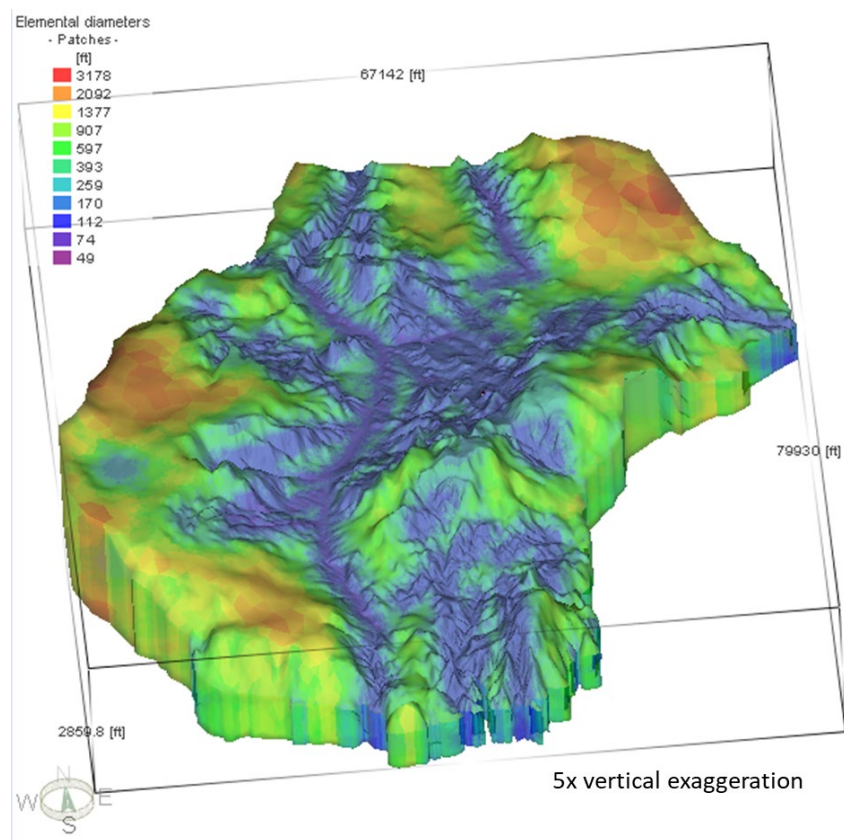


Figure 4-3: Oblique View of Model Domain, Showing Element Diameters.

4.3 Regional Boundary Conditions

The southeastern model boundary is aligned with the Owyhee Reservoir and an unnamed creek that flows directly into the reservoir along the southern edge of the model domain (Figure 4-4). The northwestern boundary is aligned with the streambed associated with Hoodoo Creek. The southwestern boundary is aligned with Sourdough Mountain. The eastern border is formed by small tributaries to the Owyhee River. The surface area of the model is 119 square miles.

The recharge distribution was imported from the SPF model and adjusted during the calibration. The final recharge distribution is shown in Figure 4-5. The total recharge over the model domain is 2,250 gpm, corresponding to an average recharge rate of 0.55 inch per year. As stated above in Section 3.2, the conceptual recharge rate is between 0.5 inch per year and 1 inch per year. The area of low recharge at the mine area, shown in Figure 4-5 roughly delineates the area of clay identified in the tailings area and present in several geological sections (*e.g.*, Figure 4-29 of Section 4.2). The low hydraulic conductivity of this surficial clay unit required to simulate observed vertical head gradients requires a lower recharge rate.

Additional boundary conditions include:

- The Owyhee reservoir, treated as a constant head boundary with a specified head of 2655 ft amsl;
- The springs listed above in Section 3.3 are defined as drains on the top of Layer 1 (see Figure 4-6);
- Two artesian wells, Darky Rock Well and Prod-1, are assigned to model layers based on their screen intervals;
- A third artesian well, Flowing Well, has no depth information and is assigned to the ground surface; and
- Stream channels are defined as drains on the top of Layer 1 (see Figure 4-4).

As shown in Figure 4-6, some of the springs are identified with more than one model node in order to capture the groundwater discharge associated with a given area of simulated groundwater discharge. The simulated heads were computed at the spring location, but the computed groundwater discharge at 11 springs and artesian wells included extra nodes as listed. In the case of Prod-1, there are two points to simulate the three screen intervals, one that is located above a clay aquitard (denoted Prod-1-Top in the calibration results), and the other two (combined as Prod-1-Bot) that are located below it (see Figure 4-29).

The northern model boundary is treated as a third-type or transfer, Cauchy (or Robin) boundary condition, in which the hydraulic head at the border is a function of a transfer rate coefficient and a reference head. The reference head was taken to be 160 ft below ground surface. Because of the uncertainty of this boundary, the sensitivity analysis includes an examination of this parameter (see Sections 4.12 and 5.2).

All other lateral boundaries, including portions of the model below the drains at the lateral boundaries, are no-flow boundaries. In other words, deep groundwater can discharge to the Owyhee Reservoir and to the northern transfer boundary, which simulates regional groundwater flow to the Malheur River. However, on all other, generally north-to-south, borders groundwater discharge occurs to surface water but does not otherwise flow out of the model domain. Therefore, groundwater is simulated to flow generally northward to the Malheur River or southward to the Owyhee Reservoir from the main recharge areas at Grassy Mountain and Sourdough Mountain.

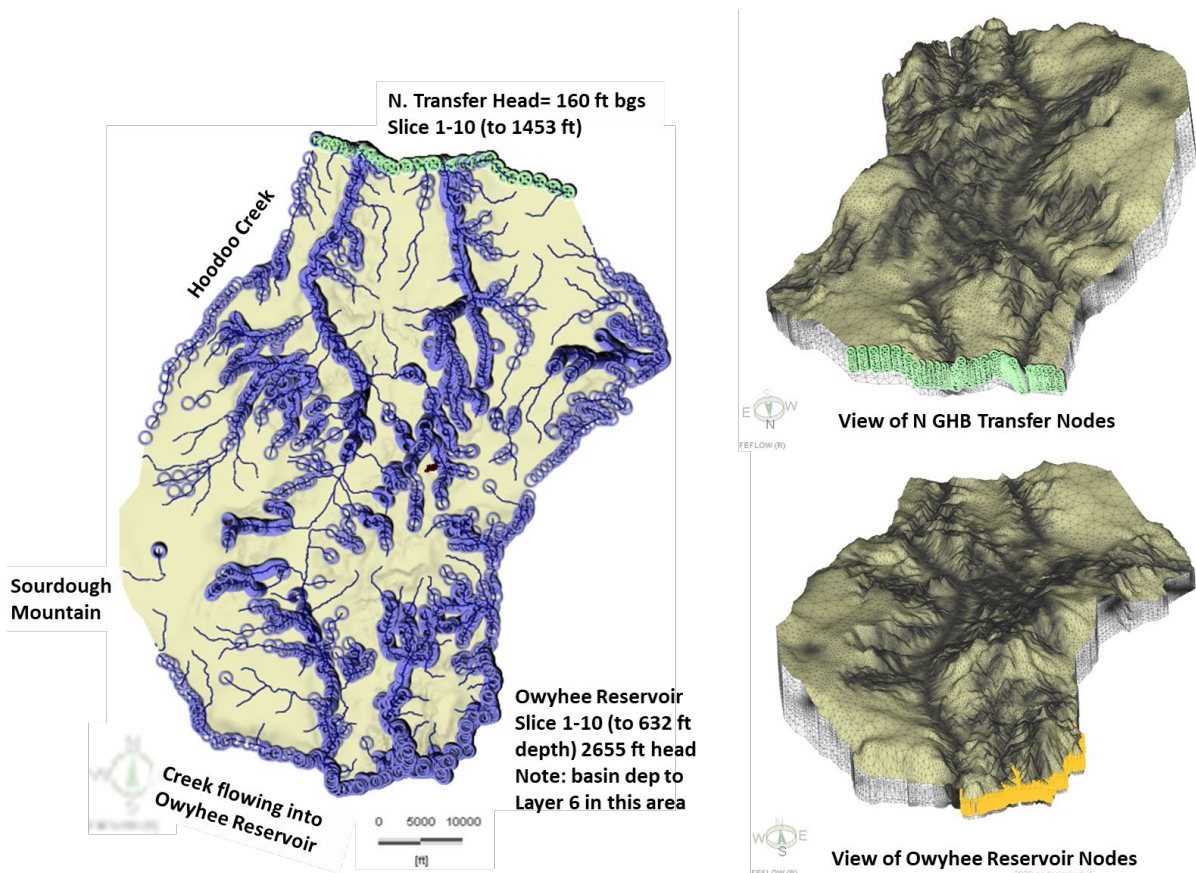


Figure 4-4: Boundary Conditions – General.

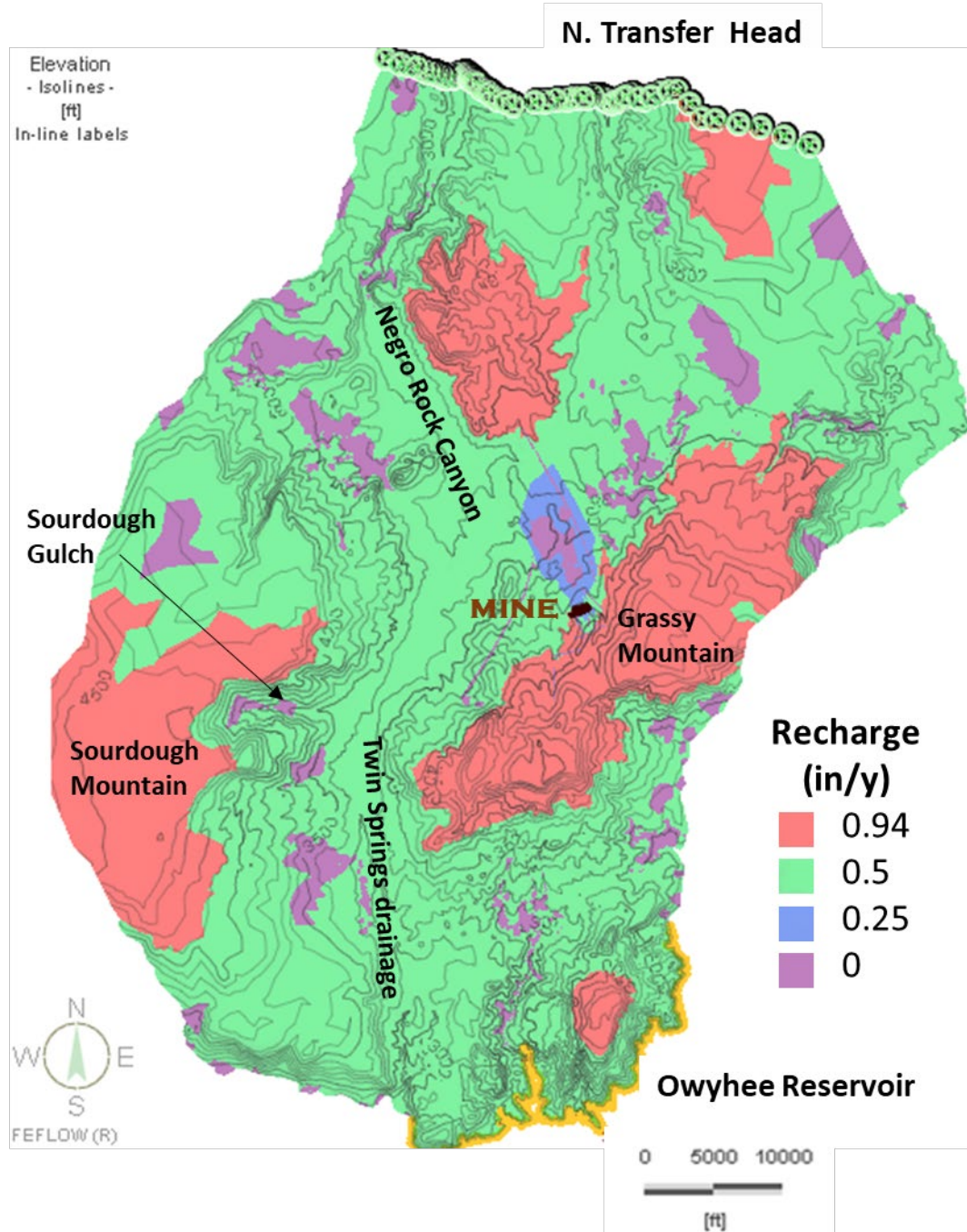


Figure 4-5: Boundary Conditions – Recharge.

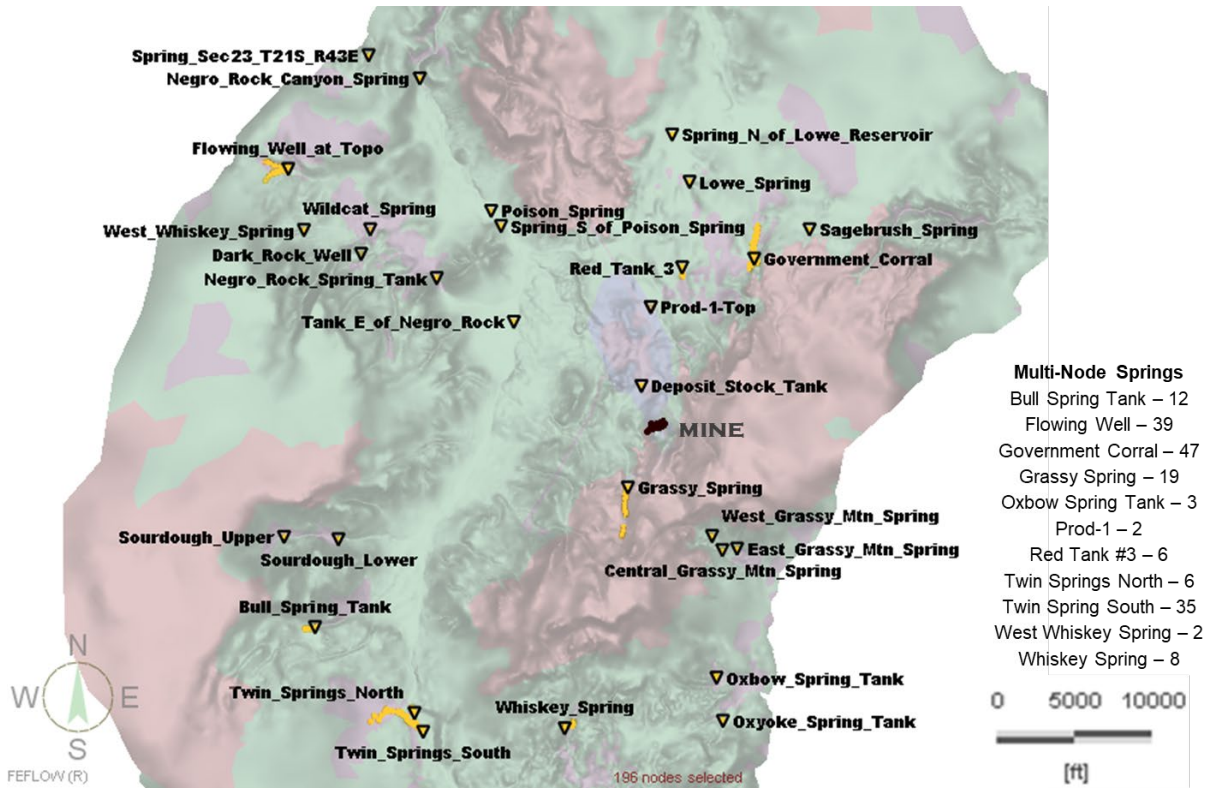


Figure 4-6: Boundary Conditions – Springs.

Figure 4-7 Summarizes the groundwater recharge to the main drainages within the model domain. The total recharge is 2,250 gpm. The largest catchment, identified in Figure 4-7 as #1, is the catchment containing Negro Rock Canyon and Poison Spring. This catchment receives 715 gpm of recharge in the groundwater model. The subcatchment #1a, containing the mine, Deposit Stock Tank and Grassy Spring, receives 131 gpm in recharge. The catchment to the east, #2, which contains Government Corral, Sagebrush Spring, and Lowe Spring, receives 345 gpm. All other catchments are separated from the mine by surface water divides that are likely to act as groundwater divides.

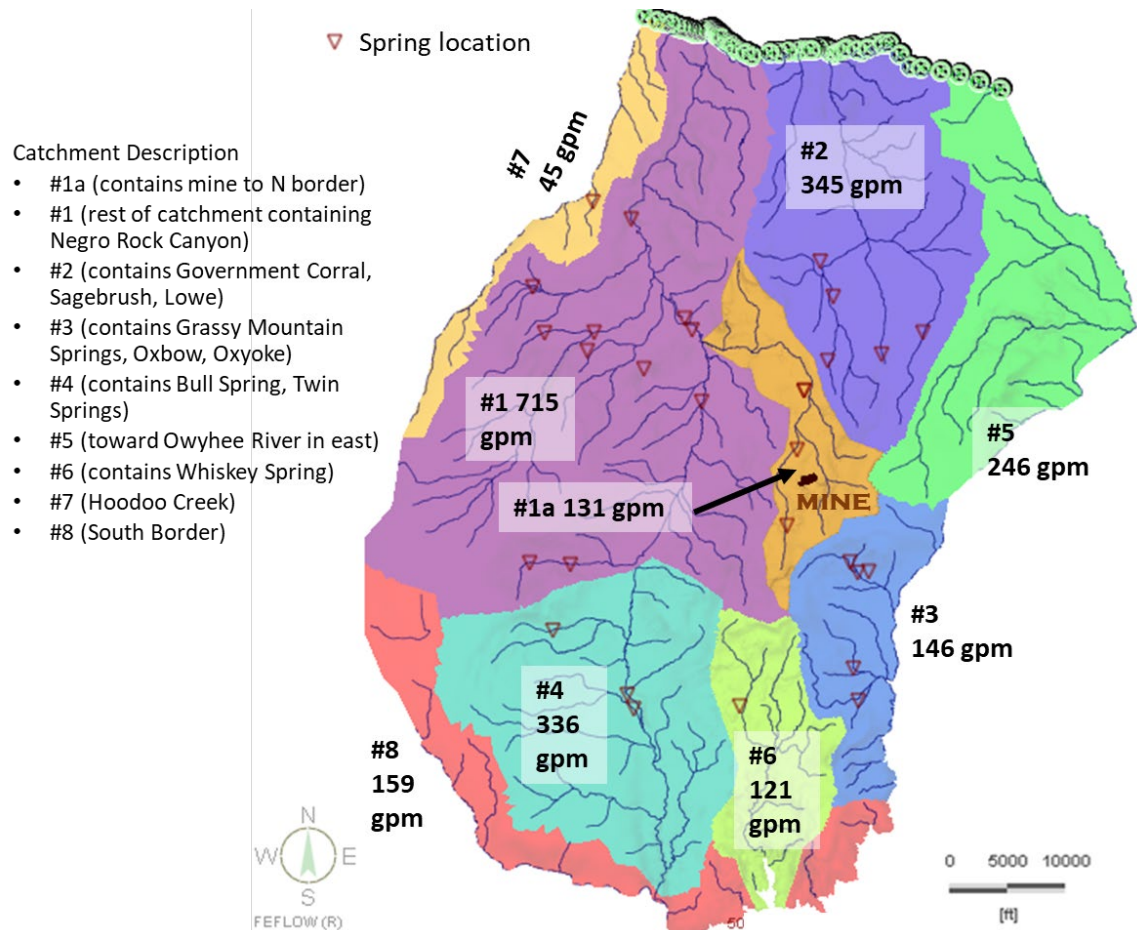


Figure 4-7: Boundary Conditions – Catchments for Recharge.

4.4 Pumping Test Calibration Boundary Conditions

The pumping tests described in 3.5.2 were simulated in two model runs. The first model simulated the pumping tests in PW-4 and PW-1. These two wells were simulated as multi-layer wells. The second model run simulated the two other pumping tests: Prod-1 and GMW17-33. In this second model run, Prod-1 and GMW17-33 were treated as multi-layer wells.

The pumping was staggered in the models, as shown in Figure 4-8 and Figure 4-9. Well configuration information is summarized in Table 4-1. Well locations are shown in Figure 4-17

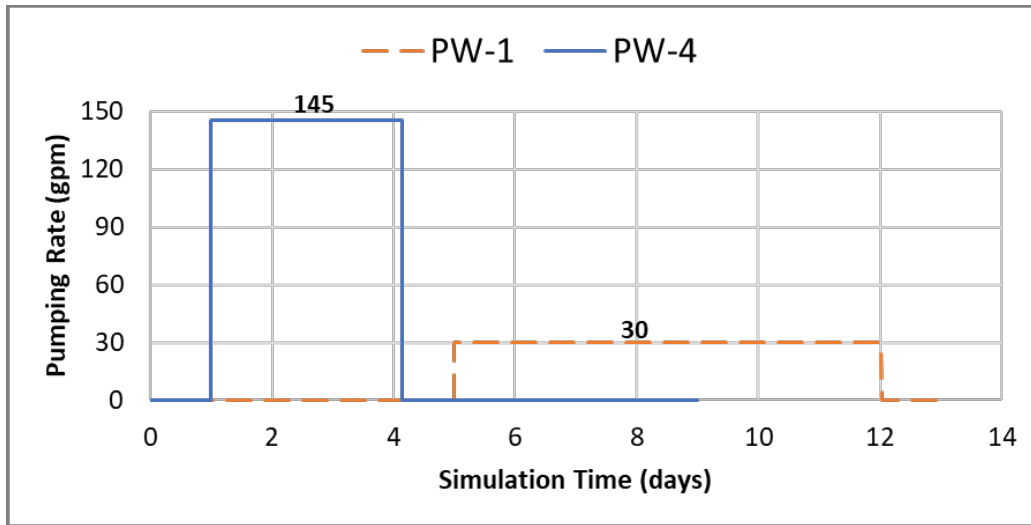


Figure 4-8: PW-1 and PW-4 Pumping Rates in Transient Calibration Run 1.

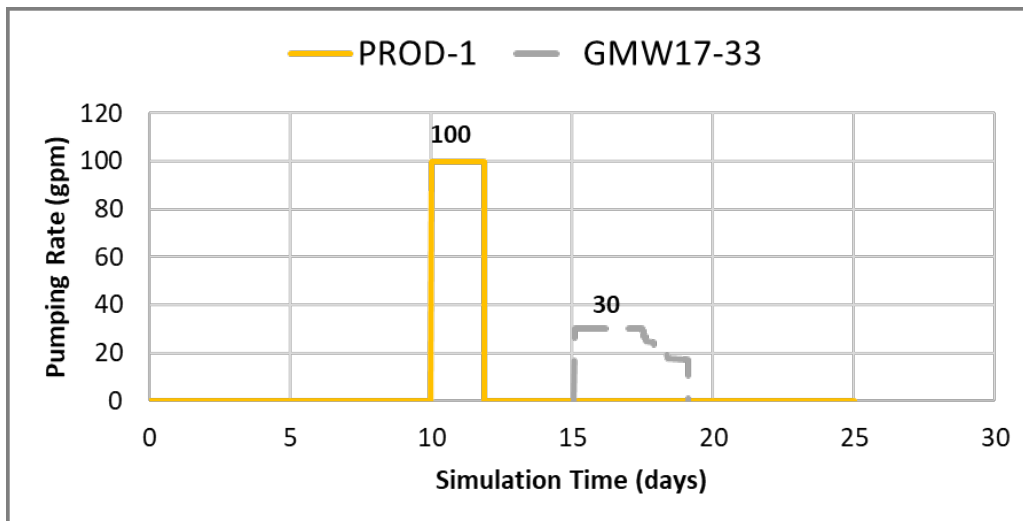


Figure 4-9: Prod-1 and GMW17-33 Pumping Rates in Transient Calibration Run 2.

Table 4-1:
Pumping Well Configuration

Well	Well B. C. Description	Pumping Rate
PW-4	Multilayer Well in Layer 4-5 (3073 ft to 2961 ft) Radius 5 in	145 gpm for 3.1 days
PW-1	Multilayer Well in Layer 5-6 (3382 ft to 3271 ft) Radius 5 in	30 gpm for 7 days
Prod-1	Multilayer Well in Layer 2-6 (3438 to 3271 ft) Radius 3 in.	100 gpm for 1.9 days
GMW17-33	Multilayer Well in Layer 3-4 (3502 ft to 3391 ft) Radius 6 in.	30 gpm for 2.4 days, followed by 1.6 days with decreasing rates to 17.2 gpm

4.5 Mine Boundary Conditions

The regional boundary conditions were first applied to a steady state model to establish pre-mining conditions. The underground mine was then simulated in a transient groundwater model. A simplified mine progression was simulated in the transient model using five stages as listed in Table 4-2.

During Year -1, the model simulates the dewatering of the tunnels and ramps that will be advanced during the first year of operations. At the same time, the production well will begin pumping at a constant rate of 72 gpm. The simulated production well location is shown in Figure 4-10. The well is approximately 1,200 ft northeast of PW-4. The new well is located on the mine property but farther from the Grassy Mountain Fault trace than PW-4, because the Grassy Mountain fault is assumed to be the barrier fault that influenced the 1989 PW-4 pumping test. The new production well was simulated as a single model node assigned a maximum pumping rate of 72 gpm and a minimum head of 519 ft below ground surface. In configuring the well in this manner, the model was able to identify if the well becomes unable to deliver 72 gpm.

The underground mine boundary conditions are shown in Figure 4-11 for Mine Year -1. This figure shows the locations of the nodes where model drains were applied. In some cases, the drain head is higher than the elevation of the node to which the drain is applied.

Figure 4-12 shows the additional drains simulated between Years 1 and 3. During this period, the tunnels advanced during Years -1 to 3 are treated as drains, and the volume around the stopes to be mined during Years 1 to 3 are also dewatered using drains.

Table 4-2:
Mine Prediction Transient Model Stages

Stage	Description
Year -1	Begin advancement and dewatering of ramps and tunnels Begin production well pumping at 72 gpm
Years 1 to 3	Dewater tunnels and ramps advanced during Years 1 to 3 and stopes to be developed during this time Continue production well pumping at 72 gpm
Years 4 to 6	Dewater tunnels and ramps advanced during Years 4 to 6 and stopes to be developed during this time Continue production well pumping at 72 gpm Simulate cemented rockfill of stopes mined during Years 1 to 3 by increasing hydraulic conductivity by a factor of 10
Years 7 to 9	Dewater tunnels and ramps advanced during Years 5 to 7 and stopes to be developed during this time Continue production well pumping at 72 gpm Simulate cemented rockfill of stopes mined during Years 4 to 6 by increasing hydraulic conductivity by a factor of 10
Post-Closure	Cease mine dewatering and production well pumping Simulate cemented rockfill of stopes mined during Years 7 to 9 by increasing hydraulic conductivity by a factor of 10

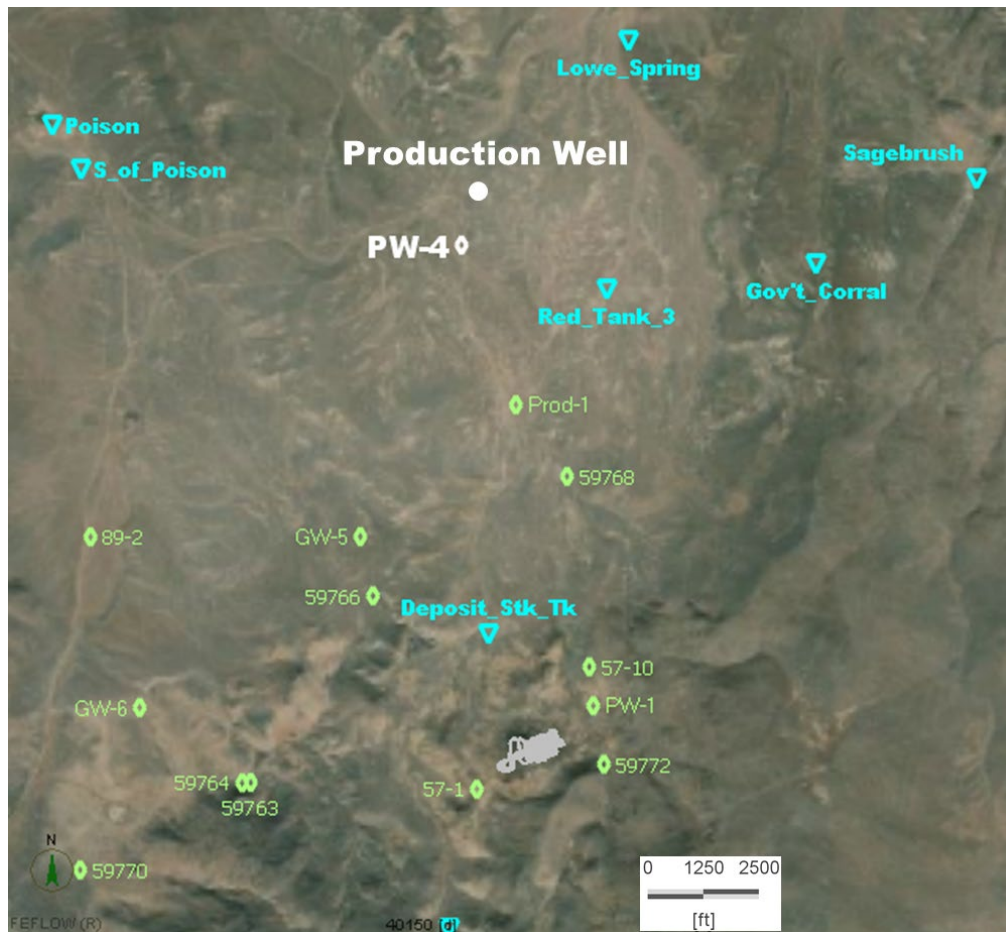


Figure 4-10: Location of Production Well.

Figure 4-13 shows the boundary conditions for the mine in Years 4 to 6. During this period, the tunnels and ramps advanced during Years -1 to 6 are treated as drains, plus the stopes to be mined in Years 4 to 6. Stopes that were mined during Years 1 to 3 are simulated to have been backfilled. The model simulates the backfill by increasing the hydraulic conductivity by a factor of 10 from the pre-mining hydraulic conductivity.

Figure 4-14 shows that the simulation for Years 7 to 9 takes the same approach as for Years 4 to 6, but the volume of backfill is greater.

Figure 4-15 shows the boundary conditions after mine closure. During this period, no dewatering or pumping is simulated. All elements containing mined out stopes are treated as higher hydraulic conductivity zones.

The simulation does not include discrete pumping points to dewater the mine. Note that the model exaggerates the influence of the backfill on the groundwater system as the entire volume of any model element containing stopes was assigned a higher hydraulic conductivity. Collectively, the mine elements, especially the ones at the bottom of the mine, are significantly larger than the mine volume (see, for example Figure 4-15d).

Mine Boundary Conditions, Year -1

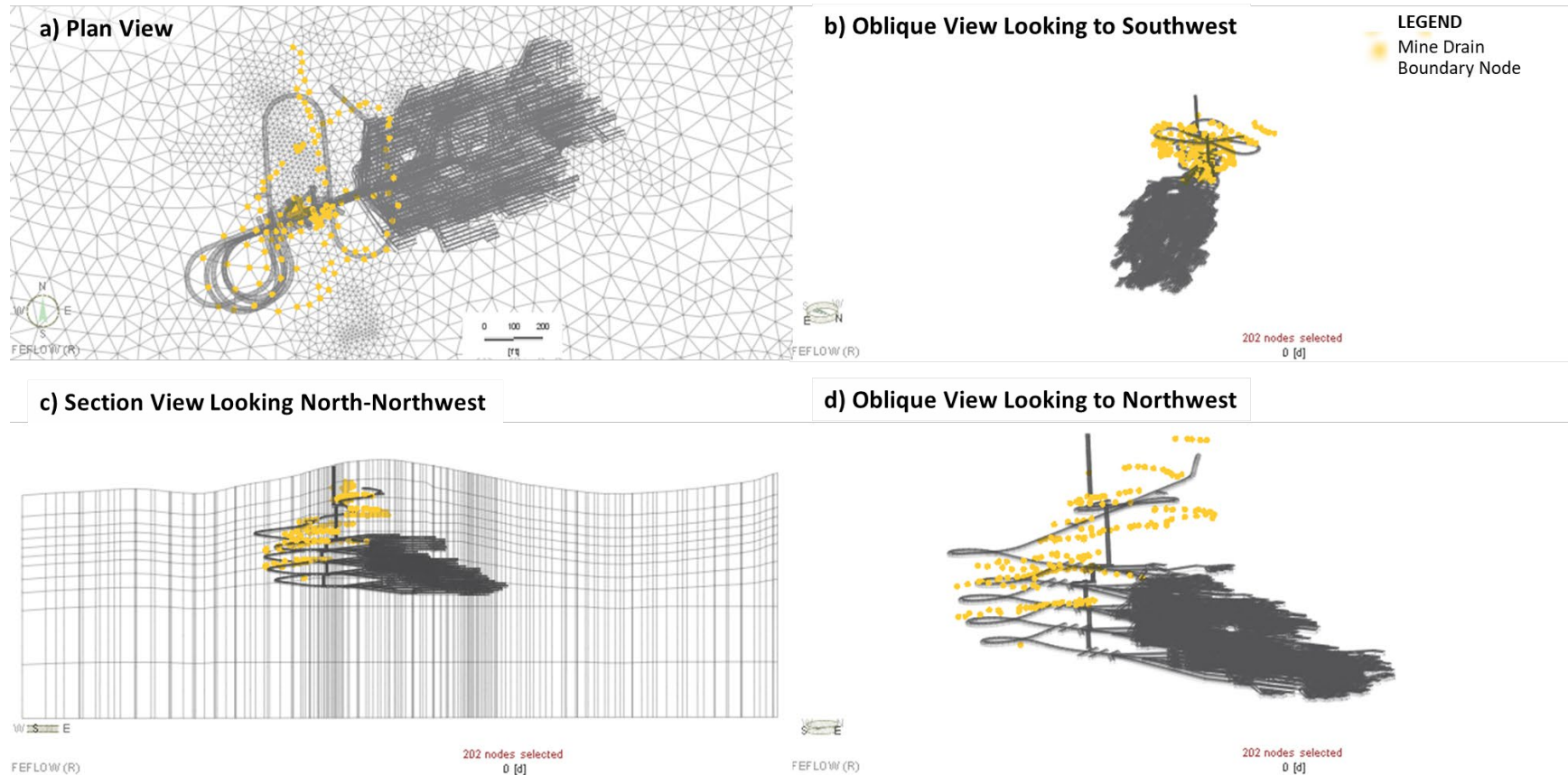


Figure 4-11: Mine Boundary Conditions, Mine Year -1.

Mine Boundary Conditions, Years 1 to 3

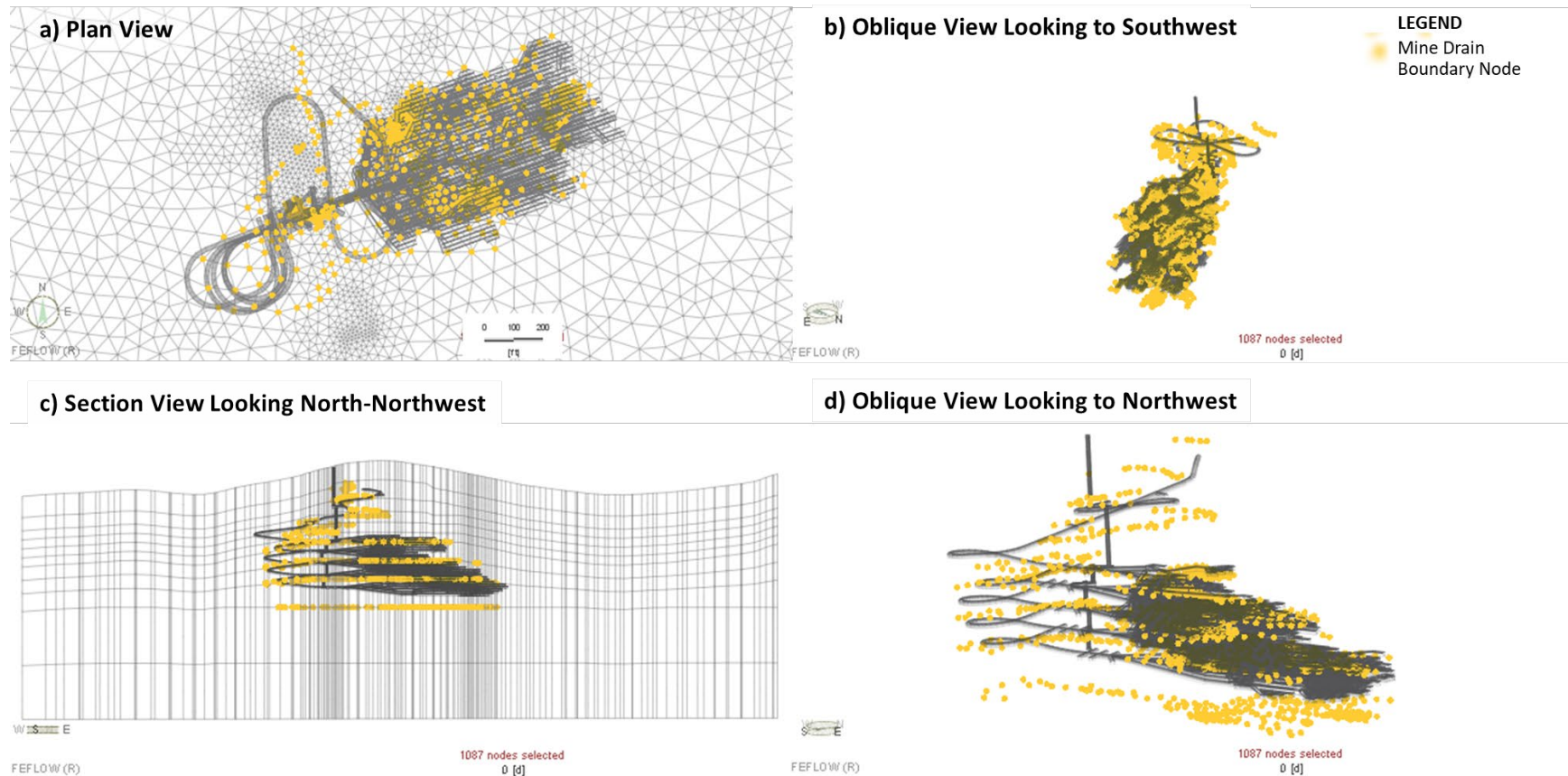


Figure 4-12: Mine Boundary Conditions, Mine Year 1 to 3.

Mine Boundary Conditions, Year 4-6

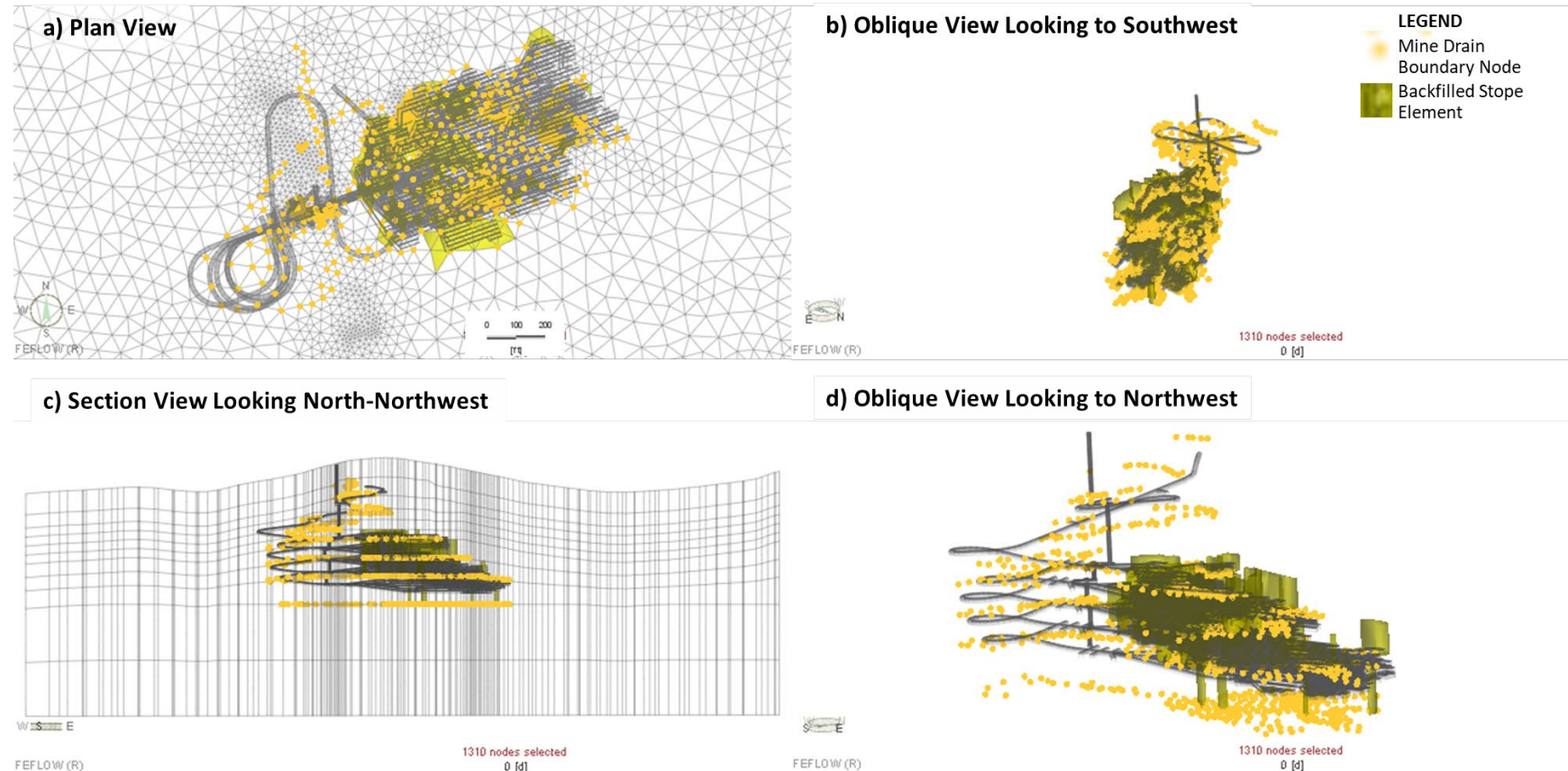


Figure 4-13: Mine Boundary Conditions and Hydraulic Conductivity Changes, Mine Year 4 to 6.

Mine Boundary Conditions, Years 7 to 9

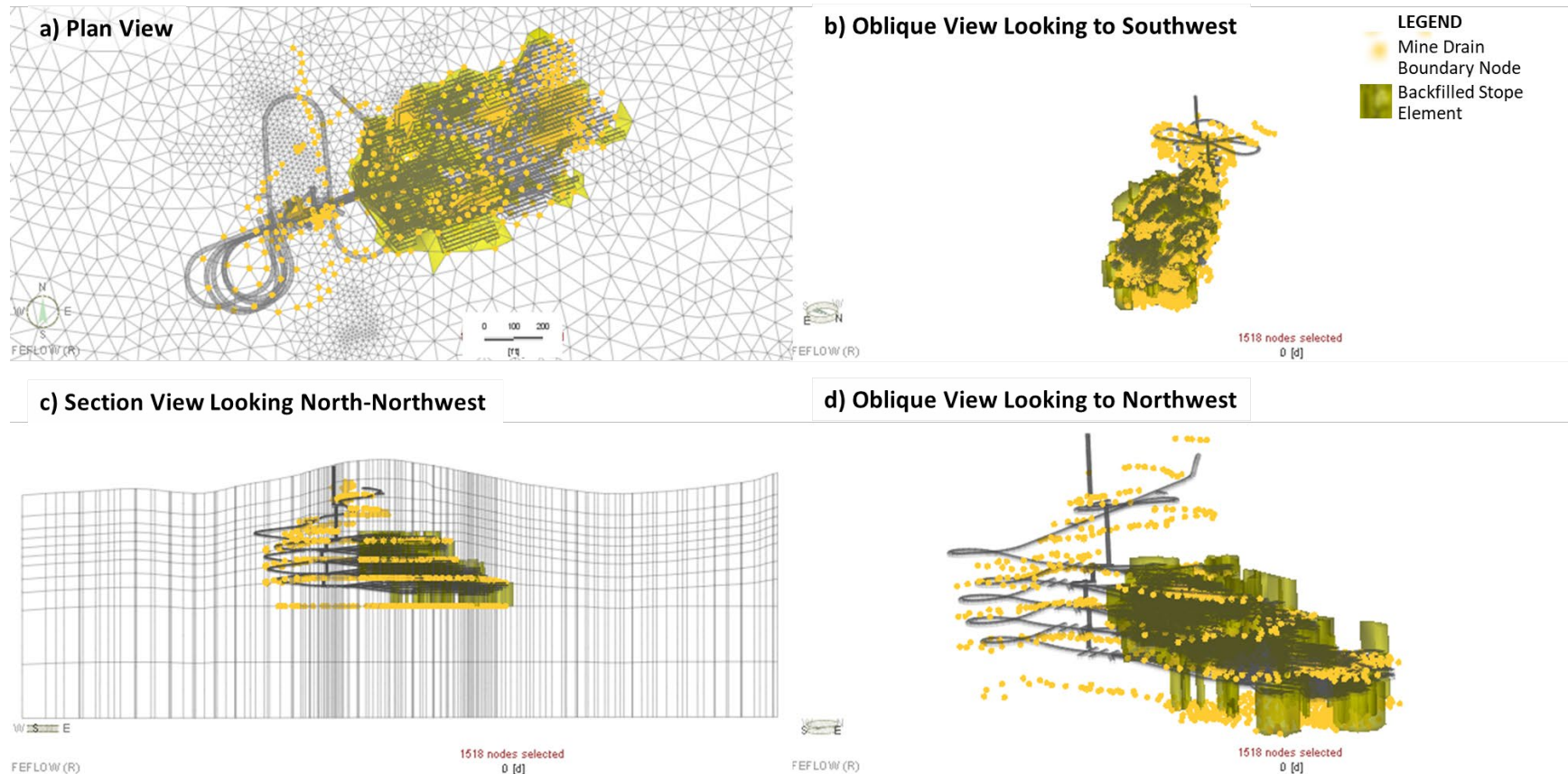


Figure 4-14: Mine Boundary Conditions and Hydraulic Conductivity Changes, Mine Year 7 to 9.

Mine Boundary Conditions, Post-Closure

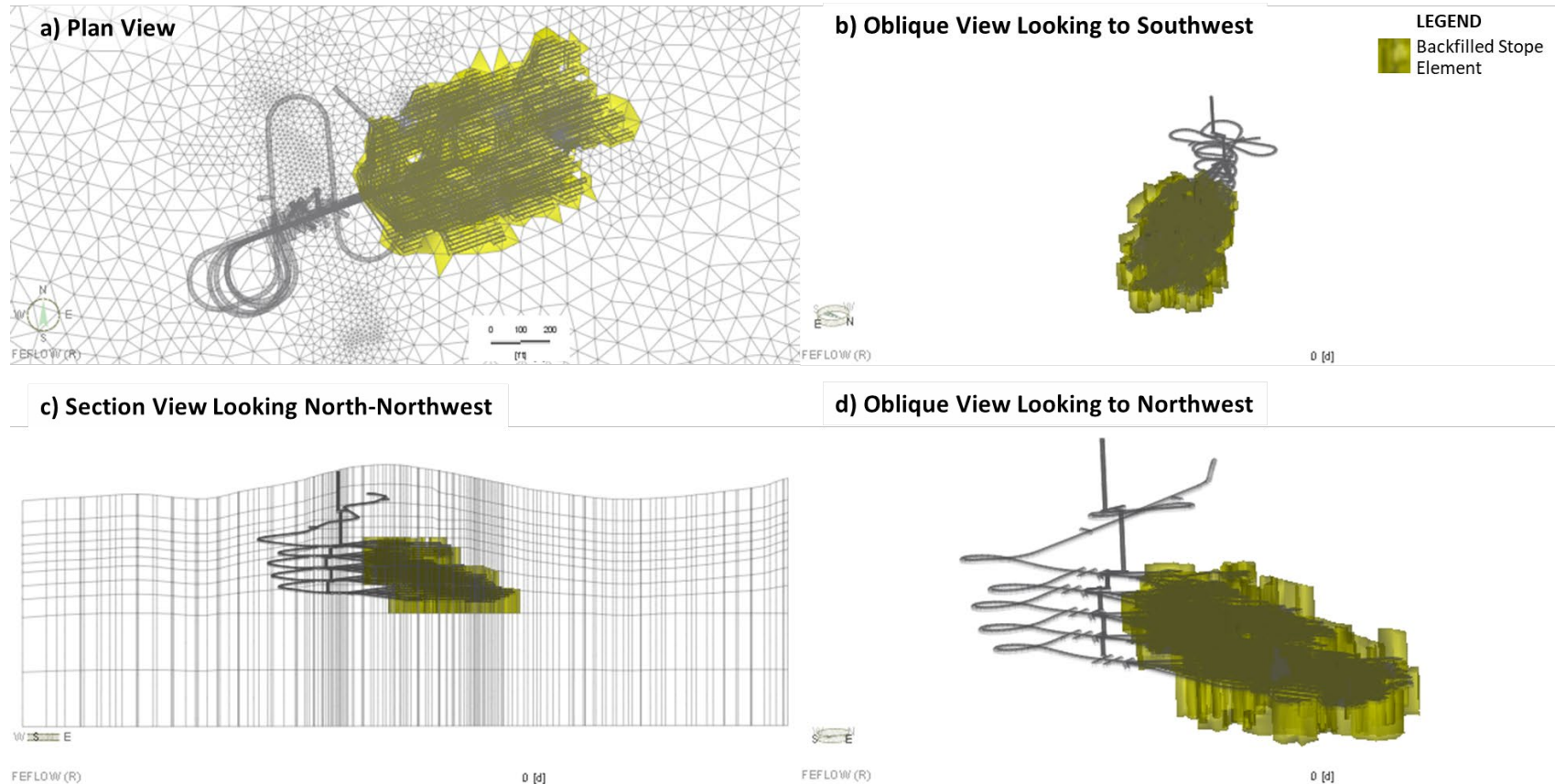


Figure 4-15: Mine Hydraulic Conductivity Changes, Post-Closure Period.

4.6 Model Stratigraphy

The model stratigraphy was derived from a combination of the baseline study (SPF, 2021c), boring logs, and the Calico's geological database. Figure 4-16 provides an overview of the model stratigraphy. As indicated in the discussion below, detail was judiciously developed in areas that lack detailed data based on the modeler's interpretation of site data. In particular, site data indicate that conditions are very heterogeneous. In developing the details of stratigraphy, there are some assumptions that the types of conditions that were observed in some areas with good characterization also exist in areas where no characterization data may exist.

In general, the hydrogeological units comprise a lower zone of Kern tuff (Figure 4-16a) overlain by basin deposits, including the Grassy Mountain Formation (Figure 4-16b). Interspersed into the Kern tuff and basin deposits are two zones of rhyodacite (Figure 4-16a). Above the basin deposits in many areas of the model domain are basalts denoted as Tbcu (upper and middle Miocene calc-alkaline lava flows). In other areas of the model domain, the basalt unit Tbou (upper Miocene olivine basalt flow) and Tbcm (middle Miocene calc-alkaline lava flows) are present (Ferns and Brooks, 1993). In the model, the two calc-alkaline lava flows, Tbcu and Tbcm, were assigned the same hydraulic properties and are shown as the dark blue zones in Figure 4-16c. The younger Tbou was assigned to a separate hydrostratigraphic unit and is shown in yellow.

The shallowest materials, the Quaternary alluvium, were divided into two zones based on assumed thickness. Layer 1 of the model has a thickness of 100 ft in the alluvial zones. The center of the alluvial zones was assigned higher hydraulic conductivity (shown in red in Figure 4-16d). In areas where the alluvium is likely thinner than 100 ft, a lower hydraulic conductivity was applied (shown as green zones in Figure 4-16d). The final regional stratigraphic unit comprises lacustrine sediments of lower Pliocene or upper Miocene age. These zones are present in the northeastern portion of the model, east of Sagebrush Spring and are shown in Figure 4-16d as light blue zones.

The portion of the basin sediments interpreted as Unit TIS—interbedded conglomerate and sandstone (SPF, 2021c)—is included in the FEFLOW model. This zone is shown in Figure 4-17. For the most part, the TIS zone is defined from Layer 1 to Layer 7 of the model, to a maximum depth of 519 ft. The TIS zone replaced elements assigned to the basin sediments/Grassy Mountain formation in earlier models. In areas where the Layer 1 zone is basalt, the TIS zone begins in Layer 2.

As shown in Figure 4-17, some areas of the mapped TIS zone were not included in the FEFLOW model. These are areas south of Prod-1, where the inclusion of a high-permeability zone resulted in a depressed water table so that artesian conditions could not

be simulated. In these areas, the lower permeability undifferentiated Grassy Mountain formation was retained in the model.

In two areas, the FEFLOW model enlarged the TIS zone. One area is in the vicinity of Prod-1, where the TIS zone was expanded westward between the two Grassy Mountain faults. In this way, Prod-1 pumping test was simulated to have occurred in the TIS zone, which is consistent with the observed drawdowns. The second area where the TIS zone was expanded is the area northwest of PW-4, where alluvium exists at ground surface according to Ferns and Brooks (1993). This area was introduced to improve the steady state calibration of PW-4, because enlarging the TIS zone here lowered the initial water table at PW-4.

Layer-by-layer hydraulic conductivities are shown in Figure 4-18 to Figure 4-21. Also noted on these figures are average layer depths. The layers were constructed to be a specified depth from the topographic elevation, except for:

- Elements below Grassy Mountain and Sourdough Mountain, where the shallow layers are thicker in order to flatten the base of the model domain. As a consequence, in all of the layers the thickness is greatest beneath the mountains.
- Under the main alluvial channel in Layer 1, where the Layer 1 thickness is 100 ft rather than 131 ft elsewhere in Layer 1.

This information is summarized in Table 4-3



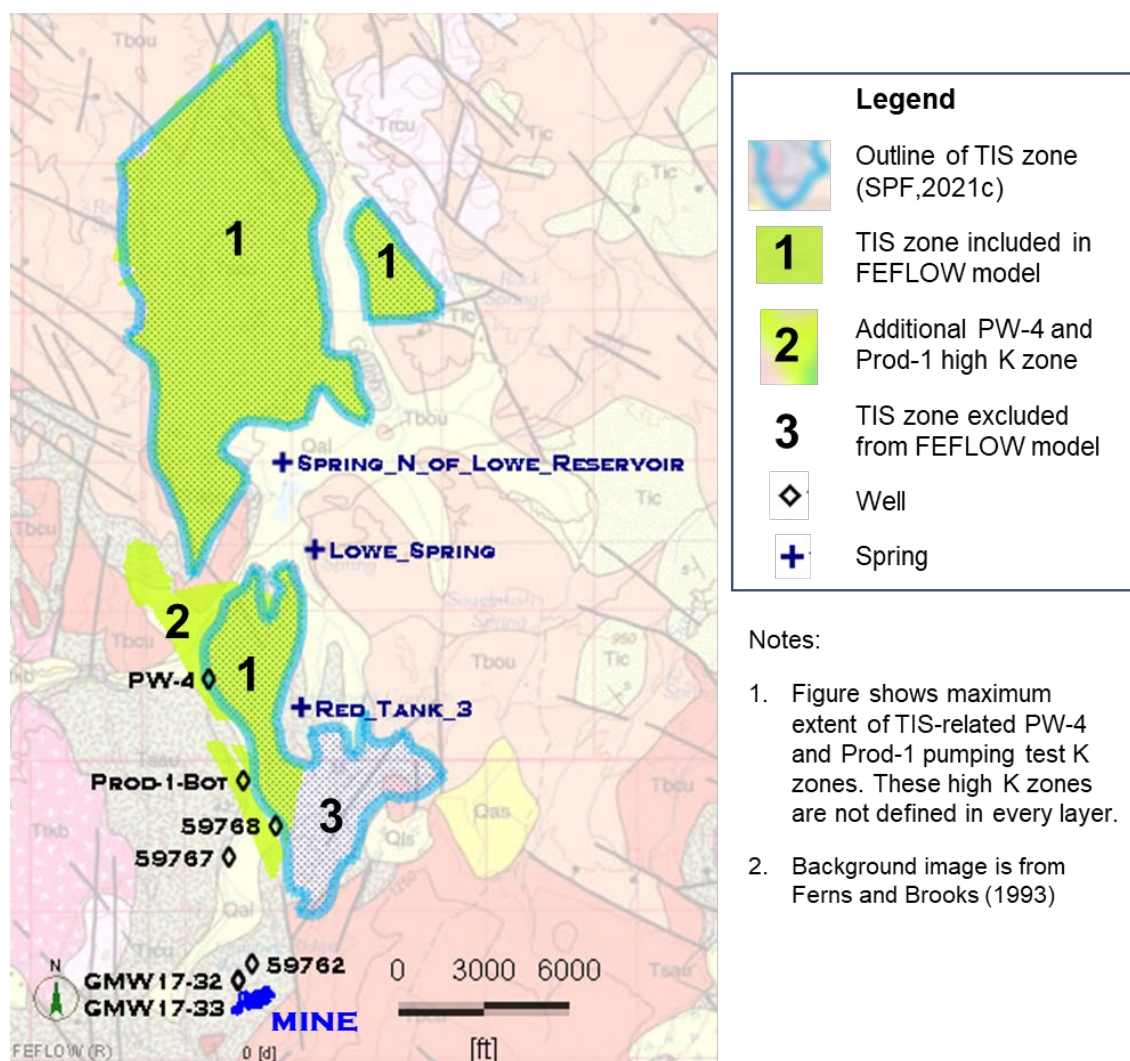


Figure 4-17: TIS (Conglomerate and Sandstone) Zone.

Table 4-3:
Model Layering

Layer	Thickness (ft)		
	At Mine	Under Alluvium	Maximum
1	131	99	328
2	82	114	437
3	56	56	246
4	56	56	151
5 and 6	56 – 63	56	103
7 and 8	98 – 115	83	123
9	56 – 174	110	191
10 and 11	345	262	346

**Table 4-4:
Stratigraphic Units**

Zone Number	Name	Description
11	Thick Alluvium	High-permeability main alluvial deposits, where the thickness of alluvium is typically 100 ft or more
12	Lacustrine	Low-permeability Tlc lacustrine sediments from Ferns and Brooks (1993) and a small zone of shallow Kern tuff near Tlc zone
13	Thinner Alluvium	Moderate-permeability alluvium at the edges of valleys
31	Basin Deposits	Moderate permeability Tsau from Ferns and Brooks (1993), Grassy Mountain Formation. This permeability was also assigned to Kern tuff located in layer 1 except where assigned lacustrine parameters were assigned (see above). The incidence of this unit in lower layers was estimated from geological sections in SPF (2021a).
41	Kern Tuff	Low-permeability Kern tuff present at the base of the model. The incidence of this unit in lower layers was estimated from geological sections in SPF (2021a) and Adrian Brown (1992).
51	Basalt	Low-permeability Tbcu and Tbcm basalt from Ferns and Brooks (1993). The incidence of this unit in lower layers was estimated from geological sections in SPF (2021a) and geological database from Calico Mining.
52	Tbou	Moderate-low permeability olivine basalt flow from Ferns and Brooks (1993).
61	Rhyo-dacite	Moderate-low permeability unit from Ferns and Brooks (1993).
71	North Structure	High-permeability zone connecting transmissive faults in the north of the model domain to the northern mine area.
72	PW-4 Zone	High-permeability TIS zone based on zone from SPF (2021c) associated with PW-4 production well.
73	Prod-1 Zone	High-permeability TIS zone based on zone from SPF (2021c) around the Prod-1 artesian well. Assigned same properties as Zone 72.
74	PW-1 Zone	Moderate permeability zone around PW-1. Similar in properties to Zone 31 but calibrated separately to pumping test data.
81	Siltstone	Moderate-low-permeability zone in mine area, generally denoted as siltstone in SPF (2021c)
82	GMW17-33 zone	High-permeability zone around GMW17-33, where pumping test was able to extract 30 gpm for a few days before encountering a barrier. Additional Zone 82 added to help depress the water table in the mine area.
83	GMW17-32 zone	Moderate permeability zone around GMW17-32, where some extraction was possible during a pumping test.
91	Clay	Low-permeability zone that includes areas identified as clay in boring logs. Additional Zone 91 added to simulate a strong vertical hydraulic gradient near the mine area.
92	Clay in Layer 1	Moderate-low permeability zone in Layer 1 of the model. This zone has a higher hydraulic conductivity than Zone 92 to accommodate a small amount of recharge, which aids in the development of strong vertical gradients.

Note: High permeability denotes $K_h > 1 \times 10^{-6}$ m/s and $K_v > 8 \times 10^{-8}$ m/s
Moderate permeability denotes $3 \times 10^{-8} < K_h < 8 \times 10^{-7}$ m/s and $2 \times 10^{-9} < K_v < 8 \times 10^{-7}$ m/s
Moderate-Low permeability denotes $5 \times 10^{-9} < K_h < 2 \times 10^{-8}$ m/s and $2 \times 10^{-10} < K_v < 5 \times 10^{-9}$ m/s
Low permeability denotes $K_v < 2 \times 10^{-9}$ m/s

Also shown in Figure 4-18 to Figure 4-21 are detailed stratigraphy in the mine area, including the production well zone north of the mine and the downgradient area. In this area, the stratigraphy was defined using the geological information presented in SPF (2021c) and borehole information. The local mine-area stratigraphic units are Zones 72 to 92 in Table 4-4. In addition, an enhanced structure zone, Zone 71, was introduced downgradient of the mine to simulate the downward hydraulic gradient evident in the mine area (see Table 4-4).

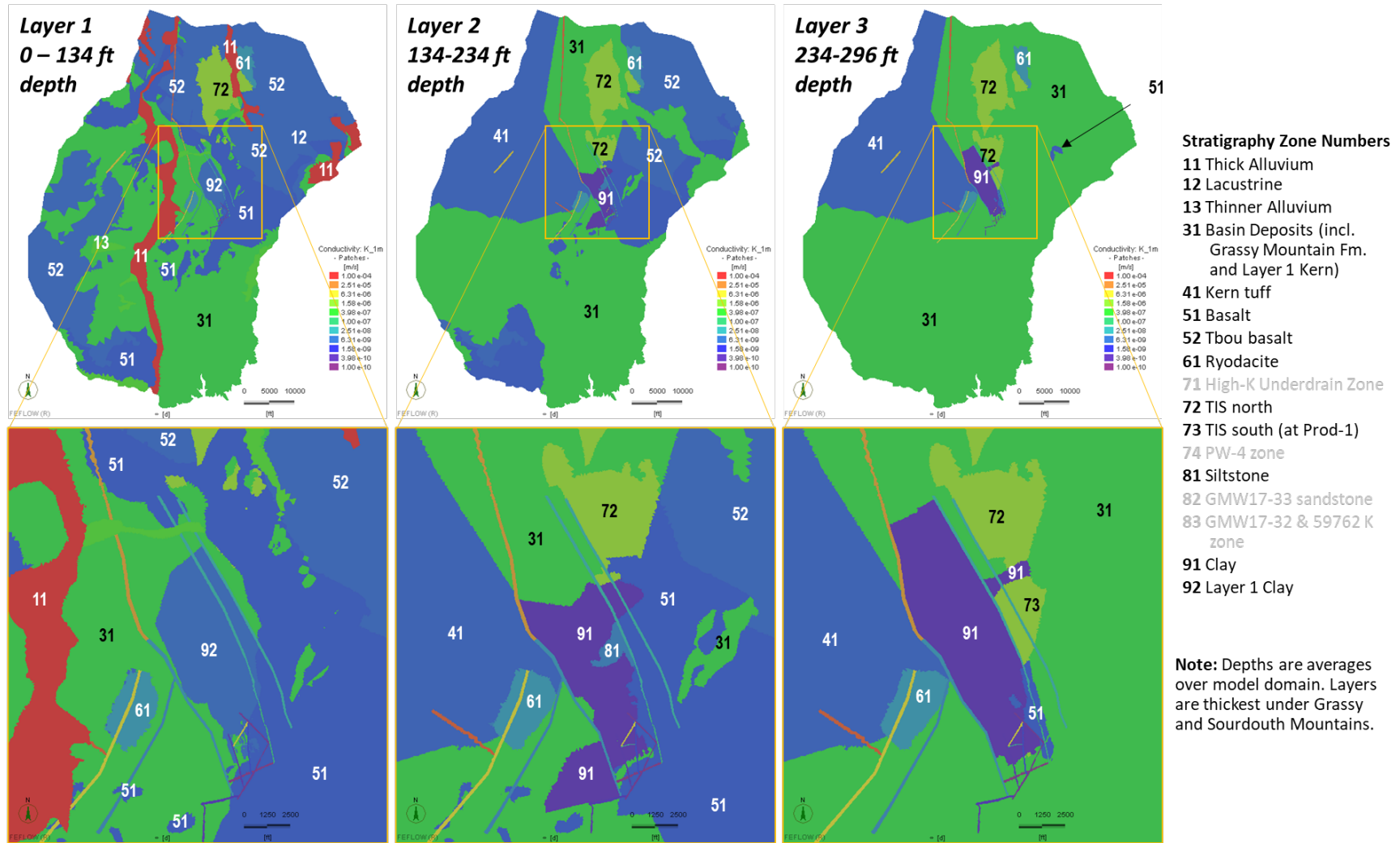


Figure 4-18: Hydraulic Conductivity Zones, Layers 1 to 3.

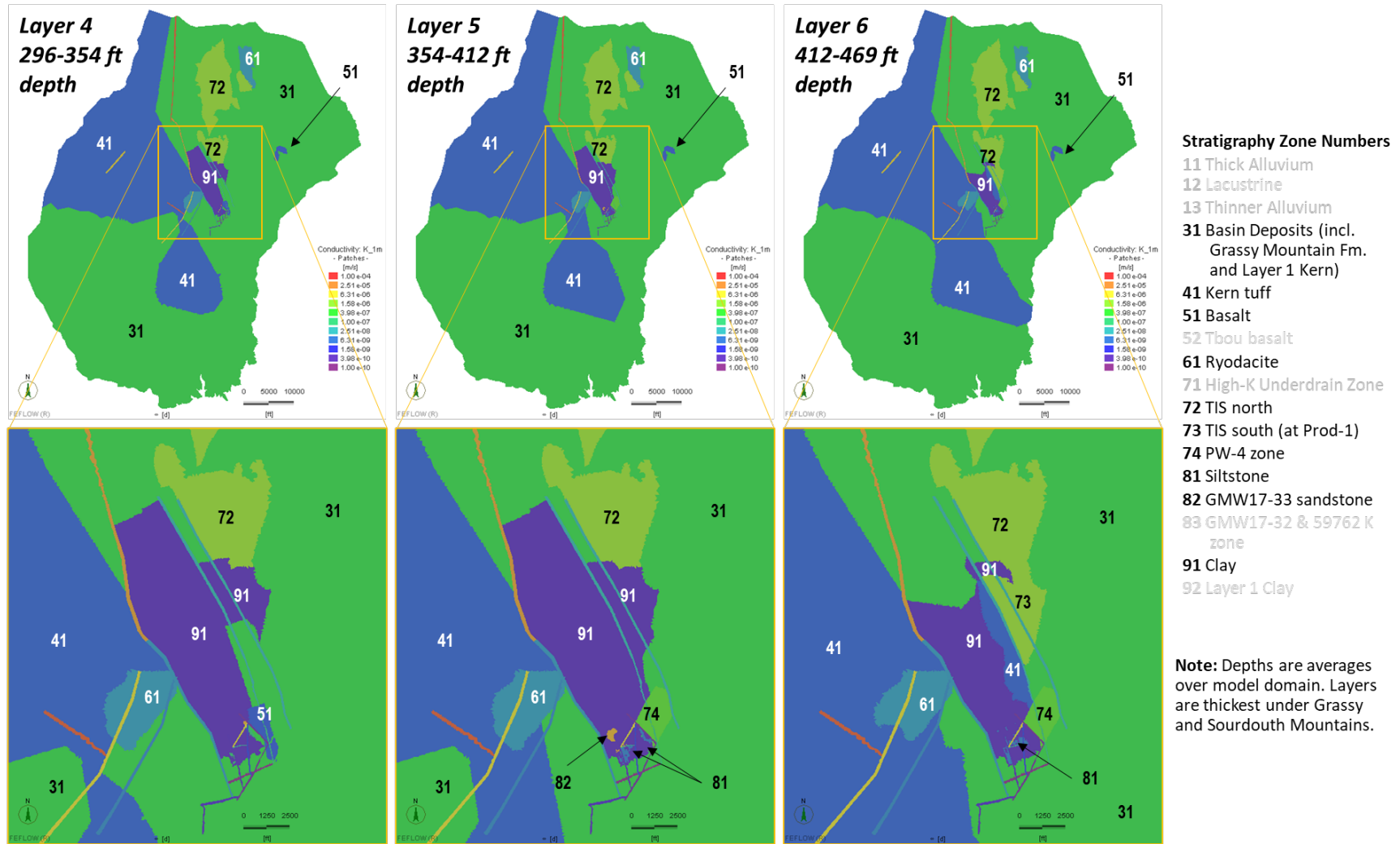


Figure 4-19: Hydraulic Conductivity Zones, Layers 4 to 6.

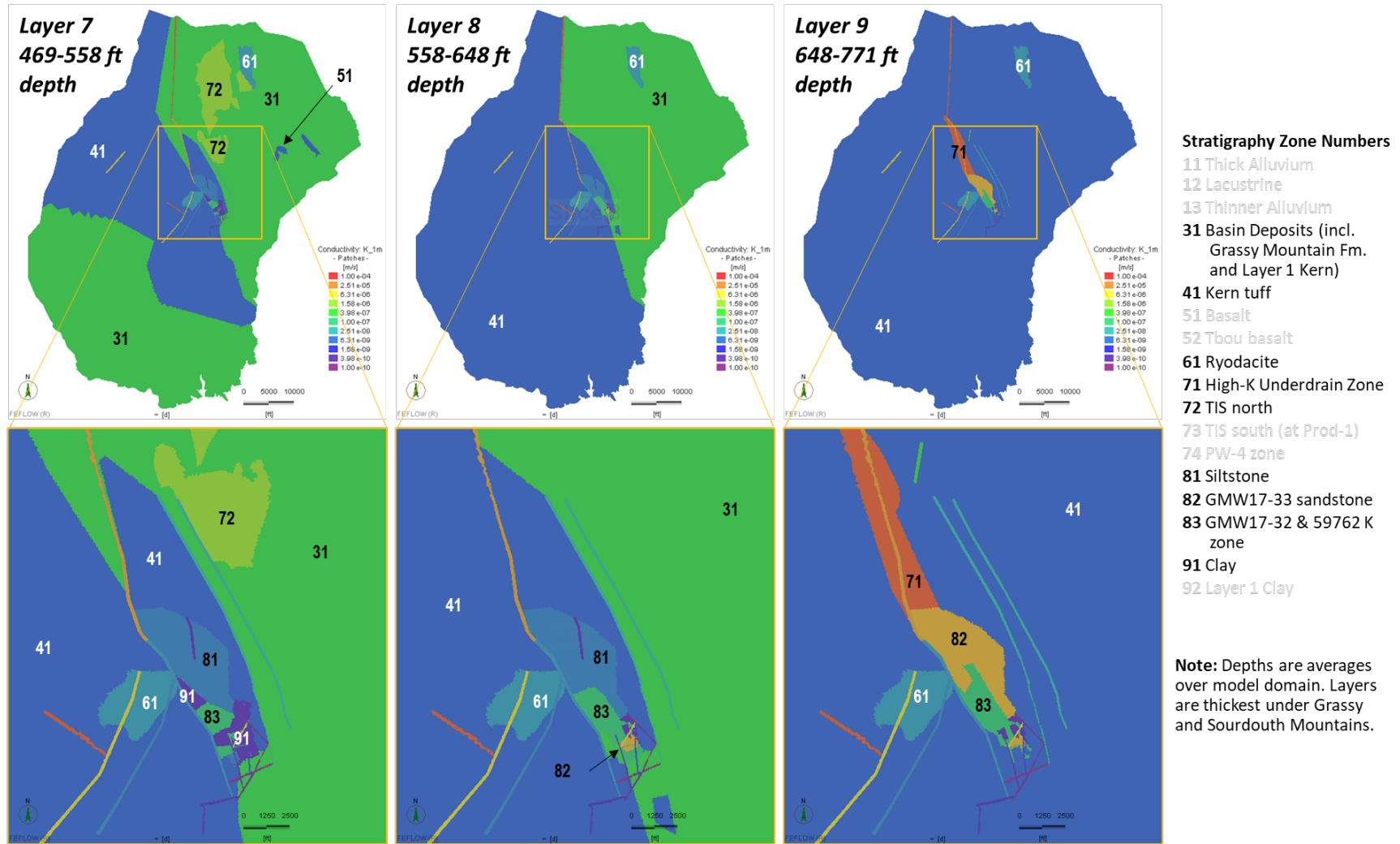


Figure 4-20: Hydraulic Conductivity Zones, Layers 7 to 9.

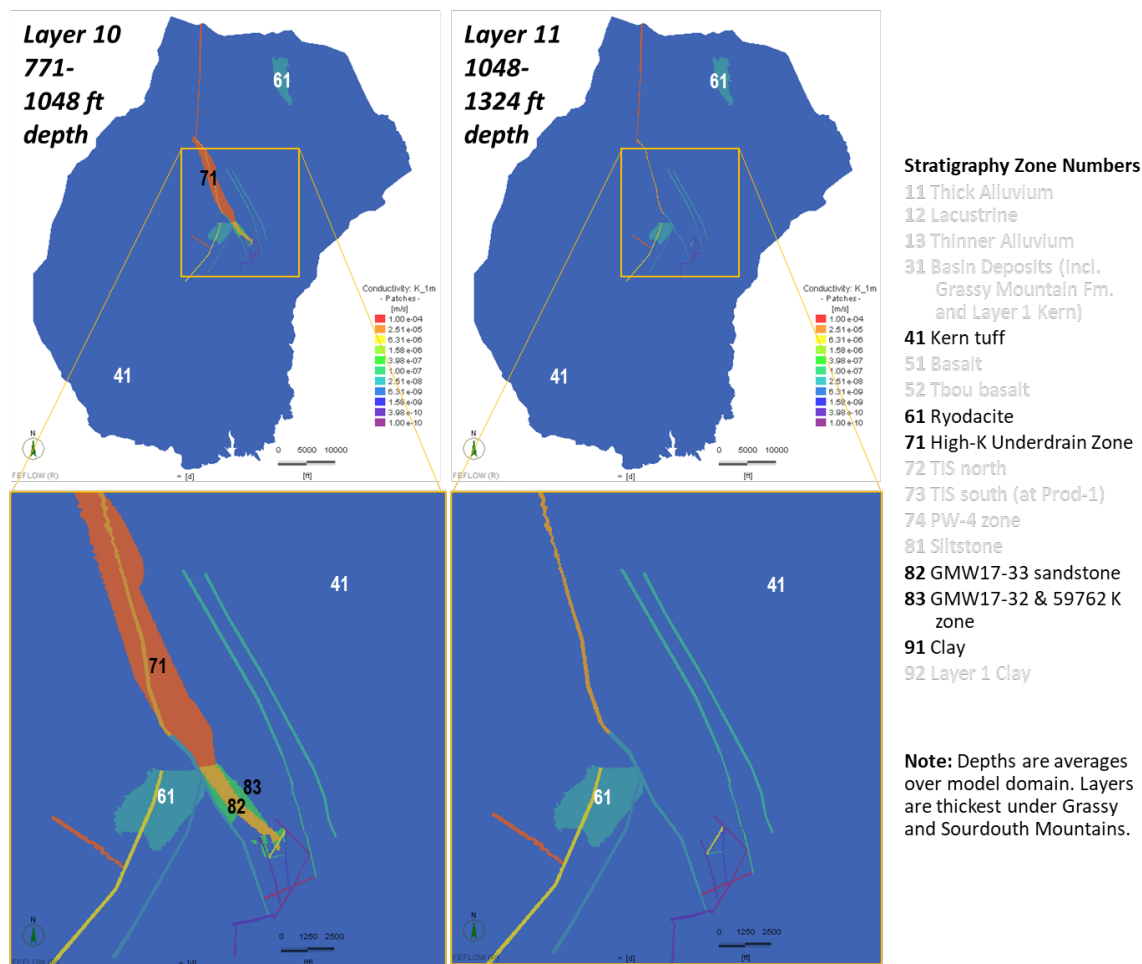


Figure 4-21: Hydraulic Conductivity Zones, Layers 10 and 11.

4.7 Structures

Figure 4-22 shows the locations of the faults included in the model domain as well as fault data obtained from Paramount Gold and from Ferns and Brooks (1993). A map of the fault zones in the mine area is presented in Figure 4-23. The site characterization data indicate that some faults are barriers to groundwater flow and some are conduits. However, not all the faults could be characterized with available data as barriers or conduits. Based on the knowledge that in this area faults can be either conduits or barriers, the modeler had judiciously assigned some faults properties (either barrier or transmissive faults) based on how well the model calibrates.

Fault traces that could explain the steep horizontal hydraulic gradient were introduced to the model as barrier faults. This group of faults includes the two Grassy Mountain Fault traces, called Grassy Mountain Fault East (Fault #2) and Grassy Mountain Fault West (Fault #1), both located east of the mine (see Figure 4-22). Southwest of the mine, two

additional fault traces in the vicinity of Grassy Spring were introduced to raise the water table at the spring relative to groundwater around it. These are identified as Faults #12 and #13 in Figure 4-22. North of Grassy Spring, Fault #14 was also treated as a barrier fault. In the mine area, Faults #4, #7a, #8, #9, #10, and #31 are barrier faults. The barrier effect of these faults was assessed in a sensitivity analysis in which the hydraulic conductivity was increased (see Sections 4.12 and 5.2).

Transmissive faults were used to simulate preferential flow zones. The main transmissive faults are Faults #25, #7, #15, #30 and #19. The first two, #25 and #7, were introduced to hydraulically connect the mine area low hydraulic head wells to the north model outflow boundary. Fault #30 is a short fault zone defined to reduce the heads at monitoring wells 59763 and 59764. Fault #15 was also calibrated to be a transmissive fault. Fault #19 is in the Wildcat Spring area and was introduced to help increase the spring flow in the artesian wells in this sector of the model. It has no influence on the mine impact predictions.

In the mine area, Fault #5 is a transmissive fault. Two additional faults, #11 and #1a, have moderate permeability. Fault #1a is the southern part of Fault #1 and is important in the PW-1 pumping test. For this reason, it was assigned a higher hydraulic conductivity than the northern part of Fault #1.

Similar to Fault #1a, which is the southern part of Fault #1, the southern part of Fault #7, a transmissive structure, is treated as a barrier fault, Fault #7a, in the FEFLOW model. The locations of these faults are shown in Figure 4-23.

All of the faults were assigned anisotropy ratios, such that it is possible for the hydraulic conductivity parallel to the fault trace to be higher than the hydraulic conductivity perpendicular to the fault trace. The FEFLOW anisotropy angle, ϕ , was defined in a manner which allows the definition of the K_z to be the hydraulic conductivity perpendicular to the fault plane. These angles are shown in Figure 4-22 and Figure 4-23.

The relationship between the mine area faults and stratigraphic zones 71 and 82 is shown in Figure 4-24. The high-permeability structure, Zone 71, is defined to widen the high-permeability zone that includes Faults #25 and #7. The hydraulic conductivity of Zone 71 is the same as that of Fault #25. Zone 71 ends approximately 1 mile northwest of the mine. The hydraulic connection between Zone 71 and the mine occurs through two areas assigned to Zone 82. Zone 82 has the relatively high hydraulic conductivity required to simulate the GMW17-33 pumping test, in which 30 gpm was pumped for approximately two days. Zone 82 comprises a western zone located in Layer 10 (see Figure 4-21) and an eastern zone located in Layer 9 (see Figure 4-20).

Table 4-5 lists the faults simulated in the model. The faults were treated as element groups in the FEFLOW model. The width of the fault zones is typically 150 ft to 200 ft. These

zones are therefore intended to simulate the hydraulic influence of a given fault zone rather than the fault itself. All faults run through the entire depth of the model domain, through all bedrock units. Faults are not defined through the alluvium zones in Layer 1.

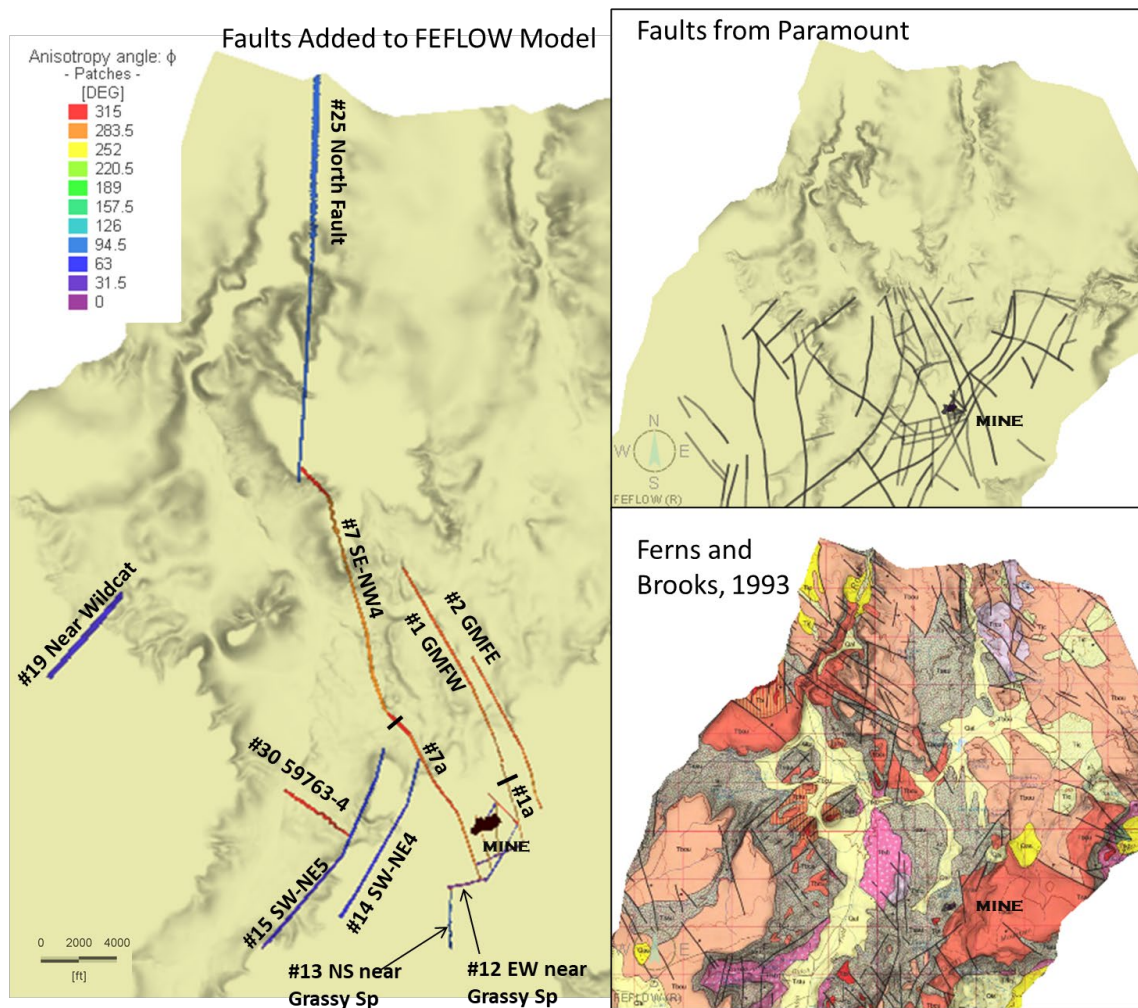


Figure 4-22: Regional Faults.

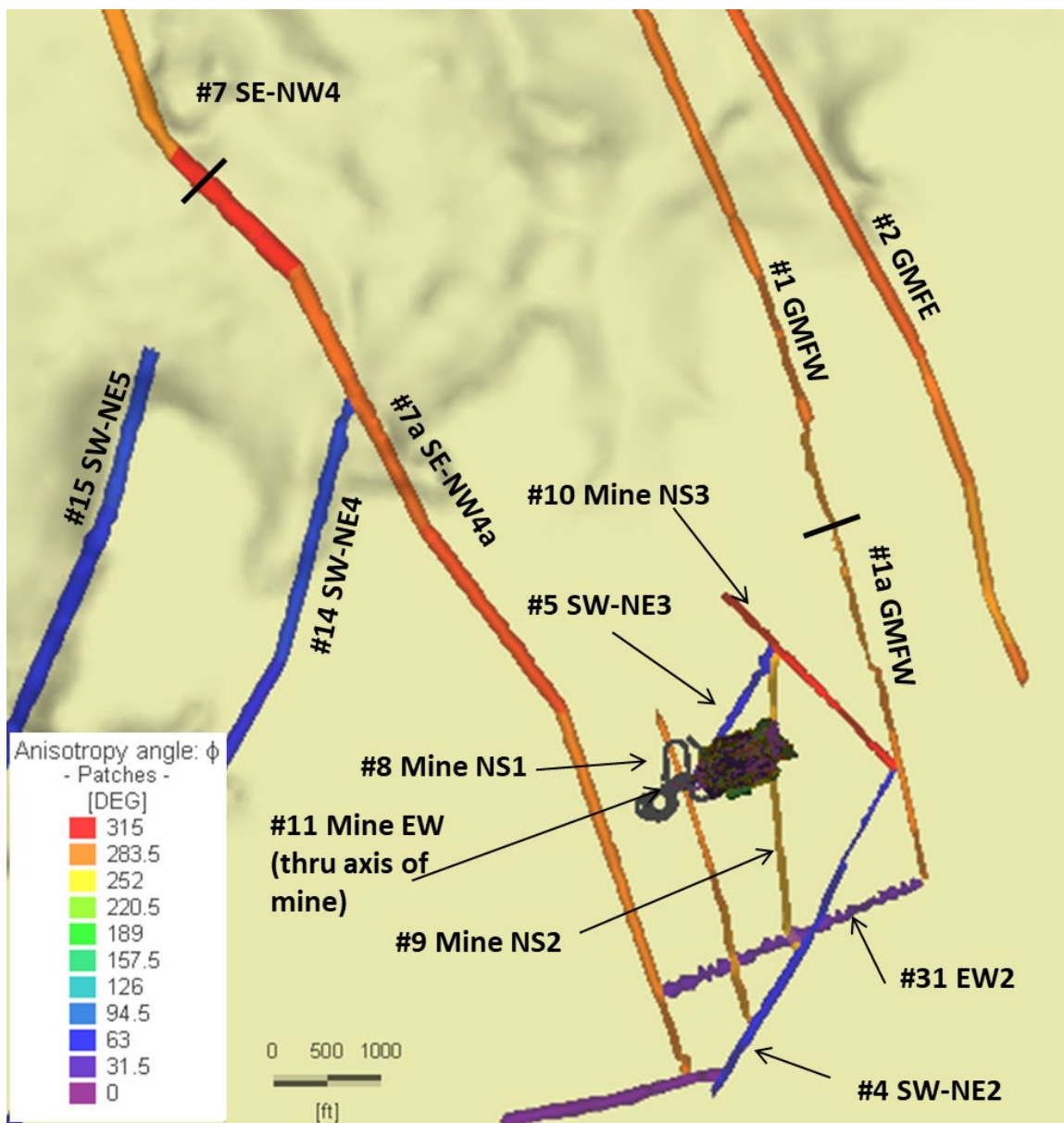


Figure 4-23: Mine Area Faults.

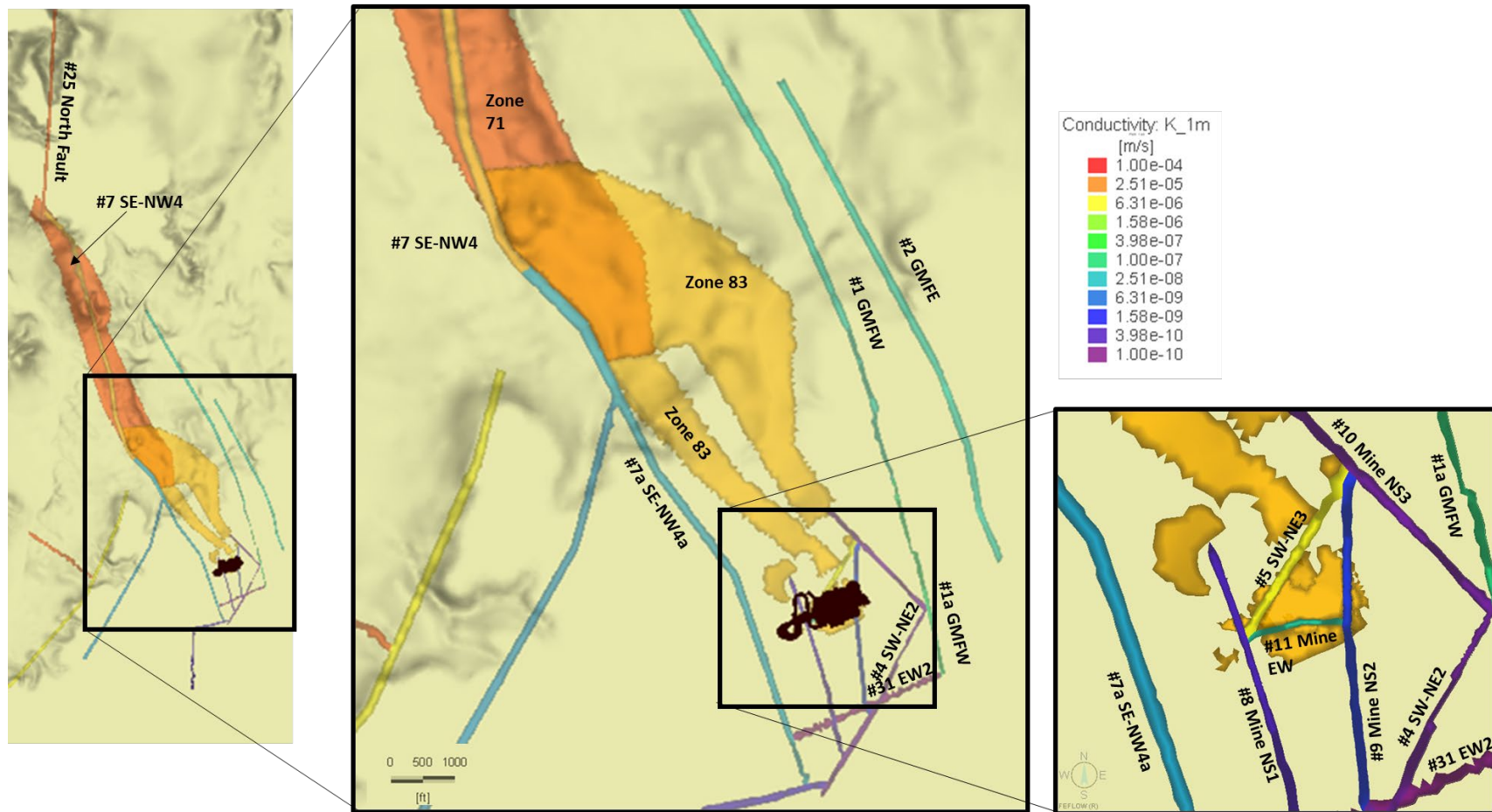


Figure 4-24: Interaction between Faults and Deep High-K Zones.

**Table 4-5:
List of Model Faults**

Fault Number	Name	Description
1	Grassy Mtn Fault W	Barrier fault first identified by Adrian Brown (1992), used to simulate the steep horizontal hydraulic gradient east of the mine property.
1a	Grassy Mtn Fault W-South	Southern portion of Grassy Mountain Fault (#1). Separated from main fault for the PW-1 calibration. The final calibrated hydraulic conductivity is similar to that of Fault #1
2	Grassy Mtn Fault E	Barrier fault first identified by Adrian Brown (1992), used to simulate the steep horizontal hydraulic gradient east of the mine property. Has the same properties as Fault #1
4	SW-NE Fault 2	Barrier fault used in conjunction with Fault #31 to simulate the steep horizontal hydraulic southeast of the mine.
5	SW-NE Fault 3	Transmissive fault located immediately west of proposed mine
7	SE-NW Fault 4	Transmissive fault associated with Fault #25 and High-K Zone 71
7a	SE-NW Fault 4 South	Barrier fault used to simulate the steep horizontal hydraulic gradient west of the mine property.
8	Mine NS Fault 1	Barrier fault that runs through the ramp area
9	Mine NS Fault 2	Barrier fault east of the mine
10	Mine NS Fault 3	Barrier fault northeast of the mine
11	Mine EW Fault 1	Transmissive fault running through the proposed stopes
12	EW Near Grassy Sp	Barrier fault north of Grassy Spring
13	NS Near Grassy Sp	Barrier fault just west of Grassy Spring
14	SW-NE Fault 5	Barrier fault west of the mine area
15	SW-NE Fault 5	Transmissive fault parallel to the main valley west of mine area (i.e., south of Negro Rock Canyon)
19	Near Wildcat Sp	Transmissive fault in the Wildcat Spring area
25	North Fault	Transmissive fault associated with Fault #7 and High-K Zone 71
30	For 59763-4	Transmissive fault used to lower the head at monitoring wells 59763 and 59764
31	Mine EW Fault 2	Barrier fault used in conjunction with Fault #30 to simulate the steep horizontal hydraulic southeast of the mine.

4.8 Sections Through Numerical Mode

The model stratigraphy in areas of interest—*i.e.*, the mine area and areas where impacts could potentially occur—is shown in 14 cross-sections in Figure 4-25 to Figure 4-38. In these figures, stratigraphic cross-sections presented in Adrian Brown (1992) and SPF (2021c) are compared to the FEFLOW model structure. The figures also show the simulated water table for the base case model discussed in Section 5.1. Note that in some cases, the fault trace is sub-parallel to the section line, which exaggerates the apparent thickness of the faults in the FEFLOW model.

4.8.1 Regional Sections

Figure 4-25 to Figure 4-38 show large-scale west-east or south-north sections through the mine area. Figure 4-25 presents a west to east section through the deposit and illustrates the location of the basalt, basin deposits/Grassy Mountain Formation and Kern basin tuff. The figure also shows the simulated faults in the model. In the area between Faults #7a and the Grassy Mountain West Fault (Fault #2), the FEFLOW model shows the depressed water table that is evident in the data (Section 3.4). The main difference between the two sections is the thinner basin deposits in the FEFLOW model compared to the conceptual section. The shallower Kern tuff contact is based on more recent geological interpretations, as shown in Figure 4-27, which shows a similar west-to-east cross-section from SPF (2021c).

Figure 4-26 presents a south-to-north section through the deposit following a section location from Adrian Brown (1992), and a section from the numerical model in approximately the same location. In this section, the basalt is thinner than in the west-to-east sections. Like the west-to-east-sections, Figure 4-26 shows that the FEFLOW model simulates a head depression bounded by the simulated faults. Figure 4-26 extends northward through the Grassy Mountain Faults and into the TIS zone that the production wells will target.

Figure 4-27 and Figure 4-28 compare the model stratigraphy with the regional sections of SPF (2021c). The overall structure of the model is similar to the sections.

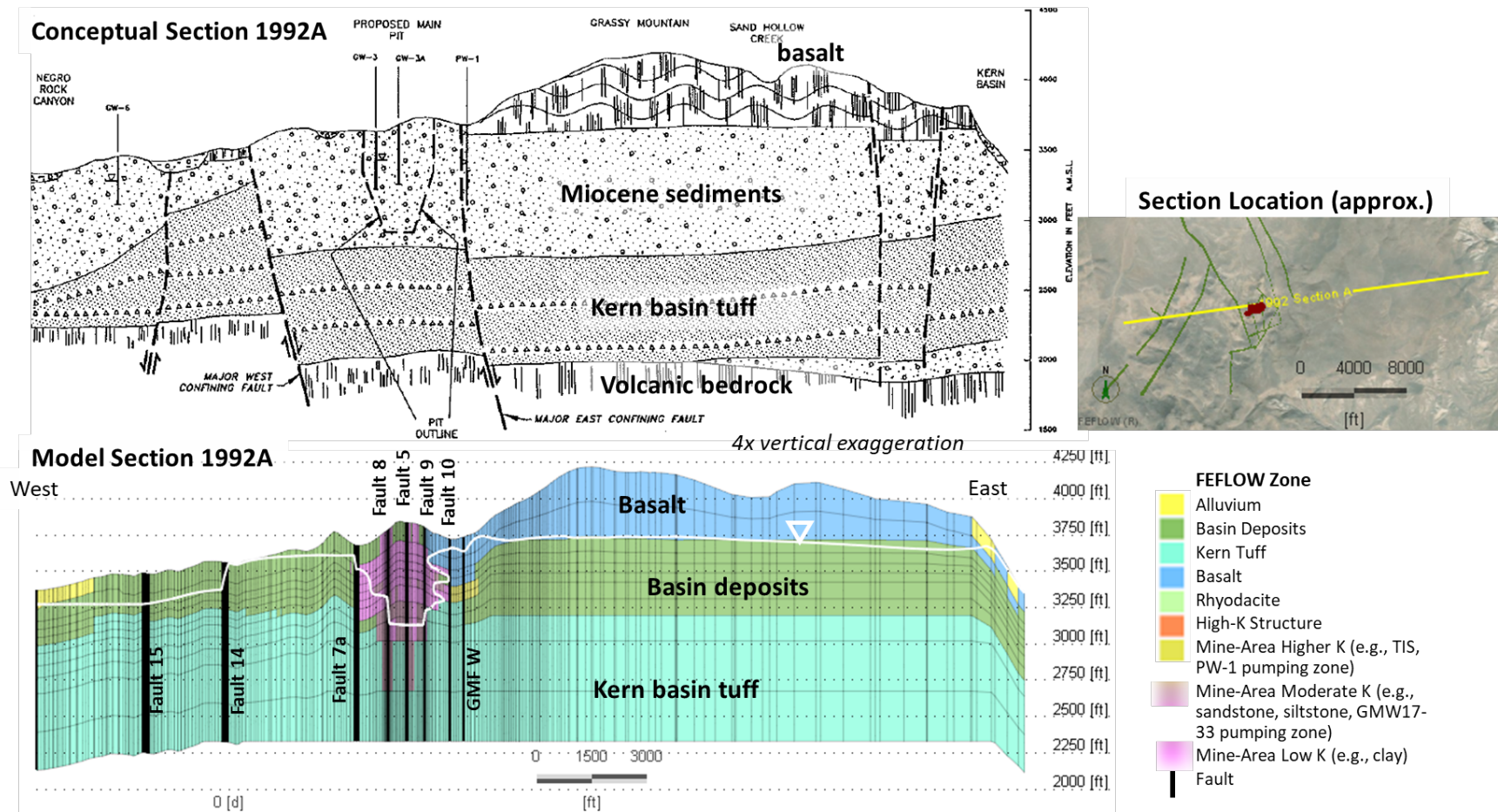


Figure 4-25: West-East Section 1992A (after Adrian Brown, 1992).

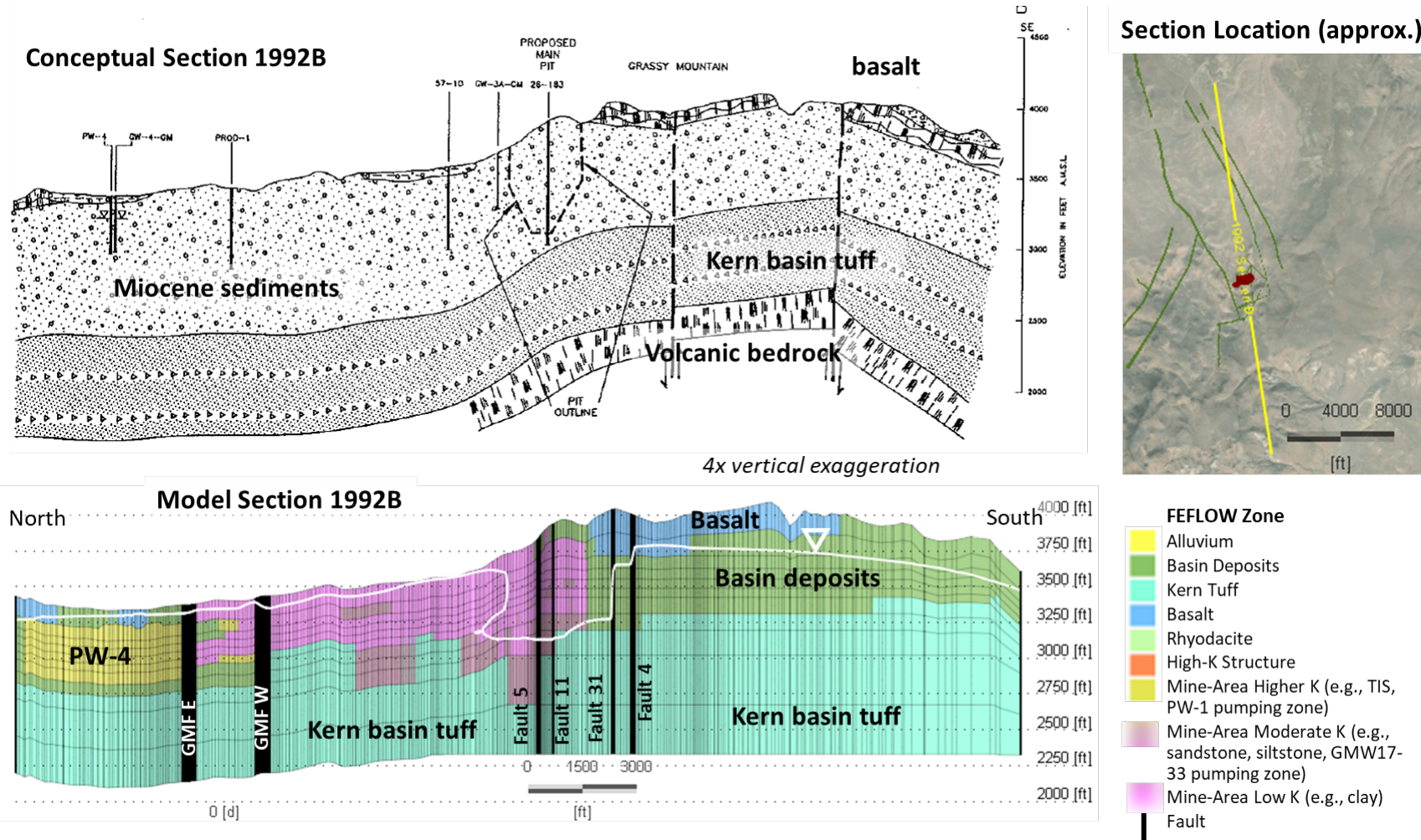


Figure 4-26: North-South Section 1992B (after Adrian Brown, 1992).

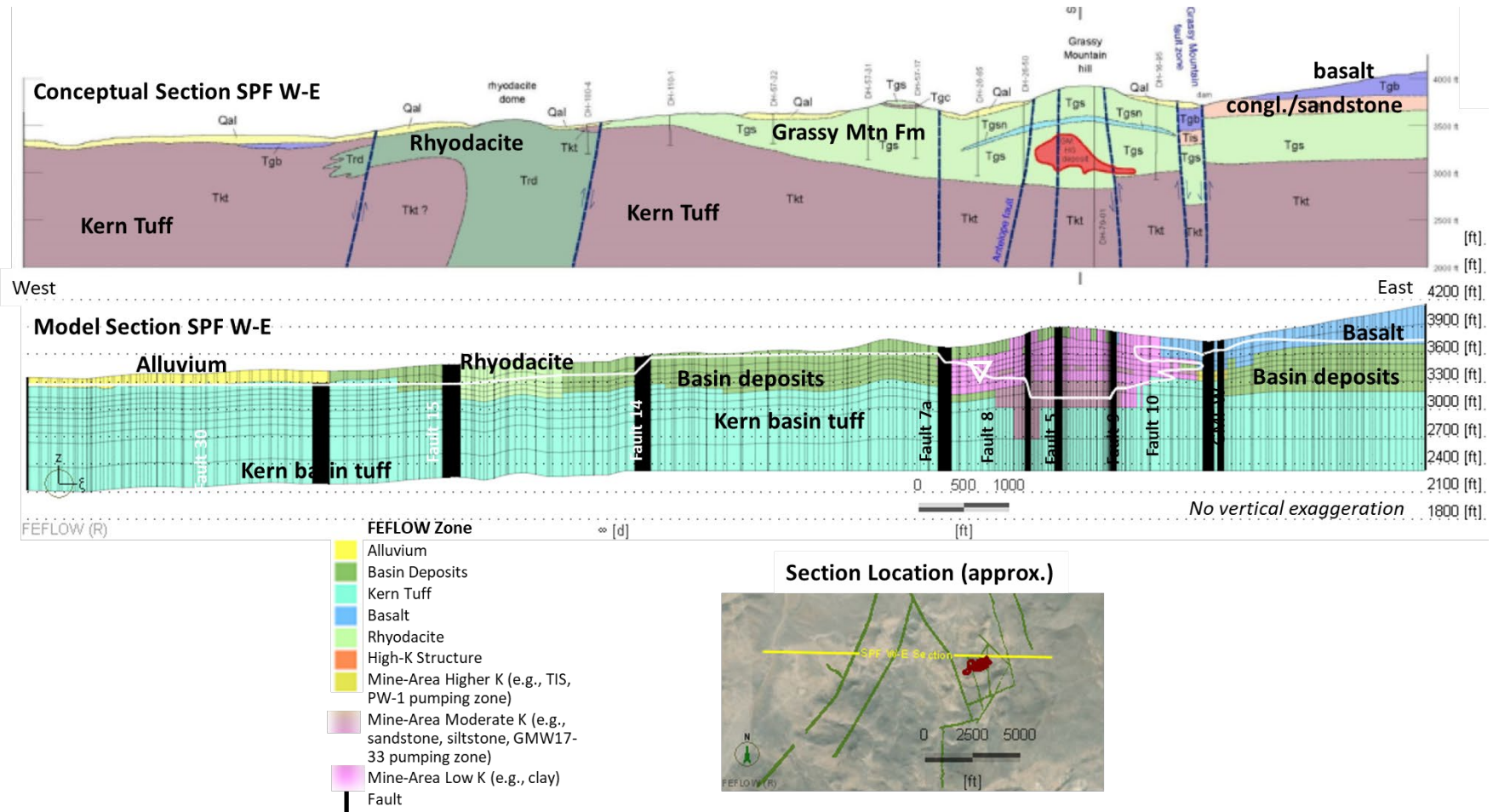


Figure 4-27: West-East Section 2021 (after SPF, 2021c).

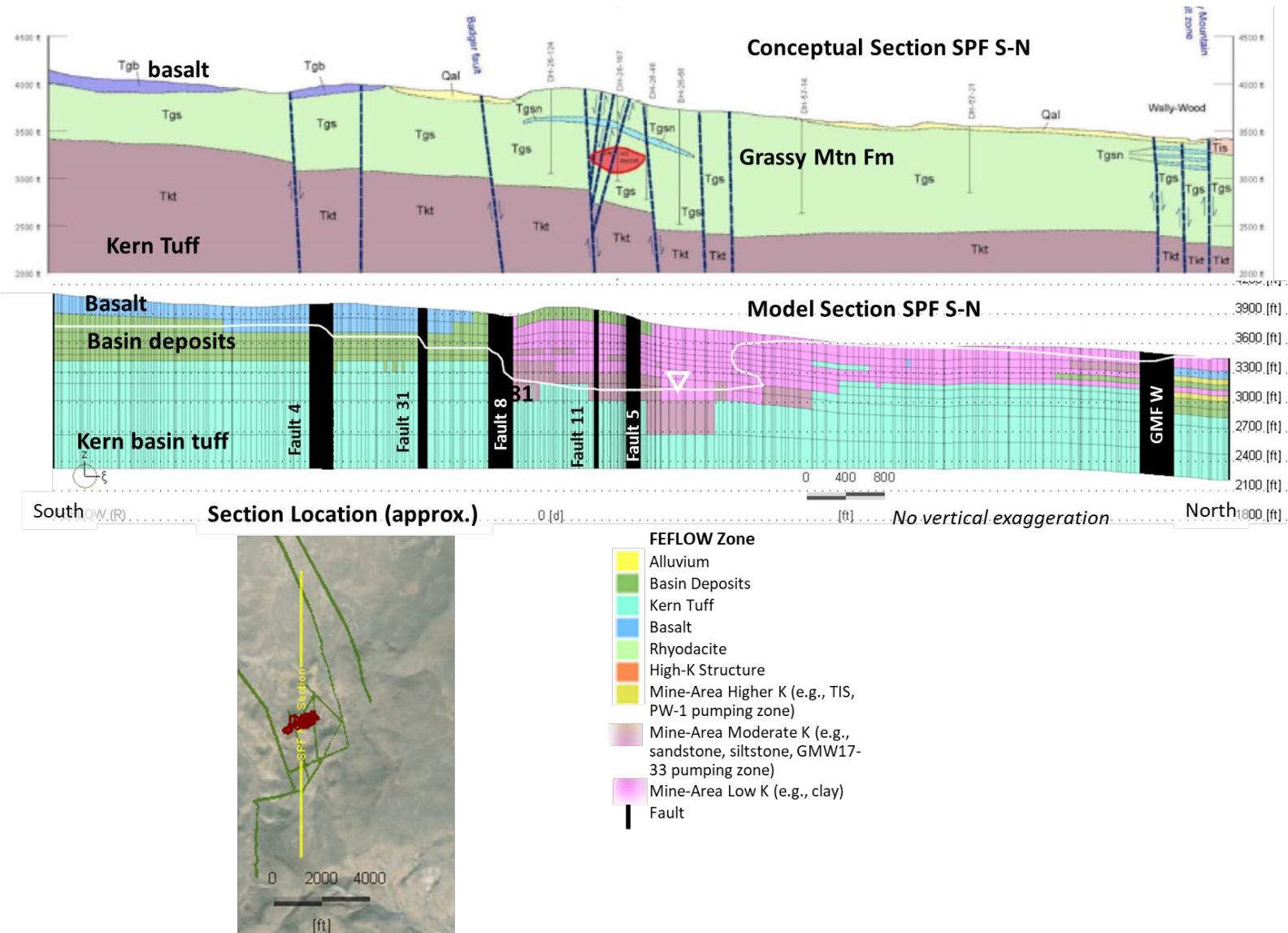


Figure 4-28: South-North Section 2021 (after SPF, 2021c).

4.8.2 Intermediate Scale Sections

Figure 4-29 to Figure 4-33 present the FEFLOW model configuration following Sections H to K of SPF (2021c). These cross-sections are intermediate in scale compared to the sections shown in Figure 4-25 to Figure 4-28. Figure 4-29 shows Section H, which is aligned generally north to south through PW-4, Prod-1, PW-1 and 59761. Figure 4-29 shows that the FEFLOW model includes a surficial clay zone consistent with SPF's Section H. The southern part of Section H runs parallel to Fault #1 (Grassy Mountain Fault West), resulting in a large swath of fault zone in the section. The southern part of the section, denoted clay, silt, sand-and-gravel and basalt in the conceptual section is treated as a zone of basalt in the FEFLOW model, underlain by a more permeable zone associated with the PW-1 pumping test. In the far north, the TIS zone can be seen as sand/conglomerate in the conceptual section and as the PW-4 pumping zone in the FEFLOW model. A combination of the Grassy Mountain Fault East (Fault #2) and clay at depth separates PW-4 and Prod-1 TIS zones in the FEFLOW model. The intervening clay zone was introduced to simulate artesian conditions at Prod-1. PW-4 and its observation well, GW-4 do not exhibit artesian conditions.

Figure 4-30 shows Section I from SPF (2021c). In this section, the conceptual model includes a thick sequence of low-permeability clay, siltstone and sinter underlain by sandstone. The clay zone becomes thinner in the north. The FEFLOW model includes a low-permeability zone at shallow portions of GMW17-32, GMW17-33 and GMW18-34, following the conceptual model. However, at the BLM well, higher permeability basin sediments are included in the model to reduce the simulated head at this well. The clay is underlain by moderate-permeability strata and then the Kern basin tuff in the FEFLOW model. In the northern part of the section, between BLM and GW-5, the section crosses Fault #7 twice. In the FEFLOW model, there is rhyodacite between the two intersections with Fault #7. Section I ends in the north in the high-K structure (Zone 71). As illustrated in Figure 4-30, this zone is located below shallow clay and moderate-permeability sandstones in the numerical model.

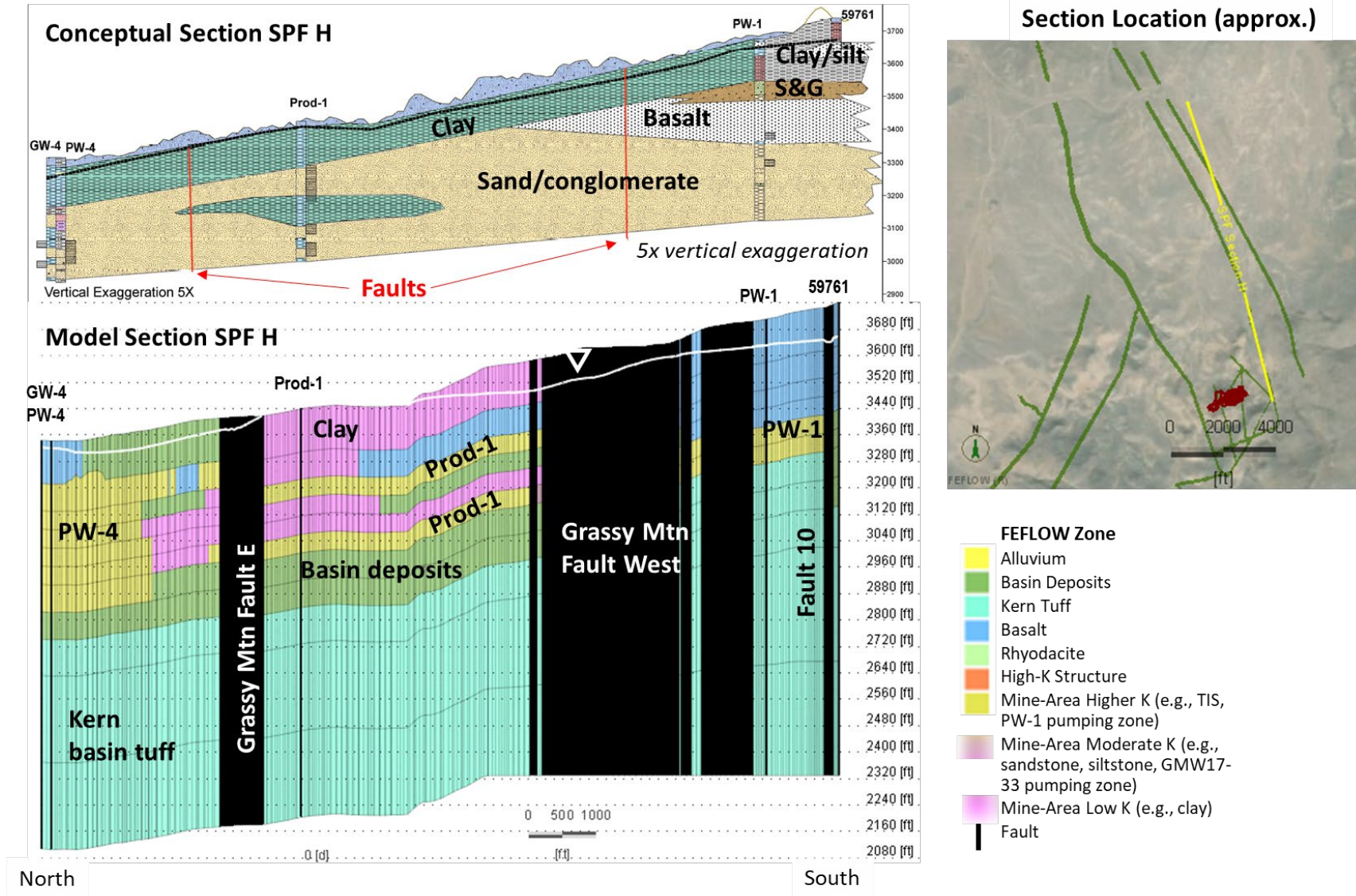


Figure 4-29: Section H (after SPF, 2021c).

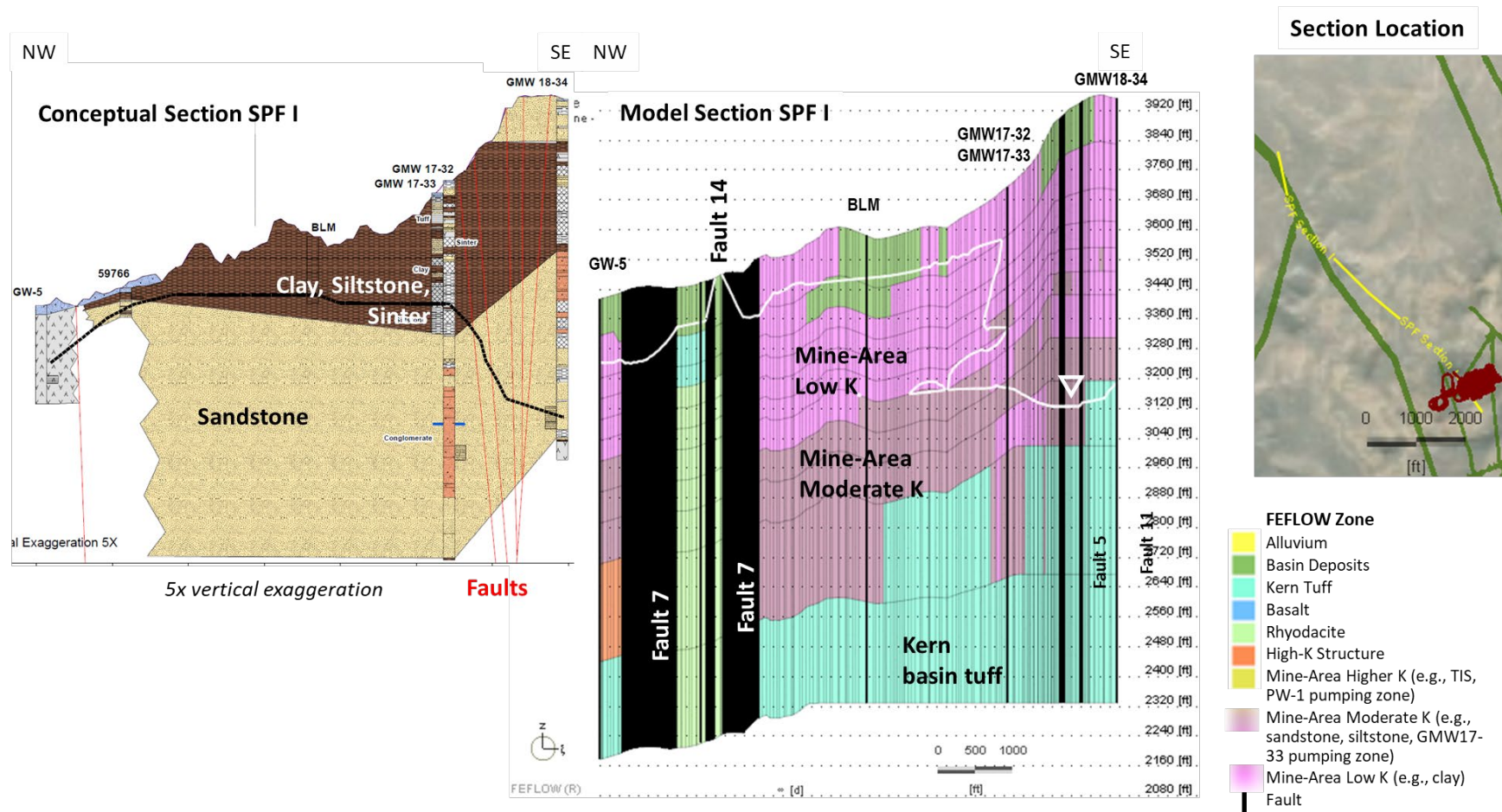


Figure 4-30: Section I (after SPF, 2021c).

Figure 4-31 presents a southwest-to-northeast section, Section J, through the rhyodacite zone. This section runs through GW-6, 59766 and 59767. The FEFLOW model matches the location of the rhyodacite area. East of the rhyodacite, the numerical model includes Kern tuff at depth and low- and moderate-permeability strata above the tuff. The conceptual model includes sandstone/conglomerate underlain by a shallower tuff zone. West of the rhyodacite, the conceptual section includes a lower sandstone zone that is absent from the FEFLOW model. It is possible that a lower permeable zone is the reason for the low piezometric head at 59643 and 59644, located southwest of GW-6.

Figure 4-32 shows the model configuration along Section K of SPF (2021c). The model has less resolution within the basin sediments, and treats the intercalated volcanic strata as a single basin deposit. As discussed below, the layering of strata within the basin deposits is indirectly simulated with anisotropy (see Section 4.11).

Figure 4-33 shows Section B of SPF (2021c). This section is similar to Section H (Figure 4-29) but trends more southward at the southern end, so that the southern part of the section is closer to the mine. The conceptual section illustrates the stratigraphic layers, which alternate between clay and sandstone in the northern part of the section. In the southern area, the stratigraphy shows alternating thicknesses of siltstone and arkose. The relatively thick layers of the numerical model do not permit the simulation of these fine lenses of material, which have been grouped into larger zones. In the northern area, the TIS/PW-4 pumping zone was defined as shown in Figure 4-17. Between the Grassy Mountain Faults, the model interleaves low permeability clayey material (shown in pink) and a higher permeability TIS zone around Prod-1, shown in yellow. South of Grassy Mountain Fault West, the numerical model has a combination of low permeability clays and moderate-permeability zones.

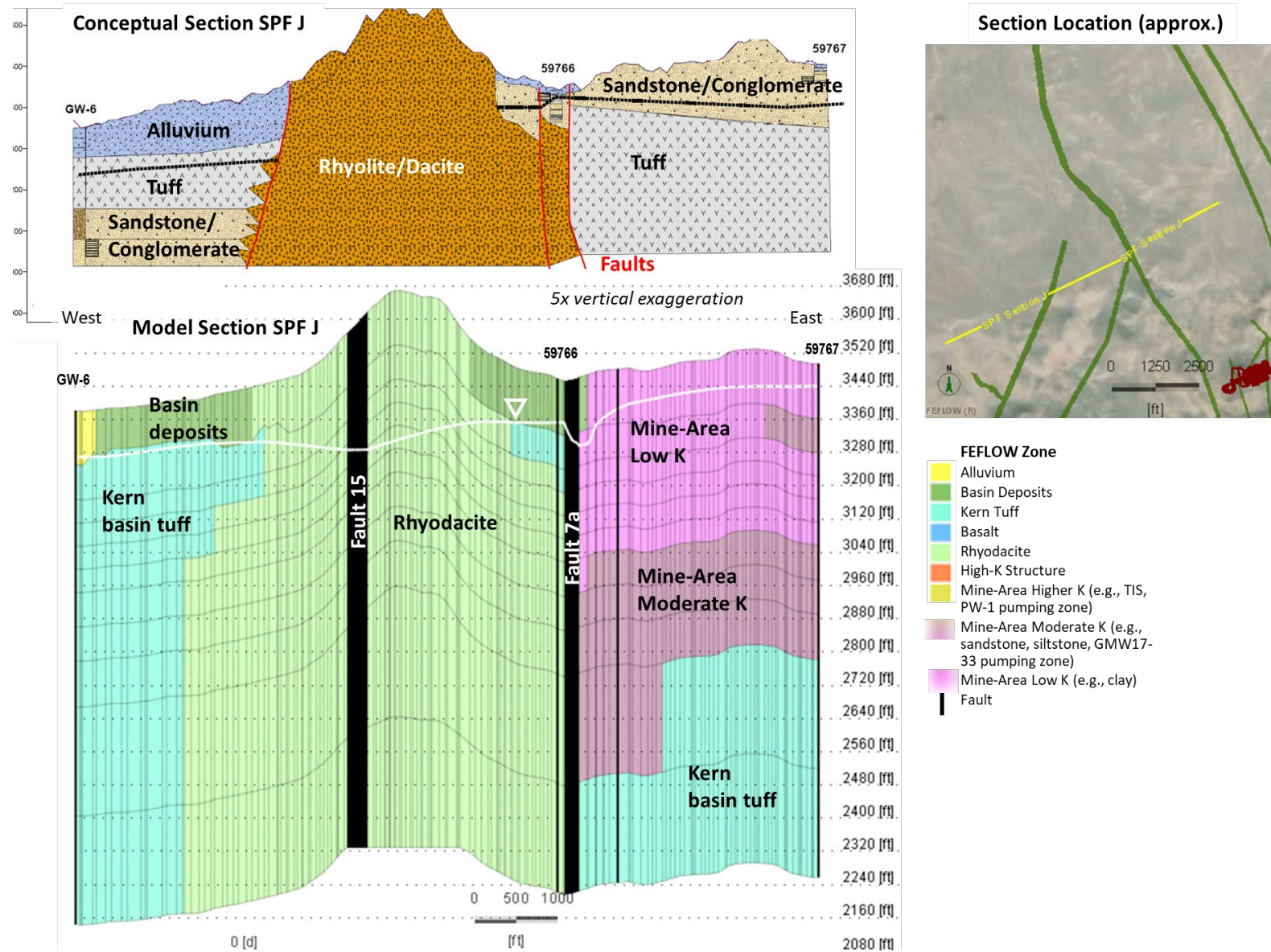


Figure 4-31: Section J (after SPF, 2021c).

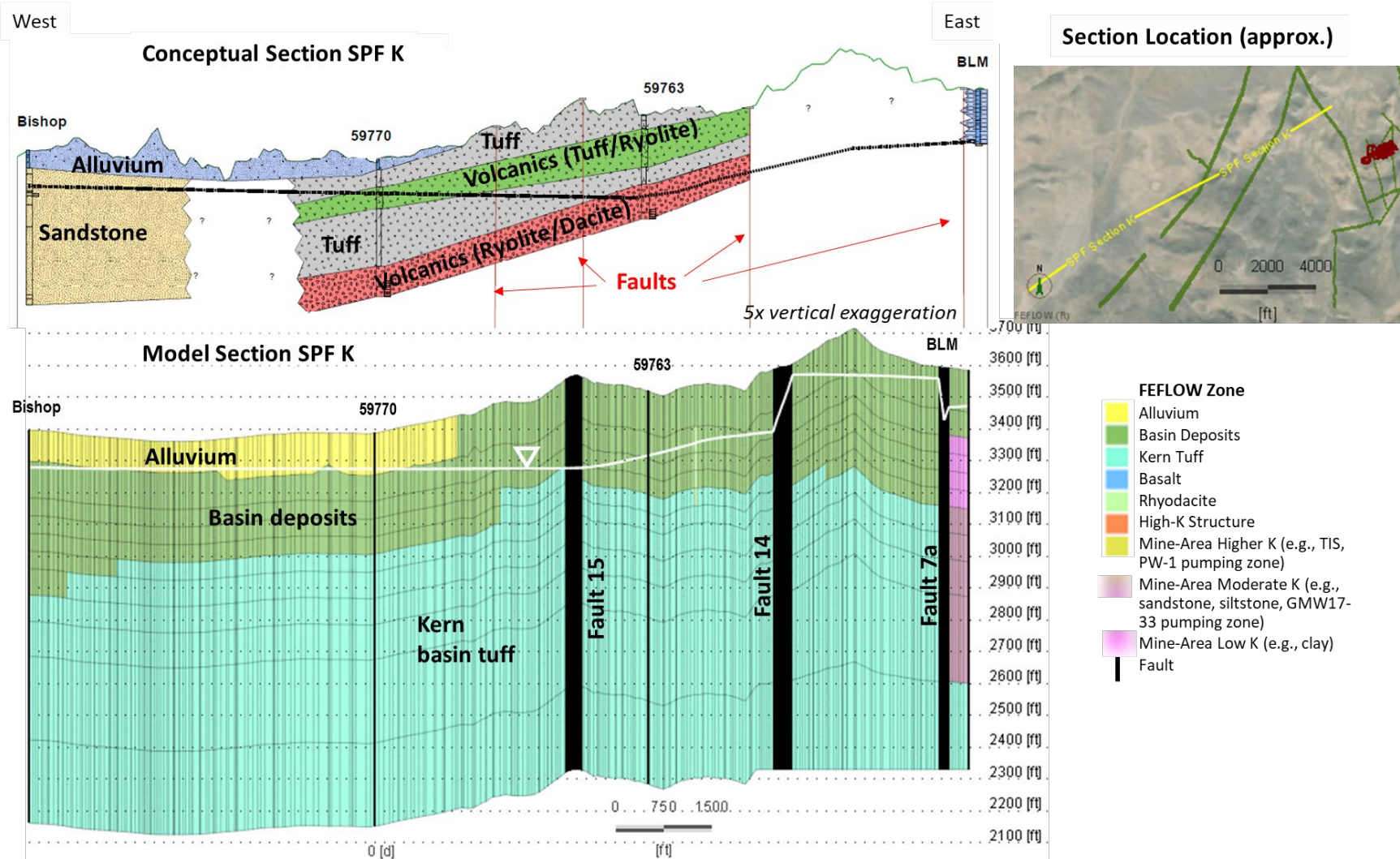


Figure 4-32: Section K (after SPF, 2021c).

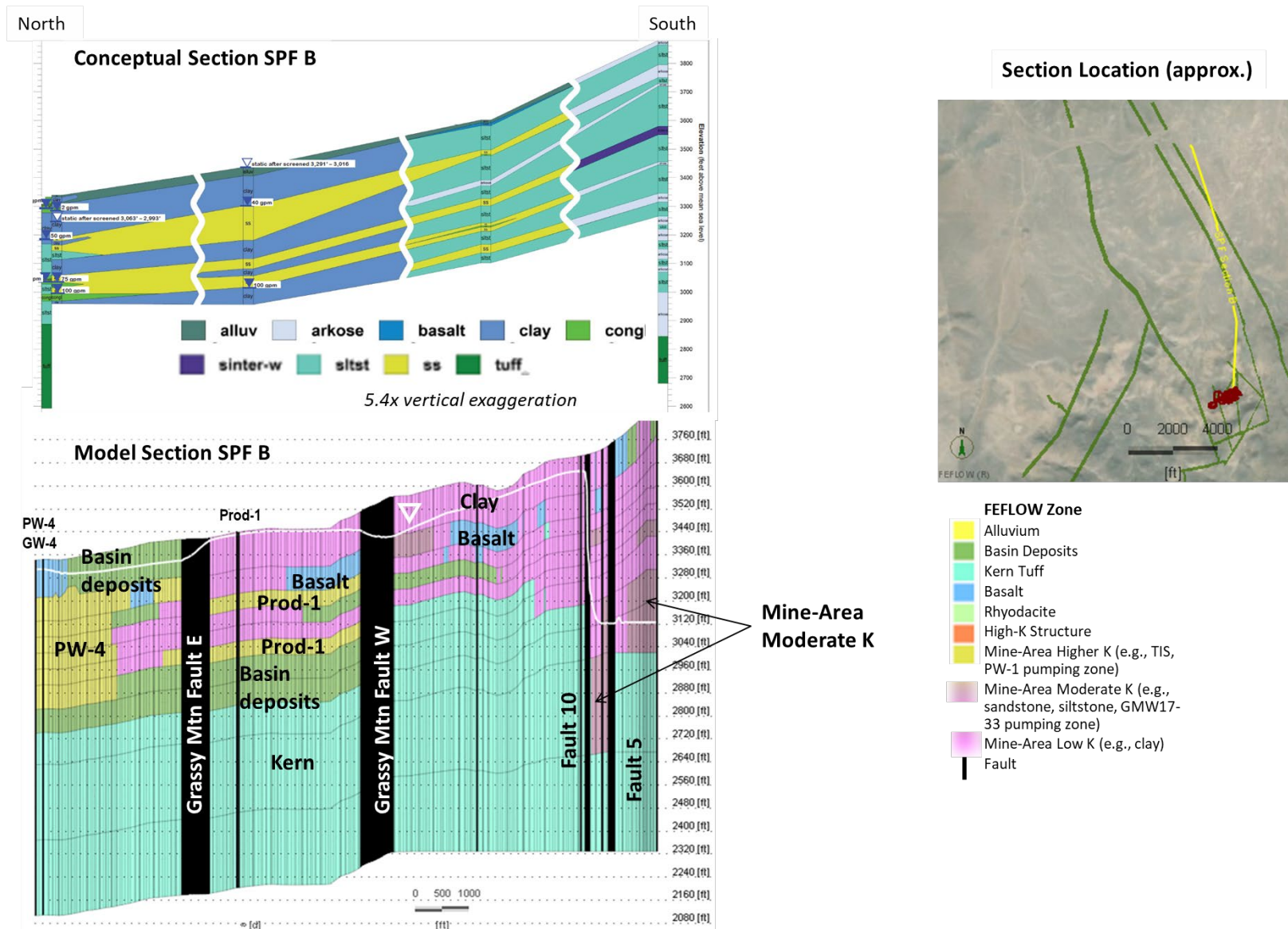


Figure 4-33: Section B (after SPF, 2021c).

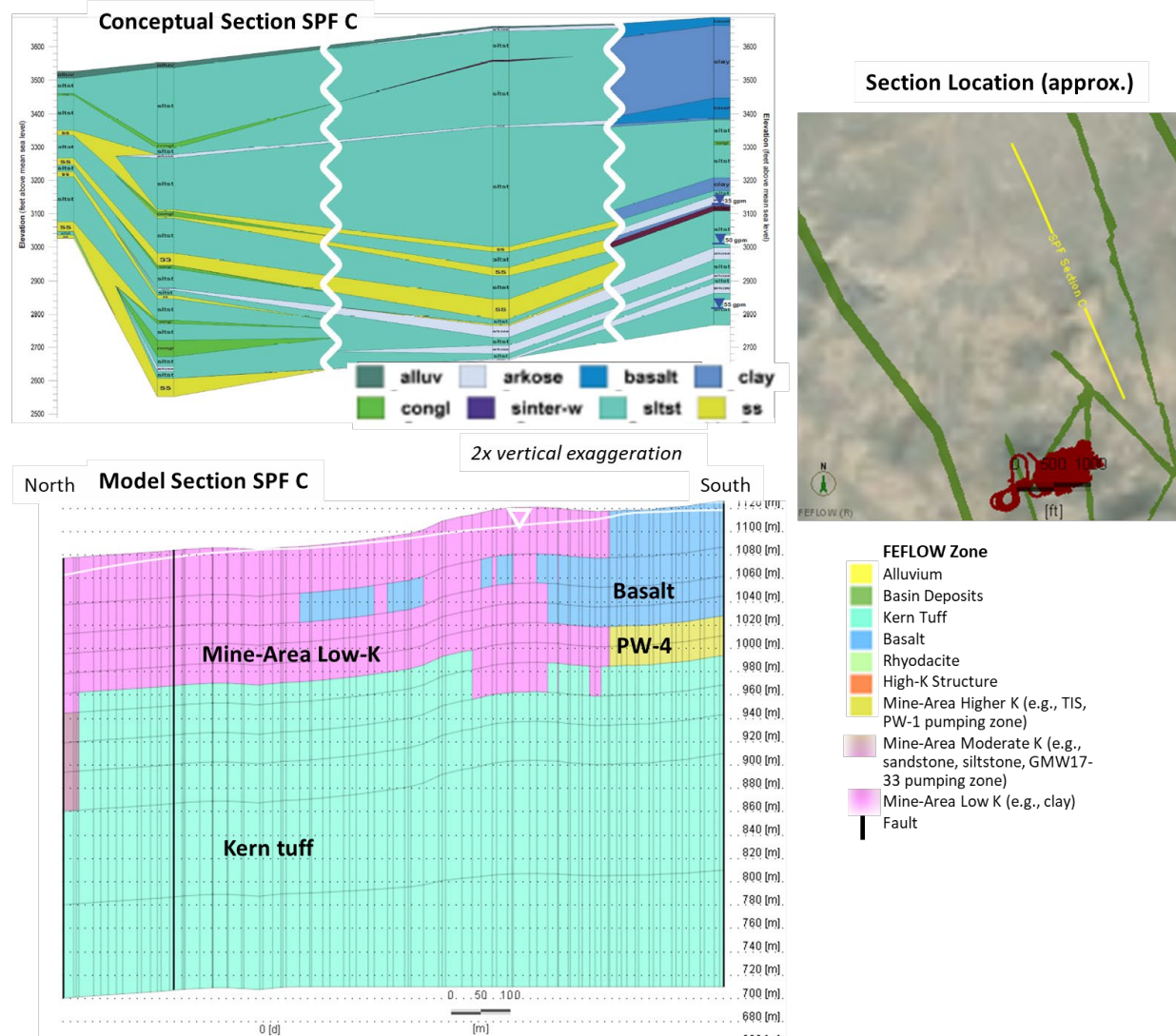


Figure 4-34: Section C (after SPF, 2021c).

4.8.3 Mine Area Sections

Figure 4-34 to Figure 4-38 show cross-sections in the vicinity of the proposed mine. Figure 4-34 shows north-to-south trending Section C of SPF (2021c). It is characterized by a thick zone of siltstone except for the southern area, which has shallow basalt. The FEFLOW model honors this trend. At lower elevations, the Section shows connected zones of sandstone, separated by two fault traces, shown as white wavy lines. The FEFLOW model does not include the fault traces and treats the lower zones as undifferentiated Kern tuff.

Figure 4-35 shows a southwest to northeast section along the southern edge of the mine. This section is intersected by seven faults. Four of these faults are present in the FEFLOW model. In the higher elevation portion of the section, SPF has noted a concentration of low-permeability units, including basalt, siltstone and sinter with some arkose. The FEFLOW model treats this zone as having low-permeability, with some zones of moderate permeability. The eastern end of the section contains basalt in both the conceptual model and the numerical model.

Figure 4-36 shows Section E of SPF (2021c). This section is dominated by siltstone, and the FEFLOW model also shows predominantly low-permeability units in this area. In the northern area, the conceptual section shows a greater frequency of sandstone in the boring logs, and the FEFLOW model has moderate permeability assigned to this zone.

Figure 4-37 shows Section F of SPF (2021c). In this section, the FEFLOW model honors the thick sequence of clay in the west, underlain by material of higher permeability. On the west, the FEFLOW model has basalt underlain by undifferentiated basin sediments.

Figure 4-38 is a short west-to-east section, Section G, at the northern edge of the proposed mine (SPF, 2021c). Note that this section is compressed vertically to show deep diamond drill logs. The stratigraphy in this section is predominantly siltstone, with intercalated sinter and arkose. The eastern area has basalt in both the conceptual model and the numerical model. In the FEFLOW model, the shallow zones are low-permeability and underlain by moderate permeability, in the area shown to have more arkose.

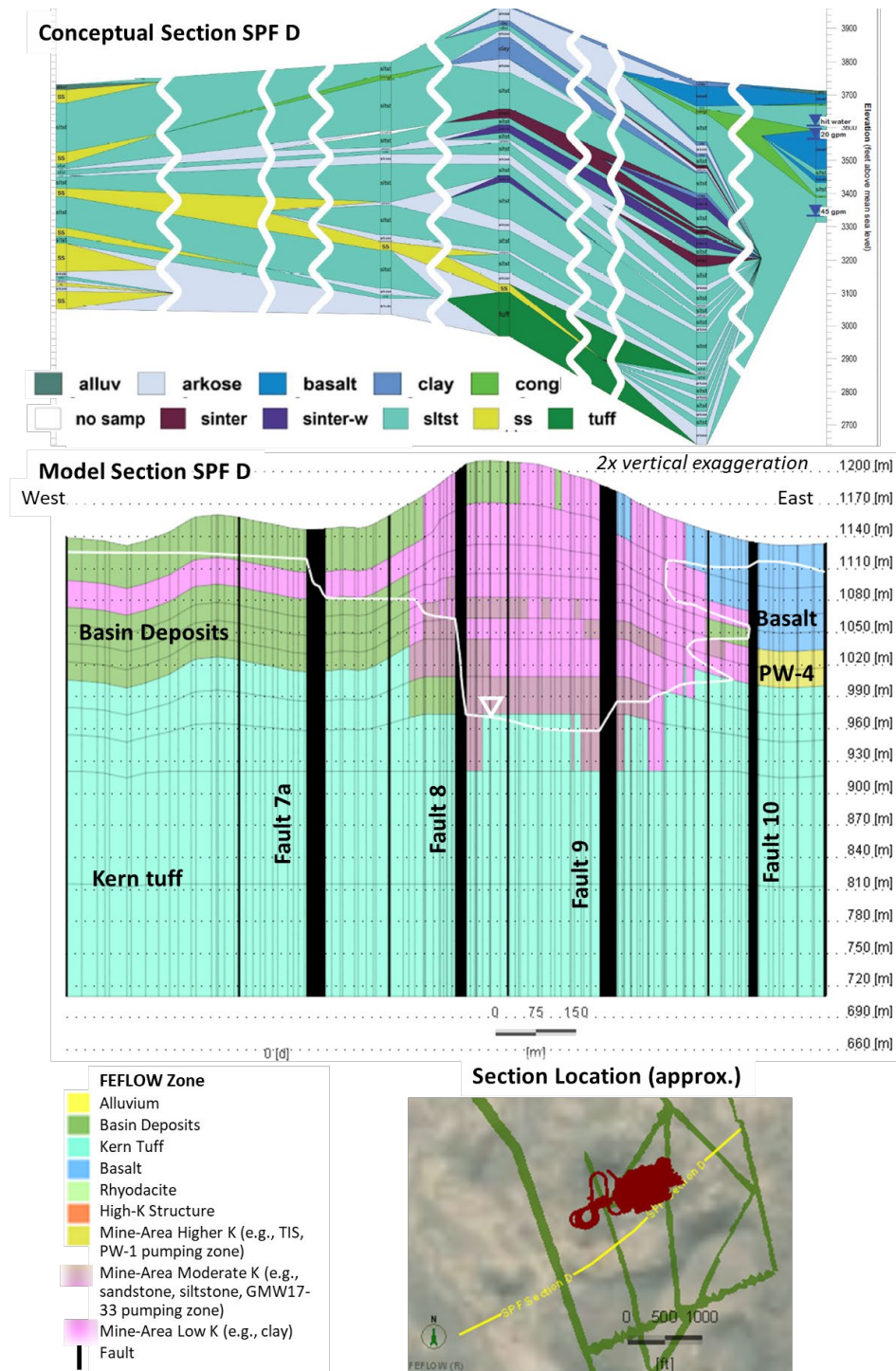


Figure 4-35: Section D (after SPF, 2021c).

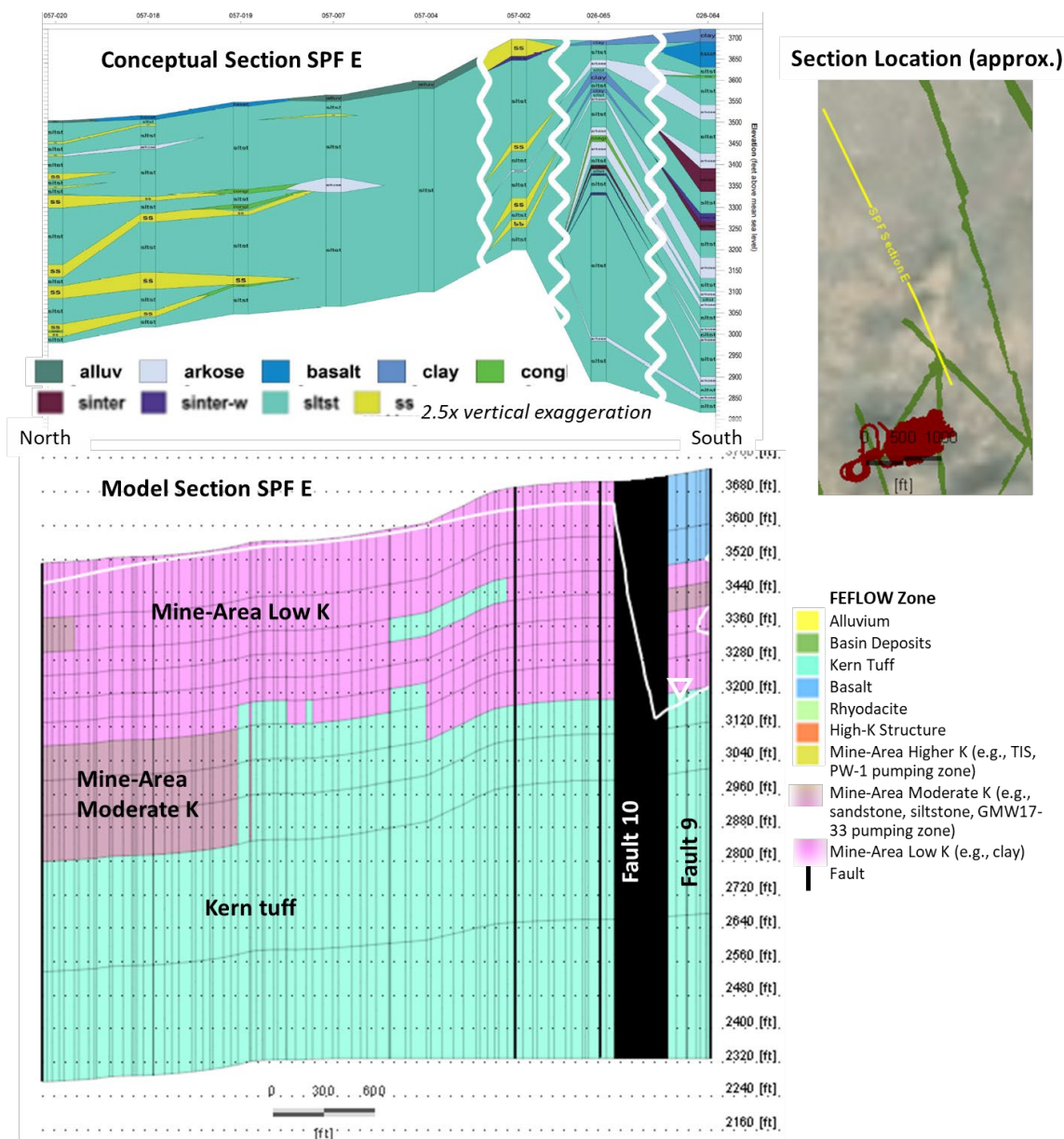


Figure 4-36: Section E (after SPF, 2021c).

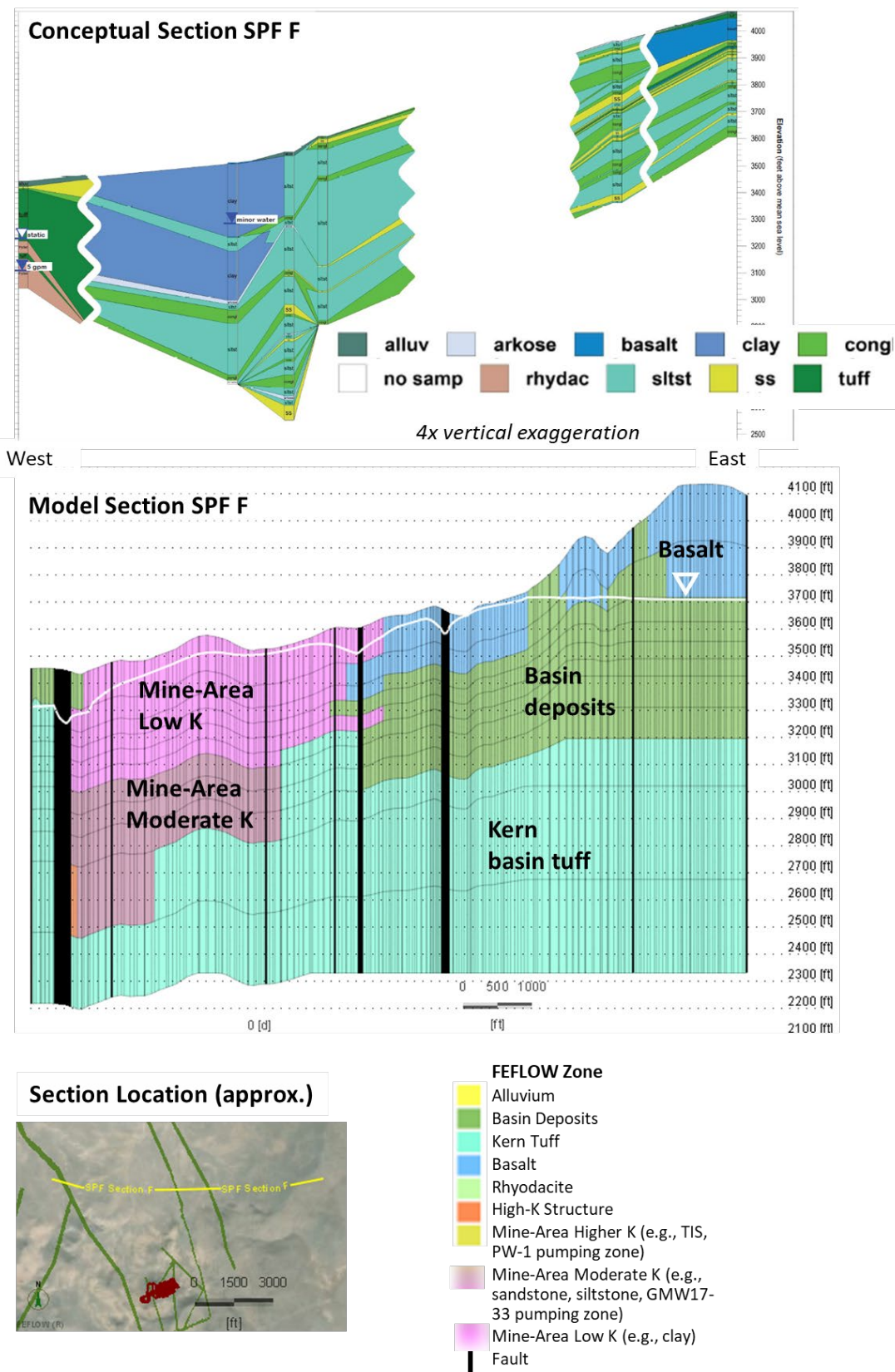


Figure 4-37: Section F (after SPF, 2021c).

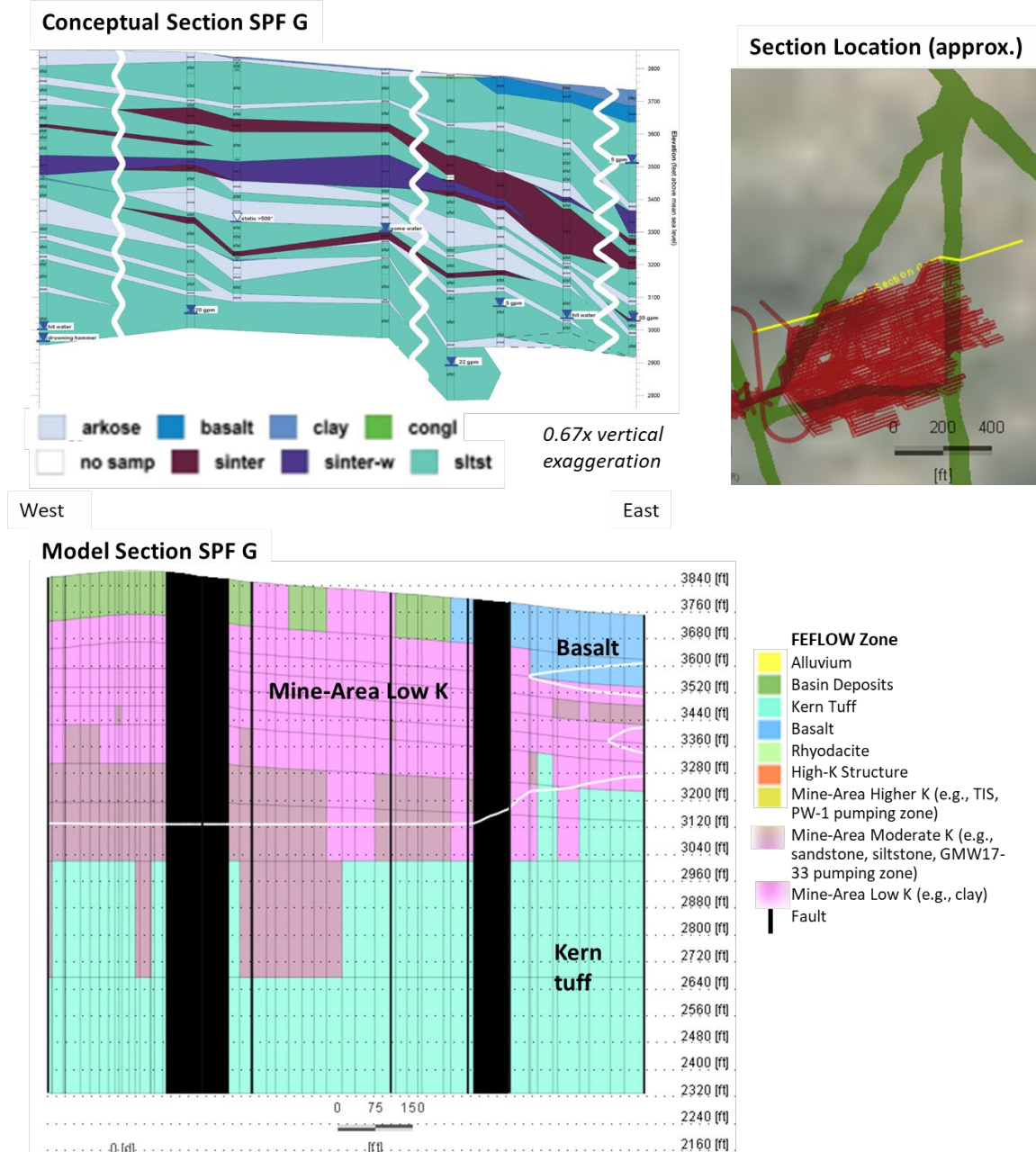


Figure 4-38: Section G (after SPF, 2021c).

4.8.4 Summary of Model Stratigraphy

The numerical model was constructed to honor as much of the available data as possible within the framework of the 11-layer finite element mesh. Regional stratigraphic units—basalt, Kern tuff, and alluvium—were imported to the model mesh. In the mine area, element hydraulic conductivities were assigned based on the borehole lithology and the hydraulic behavior, both in terms of the static water levels and the pumping test response.

The geologic cross-sections (Adrian Brown, 1992, and SPF, 2021c) indicate the high likelihood that considerable anisotropy could exist within the lithologic units, especially in the mine area.

4.9 Storage and Unsaturated Functions

The FEFLOW model was run using a variably saturated configuration. FEFLOW's modified van Genuchten parameterization was used. This formulation makes use of the pressure-saturation relationship of van Genuchten (1980), which is written as follows:

$$S_e = \left(\frac{\theta - \theta_r}{\theta_s - \theta_r} \right) = \left[\frac{1}{1 + (\alpha\psi)^n} \right]^m \quad (1)$$

where S_e is the effective saturation, θ is the volumetric moisture content; θ_s is the volumetric moisture content at the water table ($\theta_s = S_{\text{sat}}\phi$, where S_{sat} is the saturation fraction at zero pressure, and ϕ is the porosity); ψ is the matric pressure head, or the negative pressure head; and θ_r , α , n and m are fitting parameters. The first fitting parameter, θ_r , is called the residual moisture content and denotes a theoretical minimum moisture state. The second fitting parameter, α , is approximately equal to the “air entry pressure head”, the matric head at which a saturated soil begins to desaturate. The other two fitting parameters are exponents. Note that in the conventional use of the van Genuchten parameters, the two exponents, m and n , are usually linked by a relationship. They are not necessarily linked in the FEFLOW modified van Genuchten parameterization.

The FEFLOW's modified van Genuchten hydraulic conductivity relationship differs from that in the van Genuchten (1980) model. The modified van Genuchten relative hydraulic conductivity relationship is as follows:

$$K_r = \left(\frac{\theta - \theta_r}{\theta_s - \theta_r} \right)^\delta = \left[\frac{1}{1 + (\alpha\psi)^n} \right]^{m\delta} \quad (2)$$

where K_r is the relative hydraulic conductivity and δ is an exponent. The decoupling of m and n and the addition of δ adds flexibility to the modified van Genuchten model relative to the van Genuchten (1980) relationship. In addition, the modified relationship does not possess a portion of the pressure-hydraulic conductivity curve in which hydraulic conductivity becomes constant with pressure under very dry conditions.

Figure 4-39 shows the unsaturated functions used in the FEFLOW model. The parameter values are listed in Table 4-6. Table 4-6 includes the unsaturated parameters as well as the specific storage for the materials. The specific storage was calibrated using the pumping test data and set to be conservatively low in areas not influenced by the pumping tests, so as not to underestimate environmental impacts or to overestimate groundwater availability.

**Table 4-6:
Unsaturated Parameters**

Unit	Ss (m ⁻¹)	Poro- sity	Specific Yield (Sy), see text			Modified van Genuchten Parameter			
			20 ft	100 ft	500 ft	α (m ⁻¹)	n	m	δ
Alluvium	1.0E-04	0.25	0.091	0.15	0.19	0.5	1.35	0.26	1
Lacustrine Deposits	1.0E-04	0.3	0.11	0.18	0.23	0.5	1.35	0.26	1
TIS (PW-4 and Prod-1)	1.5E-05	0.15	0.017	0.054	0.092	0.1	1.35	0.26	6
Basin Deposits	1.5E-05	0.15	0.017	0.054	0.092	0.1	1.35	0.26	4
PW-1 Zone	5.0E-06	0.15	0.017	0.054	0.092	0.1	1.35	0.26	4
Kern Tuff	1.0E-06	0.05	0.004	0.014	0.025	0.1	1.25	0.2	2
Basalt, Rhyodacite	5.0E-06	0.01	0.001	0.003	0.005	0.1	1.25	0.2	2
Fault Zones	5.0E-06	0.01	0.001	0.004	0.006	0.1	1.35	0.26	4

Table 4-6 lists three values of the specific yield for each unit. In a saturated-unsaturated formulation of the groundwater flow equations, a unique specific yield value is not used. Instead, FEFLOW computes the amount of water released from storage due to dewatering by integrating the change in the unsaturated moisture state as the water table declines. As a consequence, the specific yield, which equals the amount of water released per unit drop in head, may increase as dewatering progresses. Generally, the specific yield that is sampled during a pumping test can be on the low end of the ultimately available storage release. For instance, in the case of the TIS zone intercepted by PW-1 and Prod-1, the specific yield is 0.017 for a water table decline of 20 ft, 0.054 for a water table decline of 100 ft, and 0.092 for a water table decline of 500 ft. The assumed porosity of this unit is 0.15. As for the specific storage, conservatively low values of the porosity and specific yield were applied to the FEFLOW model.

Due to the uncertainty in the storage properties, the sensitivity analysis included the specific storage—which quantifies confined storage release—and porosity. The porosity was selected as an analogue for the specific yield because the specific yield is proportional to the porosity for a given set of modified van Genuchten parameters.

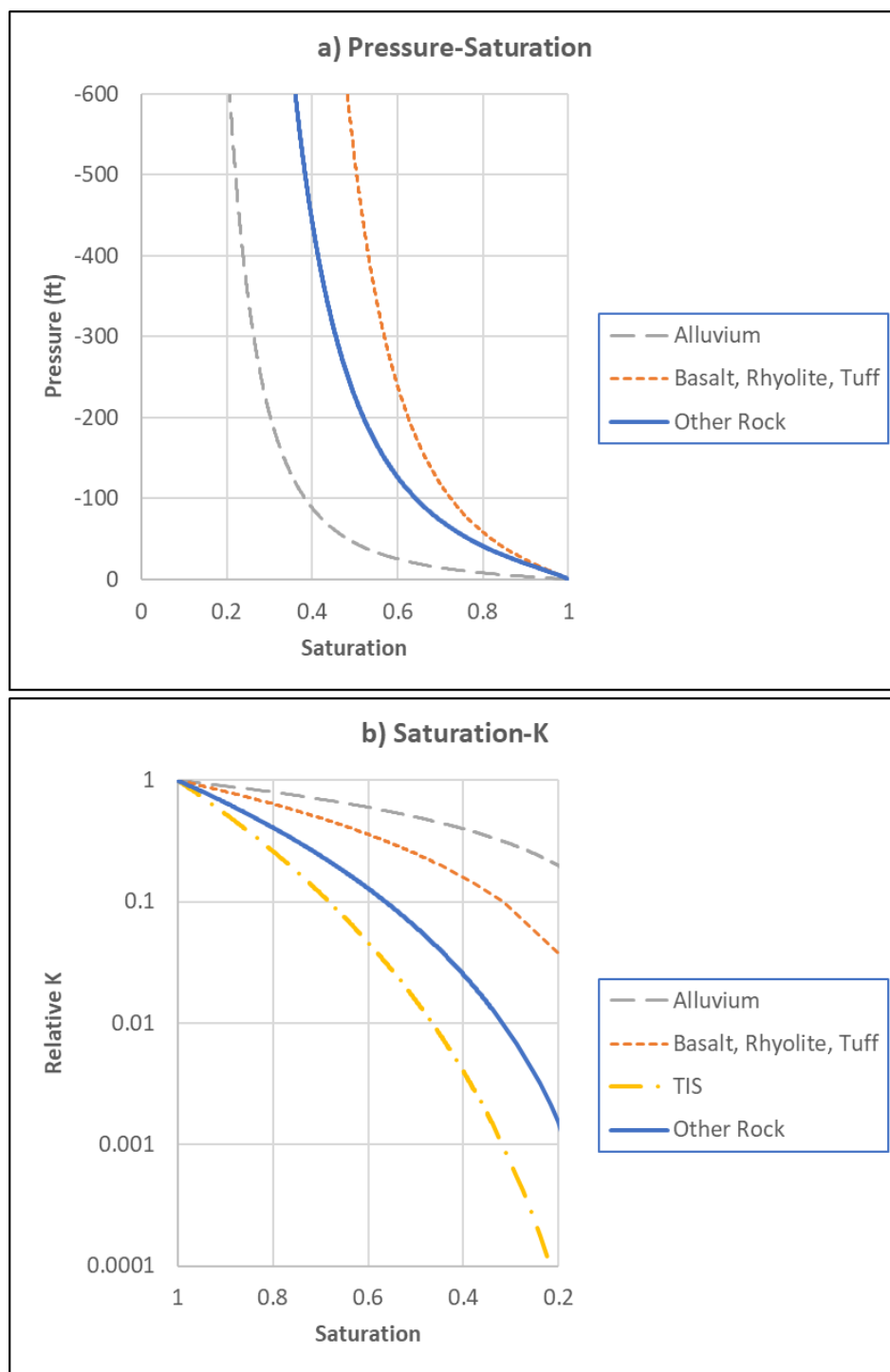


Figure 4-39: Unsaturated Functions.

4.10 Calibration Methodology

A two-step calibration was completed for the Grassy Mountain project. An initial steady state analysis was completed using the head targets listed above in Table 3-2 and Table 3-3 and the spring flows listed in Table 3-1. Of the two types of parameters, the head targets were given precedence.

The second step in the calibration was the simulation of the pumping tests in PW-4, Prod-1, PW-1, and GMW17-33. An assessment of the pumping test at GMW17-32 and 59762 was also completed, but due to the low permeability of these zones, as evidenced by the inability to pump even 1 gpm over one day, the model mesh was not adequate to accurately simulate these tests. Smaller finite element sizes would have been required.

To reduce the computational time, the pumping tests at PW-4 and PW-1 were simulated in the same model run. A second run included the consideration of the other four pumping tests. The pumping was staggered as discussed in Section 4.4.

4.11 Calibration Results

4.11.1 Steady State Heads

Figure 4-40 shows the simulated and observed steady state, pre-mining heads in the calibrated model. The residual mean for all head observation points in the model domain is -7.1 ft, and the absolute residual mean is 23.4 ft. The normalized root mean squared error is 4.1%. When only the 21 calibration targets that are closest to the mine are considered, the residual mean is -12.4 ft, the absolute residual mean is 31.6 ft, and the normalized root mean squared error is 5.8%. Table 4-7 and Table 4-8 list the measured and simulated heads, and the residual, defined to be the simulated head minus the measured head. Table 4-7 and Table 4-8 identify the 20 wells nearest to the mine and the one spring, Deposit Stock Tank, included in the mine-area statistic.

Figure 4-41 plots the head residuals shown in Figure 4-40 as a function of the observed head. There is a slight trend of decreasing residuals with observed head value, especially in the southwestern part of the model domain. In the wells near the mine, even with the barrier faults and the high-permeability structure to reduce heads in the deep wells, the model underestimates the hydraulic gradient, as indicated by the generally lower residuals at higher head elevations. Aside from the mine area—where more significant compartmentalization would have been required to simulate the steep gradients—the residuals do not show a significant bias with groundwater elevation.

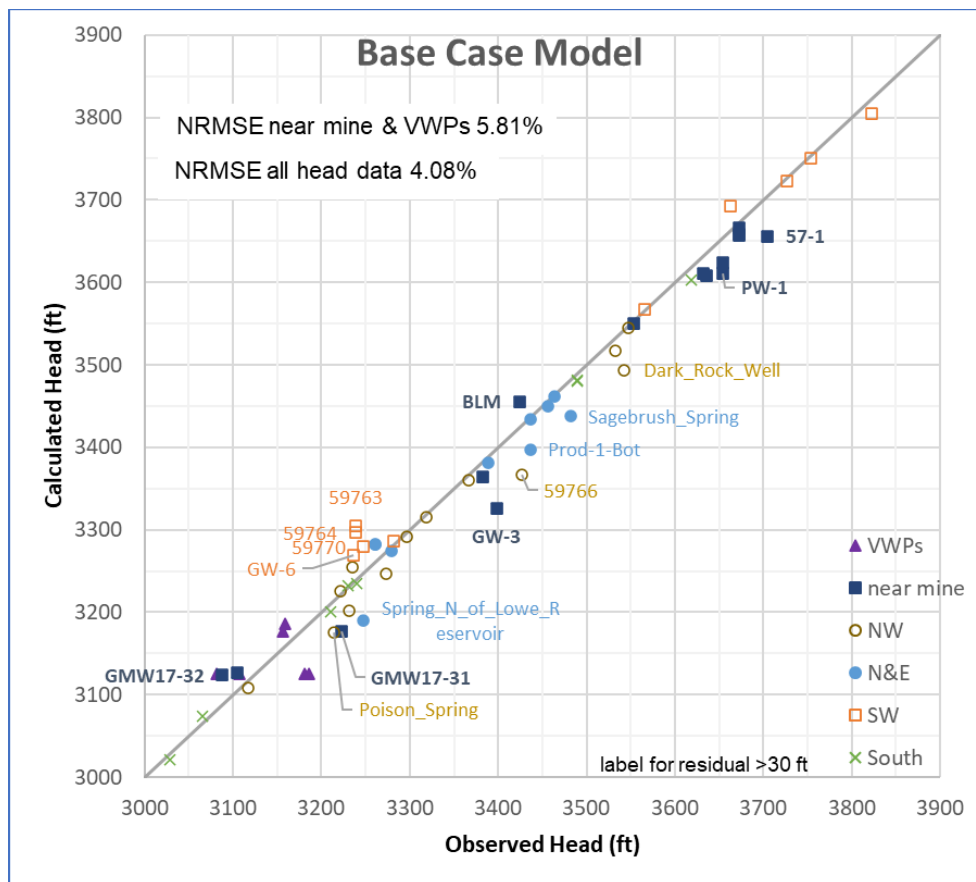


Figure 4-40: Simulated versus Observed Heads.

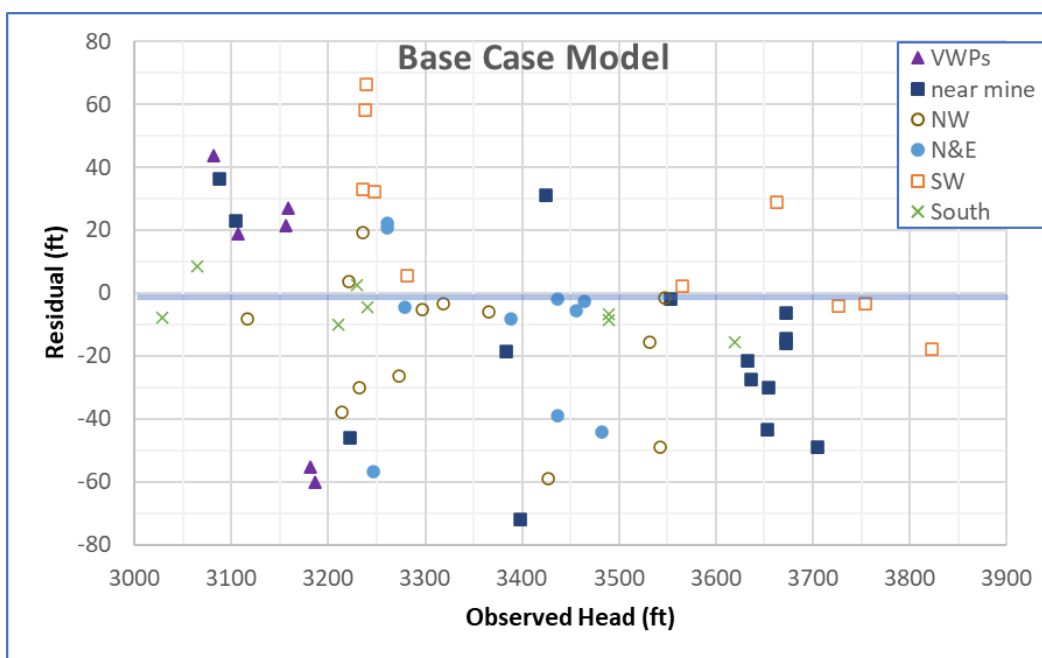


Figure 4-41: Residual versus Observed Heads.

**Table 4-7:
Simulated and Predicted Head, Monitoring Wells**

Well ID	Measured (ft)	Calculated (ft)	Residual (ft)
59760 (mine area)	3672.9	3657.1	-15.8
59761 (mine area)	3672.9	3658.5	-14.5
59762 (mine area)	3104.4	3127.2	22.8
59763	3239.2	3305.3	66.2
59764	3238.3	3296.3	58.0
59765	DRY (<3410)	3299.1	DRY in model
59766	3426.5	3367.5	-59.0
59767	DRY (<3455)	3430.6	DRY in model
59768	3464.2	3461.7	-2.5
59770	3247.8	3279.9	32.1
59772 (mine area)	3673.0	3666.8	-6.2
26-092-915 (mine area)	3632.3	3610.8	-21.5
57-1 (mine area)	3704.7	3655.9	-48.8
57-10 (mine area)	3635.7	3608.2	-27.5
89-2	3235.7	3254.8	19.1
Bishop	3281.4	3287.0	5.6
BLM (mine area)	3424.3	3455.5	31.2
GM17-16-D (mine area)	3081.5	3125.4	43.9
GM17-16-I (mine area)	3181.0	3125.6	-55.4
GM17-16-S	DRY (<3443.6)	3278.3	DRY in model
GM17-20-D (mine area)	3156.0	3177.5	21.5
GM17-20-I (mine area)	3159.0	3186.1	27.1
GM17-20-S	DRY (<3485.3)	3376.5	DRY in model
GM17-21-D	DRY (<3059.1)	3126.0	>67
GM17-21-I (mine area)	3107.0	3126.1	19.1
GM17-21-S	DRY (<3342.9)	3198.5	DRY in model
GM17-28-D	DRY (<3173.8)	3138.7	DRY in model
GM17-28-I	DRY (<3237.6)	3131.6	DRY in model
GM17-28-S	DRY (<3459.1)	3212.5	DRY in model
GM17-30-D	DRY (<3087.9)	3125.7	>38.2
GM17-30-I (mine area)	3186.0	3125.8	-60.2
GM17-30-S	DRY (<3352.9)	3186.8	DRY in model
GMW17-31 (mine area)	3222.6	3176.5	-46.1
GMW17-32 (mine area)	3087.8	3124.1	36.3
GMW17-33 (mine area)	3383.1	3364.6	-18.5
GMW18-34	DRY (<3067)	3190.0	>123.3
GW-1 (mine area)	3654.0	3624.0	-30.0
GW-2	3663.0	3692.0	29.1
GW-3 (mine area)	3398.1	3326.2	-71.9
GW-3A	DRY (<3235)	3193.5	DRY in model
GW-4	3260.8	3282.8	22.0
GW-5	3221.5	3225.1	3.6
GW-6	3236.2	3269.3	33.1
Prod-1-Bot	3436.4	3397.5	-38.9
Prod-1-Top	3436.4	3434.4	-2.0
PW-1 (mine area)	3653.7	3610.4	-43.3
PW-4	3261.4	3282.0	20.7

Table 4-8:
Simulated and Predicted Head, Springs and Regional Artesian Wells

Well ID	Measured (ft)	Calculated (ft)	Residual (ft)
Bull Spring Tank	3727.0	3723.1	-3.9
Central Grassy Mtn Spring	3489.0	3480.4	-8.6
Darky Rock Well	3542.6	3493.6	-49.0
Deposit Stock Tank (mine area)	3552.8	3550.8	-1.9
East Grassy Mtn Spring	3489.0	3482.2	-6.8
Flowing Well at Topo	3532.0	3516.6	-15.4
Government Corral	3456.0	3450.6	-5.4
Grassy Spring	3822.8	3805.0	-17.9
Lowe Spring	3279.0	3274.5	-4.4
Negro Rock Canyon Spring	3117.0	3108.8	-8.2
Negro Rock Spring Tank	3319.0	3315.5	-3.5
Oxbow Spring Tank	3065.0	3073.5	8.5
Oxyoke Spring Tank	3029.0	3021.3	-7.7
Poison Spring	3213.9	3176.0	-37.8
Red Tank 3	3389.0	3380.9	-8.1
Sagebrush Spring	3481.9	3437.8	-44.1
Sourdough Lower	3565.4	3567.6	2.2
Sourdough Upper	3754.1	3750.7	-3.3
Spring N of Lowe Reservoir	3247.0	3190.3	-56.7
Spring S of Poison Spring	3232.0	3202.1	-29.9
Spring Sec23 T21S R43E	3297.0	3291.8	-5.2
Tank E of Negro Rock	3273.0	3246.6	-26.4
Twin Springs North	3240.0	3235.6	-4.4
Twin Springs South	3210.3	3200.3	-10.0
West Grassy Mtn Spring	3619.0	3603.5	-15.5
West Whiskey Spring	3547.0	3545.3	-1.7
Whiskey Spring	3230.0	3232.8	2.7
Wildcat Spring	3366.0	3359.9	-6.1

Figure 4-42 and Figure 4-43 show the approximate water table elevation simulated in the calibrated model for the top of Layer 2 (slice 2) of the FEFLOW model. Figure 4-44 shows the simulated head distribution on other slices in the model. This figure clearly shows the downward vertical gradient at Sourdough and Grassy Mountains, indicating that these are major groundwater recharge zones. The model also shows a change in the local hydraulic gradient above the north structure: at shallow depths, the head distribution is a muted version of the topography, whereas at depth, the heads are depressed following the combination of Zone 71, the North Structure, and Fault #25, the North Fault.

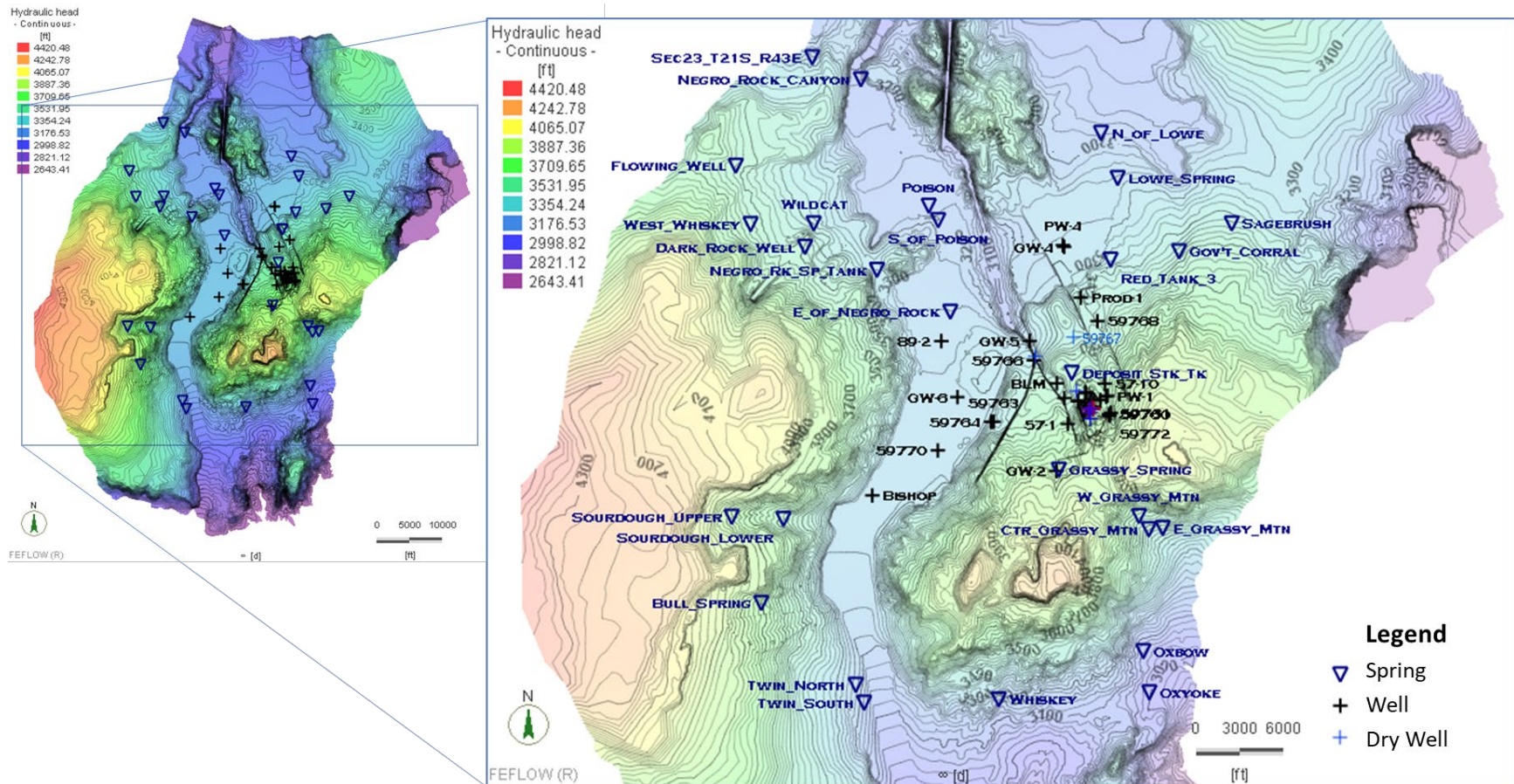


Figure 4-42: Calibrated Piezometric Head, Top of Layer 2, at Approximate Water Table Elevation.

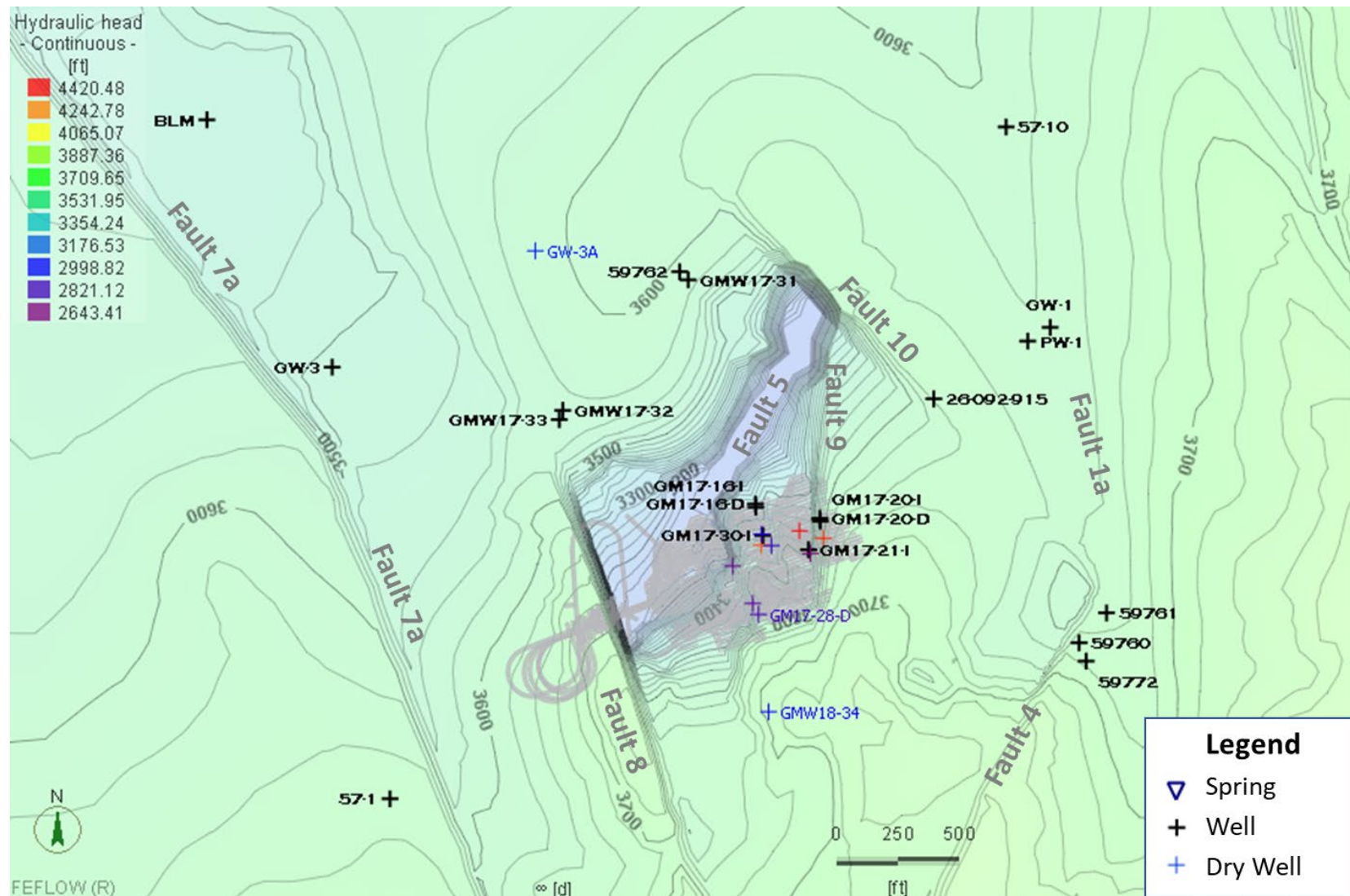


Figure 4-43: Calibrated Piezometric Head, Top of Layer 2, in Mine Area.

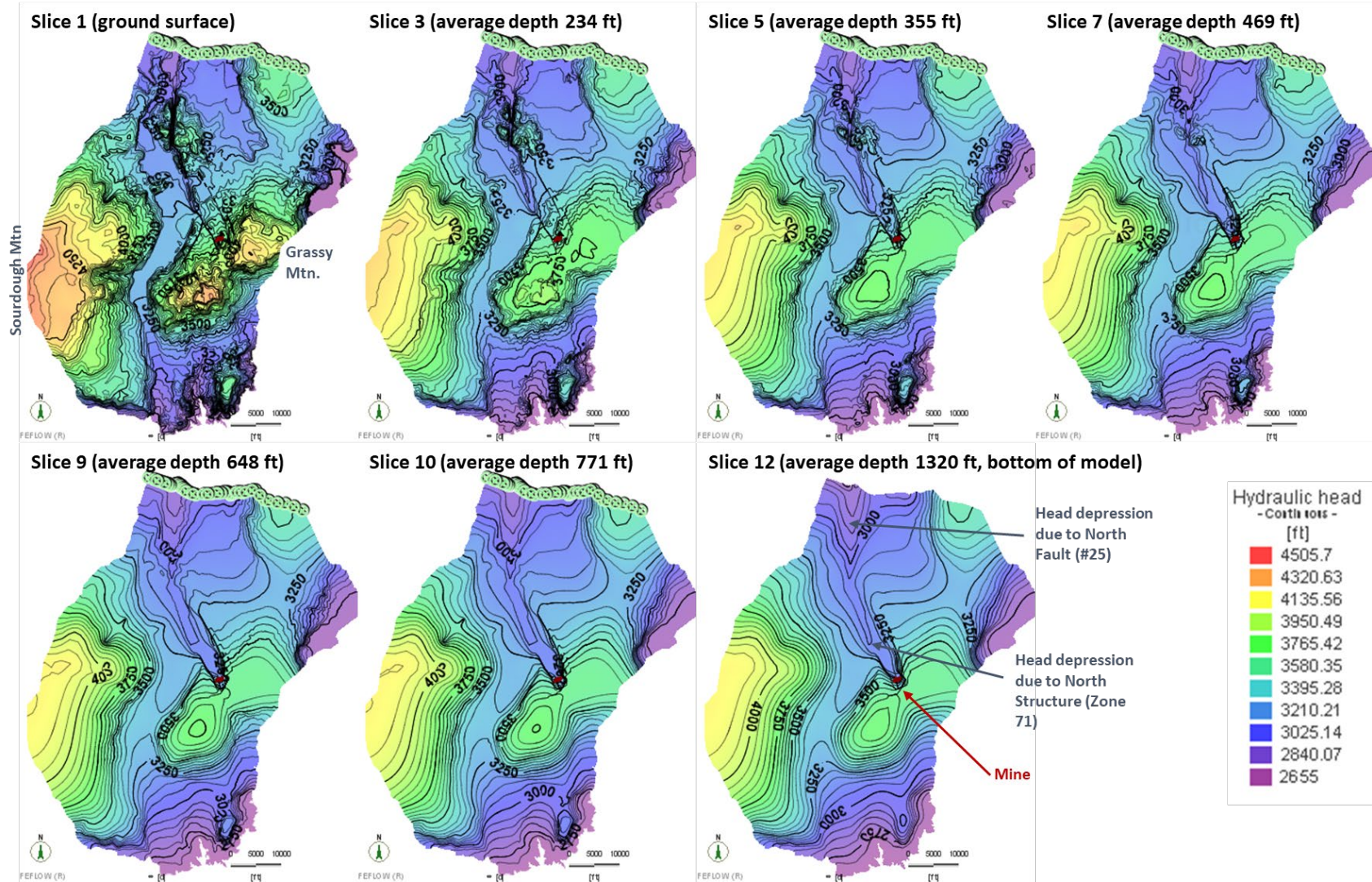


Figure 4-44: Calibrated Piezometric Head, Slices 1, 3, 5, 7, 9, 10 and 12.

4.11.2 Water Balance and Steady State Spring Flow Rates

The model-wide water balance is presented on Table 4-9. Groundwater enters the model at a rate of 2,247 gpm via recharge on the surface. Groundwater exits the model at the Owyhee reservoir (486 gpm) and the north transfer boundary (604 gpm). Sixteen (16) gpm leaves the groundwater model at the springs and artesian wells. The remainder of the groundwater discharge occurs through drain nodes in the streambeds. Of this last quantity, 434 gpm discharges through stream nodes at east edge of the model domain, 234 gpm exits the model domain downstream of the Lowe Spring, 116 gpm discharges to the tributary entering the Owyhee Reservoir from the west, and 70 gpm discharges at Hoodoo Creek in the northwest border of the model. The remaining 288 gpm discharges to internal seepage nodes, mostly to the north part of the Negro Rock Canyon drainage near the model boundary.

**Table 4-9:
Model-Wide Water Balance**

Source	Inflow (gpm)	Outflow (gpm)	Discrepancy (%)
Recharge	2,246.7		
Owyhee Reservoir		485.7	
North Boundary		603.6	
East Boundary, including Oxbow Creek Area		433.8	
Northeast Boundary		234.0	
South Border West of Owyhee Reservoir		115.5	
Northwest Boundary (Hoodoo Creek)		69.9	
Springs and Artesian Wells		16.2	
Other Streams		288.1	
Total	2,246.7	2,246.8	<0.01%

Discharge to individual springs is shown in Figure 4-45 and listed in Table 4-10 and Table 4-11. The model is able to predict the general magnitude of the discharge at Bull Spring Tank, Twin Springs South, Whiskey Spring, Oxbow Spring Tank, and Wildcat Spring. It is also able to simulate zero or nearly zero discharge at Grassy Spring, Lowe Spring, Negro Rock Canyon Spring, Oxyoke Spring Tank, Red Tank #3, the spring North of Lowe Reservoir, the spring South of Poison Spring, the spring in Section 23/T21S/R43E, West Grassy Mountain Spring, and West Whiskey Spring.

The model overestimates groundwater discharge at Sourdough Upper and Lower Springs, Central Grassy Mountain Spring, East Grassy Mountain Spring, and Negro Rock Spring Tank.

The model underestimates the flow at Deposit Stock Tank, Government Corral spring, Prod-1, Poison Spring, Twin Springs North, Darky Rock Well, Flowing Well and the Tank

East of Negro Rock. At Deposit Stock Tank, the model simulates groundwater discharge in the general vicinity of the spring, and more detailed geological information at the spring would lead to a better calibration to spring flows. Although the model simulates some discharge at Government Corral, it is approximately one-third of the recorded flow. At Prod-1, the FEFLOW model underestimates the head (see Table 4-7), and, although the simulated head for the shallow screen of Prod-1 is within 2 ft of ground surface, artesian flow is not simulated. The underestimate of spring discharge at Twin Springs North is similar in magnitude to the overestimate of spring discharge at Twin Springs South, and the simulated total flow at the two springs is similar to the observed value. Additional refinements to the model in this area would help with the flow calibration at Twin Springs.

At Poison Spring and the Tank East of Negro Rock, the lack of groundwater discharge is due to the proximity of the highly permeable alluvial deposits in the area of these springs. Reconfiguring the properties of the alluvium in this area or adjusting the width of the alluvial channel would help with the calibration here. Darky Rock Well is a relatively shallow artesian well located in the northwestern area of the model, where the conceptual model has assigned shallow Kern tuff. Nearby artesian well Flowing Well also has more observed flow than the model is able to simulate. The calibration of flow at this location is complicated by uncertainty in the location of the well screen. The mechanism by which more than 10 gpm of groundwater discharges at Darky Rock Well and 7 gpm discharges at Flowing Well are not clear. However, both are background wells and are not in the area of influence of the mine, as discussed in Section 5.

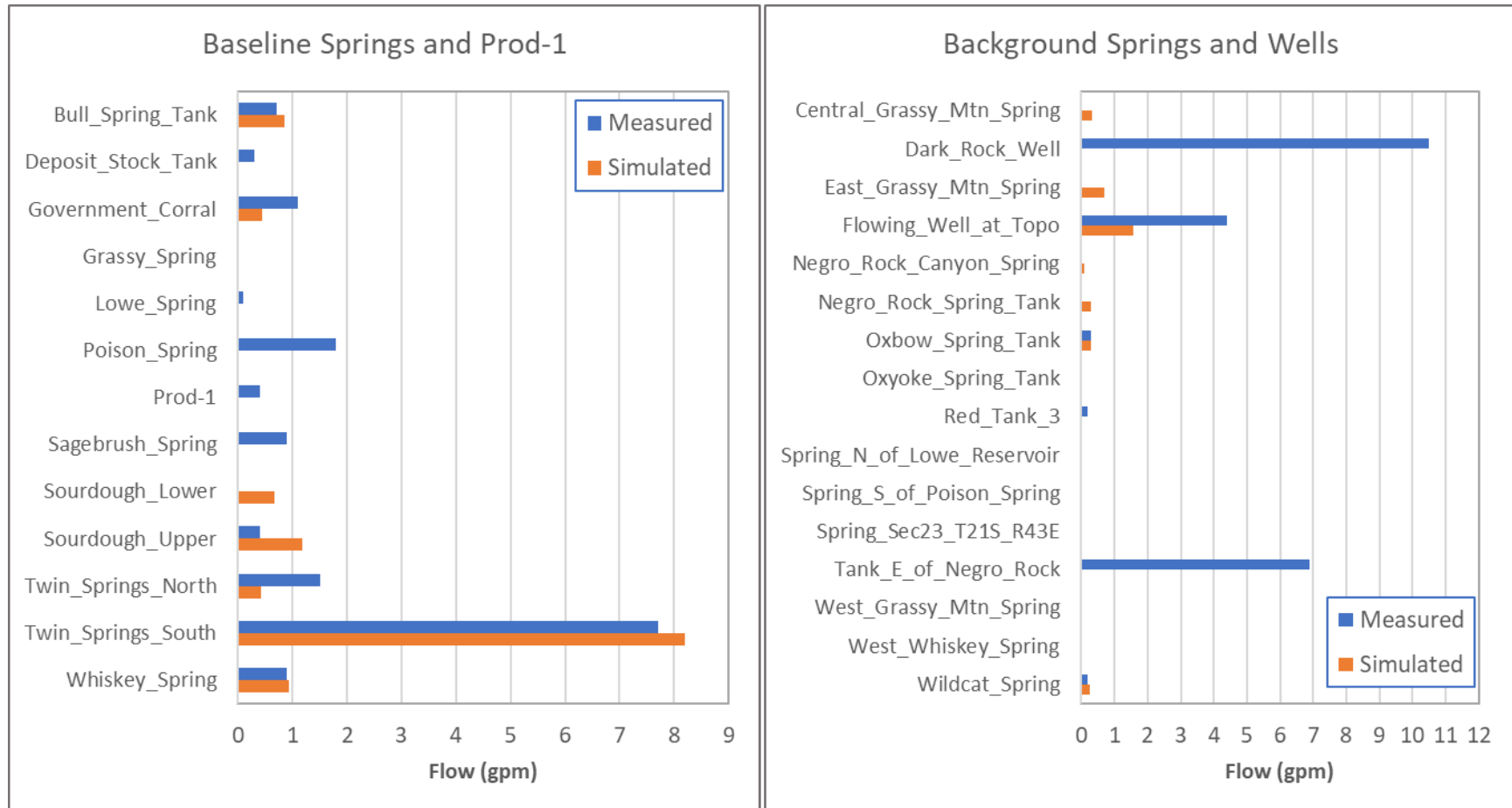


Figure 4-45: Measured and Simulated Spring and Artesian Well Discharge.

**Table 4-10:
Simulated and Predicted Flow, Baseline Springs and Artesian Wells**

Well ID	Measured (gpm)	Calculated (gpm)	Residual (gpm)
Bull_Spring_Tank	0.7	0.8	0.1
Deposit Stock Tank	0.3	0.0	-0.3
Government Corral	1.1	0.4	-0.7
Grassy Spring	0.0	0.0	0.0
Lowe_Spring	0.1	0.0	-0.1
Poison Spring	1.8	0.0	-1.8
Prod-1	0.4	0.0	-0.4
Sagebrush Spring	0.9	0.0	-0.9
Sourdough_Lower	0.0	0.7	0.7
Sourdough_Upper	0.4	1.2	0.8
Twin_Springs_North	1.5	0.4	-1.1
Twin_Springs_South	7.7	8.2	0.5
Whiskey_Spring	0.9	0.9	0.0

**Table 4-11:
Simulated and Predicted Flow, Background Springs and Artesian Wells**

Well ID	Measured (gpm)	Calculated (gpm)	Residual (gpm)
Central Grassy Mtn Spring	0.0	0.3	0.3
Dark Rock Well	10.5	0.0	-10.5
East Grassy Mtn Spring	0.0	0.7	0.7
Flowing Well at Topo	4.4	1.6	-2.8
Negro Rock Canyon Spring	0.0	0.1	0.1
Negro Rock Spring Tank	0.0	0.3	0.3
Oxbow Spring Tank	0.3	0.3	0.0
Oxyoke Spring Tank	0.0	0.0	0.0
Red Tank 3	0.2	0.0	-0.2
Spring_N_of_Lowe_Reservoir	0.0	0.0	0.0
Spring_S_of_Poison_Spring	0.0	0.0	0.0
Spring_Sec23_T21S_R43E	0.0	0.0	0.0
Tank E of Negro Rock	6.9	0.0	-6.9
West Grassy Mtn Spring	0.0	0.0	0.0
West Whiskey Spring	0.0	0.0	0.0
Wildcat Spring	0.2	0.3	0.1

4.11.3 Pumping Test Calibration

Figure 4-46 and Figure 4-47 present the predicted drawdowns for the pumping tests. Figure 4-46 shows the pumping test simulation for the tests in the most permeable strata in the mine area. These two tests, PW-4, and Prod-1, are located in the TIS sandstone and conglomerate zone of the numerical model. Both of the pumping wells and the observation well GW-4 are located in hydrostratigraphic zones that were assigned the same hydraulic properties. The base model matches the magnitude of the drawdown at observation well GW-4. At the pumping wells, the model overestimates the drawdown at PW-4 and underestimates the drawdown at Prod-1. Prod-1 is a narrow-diameter well (see Table 4-1) and it is expected that there could be well losses in this well during pumping of 100 gpm. The calibrated model underpredicts the observed drawdown at Prod-1 by approximately 40 ft. At PW-4, the model overestimates the drawdown by approximately 20 ft. The calibration target for the pumping test was the observation well, GW-4, and these parameters were retained in the simulation because the hydraulic conductivity used will tend to overestimate the drawdown from a future production well in the PW-4 area. It will therefore tend to lead to a conservative impact prediction. Looking at the temporal signature, the model may overestimate the storage at these wells due to the slower simulated drawdown and recovery compared to the data. The storage properties of the TIS zone were examined in the sensitivity analysis (Section 4.12).

Figure 4-47 presents the numerical model simulation of the pumping tests in the two moderate-permeability mine area tests, at PW-1 and GMW17-33. At both locations, the model is able to simulate the general magnitude of the drawdown. At PW-1 and GW-1, the model slightly overestimates the drawdown at the end of the test, and in the case of PW-1, underestimates the speed of the recovery. Therefore, it is expected that the model will overestimate drawdown in the area southeast of the mine. The calibration parameters will therefore tend to lead to a conservative impact prediction in the PW-1 area. At GMW17-33, the model is able to simulate the general magnitude of the drawdown. Although it does not simulate the peak drawdown of 90 ft that occurred before the pumping rates at this well were reduced (see Section 3.5.2), the model captures the general shape of the drawdown during the recovery period.

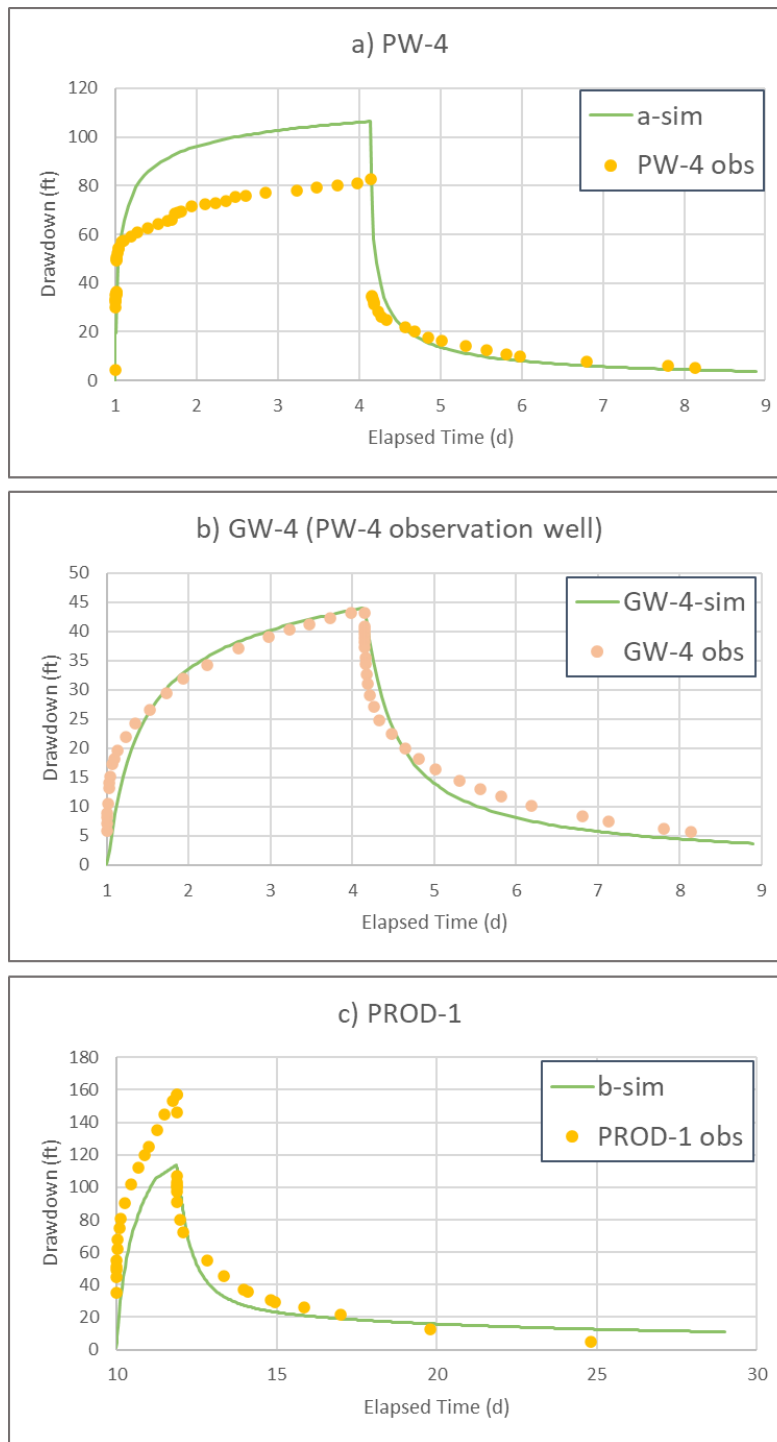


Figure 4-46: TIS Zone Pumping Test Calibration – PW-4 and Prod-1.

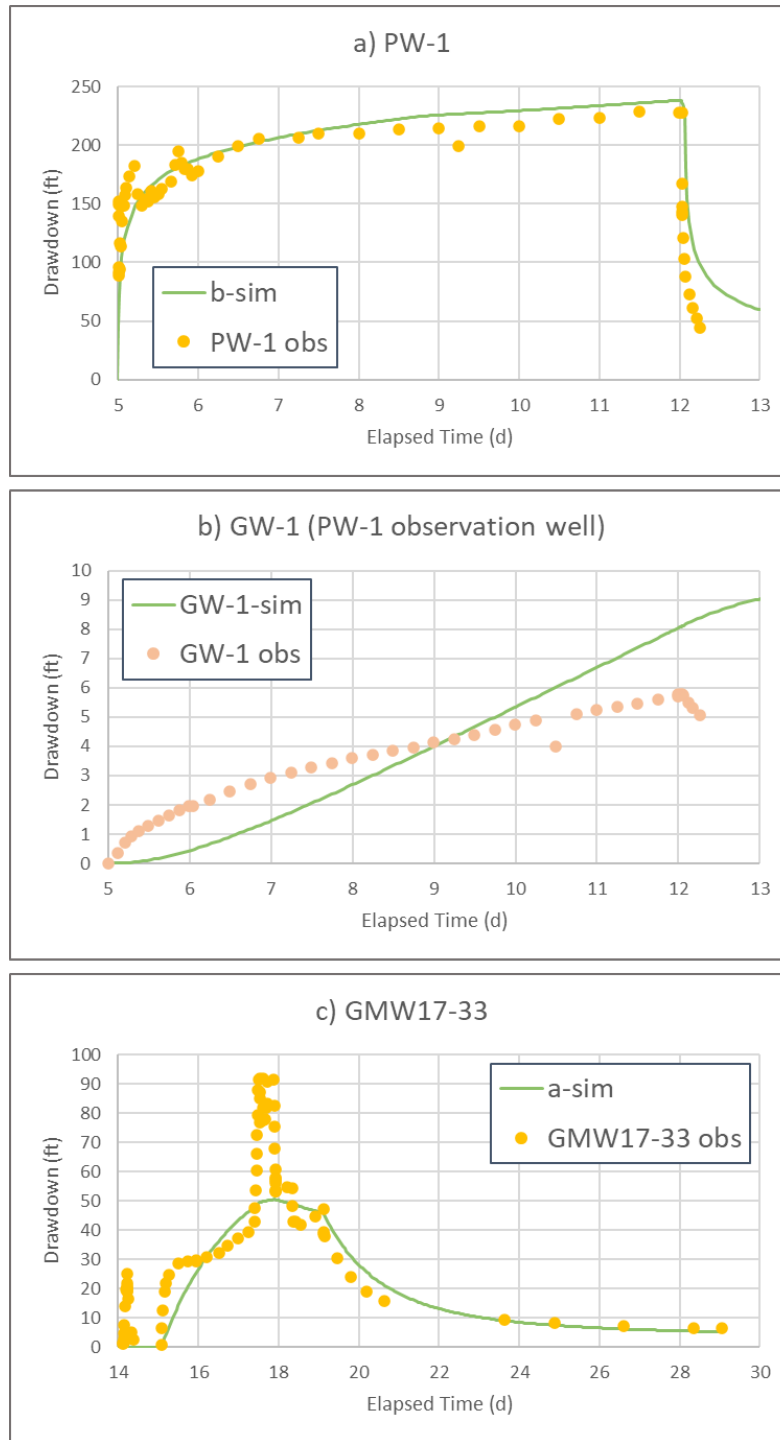


Figure 4-47: Mine-Area Sandstone Pumping Test Calibration – PW-1 and GMW17-33.

4.11.4 Calibrated Parameters

The calibrated hydraulic conductivities for the bulk bedrock and soil zones are listed in Table 4-12 and displayed in Figure 4-48. The units are listed with the shallowest units

shown first, down to the deepest unit, the Kern tuff, listed at the bottom. The highest hydraulic conductivities are assigned to the thicker alluvial deposits and the structure defined to lower the hydraulic heads at depth in the mine area. The lowest hydraulic conductivity was assigned to the clay, Zone 91.

**Table 4-12:
Calibrated Hydraulic Conductivity of Hydrogeological Units**

Unit	Kh (m/s)	Kv (m/s)	Kh/Kv
11-Thick Alluvium	1.00E-04	5.00E-05	2
12-Lacustrine	5.15E-09	1.67E-09	3.1
13-Thinner Alluvium	5.93E-07	5.93E-09	100
51-Basalt	2.86E-09	1.39E-09	2.0
52-Tbou	5.08E-09	5.08E-09	1
92-Clay in Layer 1	5.62E-09	5.62E-09	1
91-Clay	4.63E-10	3.71E-11	12
72-PW-4 Zone	3.60E-06	9.00E-08	40
73-Prod-1 Zone	3.60E-06	9.00E-08	40
74-PW-1 Zone	7.50E-07	7.50E-07	1
31-Basin Deposits	2.50E-07	2.50E-09	100
81-Siltstone	8.70E-09	2.37E-10	37
82-GMW17-33 zone	1.35E-05	9.05E-07	15
83-GMW17-32 zone	1.00E-07	1.00E-08	10
71-North Structure	5.00E-05	5.00E-05	1
61-Rhyodacite	1.57E-08	1.35E-09	12
41-Kern Tuff	4.57E-09	1.39E-09	3.3

The majority of stratigraphic units have some anisotropy. The isotropic units are the Layer 1 clay (Zone 92), the PW-1 pumping test zone (Zone 74), the structure defined to depress the water table in the mine area (Zone 71), and Zone 52 (the Tbu basalt zones at Sourdough Mountain and in the Government Corral spring area). All other zones have some anisotropy, ranging from a value of between 2 for the thick alluvial deposits, to 100 for the thinner alluvium and the basin deposits. The units with the highest anisotropy are expected to contain sediment layers with a range of permeabilities, and the low vertical hydraulic conductivity acts to simulate the presence of fine-grained strata within these units.

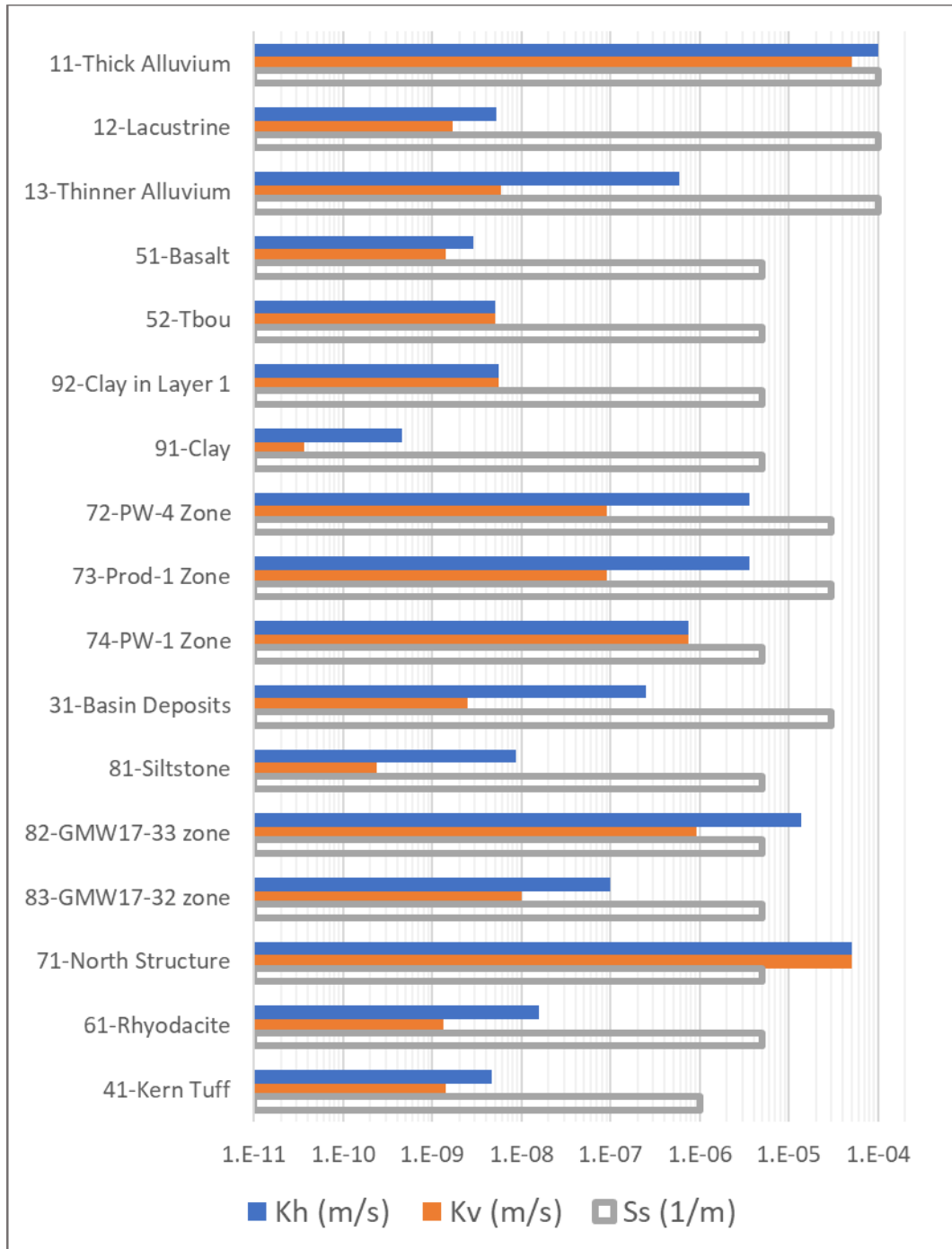


Figure 4-48: Calibrated Hydraulic Conductivity and Specific Storage of Hydrogeological Units.

Table 4-13 and Figure 4-49 show the calibrated hydraulic conductivity of the fault zones. The faults are listed in numerical order. The most permeable fault zones are the North Fault, which in conjunction with Zone 71 acts to reduce the head in the deep mine area

(Figure 4-24). The short fault connecting the alluvial zone with monitoring wells 59763 and 59764 also has a high hydraulic conductivity. The lowest hydraulic conductivity is present in faults in and around the mine area, especially Fault #31, located south of the mine. Approximately half of the fault zones are isotropic, and the rest have generally low anisotropy ratios that are less than 10. The fault zones with highest anisotropy ratios are the two Grassy Mountain Faults (#1 and #2) and the fault in the northwest near Wildcat Spring.

Table 4-13:
Calibrated Hydraulic Conductivity of Fault Zones

Fault Zone	K_{parallel} (m/s)	K_{perpendicular} (m/s)	Kh/Kv
1-Grassy Mtn Fault W	3.05E-08	6.70E-10	45
2-Grassy Mtn Fault E	3.05E-08	6.70E-10	45
1a-Grassy Mtn Fault W-South	7.20E-08	3.60E-08	2
4-SW-NE Fault 2	2.00E-10	2.00E-10	1
5-SW-NE Fault 3	6.28E-06	6.28E-06	1
7-SE-NW Fault 4	1.76E-05	1.76E-05	1
7a-SE-NW Fault 4 South	1.45E-08	1.15E-09	13
8-Mine NS Fault 1	5.00E-10	5.00E-11	10
9-Mine NS Fault 2	2.40E-09	2.40E-09	1
10-Mine NS Fault 3	2.00E-10	5.00E-11	4
11-Mine EW Fault 1	4.15E-08	4.15E-08	1
12-EW Near Grassy Spring	6.59E-10	1.00E-10	6.6
13-NS Near Grassy Spring	5.00E-10	5.00E-10	1
14-SW-NE Fault 5	1.05E-08	1.31E-09	8
15-SW-NE Fault 5	6.80E-06	3.73E-07	18
19-Near Wildcat Spring	8.71E-06	8.71E-08	100
25-North Fault	5.00E-05	5.00E-05	1
30-For 59763-4	5.00E-05	5.00E-05	1
31-Mine EW Fault 2	1.00E-10	5.00E-11	2

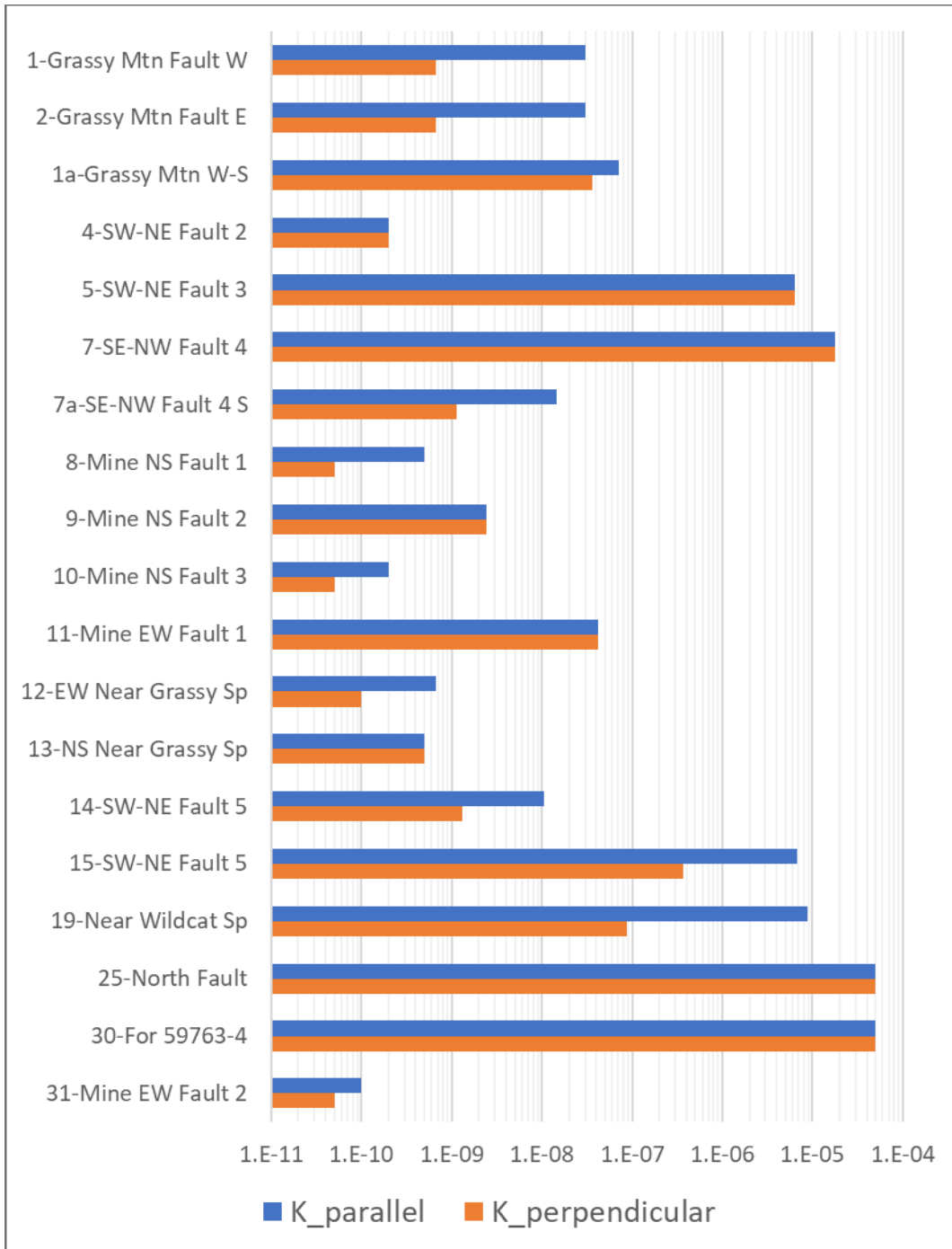


Figure 4-49: Calibrated Hydraulic Conductivity of Fault Zones.

4.12 Sensitivity Analysis

4.12.1 Introduction

A sensitivity analysis was completed on the numerical model to determine the importance of key parameters on the calibration and the predictions of the model. Table 4-14 lists the runs completed. A full list of the parameters is presented in Appendix I – Sensitivity Analysis Parameter Tables. The sensitivity runs are designed to yield a prediction of more drawdown impacts due to mining. Two runs were evaluated on the storage properties, because a lower storage results in more drawdown during mine operations but predicts a more rapid recovery of water levels after closure than the base case model. Conversely, a high storage model would predict smaller drawdown impacts but a longer period of water level recovery after mining. The sensitivity runs include parameter sets that predict higher mine inflows as well as some that predict lower mine inflows.

**Table 4-14:
Sensitivity Runs**

Run	Description	Parameter Changes
1	Reduce Zone 71 (North Structure) K	Zone 71 K \times 0.1
2	Raise K of Barrier Faults	Barrier Fault K \times 50
3a	Reduce storage	All Ss \times 0.4 All Porosity \times 0.5, except lacustrine sediments, which have Porosity \times 0.42
3b	Increase Storage	All Ss \times 1.5 All Rock Porosity \times 1.5
4	Reduce Recharge	Recharge \times 0.75
5	Raise Clay/Siltstone K	Zone 81 K \times 10 Zone 91 K \times 10 Zone 92 K \times 10
6	Raise Basin Deposit K	Zone 31 K \times 2
7	Reduce Transfer Coefficient	Transfer Rate Coefficient \times 0.001

4.12.2 Steady State Calibration

The steady state calibration statistics of the sensitivity runs are presented in Figure 4-50, Figure 4-51, and Table 4-15. Three of the sensitivity runs have steady state statistics that are similar to the base case. These are:

- Sens 3a and Sens 3b on the storage properties. These runs are slightly different from the base case because the porosity that was altered to simulate a change in the

specific yield has a minor effect on the water table elevation due to unsaturated flow

- Sens 7 on the transfer rate coefficient of the northern boundary. This transfer rate coefficient controls the amount of groundwater that exits at the north model boundary but does not have a noticeable influence on the heads at the head calibration points.

One of the sensitivity runs, Sens1, has a generally higher piezometric surface than the base case. In this run, the hydraulic conductivity of the North Structure that reduces the heads in the deep mine-area piezometers was reduced. The reduction in permeability of the North Structure has a minor influence on the heads in shallow wells in the model domain but significantly increases the head at wells 59762, GMW17-32 and the VWP.

The other four sensitivity runs have generally lower piezometric heads than the base case model. These runs are:

- Sens 2, in which the hydraulic conductivity of all of the barrier faults was increased
- Sens 4, in which the recharge rate was reduced
- Sens 5, in which the mine-area clay and siltstone hydraulic conductivity was increased
- Sens 6, in which the hydraulic conductivity of the regional basin deposits, including the Grassy Mountain Foundation, was increased.

None of the sensitivity models had a *significantly* better steady state calibration than the base case model. However, Sens 7, in which the groundwater throughflow at the north boundary was reduced, has a slightly better steady state calibration, with a residual mean of -6.8 feet, compared to -7.1 feet in the base case model.



Figure 4-50: Sensitivity Run Steady State NRMSE and Residual Mean.

Table 4-15:
Sensitivity Run Calibration Statistics

Model	Description	Residual Mean (ft), All Data	MAE (ft), All Data	NRMSE (%), All Data	Residual Mean (ft), Mine Area	MAE (ft), Mine Area	NRMSE (%), Mine Area
Base Case		-7.1	23.4	4.1%	-12.4	32	5.8%
Sens 1	Reduce north structure K	7.4	27.6	5.4%	24.7	42	9.1%
Sens 2	Raise barrier fault K	-27.3	53.4	10.2%	-48.7	98	17.9%
Sens 3a	Reduce storage	-7.1	23.4	4.1%	-12.4	32	5.8%
Sens 3b	Raise storage	-7.1	23.4	4.1%	-12.4	32	5.8%
Sens 4	Reduce recharge	-45.4	48.2	8.5%	-72.4	73	13.6%
Sens 5	Raise clay, siltstone K	-14.9	31.0	5.5%	-31.3	50	9.4%
Sens 6	Raise Grassy Mtn Fm K	-34.8	56.3	9.8%	-46.9	79	15.1%
Sens 7	Reduce N Transfer coefficient	-6.8	23.3	4.1%	-12.1	32	5.8%

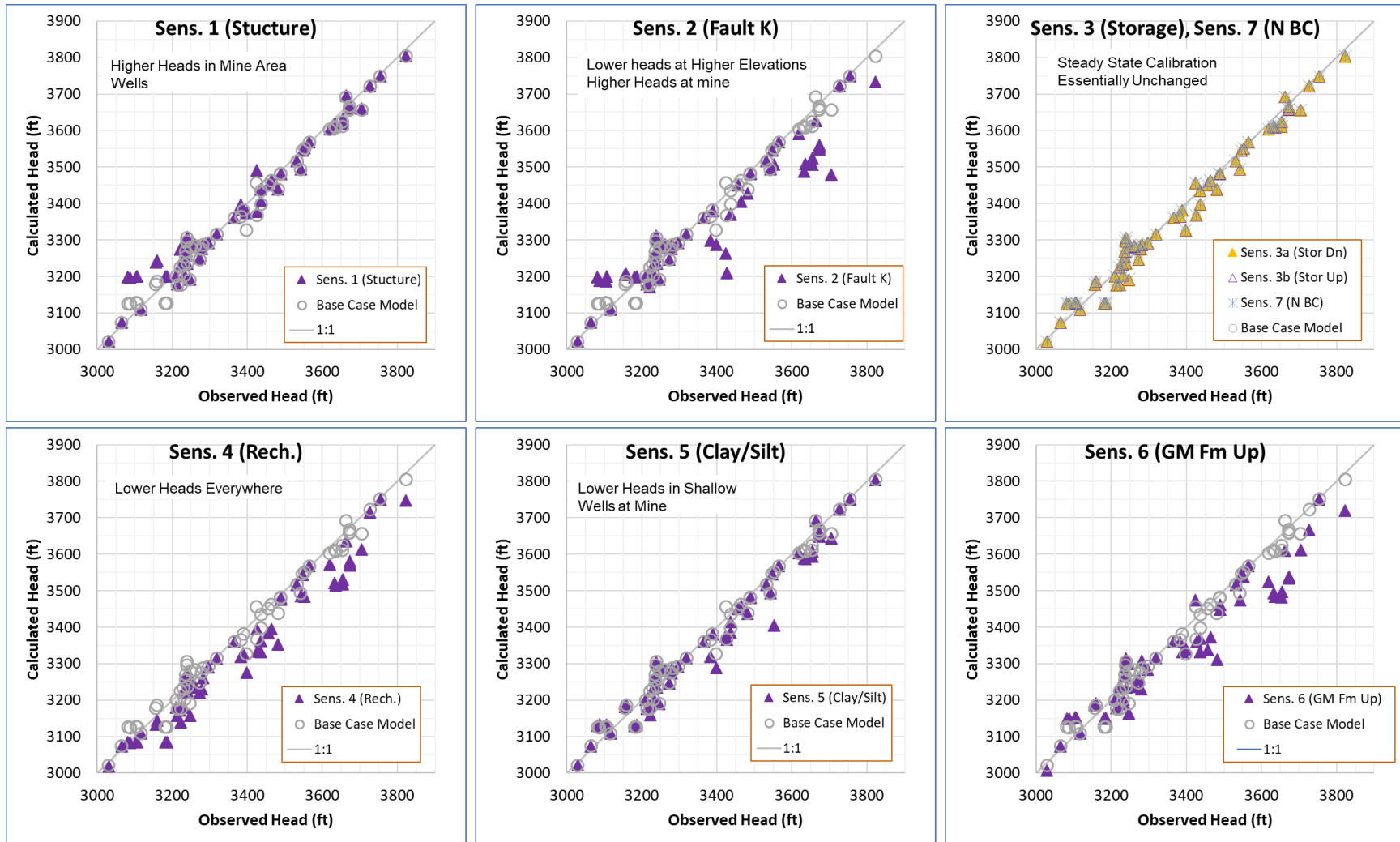


Figure 4-51: Sensitivity Run Steady State Calibration Statistics.

A comparison of the predicted flow to springs from the sensitivity analysis is presented in Figure 4-52 and Figure 4-53. In some of the simulations, notably Sens 4, with lower recharge, and Sens 6, with a higher hydraulic conductivity applied to the regional basin deposit, the simulated spring flows were lower than the base case value. Except for these, the flows were similar to the base case model.

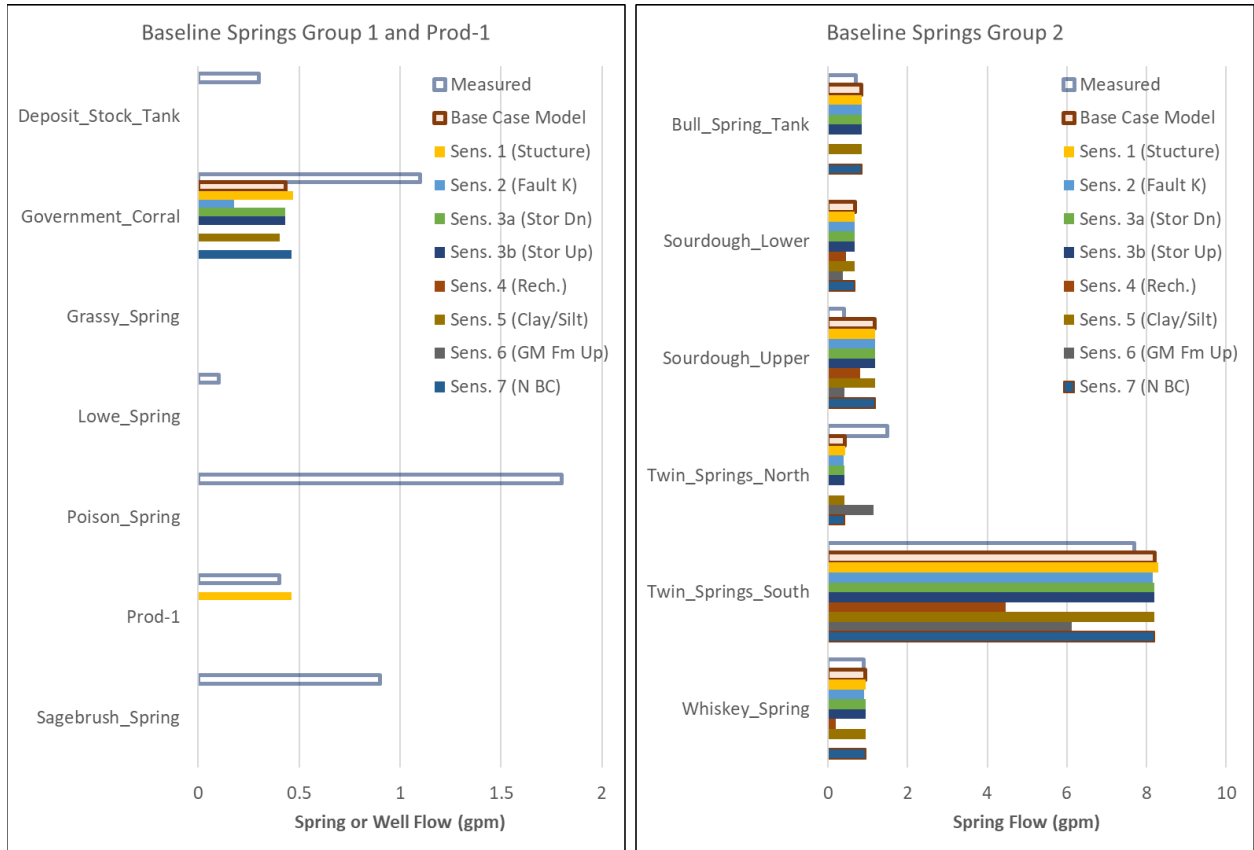


Figure 4-52: Baseline Spring and Well Flow – Sensitivity Runs

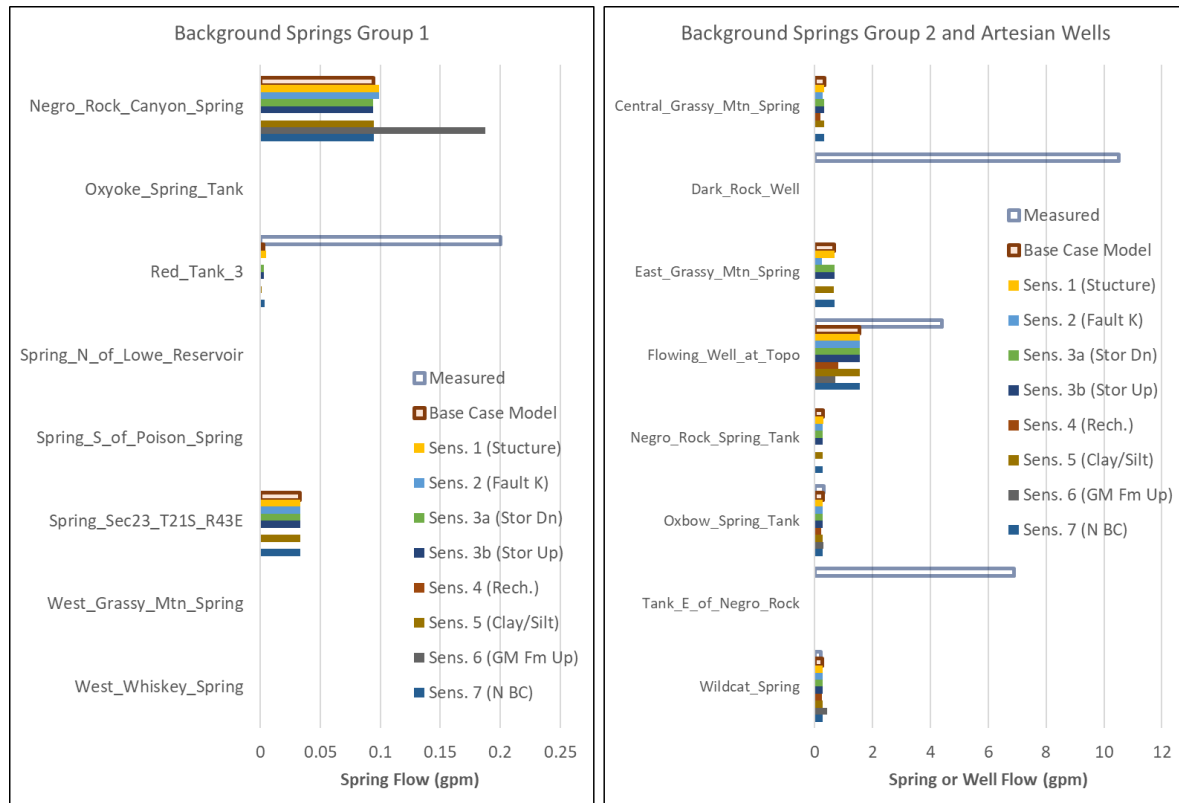


Figure 4-53: Background Spring and Well Flow – Sensitivity Runs

4.12.3 Transient Calibration

The pumping test calibration for the sensitivity runs is presented in Figure 4-54 and Figure 4-55. Figure 4-54a and Figure 4-54b show that most of the sensitivity runs had no influence on the simulated behavior during the PW-4 pumping test. Specifically, the following parameter changes did not influence the predicted drawdown at either the pumping well, PW-4, or the observation well, GW-4:

- S1, in which the North Structure (Zone 71) hydraulic conductivity was reduced to illustrate the importance of this zone in the steady state calibration (see Figure 4-50);
- S2, in which the hydraulic conductivity of all barrier faults was increased to reduce the compartmentalization of the groundwater flow field;
- S4, in which the recharge rate was reduced;
- S5, in which the mine-area clay and siltstone hydraulic conductivity was increased, again to reduce the compartmentalization of the flow field;
- S6, in which the basin deposits, including the Grassy Mountain Formation, was simulated as a more permeable material; and

- S7, in which the transfer rate coefficient at the north model boundary was reduced to reduce the groundwater discharge at this border.

The two sensitivity runs that influenced the PW-4 pumping test result are:

- **S3a:** In S3a, the specific storage coefficient and effective specific yield of all units in the model was reduced. This results in an increase in the simulated drawdown for both wells. The shape of the drawdown curve at GW-4 is somewhat better than in the base case model, so lower storage coefficients could be preferred. However, the lower storage coefficients would have to be assigned in conjunction with a higher hydraulic conductivity, and it is not anticipated that the model predictions will change significantly.
- **S3b:** In this run, the specific storage coefficient of all units was increased, and the effective specific yield of all rock units was increased. This run predicts lower drawdowns at both locations and yields a flatter drawdown and recovery curve than the observed data.

Figure 4-54c presents the simulated result for Prod-1 for the sensitivity analysis. Prod-1 is screened in two zones of sandstone-and-conglomerate (TIS) simulated as Zone 73 in the model (see Figure 4-18, Figure 4-19, Figure 4-20, and Figure 4-29). In addition, the artesian well is located between the two Grassy Mountain Faults (#1 and #2). As a result, the predicted drawdown is influenced by the hydraulic conductivity of the barrier faults (tested in Run S2), the tailings area clay (Zone 91, test in Run S5), the underlying basin deposits (Zone 31, tested in Run S6), the strength of the Zone 71 Structure (Run S1), and the recharge rate (Run S4). The Prod-1 pumping test drawdown is also affected by the storage coefficients, as shown in Figure 4-54c. The only parameter that does not influence the simulated Prod-1 pumping test is the conductance of the north boundary condition (Run S7).

Figure 4-55 presents the results of the sensitivity analysis on the PW-1 pumping test. As indicated in the charts in Section 3.5.2, the drawdown in the pumping well, PW-1, is the highest recorded drawdown, 230 ft, in any mine area pumping test. By contrast, nearby observation well GW-1 has minor drawdown of up to 6 ft. The base case water level at PW-1 is 3610.4 ft (Table 3-2). The bottom of the lower screen at this well is 3298 ft (SPF, 2021a). Therefore, the maximum allowable drawdown is on the order of 310 ft. In some of the sensitivity runs—S2 with higher hydraulic conductivity in the barrier faults, S4 with lower recharge, and S6 with a higher Grassy Mountain formation hydraulic conductivity—the initial water table is depressed (see Figure 4-51). In these three runs, the piezometric head in PW-1 drops below the well screen at some point in the pumping test, and the simulated drawdown is erratic (see Figure 4-55c). All of the runs in Figure 4-55c and the

corresponding observation well drawdowns in Figure 4-55d are not reasonable simulations because the parameters do not permit the pumping of PW-1 as specified in the well boundary conditions. Of the remaining sensitivity runs, in which PW-1 does not go dry, only the two simulations with higher and lower storage properties have an influence on the drawdown predictions, as shown in Figure 4-55a and Figure 4-55b.

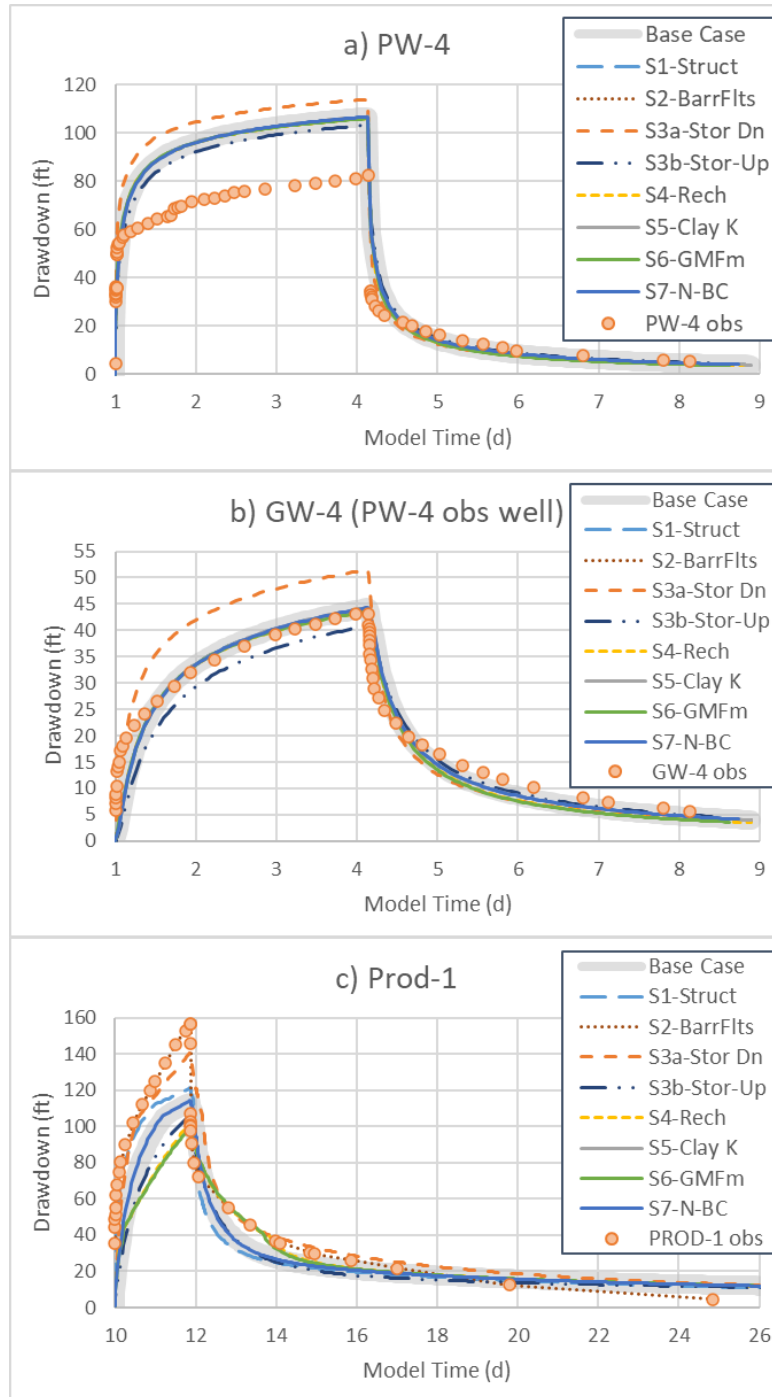


Figure 4-54: TIS Zone Pumping Test Calibration – Sensitivity Runs

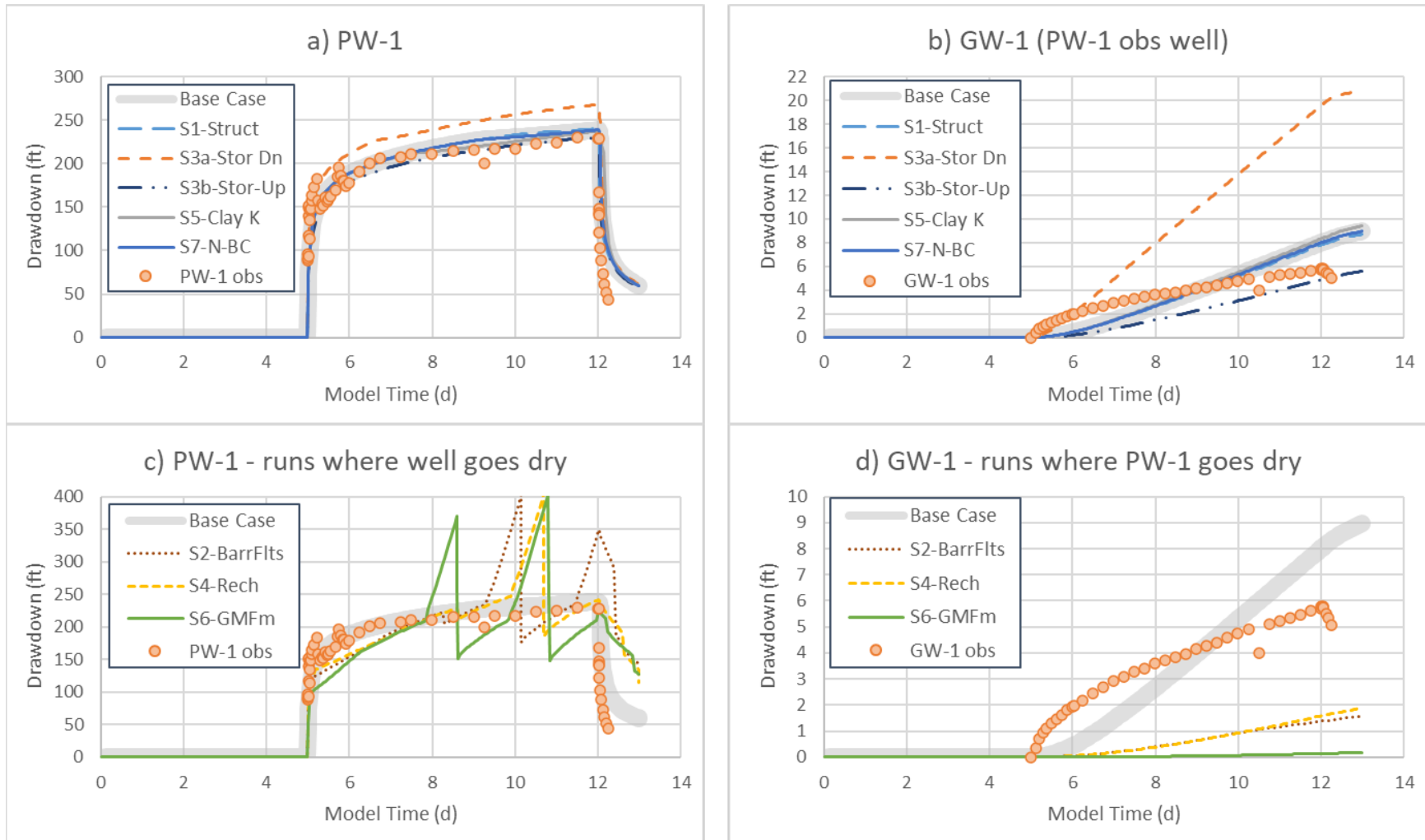


Figure 4-55: PW-1 Pumping Test Calibration – Sensitivity Runs

Figure 4-56 shows the drawdowns predicted for the GMW17-33 pumping test.

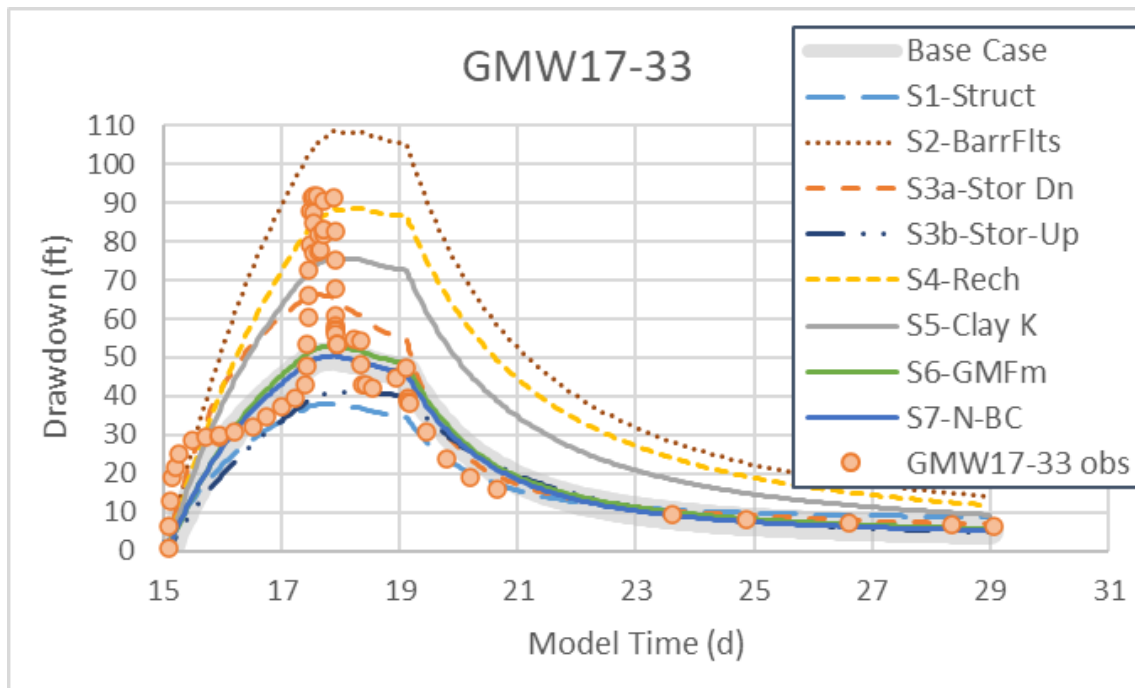


Figure 4-56: GMW17-33 Pumping Test Calibration – Sensitivity Runs

5. Model Predictions

5 Model Predictions

5.1 Base Case Predictions

Figure 5-1 presents the predicted inflows to the underground mine during operations, using the boundary condition configuration shown in Section 4.5. The figure shows average inflows for five time periods. As discussed in Section 4.5, the mine operational period is simulated in four phases: (1) a one-year construction period (Year -1), (2) the tunnel and ramp configuration for mining Years 1 to 3, (3) the tunnel and ramp configuration for mining Years 4 to 6, and (4) the tunnel and ramp configuration for mining Years 7 to 9. The results for the second phase have been divided into two time periods: Year 1 and Years 2 to 3 in Figure 5-1, because the predicted flow into the mine is highest during the first year of mining. Also shown on Figure 5-1 is the groundwater extracted from the production well shown in Figure 4-10.

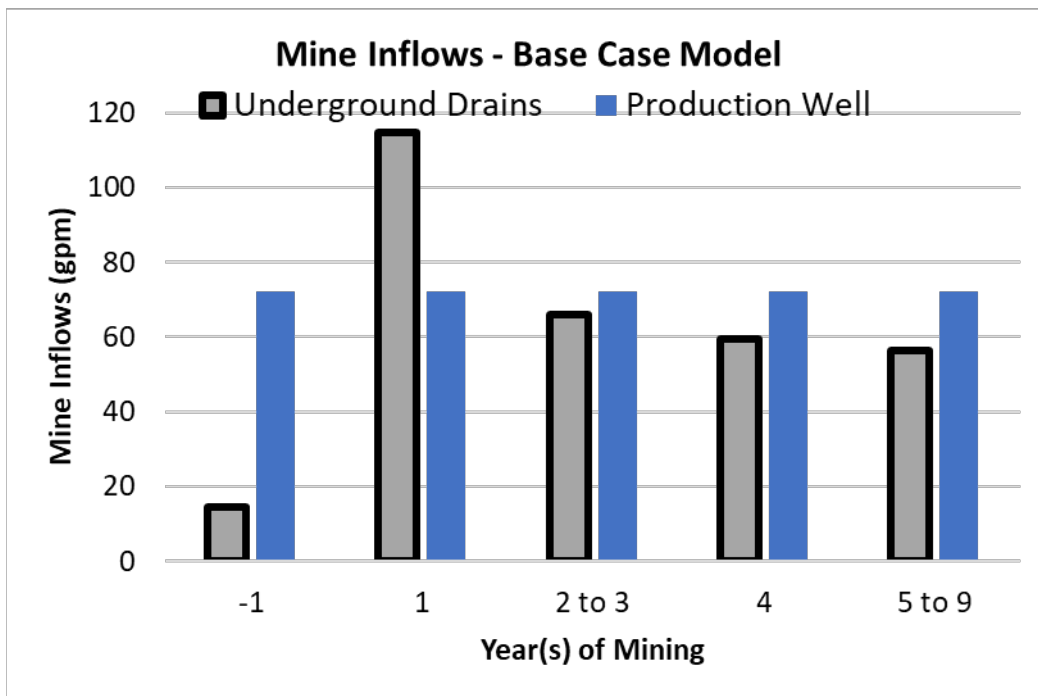


Figure 5-1: Predicted Groundwater Inflows, Base Case Model.

The groundwater inflow to the underground workings is predicted to be on the order of 15 gpm during the pre-construction year, before active mining begins. The average mine inflows during mine operations are predicted to range from approximately 115 gpm during the first year to 56 gpm during the final years. These estimates are based on the simplified

mine staging (see Table 4-2). The flow predictions are higher than the Lorax (2021) estimates, which used a steady state model and did not account for the release of water from storage. The Lorax (2021) model also uses lower regional recharge rates than the current model.

The production well is simulated to extract 72 gpm over the 10-year period of construction and operation. The predicted water level in groundwater in the vicinity of the production well at the end of operations is 3122 ft amsl.

The drawdown predicted during and after operations in Slice 1 of the model, at the top of Layer 1 of the model, and at Slice 5 of the model, located at a depth of approximately 325 ft below ground surface (bgs) is shown Figure 5-2 to Figure 5-4. Figure 5-2 shows predicted drawdowns during operations. During this period, the drawdown from the underground mining is, for the most part, restricted to deeper groundwater. Shallow groundwater near the mine is not predicted to be influenced by dewatering of the mine. This is due to the low-permeability clay and siltstone in the mine area. These low-permeability strata are evident in the boring logs and in the strong vertical gradient evident in the monitoring wells and VWPs in the mine area. The more extensive zone of drawdown is associated with the production well, located in a zone of higher permeability, shown as Zones 72 and 73 in Figure 4-18. This zone of high permeability extends to ground surface (Layer 1 of the numerical model), and this results in the predicted drawdown zone in Figure 5-2. As shown in the figure, the springs that are predicted to fall within the zone of influence of the proposed production well are those located northeast of the mine, and in particular Lowe Spring and Red Tank #3. The time-series of the drawdown predicted at the wells and springs is presented in Figure 5-5 to Figure 5-7. As shown in Figure 5-7, maximum drawdowns greater than 1 foot are predicted for four springs: Lowe Spring, Red Tank #3, Sagebrush Spring, and the Spring North of Lowe Reservoir. Nearby Government Corral is not predicted to experience significant drawdown because this spring is located in a zone of shallow groundwater discharge associated with recharge on Grassy Mountain, and reductions in the water table in the TIS zone is not predicted to cause this spring to dry out in the base case model. Sensitivity runs (see Section 5.2) show that Government Corral could be experience drawdown impacts under some parameter sets.

Figure 5-3 shows that the recovery of drawdown at the underground mine and production well area after mine closure. The magnitude of drawdown at the mine and production well recovers relatively quickly at the lower elevation (Slice 5) shown in the figure. At the same time that drawdown recovery occurs at the mine and production well, the low-drawdown contours (*e.g.*, 0.5 ft, 1 ft) at the outer edge of the zone of influence expand outward for the first 20 years, as the impact of the dewatering propagates into adjacent areas. The area of influence begins to shrink after approximately 20 to 50 years after mine closure. Continued

reduction of the predicted zone of influence at 80 years and 100 years after mine closure is shown on Figure 5-4.

Figure 5-5b shows that the highest drawdowns are predicted for the deep VWP in the mine area. The water levels in the deep mine area are predicted to recover rapidly in these locations after the end of mining. Some of them—notably GM17-20-I and GM17-20-D—are predicted to have final water levels below current conditions due to the higher simulated permeability of the backfilled stopes. Some of the shallow VWP and monitoring wells are predicted to experience drawdown, as shown in Figure 5-5b and Figure 5-5c. At some locations—most notably GM17-16S, GM17-21S, and GM17-28S—the drawdown is not predicted to recover; however, it should be noted that these three VWPs are currently dry, and the model is predicting that the water table below these VWPs will be lower after mining. Because of the low permeability of the bedrock around the mine, the drawdown at the mine is of relatively limited extent. Downgradient of the mine area, minor residual drawdowns of less than 4 feet are predicted for GW-3, GMW17-31, and GMW17-33 (Figure 5-5c and Figure 5-5d). PW-4 and GW-4 in the vicinity of the production well are also predicted to recover within a few decades after the end of mining (Figure 5-5a).

Figure 5-6 shows the predicted drawdowns at other monitoring wells in the numerical groundwater model. Long-term drawdowns of less than 3 ft are predicted for these wells. Short- and medium-term drawdowns of more than 3 ft and up to approximately 7 feet are predicted for BLM, located in the tailings area; PW-1, GW-1, 26-092-915 located northeast of the mine; 59768 located above the TIS sandstone/conglomerate zone southeast of Prod-1; GW-5 located northwest of the mine; and 59765, a dry well located near GW-5; and 59761, located east of the mine.

Figure 5-7 shows that, except for the springs noted above—Lowe Spring, Red Tank #3, Sagebrush Spring and the Spring North of Lowe Reservoir—none of the springs are predicted to experience drawdowns greater than 0.5 ft. Government Corral is included in Figure 5-7a with the four springs that are inside the drawdown zone. Although the base case model predicts no change in the head at Government Corral, the discharge predicted for this spring is predicted to drop, because the water table around the spring is predicted to drop.

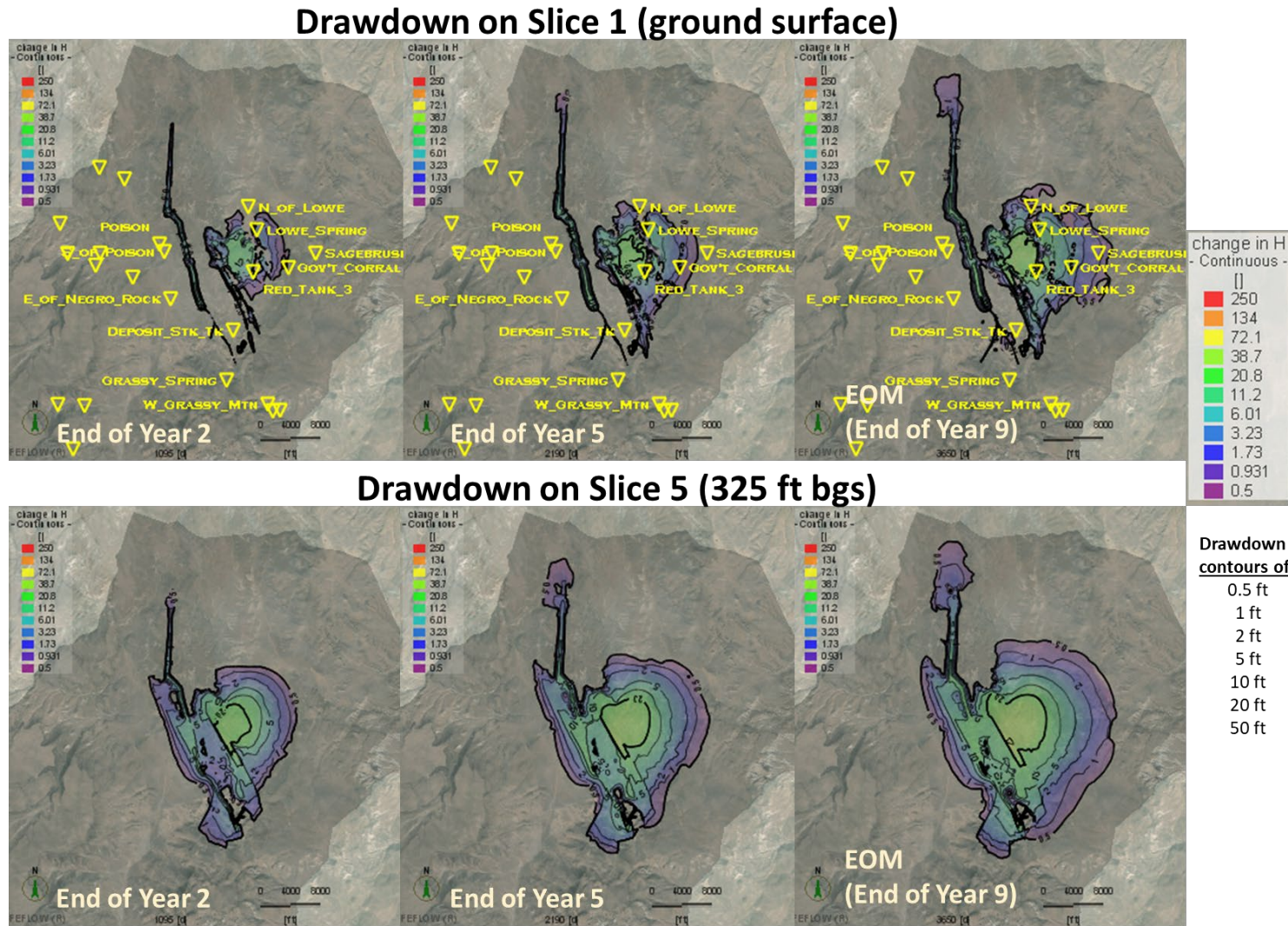


Figure 5-2: Predicted Drawdown, Model Slices 1 and 5, End of Mine Years 2, 5 and 9.

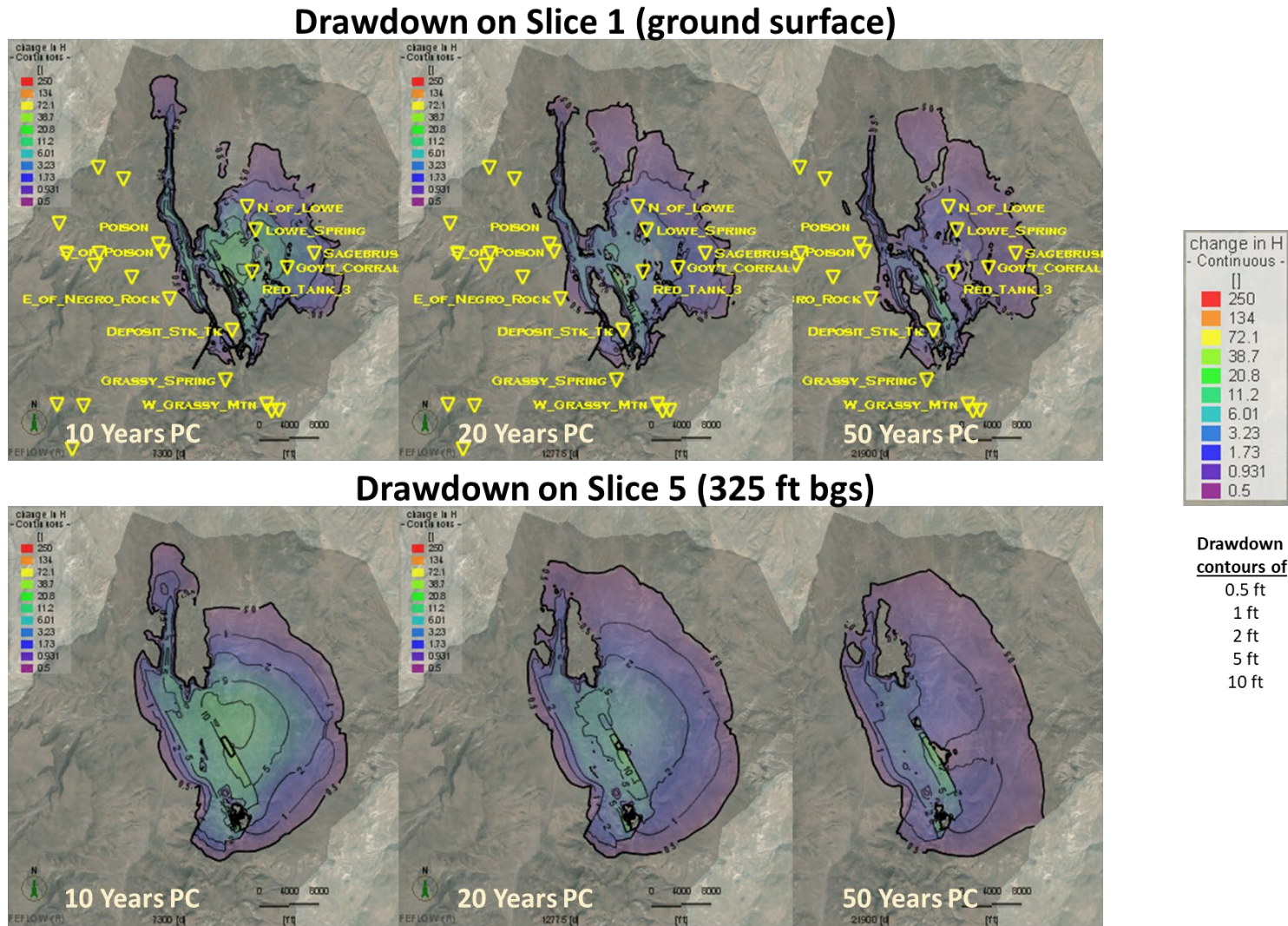
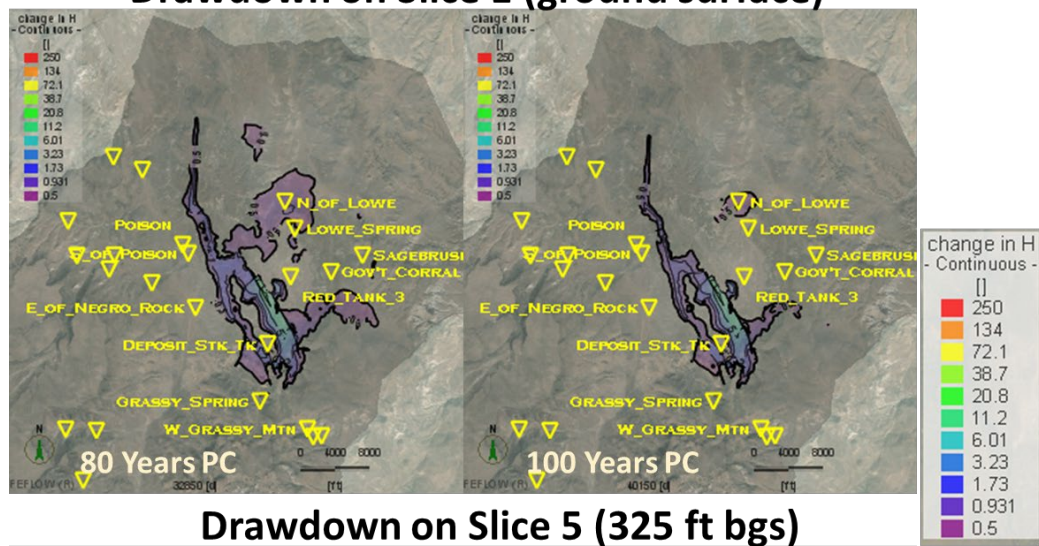


Figure 5-3: Predicted Drawdown, Model Slices 1 and 5, 10, 20 and 50 Years After End of Mining.

Drawdown on Slice 1 (ground surface)



Drawdown on Slice 5 (325 ft bgs)

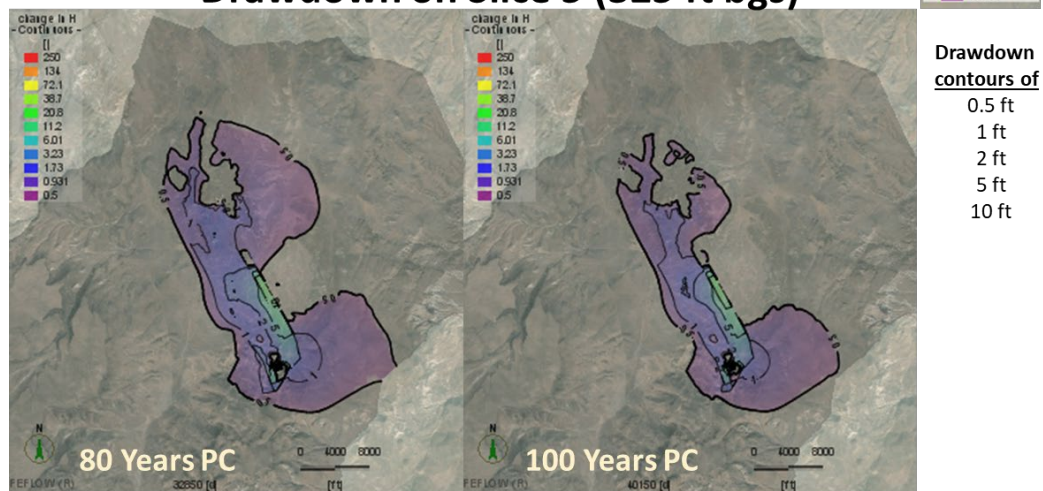


Figure 5-4: Predicted Drawdown, Model Slices 1 and 5, 80 and 100 Years After End of Mining

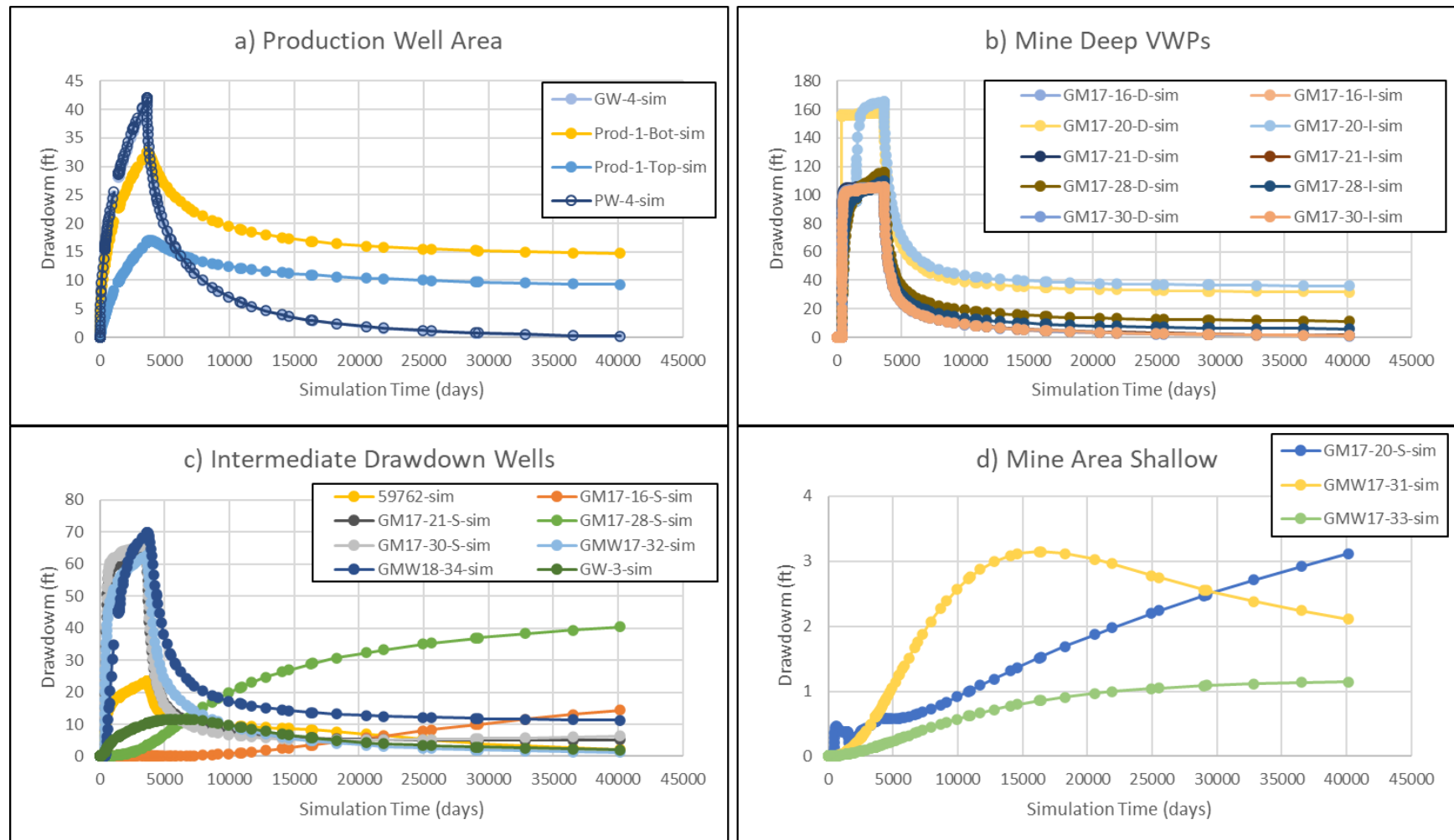


Figure 5-5: Time-Series of Simulated Drawdown, Higher Drawdown Wells.

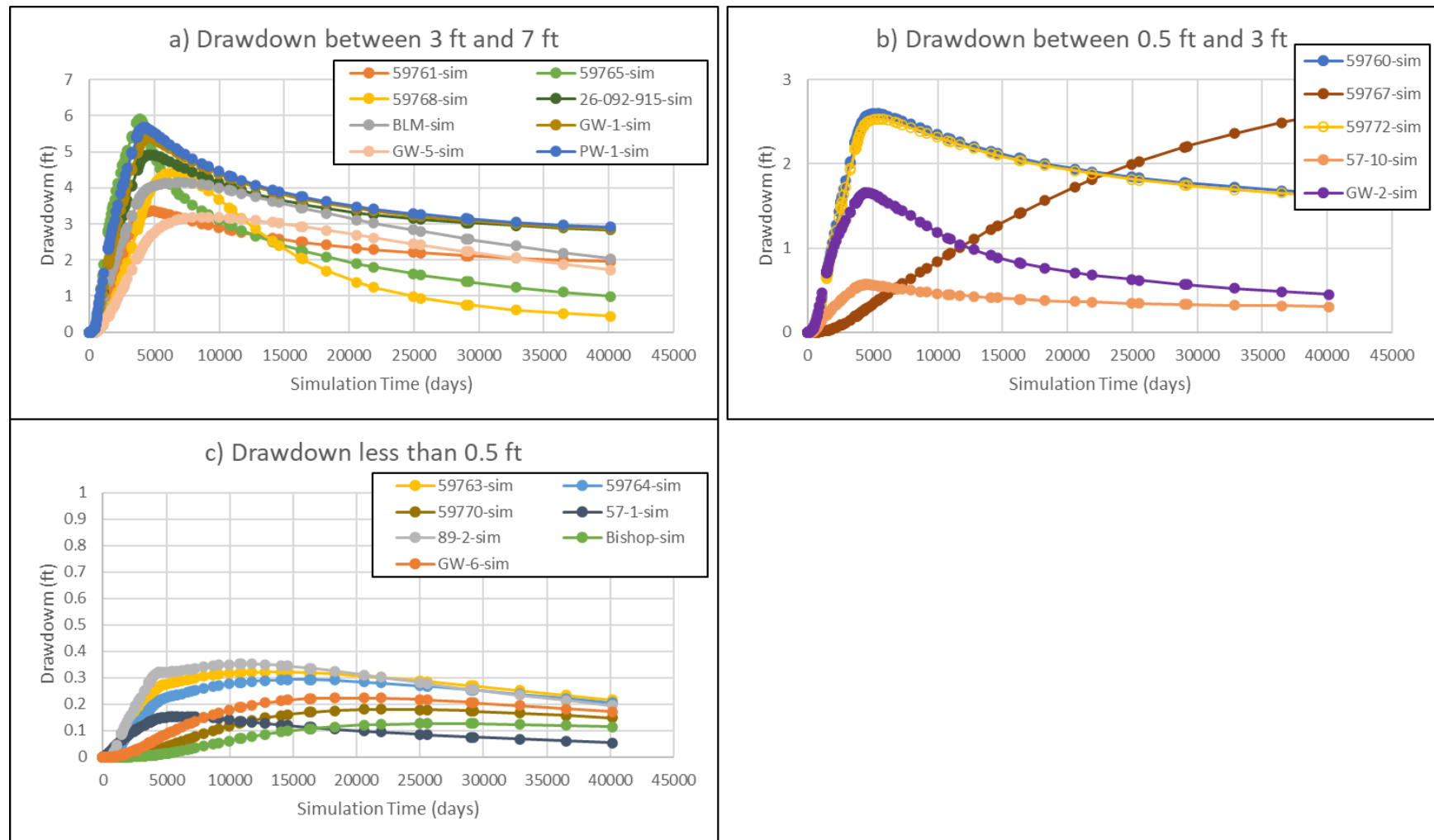


Figure 5-6: Time-Series of Simulated Drawdown, Lower Drawdown Wells.

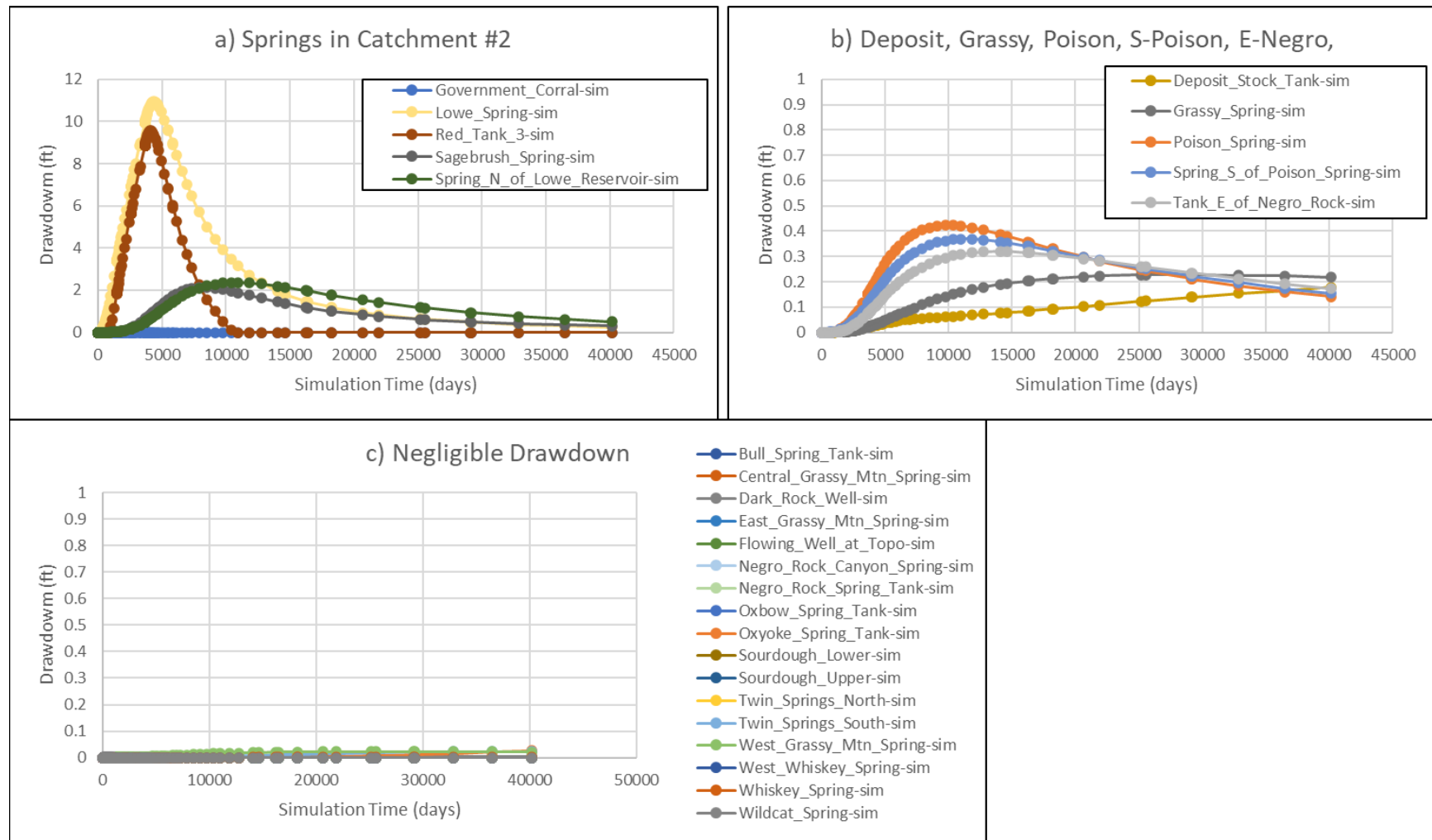


Figure 5-7: Time-Series of Simulated Drawdown, Springs.

5.2 Sensitivity Analysis

Eight sensitivity models were run to model the impact of mining on groundwater (see Section 4.12). Figure 5-8 shows the predicted underground mine inflows for the sensitivity runs. The sensitivity runs yield a range of inflows, with the lowest average inflows predicted when the recharge is reduced (S4) and when the storage coefficient is lowered (S3a). The highest inflows are predicted when the degree of hydraulic compartmentalization with barrier faults is reduced (S2) and when the North Structure hydraulic conductivity is decreased (S1), which results in a higher initial water table in the deep groundwater system that will be tapped by the mine.

Table 5-1 lists the average groundwater inflow to the mine from Year -1 to the end of mining in Year 9. The table also shows the steady state statistics associated with the sensitivity run. It is relevant that the highest mine inflows are predicted for the model, S3, that has the poorest steady state calibration statistics.

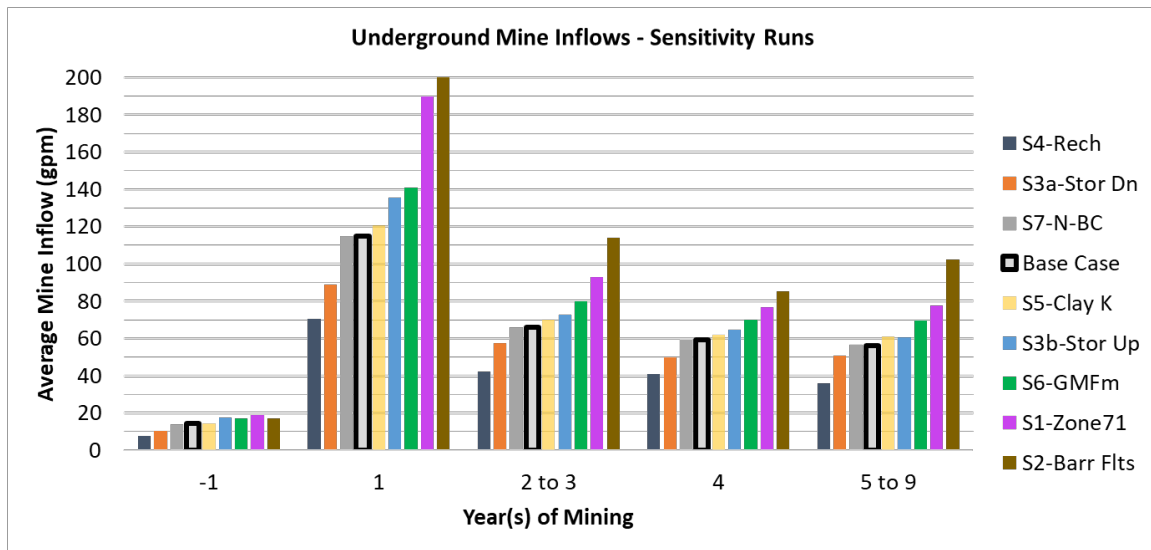


Figure 5-8: Predicted Underground Mine Inflows, Sensitivity Runs.

**Table 5-1:
Predicted Underground Mine Inflow, Sensitivity Run Prediction**

Model	Description	UG average Q (gpm)	Final PW Head (ft)	NRMSE (%), All Data	NRMSE (%), Mine Area
	Base Case	60	3,122	4%	6%
S1	Reduce structure K	84	3,126	5%	9%
S2	Raise barrier fault K	102	3,125	10%	18%
S3a	Reduce storage	51	3,112	4%	6%
S3b	Raise storage	66	3,130	4%	6%
S4	Reduce recharge	38	3,082	8%	14%
S5	Raise clay, siltstone K	64	3,122	6%	9%
S6	Raise Grassy Mtn. Fm K	73	3,088	10%	15%
S7	Reduce N Transfer coeff	60	3,123	4%	6%

The influence of the sensitivity analysis parameters on the predicted drawdown at the end of mining is shown in Figure 5-9. This figure shows the zone of predicted drawdown in the base case model using the color shading of Figure 5-2 to Figure 5-4. However, rather than using a 0.5 ft minimum drawdown contour, a 1-ft minimum contour is used. The 1-ft drawdown contour of the sensitivity analyses is also shown. Additional drawdown contour plots for the sensitivity runs, down to 0.5 ft, are presented in Appendix II: Sensitivity Analysis Individual Drawdown Maps. As in Figure 5-2 to Figure 5-4 for the base case model, Figure 5-9 to Figure 5-17 show simulated drawdowns at ground surface (Slice 1) and at an approximate depth of 325 ft (Slice 5). As mentioned in Section 4.12, the sensitivity analysis parameters were selected to yield predictions of greater drawdown from the proposed project. This is evident in Figure 5-9, where most of the simulations, except for S3b, in which the storage parameters were increased, show a smaller zone of drawdown than the base case model.

Figure 5-10 shows the drawdowns in Slice 1 at the end of mining. Five of the eight sensitivity runs—S1, S2, S4, S5, and S7—predict drawdown zones that are similar to the base case model, with minor changes at the margins (Figure 5-11a). The three scenarios that predict significantly different drawdown zones are S3b, which predicts a smaller drawdown zone, as mentioned above; S3a, in which the storage properties were reduced, leading to the largest predicted zone of drawdown; and S6, in which the Grassy Mountain Formation K was doubled, leading to a larger zone of drawdown in the north, but a smaller zone of drawdown in the south (Figure 5-11b).

End of Mining

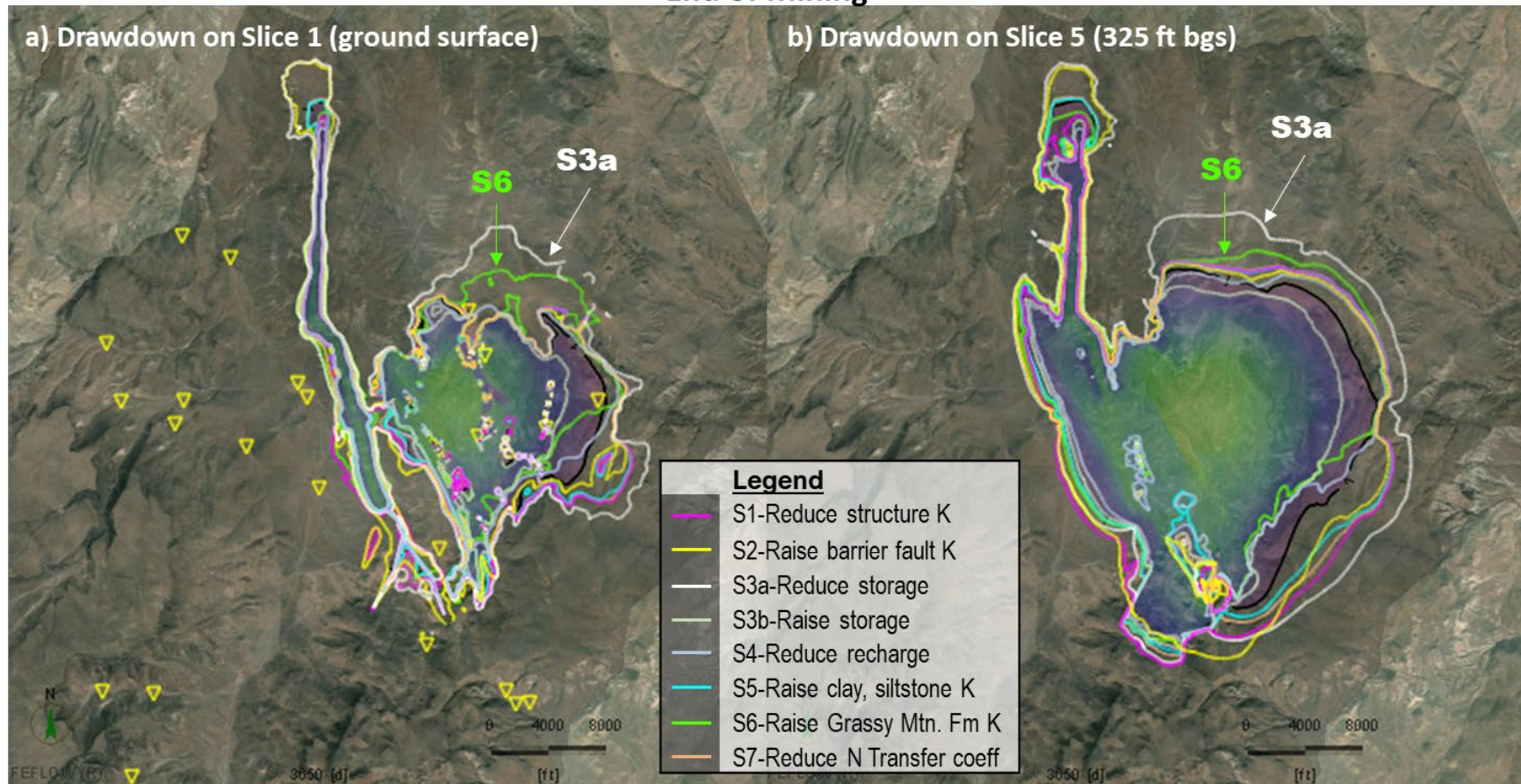


Figure 5-9: Comparison of 1-ft Drawdown Contours, Sensitivity Runs, At End of Mining.

Drawdown on Slice 1 (ground surface) – End of Mining

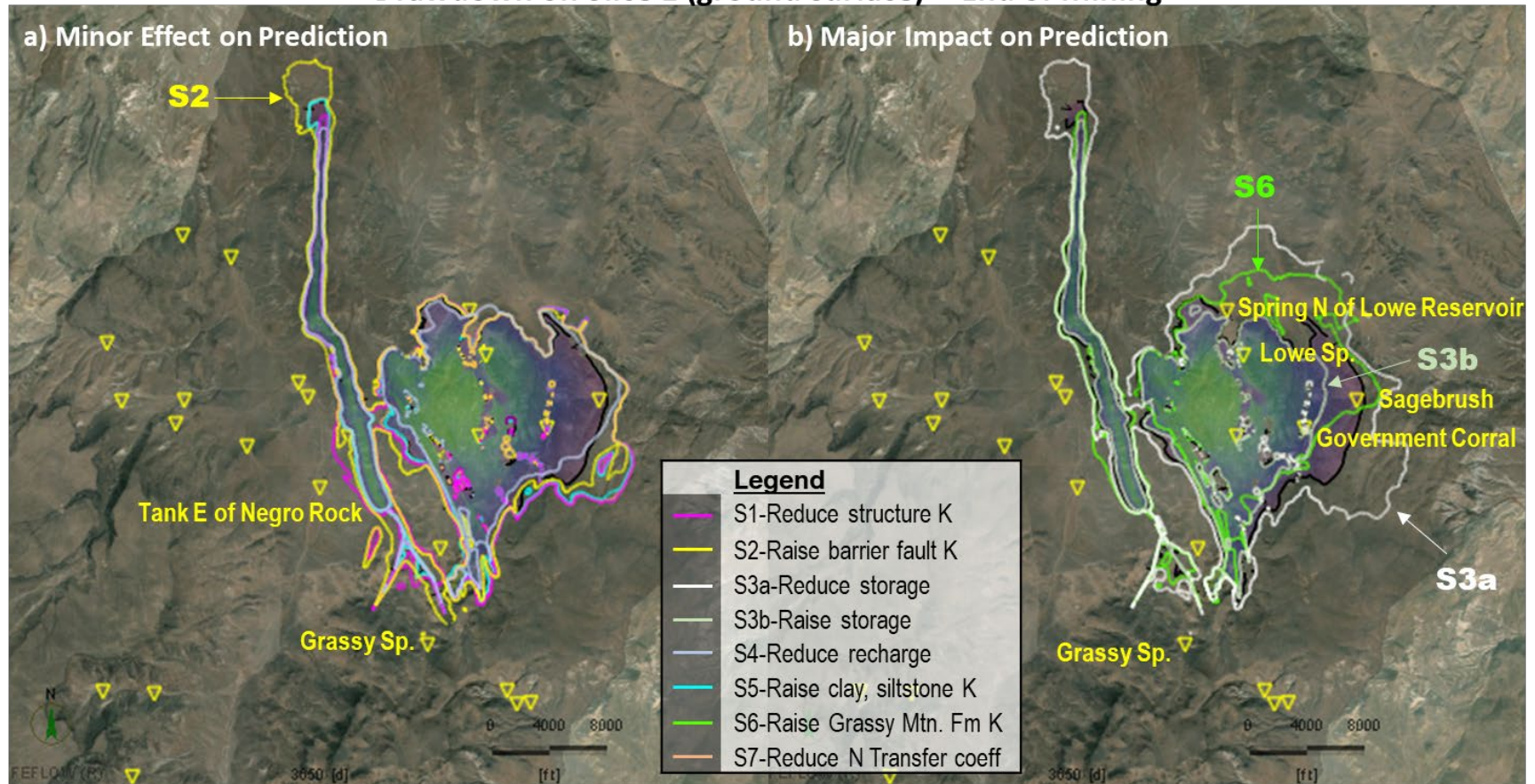


Figure 5-10: Comparison of 1-ft Drawdown Contours on Slice 1, End of Mining.

Drawdown on Slice 5 (325 ft bgs) – End of Mining

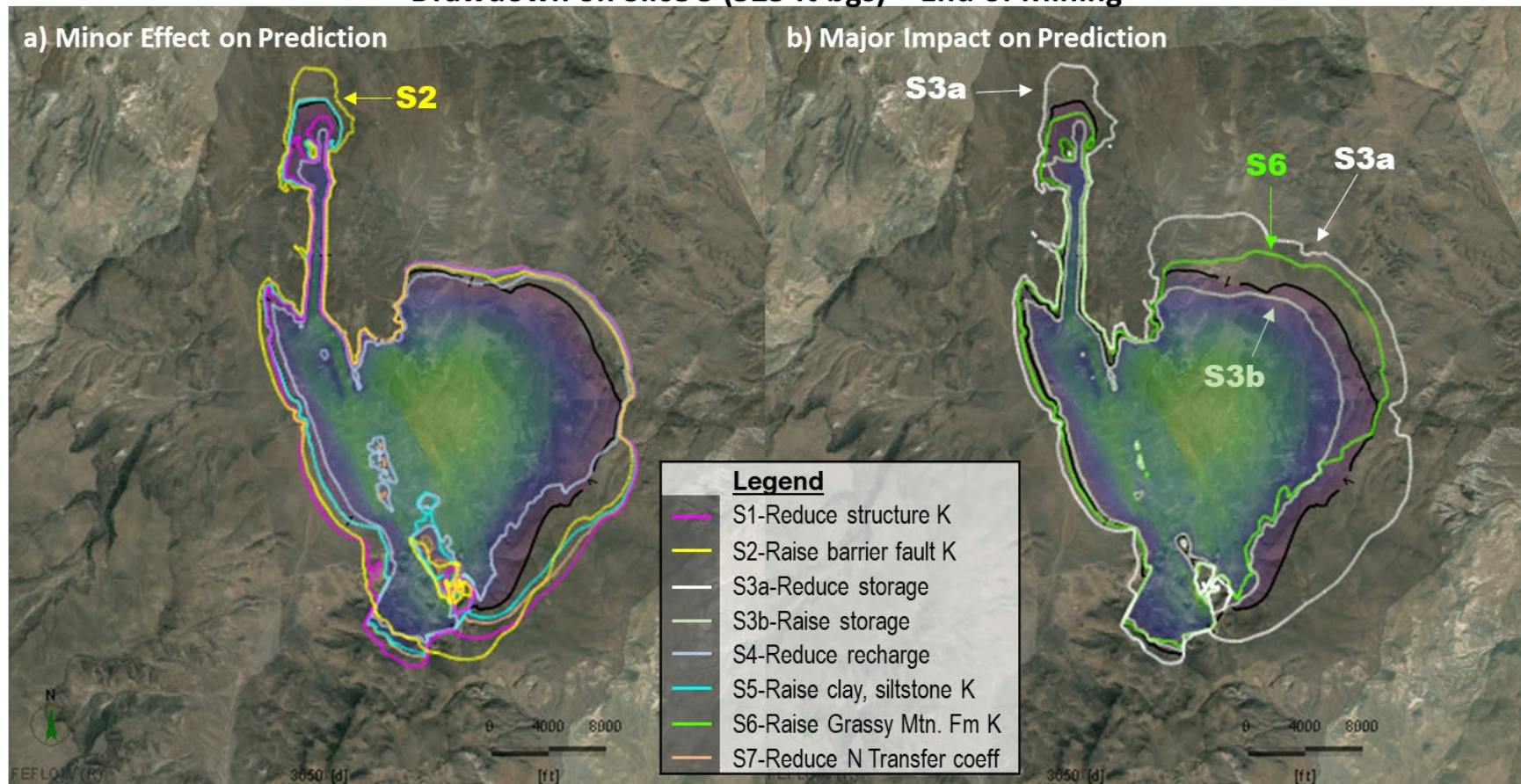


Figure 5-11: Comparison of 1-ft Drawdown Contours on Slice 5, End of Mining.

Figure 5-11 shows the drawdowns predicted at the end of mining in Slice 5. On Slice 5, the three sensitivity runs shown in Figure 5-10b—S3a, S3b, and S6—show similar behavior to that observed on Slice 1. The other five runs have predicted drawdowns that are similar to that of the base case.

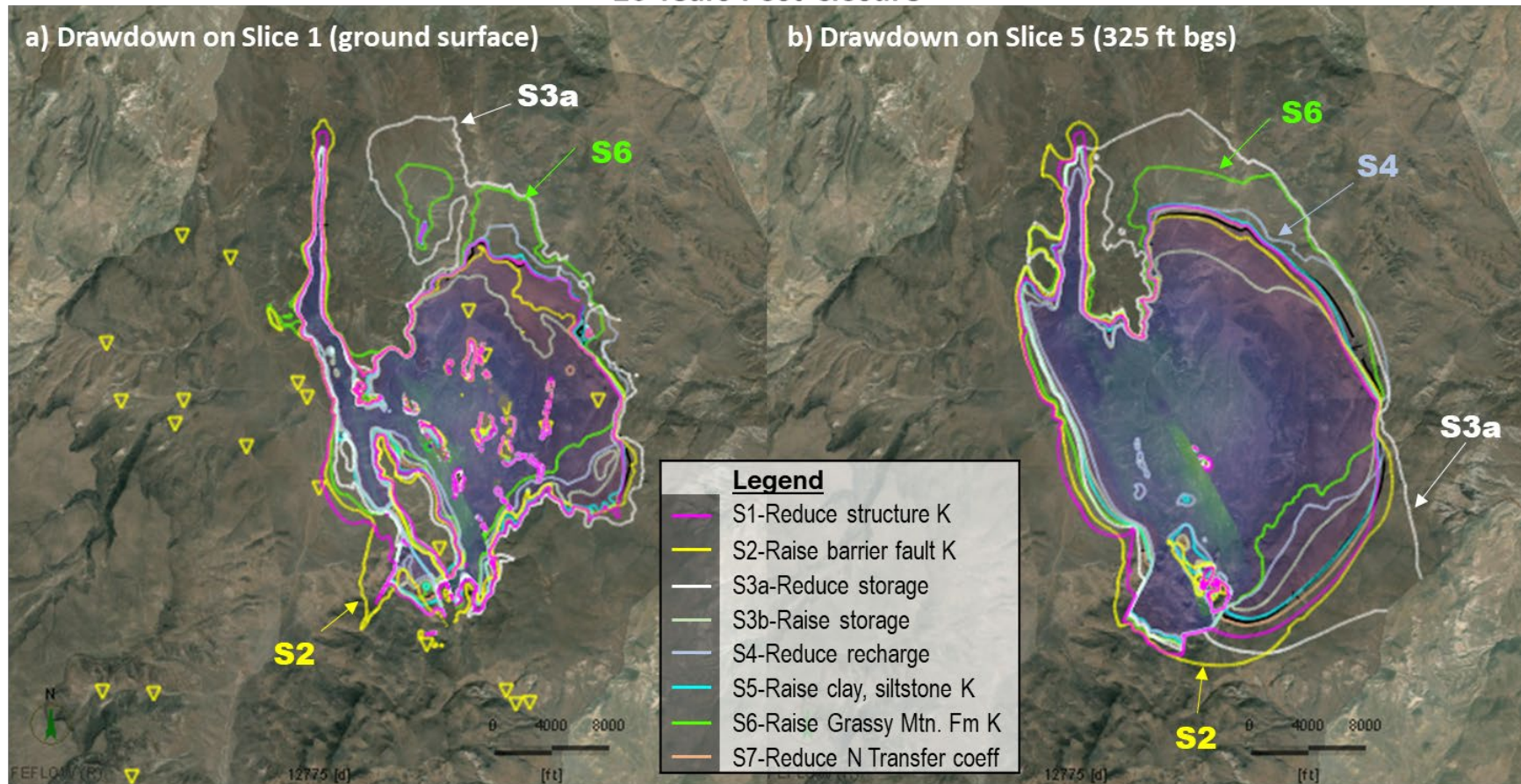
Figure 5-12 shows the simulated drawdowns 20 years after the end of mining. On Slice 1, two of the models—S5 and S7—have drawdowns that are very similar to those of the base case model. S1, in which the north high-K structure permeability was reduced, and S2, in which the barrier fault hydraulic conductivities were increased, have predicted drawdowns that are similar to the base case in the production well area but predict higher drawdowns west of the mine (Figure 5-13a). Three runs—S3a (lower storage), S4 (lower recharge) and S6 (lower Grassy Mountain Formation K)—have larger zones of predicted drawdown north and east of the production well area (Figure 5-13b). As in the end-of-mining runs, sensitivity run S3b, with lower storage properties, has the smallest predicted drawdown zone (Figure 5-13b).

Figure 5-14 shows the predicted drawdowns 20 years after the end of mining on model Slice 5. Run S3b (higher storage), predicts a smaller zone of drawdown. Three runs predict larger zones of drawdown: S3a (lower storage), S4 (lower recharge), and S6 (higher Grassy Mountain Formation hydraulic conductivity).

Figure 5-15 shows the predicted drawdowns 100 years after the end of mining. On Slice 1, the zone of drawdown greater than 1 ft is predicted to have shrunk significantly (Figure 5-16a). Three runs have significantly higher zones of residual drawdown (Figure 5-16b). Two of these have higher predicted drawdowns 20 years after the end of mining: these are S4 (25% lower recharge) and S6 (higher Grassy Mountain Formation hydraulic conductivity). A third sensitivity run, S2, also predicts a larger zone of drawdown; S2 is the run in which the hydraulic conductivity of the barrier faults was increased to reduce the compartmentalization of the groundwater flow system. Models S2, S4 and S6 are the models with the three worst steady state calibration statistics (see Figure 4-50)

Figure 5-17 shows similar relative drawdown predictions on Slice 5. The three models with the highest predicted drawdown are S2, S4 and S6. Figure 5-17a also shows that the model with the smallest zone of residual drawdown is S3a (lower storage). By comparison, S3b (higher storage) has a slightly higher zone of drawdown at the end of the simulation.

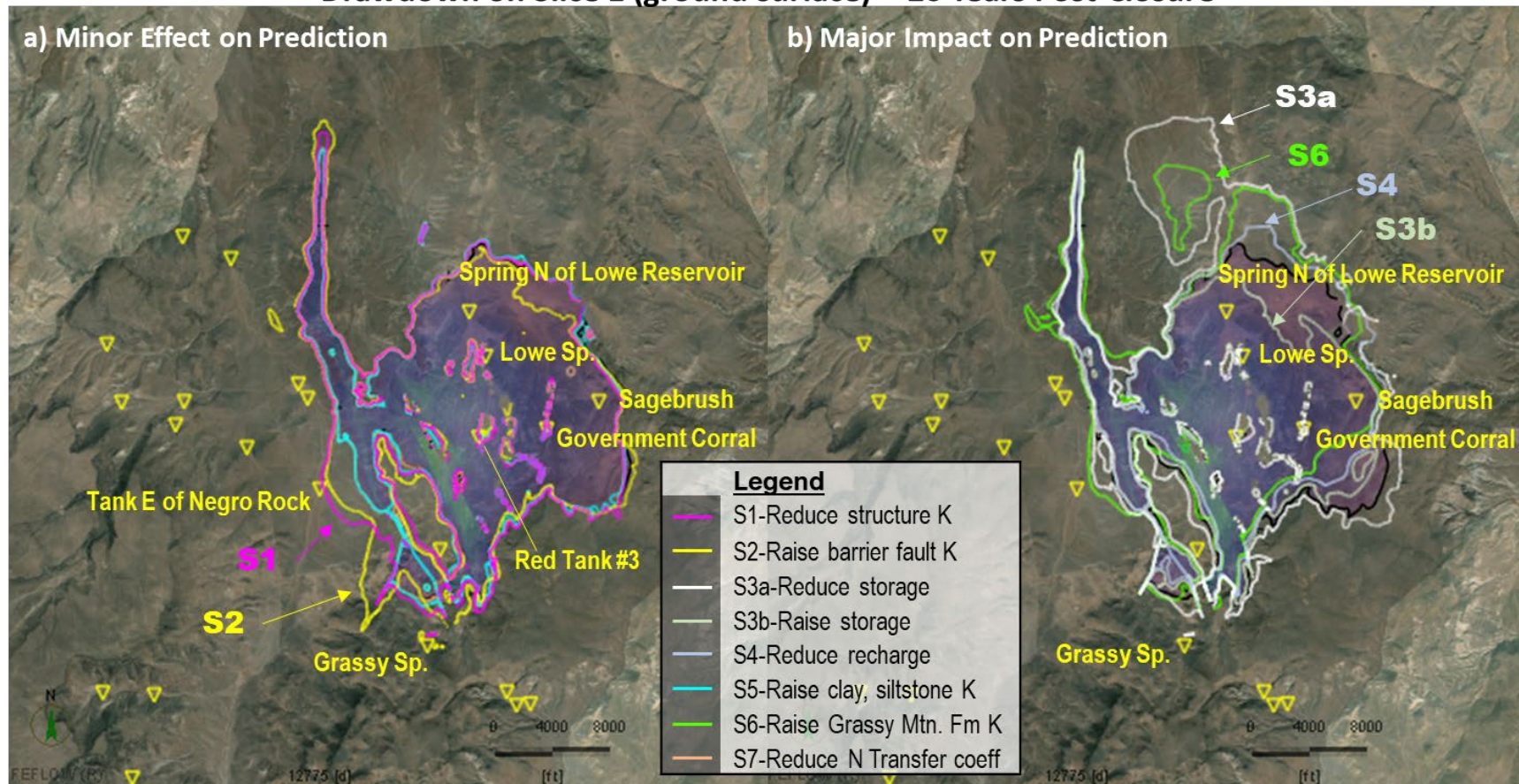
20 Years Post-Closure



Notes: Shaded area shows Base Case drawdowns greater than 1 ft.
Contour lines show Sensitivity analysis 1-ft drawdown contour.

Figure 5-12: Comparison of 1-ft Drawdown Contours, Sensitivity Runs, 20 Years After End of Mining.

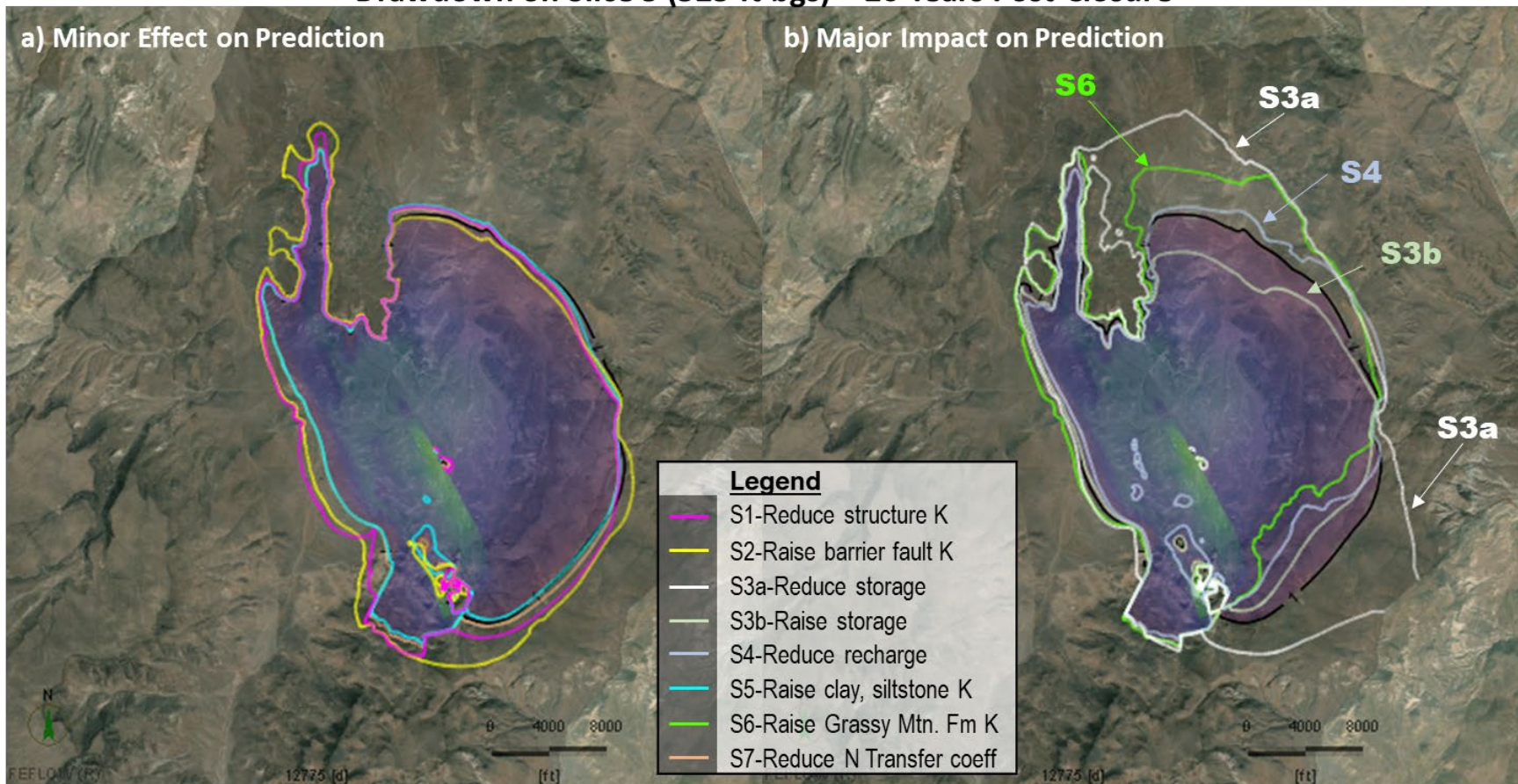
Drawdown on Slice 1 (ground surface) – 20 Years Post-Closure



Notes: Shaded area shows Base Case drawdowns greater than 1 ft.
Contour lines show Sensitivity analysis 1-ft drawdown contour.

Figure 5-13: Comparison of 1-ft Drawdown Contours on Slice 1, 20 Years End of Mining.

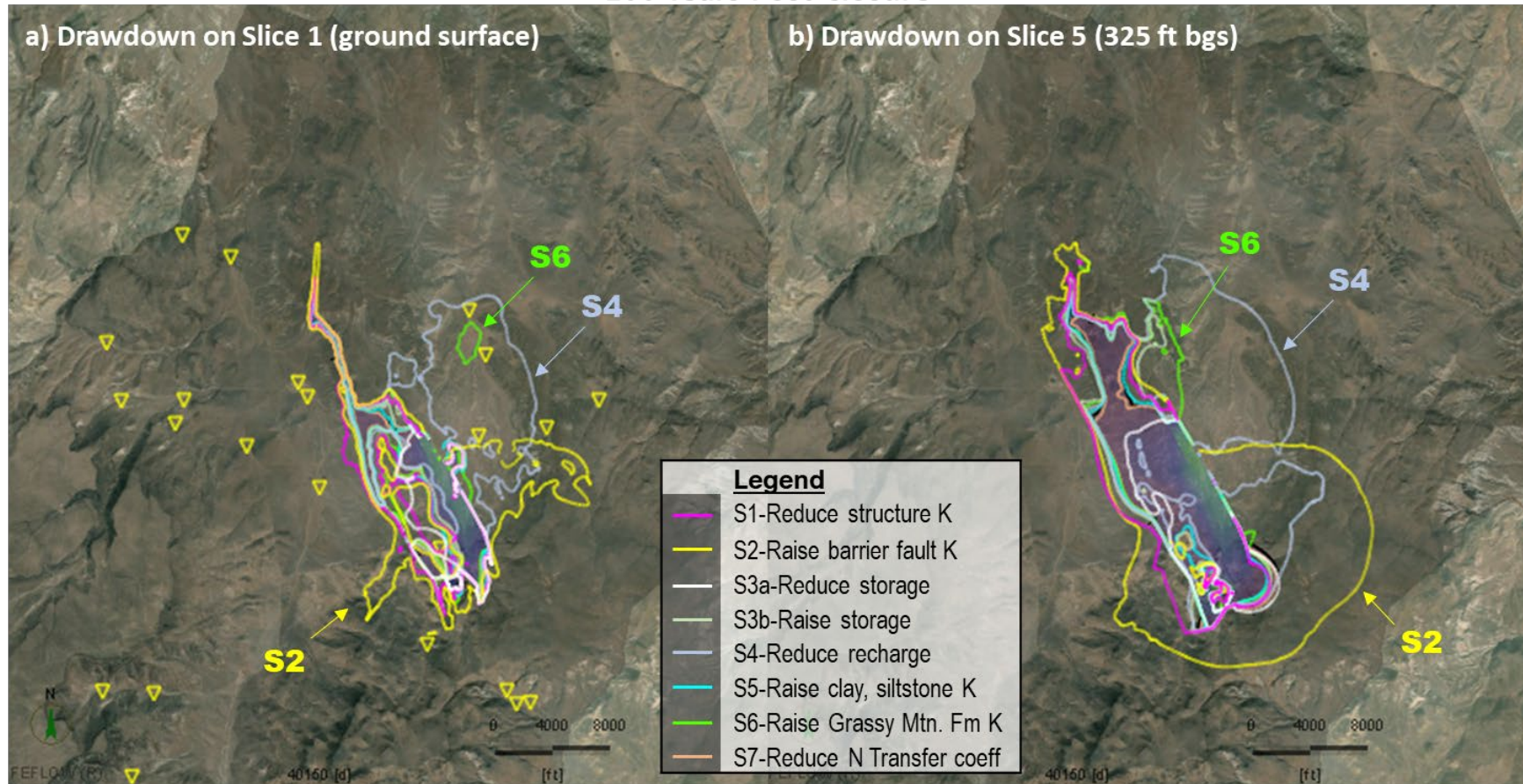
Drawdown on Slice 5 (325 ft bgs) – 20 Years Post-Closure



Notes: Shaded area shows Base Case drawdowns greater than 1 ft.
Contour lines show Sensitivity analysis 1-ft drawdown contour.

Figure 5-14: Comparison of 1-ft Drawdown Contours on Slice 5, 20 Years End of Mining.

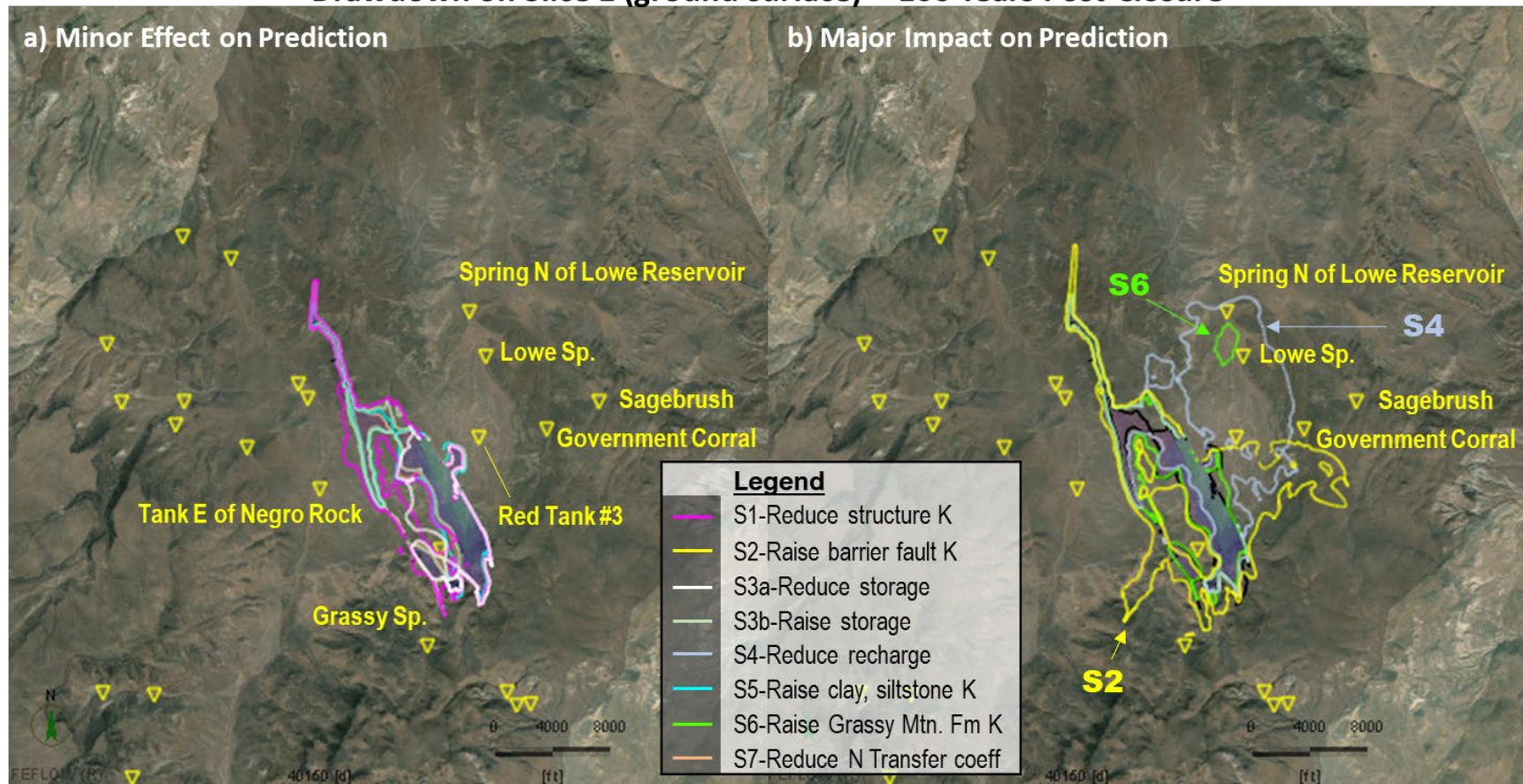
100 Years Post-Closure



Notes: Shaded area shows Base Case drawdowns greater than 1 ft.
Contour lines show Sensitivity analysis 1-ft drawdown contour.

Figure 5-15: Comparison of 1-ft Drawdown Contours, Sensitivity Runs, 100 Years After End of Mining.

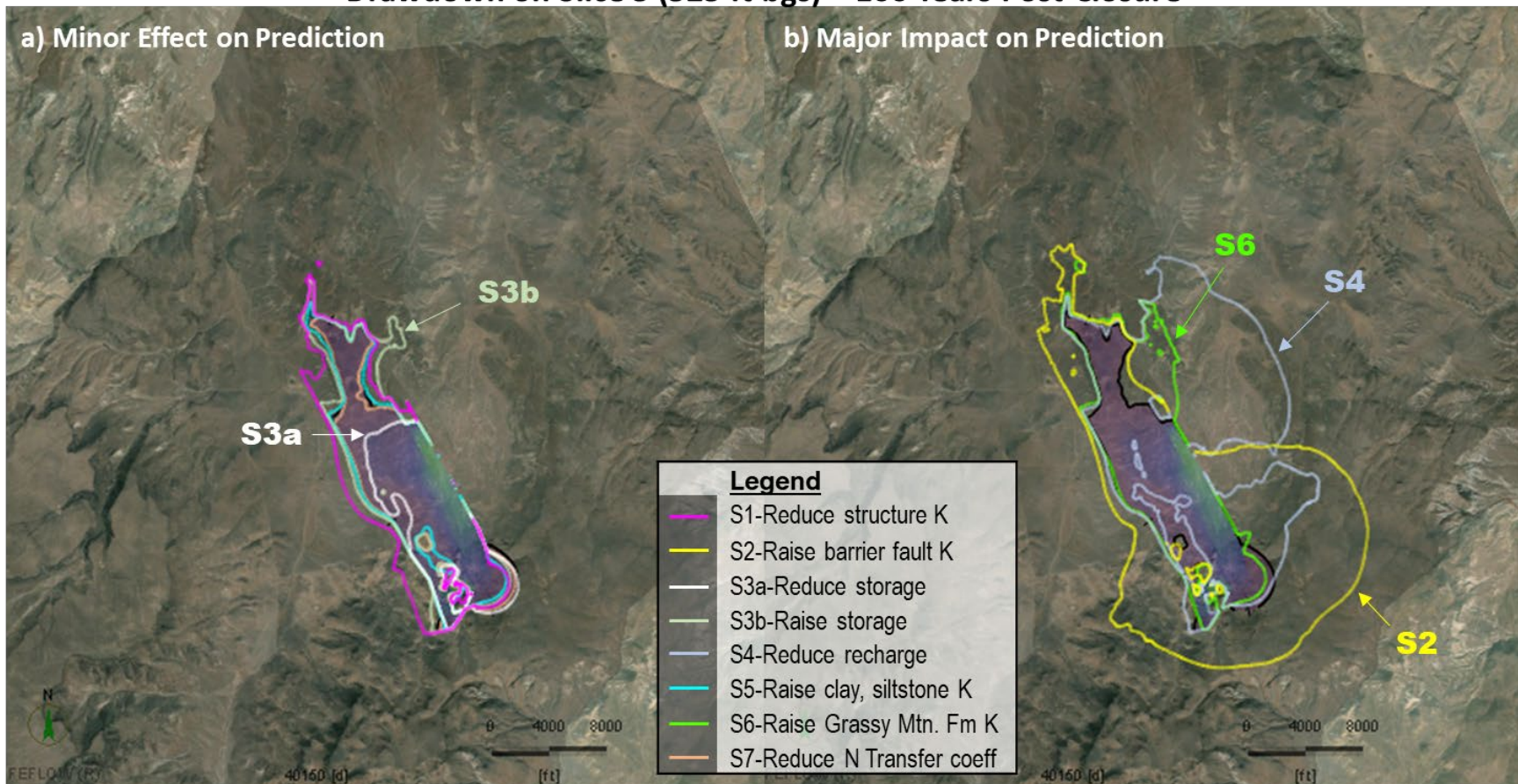
Drawdown on Slice 1 (ground surface) – 100 Years Post-Closure



Notes: Shaded area shows Base Case drawdowns greater than 1 ft.
Contour lines show Sensitivity analysis 1-ft drawdown contour.

Figure 5-16: Comparison of 1-ft Drawdown Contours on Slice 1, 20 Years End of Mining.

Drawdown on Slice 5 (325 ft bgs) – 100 Years Post-Closure



Notes: Shaded area shows Base Case drawdowns greater than 1 ft.
Contour lines show Sensitivity analysis 1-ft drawdown contour.

Figure 5-17: Comparison of 1-ft Drawdown Contours on Slice 5, 100 Years End of Mining.

5.3 Discussion

The FEFLOW model predicts that the extent of the drawdown zone from mine operations will be primarily due to the proposed production well, which will target a permeable sandstone and conglomerate zone. The mine area drawdown is predicted to be constrained by the barrier faults that create significant hydraulic compartmentalization (see Section 3.4). The base case model predicts an underground inflow of 15 gpm during construction and mine inflow rates of 56 gpm to 115 gpm during operations, for an average mine-life average inflow of 60 gpm. The predicted mine inflows from the sensitivity runs, averaged over nine years of operations plus one year of construction range from an annual average value of 38 gpm to 100 gpm, much of it derived from storage during the early years of mining, when the higher permeability strata intercepted by GMW17-33 will be dewatered (see Table 5-1). Collected groundwater inflow to the mine workings would provide some operational water supply, allowing for lower extraction from the production well. Note that lower pumping from the production well would reduce the zone of drawdown due to the Grassy Mountain project.

The drawdown from mining the underground is predicted to be higher at depth than at the ground surface due to the presence of a low-permeability clay layer in the mine area, and in particular in the tailings area (see for example Figure 4-18 and Figure 4-29). Because of this clay zone, the model does not predict any drawdown at the location of Deposit Stock Tank. The springs that the modeling predicts could experience a drawdown of greater than 0.5 ft as a result of the project are located northeast of the underground mine. These are Red Tank #3, Low Spring, Sagebrush Spring, the Spring North of Lowe Reservoir, and Government Corral. These springs are impacted by the drawdown from the proposed production well. Reducing the extraction from the production well will mitigate these impacts.

6. Summary and Conclusions

6 *Summary and Conclusions*

A numerical groundwater model was developed using FEFLOW 7.4. The primary objective of the model was to refine estimates of groundwater inflows to the underground mine and to estimate drawdown and recovery that results from mine dewatering and water production. The model was calibrated to steady state heads at wells and springs in the mine area. Secondary calibration targets included the baseflow to the springs and the drawdown response at four pumping wells—PW-4, Prod-1, PW-1, and GMW17-33.

The calibrated model simulates the observed hydraulic compartmentalization with a combination of stratigraphic units, including:

- A shallow clay zone mapped in the tailings area;
- A permeable sandstone/conglomerate zone (TIS) present in the production well area (see Figure 4-17 in Section 4.6); and
- A high-permeability zone (Zone 71) providing hydraulic connection between the mine area and lower hydraulic heads at the northern boundary. This zone can also be seen as a proxy for a regional groundwater system flowing toward the Malheur River (see Figure 3-16 in Section 3.6), and depresses the piezometric head in deep groundwater in the immediate area of the mine.

Compartmentalization is also simulated with 19 fault zones (see Section 4.7), of which 11 are barrier faults, and 8 are transmissive features.

The model also includes the main stratigraphic units in the model domain—alluvium (Zone 11), shallow basin deposits, including the Grassy Mountain Formation (Zone 31), the Kern basin tuff (Zone 41), basalt (Zones 51 and 52), rhyodacite (Zone 61).

Within the mine area, the mine includes local permeability zones at PW-1 (Zone 74) and GMW17-33 (Zone 82) to simulate the pumping tests completed in these wells. The mine area local stratigraphy was divided into clayey, low-permeability zones (Zones 91 and 92) and moderately-low-permeability siltstones (Zones 81 and 83). The mine-area hydraulic conductivity zones were defined based on the borehole logging information and drawdown responses to the PW-1 and GMW17-33 pumping tests.

The normalized root mean squared error for the steady state calibration was 4.1% for all piezometers and springs and 5.8% in the mine area. The model is able to simulate the general behavior of the pumping tests in the TIS zone at GW-4 and Prod-1. The model overestimates the drawdown at PW-4 during the pumping test, and therefore can be considered conservative with respect to the drawdown prediction from the proposed production well. The model is able to simulate the observed general behavior of the PW-1

pumping test, both at the pumping well and at the observation well GW-1. In some of the sensitivity simulations, PW-1 went dry during the simulation due to a low initial water table; these results are not considered plausible but are included in Figure 4-55 for the sake of completeness.

The base case model is also able to simulate the general shape of the drawdown curve at GMW17-33. The drawdown at this well is strongly affected by several of the parameters adjusted in the sensitivity analysis (see Figure 4-56).

The base case simulation predicts groundwater inflows to the underground mine ranging from 15 gpm during the mine-construction Year -1 to 115 gpm in Year 1. The average annual mine inflow is predicted to be 60 gpm. Therefore, there may be opportunities to reduce the pumping from the proposed production well.

The drawdown predicted due to the underground mine is relatively limited to the area in the immediate vicinity of the mine, due to the compartmentalization evident in the field data. Much greater drawdown is predicted from the 10-year duration operation of the proposed production well at an extraction rate of 72 gpm. If the pumping rate at the production well is lowered, the simulated drawdown will reduce.

A series of eight sensitivity runs were completed for the calibration and prediction phases of the model. In each of the eight runs, one or more individual parameters were adjusted with the objective of producing a greater zone of drawdown. Recharge, hydraulic conductivity and storage properties were adjusted in the sensitivity analysis. Within the sensitivity model runs, the range of groundwater inflows averaged over the entire life of mine including the construction period is 38 gpm to 100 gpm (Table 5-1). The simulated drawdown in about half of the sensitivity runs was noticeably greater than the base case drawdown zone. However, only four or five regional springs predicted to experience a drawdown of greater than 0.5 ft due to the operation of the production well. These are Red Tank #3, Lowe Spring, Sagebrush Spring, the Spring North of Lowe Reservoir and Government Corral.

7. Limitations

7 *Limitations*

7.1 *Limitations*

This report was prepared for the exclusive use of SLR and Paramount Gold Nevada. The report is based, in part, on a review of existing information from readily available sources. Lorax Environmental Services Ltd. or its employees will not be responsible for any use of the information contained in this report or any reliance on or decisions made based on it by any unauthorized third party.

The numerical groundwater analysis presented here is subject to limitations and uncertainties. There are uncertainties inherent to the numerical simulation of groundwater flow. The accuracy of the model depends on the quality and quantity of data and the time frame over which the data were collected. Furthermore, model calibration is non-unique, meaning that more than one set of parameters can lead to a model solution that meets the calibration targets. It is possible that this analysis has not been exhaustive and that there exist other viable parameter combinations that were not considered. The analysis does not and cannot include all potential, but as-yet-unobserved flow pathways.

The estimation of seepage paths and flow rates to and from the underground mine is subject to uncertainties related to the non-homogenous nature of fractured rocks. Flow through fractured bedrock occurs primarily through secondary porosity or fracture conduits. The location, degree of fracturing, and interconnectedness of fracture networks are not known and cannot be estimated with absolute certainty. Therefore, multiple sources of information were brought together to inform the model development. For the Grassy Mountain model, these data include geological interpretation, groundwater and spring level measurements, and hydraulic conductivity tests in the field. The data also include an estimate of the groundwater recharge distribution, which is also subject to uncertainty. However, even with this integrated data set, there is still uncertainty in the calibration of the model, as shown in the nonzero average residual and in the NRMS error. The NRMS meets the desired criteria of an acceptable calibration but demonstrates the degree of uncertainty that still exists.

The simulations described in this report were designed to evaluate potential groundwater behavior in response to the Grassy Mountain project in an idealized numerical model. Finite-element-scale and sub-finite-element-scale local heterogeneities in material properties and the consequent preferential flow paths are not explicitly modeled. These

local heterogeneities would play a significantly larger role in contaminant movement than in groundwater flow analysis.

Additional uncertainties arise from potential future events. For instance, future groundwater flow will be influenced by changes in climate dynamics, including precipitation rates. Future seismic events may also influence the groundwater flow regime.

In all cases, the uncertainty in the model is directly related to the quality and quantity of monitoring information. Increasing the number of monitoring points will improve the accuracy of the model calibration and improve the impact predictions. The current model is the best estimate based on the information available at the time the model was completed. However, it is not a single solution and should be seen as such. The results presented in the sensitivity analysis are feasible based on our current understanding of the system and the behavior of the model during the calibration period.

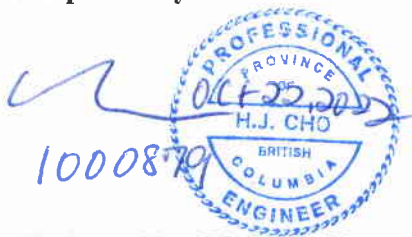
8. Closure

8 Closure

We trust that this report meets the current needs of SLR. Please contact us should you require further information or have any questions.

Yours sincerely,
Lorax Environmental Services Ltd.

Prepared By:



H. Jean Cho, Ph.D., P.Eng.
Groundwater Modeling Specialist

Reviewed By:

Justin Bourne, M.Eng., P.Eng.
Principal Hydrogeological Engineer

Engineers and Geoscientists British Columbia Permit to Practice Number: 1001840.

References

References

- Abrams, Mark J., 2018. Calico Resources USA Corp, Grassy Mountain Mine Project, Malheur County, Oregon, Geology and Soils Baseline Report; October 2018.
- Adrian Brown Consultants, Inc, 1992. Water Resources Technical Memorandum for Atlas Precious Metals Inc., Grassy Mountain Project Environmental Impact Statement.
- Calico Resources, 2021. Grassy Mountain Mine Project, Mine Plan of Operations, Prepared for Bureau of Land Management, December 2021.
- Ferns, Mark L. and Howard C. Brooks, 1993. Geologic Map of the Vale 30x60 Minute Quadrangle, Malheur County, Oregon, and Owyhee County, Idaho, DOGAMI Geological Map Series GMS-77.
- Lorax Environmental, 2021. Grassy Mountain Gold and Silver Project Mine Dewatering Hydrogeologic Assessment, draft technical memorandum prepared for Ausenco Canada, Inc.
- SPF Water Engineering, LLC, 2021a. Grassy Mountain Gold Project Groundwater Vol. I, Groundwater Baseline Data Report. Prepared for Calico Resources USA Corp 665 Anderson Street Winnemucca, Nevada 89445. February 19, 2019.
- SPF Water Engineering, LLC, 2021b. Grassy Mountain Gold Project Groundwater Vol. II, Groundwater Characterization Report. Prepared for Calico Resources USA Corp 665 Anderson Street Winnemucca, Nevada 89445. August 13, 2019.
- SPF Water Engineering, LLC, 2021c. Grassy Mountain Gold Project Groundwater Vol. III, Dewatering Projections and Evaluation of Potential Pumping Impacts. Prepared for Calico Resources USA Corp 665 Anderson Street Winnemucca, Nevada 89445. August 13, 2019.
- van Genuchten, M. Th. 1980. A closed form equation predicting the hydraulic conductivity of unsaturated soils. Soil Science Society of America Journal, 44: 892–898.

Appendix I: Sensitivity Analysis Parameter Tables

Appendix I:

Sensitivity Analysis Parameter Tables

Table I-1:
Sensitivity Runs on Hydraulic Conductivity

Unit	Kmax (m/s)			Kmin (m/s)			Run #
	Base Case	Sensi-tivity Run	factor	Base Case	Sensi-tivity Run	factor	
31 Basin Deposits	2.5E-07	5.0E-07	2	2.5E-09	5.0E-09	2	6
71 North Structure	5.0E-05	5.0E-06	0.1	5.0E-05	5.0E-06	0.1	1
81 Siltstone	8.7E-09	8.7E-08	10	2.4E-10	2.4E-09	10	5
91 Clay	4.6E-10	4.6E-09	10	3.7E-11	3.7E-10	10	5
92 Clay in Layer 1	5.6E-09	5.6E-08	10	5.6E-09	5.6E-08	10	5
F#1&2 Grassy Mtn Fault W&E	3.0E-08	1.5E-06	50	6.7E-10	3.4E-08	50	2
F#4 SW-NE Fault 2	2.0E-10	1.0E-08	50	2.0E-10	1.0E-08	50	2
F#7a SE-NW Fault 4 South	1.4E-08	7.2E-07	50	1.2E-09	5.8E-08	50	2
F#8 Mine NS-Fault 1	5.0E-10	2.5E-08	50	5.0E-11	2.5E-09	50	2
F#9 Mine NS-Fault 2	2.4E-09	1.2E-07	50	2.4E-09	1.2E-07	50	2
F#10 Mine NS Fault 3	2.0E-10	1.0E-08	50	5.0E-11	2.5E-09	50	2
F#12 EW Near Grassy Spring	6.6E-10	3.3E-08	50	1.0E-10	5.0E-09	50	2
F#13 NS Near Grassy Spring	5.0E-10	2.5E-08	50	5.0E-10	2.5E-08	50	2
F#14 SW-NE Fault 4	1.0E-08	5.2E-07	50	1.3E-09	6.5E-08	50	2
F#31 Mine EW Fault 2	1.0E-10	5.0E-09	50	5.0E-11	2.5E-09	50	2

**Table I-2:
Sensitivity Runs on Storage and Porosity**

Unit	Ss (1/m)			Porosity			Run #
	Base Case	Sensi- tivity Run	factor	Base Case	Sensi- tivity Run	factor	
11, 13 Alluvium	1.0E-04	4.0E-05	0.4	0.25	0.125	0.5	3a
12 Lacustrine Sediments	1.0E-04	4.0E-05	0.4	0.3	0.125	0.417	3a
31 Basin Deposits; 72, 73 PW-4 and Prod-1 Zones	4.0E-05	1.2E-05	0.4	0.15	0.075	0.5	3a
74 PW-1 Zone ; 82, 83 GMW17-33 and GMW17-32 Zones	1.2E-05	2.0E-06	0.4	0.15	0.075	0.5	3a
81, 91 Mine-Area Low-K and Moderate-K, 92 Clay in Layer 1	2.0E-06	2.0E-06	0.4	0.15	0.075	0.5	3a
41 Kern Tuff	2.0E-06	4.0E-07	0.4	0.05	0.025	0.5	3a
Faults and 51, 52, 61 Basalt, Ryodacite	2.0E-06	2.0E-06	0.4	0.01	0.005	0.5	3a
11, 13 Alluvium	4.0E-07	1.5E-04	1.5	0.25	0.25	-	3b
12 Lacustrine Sediments	2.0E-06	1.5E-04	1.5	0.3	0.3	-	3b
31 Basin Deposits; 72, 73 PW-4 and Prod-1 Zones	3.0E-05	4.5E-05	1.5	0.15	0.225	1.5	3b
74 PW-1 Zone ; 82, 83 GMW17-33 and GMW17-32 Zones	5.0E-06	7.5E-06	1.5	0.15	0.225	1.5	3b
81, 91 Mine-Area Low-K and Moderate-K, 92 Clay in Layer 1	5.0E-06	7.5E-06	1.5	0.15	0.225	1.5	3b
41 Kern Tuff	1.0E-06	1.5E-06	1.5	0.05	0.075	1.5	3b
Faults and 51, 52, 61 Basalt, Ryodacite	5.0E-06	7.5E-06	1.5	0.01	0.015	1.5	3b

**Table I-3:
Sensitivity Runs on Other Parameters**

Parmeter	Base Case	Sensitivity Run	factor	Run #
Highest Recharge Rate (in/y)	0.94	0.71	0.75	5
Intermediate Recharge Rate (in/y)	0.50	0.38	0.75	5
Low Recharge Rate (in/y)	0.25	0.19	0.75	5
Transfer coeff (x1e-4 1/d)	1	0.001	0.001	8

***Appendix II:
Sensitivity Analysis Individual
Drawdown Maps***

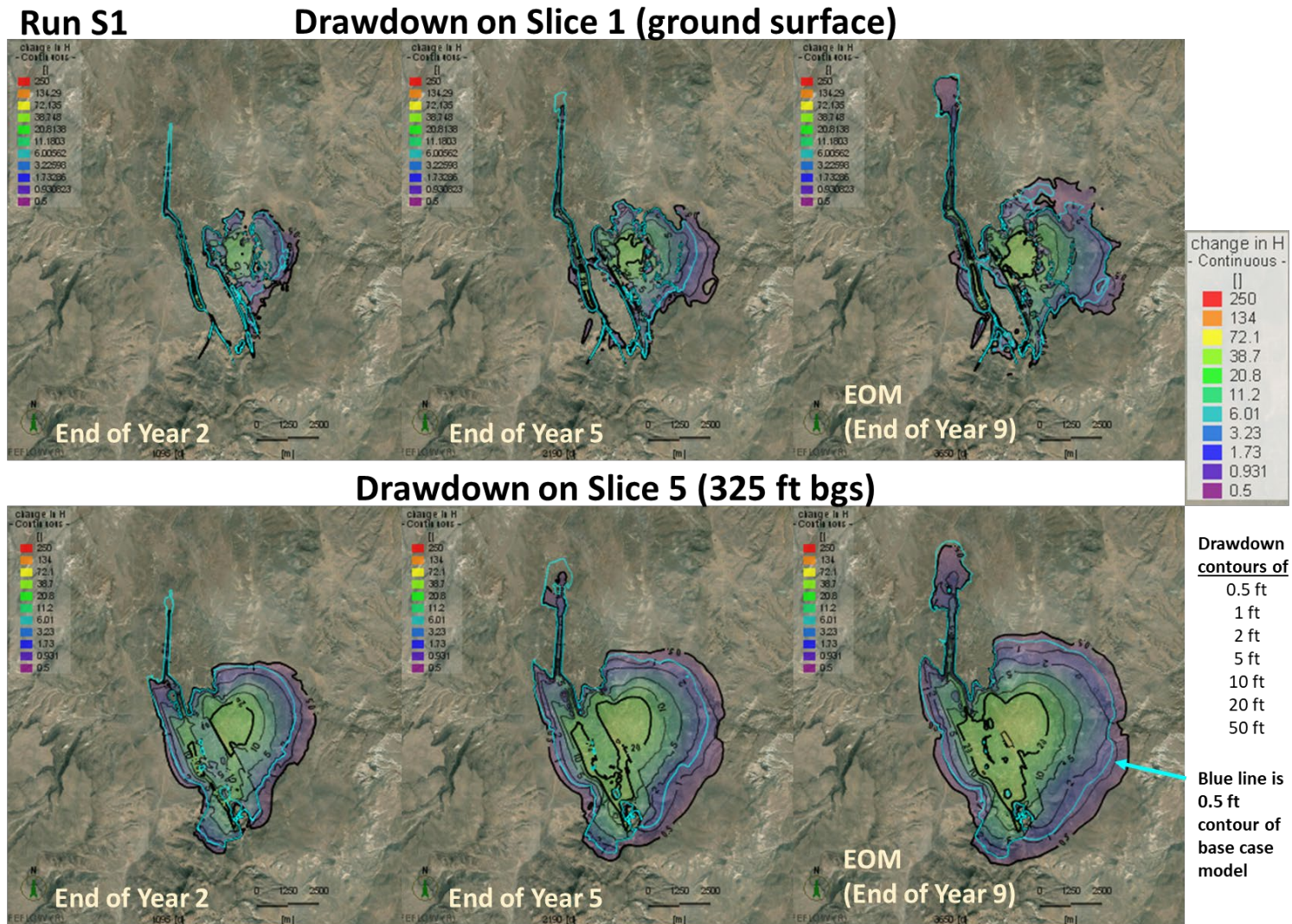


Figure II-1: Predicted Drawdown, Model Slices 1 and 5, End of Mine Years 2, 5 and 9, Sensitivity Run S1.

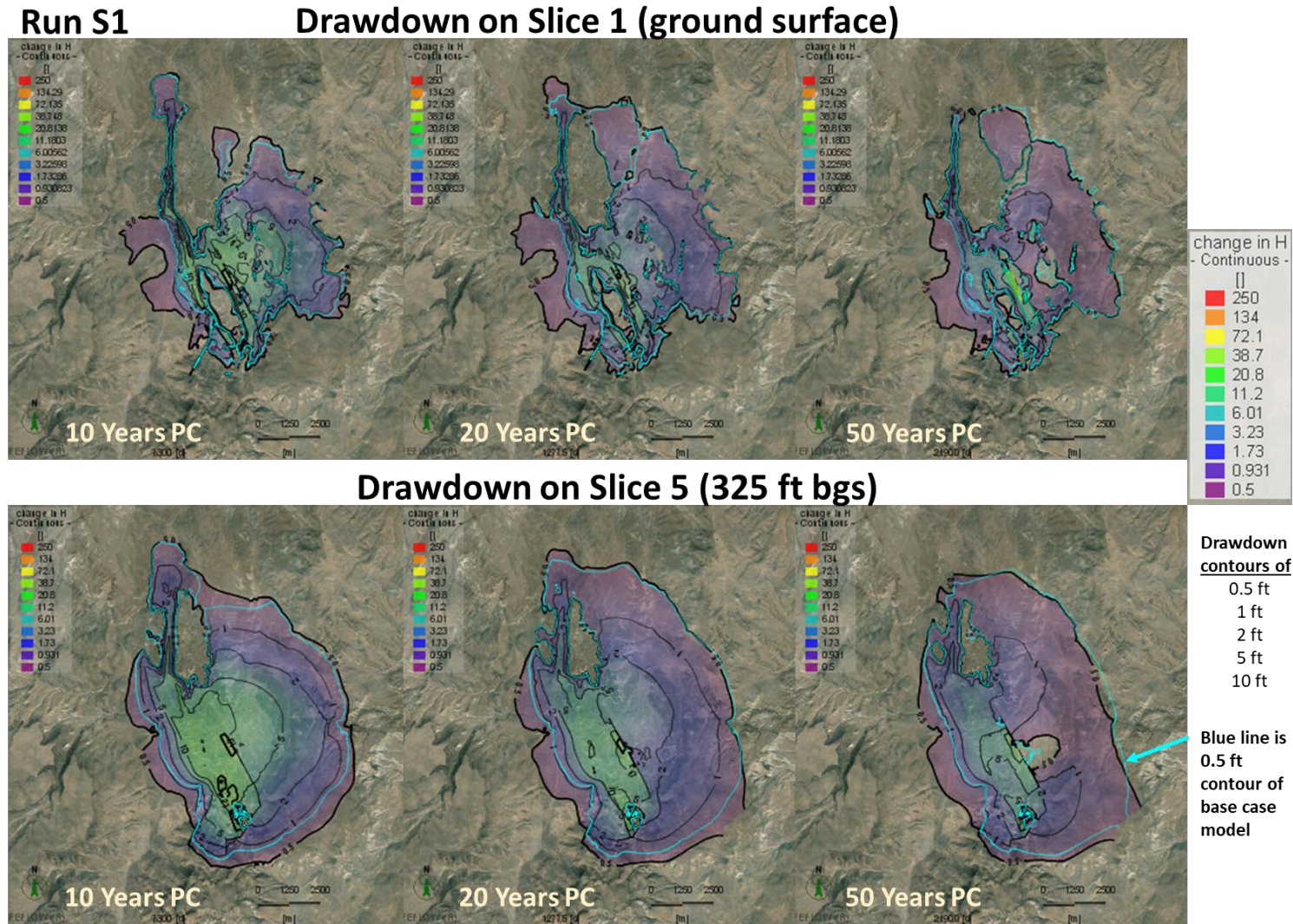
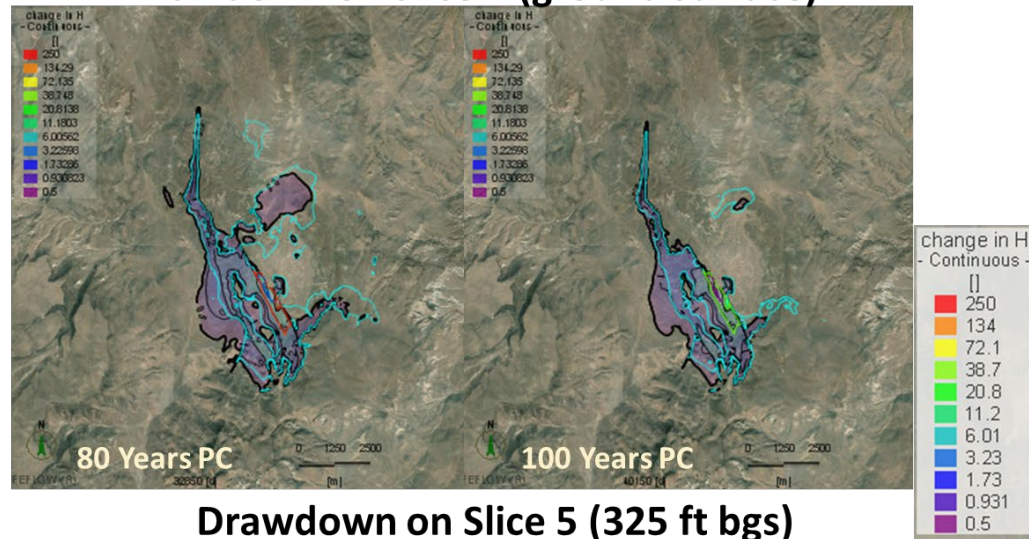


Figure II-2: Predicted Drawdown, Model Slices 1 and 5, 10, 20 and 50 Years After End of Mining, Sensitivity Run S1.

Run S1

Drawdown on Slice 1 (ground surface)



Drawdown on Slice 5 (325 ft bgs)

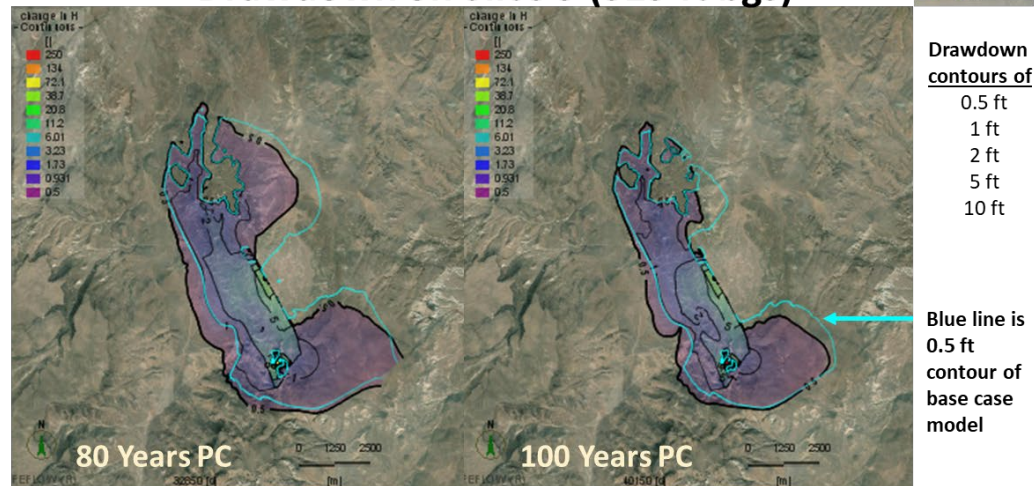


Figure II-3: Predicted Drawdown, Model Slices 1 and 5, 80 and 100 Years After End of Mining, Sensitivity Run S1.

Run S1

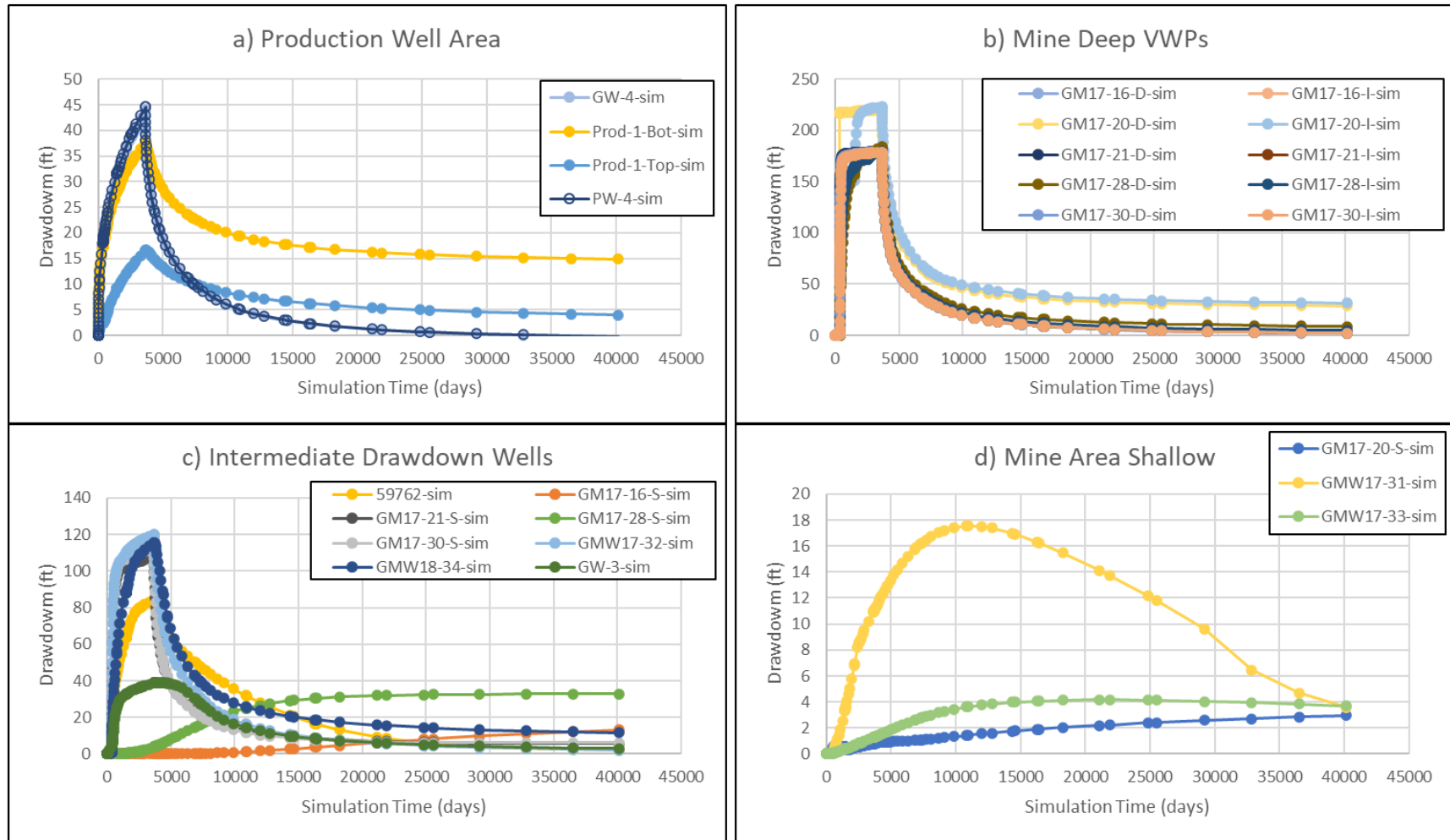


Figure II-4: Time-Series of Simulated Drawdown, Higher Drawdown Wells, Sensitivity Run S1.

Run S1

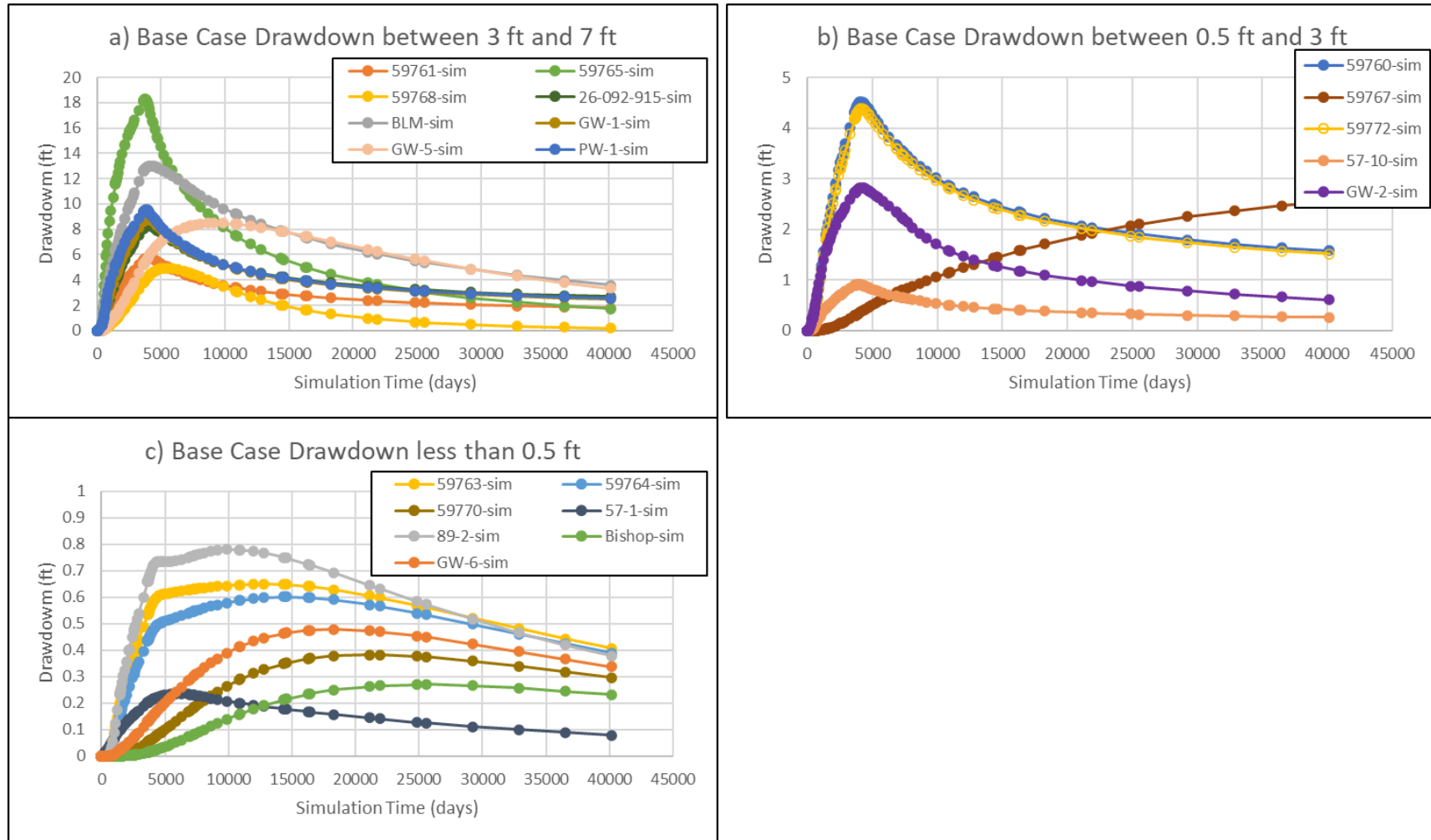


Figure II-5: Time-Series of Simulated Drawdown, Lower Drawdown Wells, Sensitivity Run S1.

Run S1

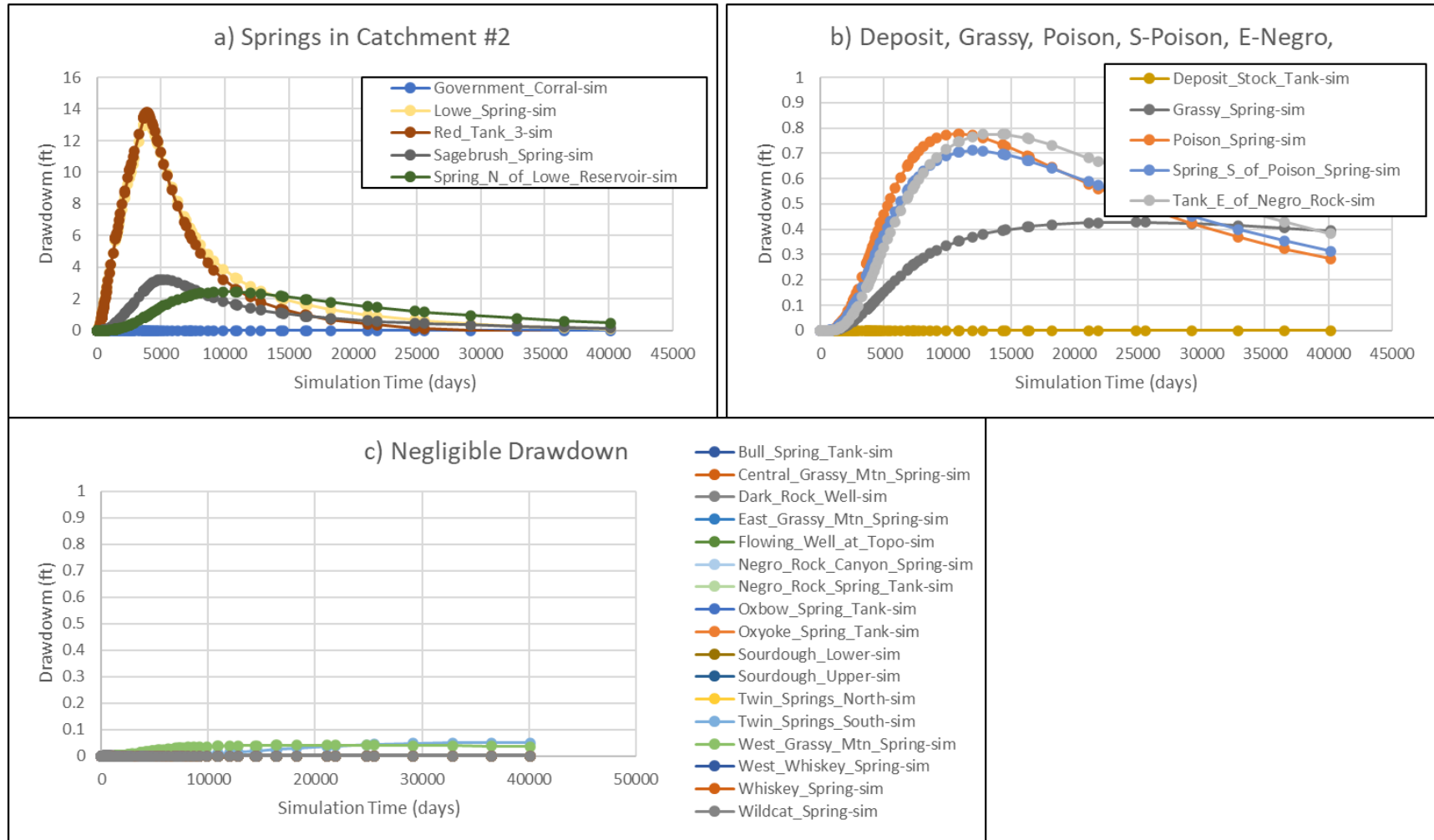


Figure II-6: Time-Series of Simulated Drawdown, Springs, Sensitivity Run S1.

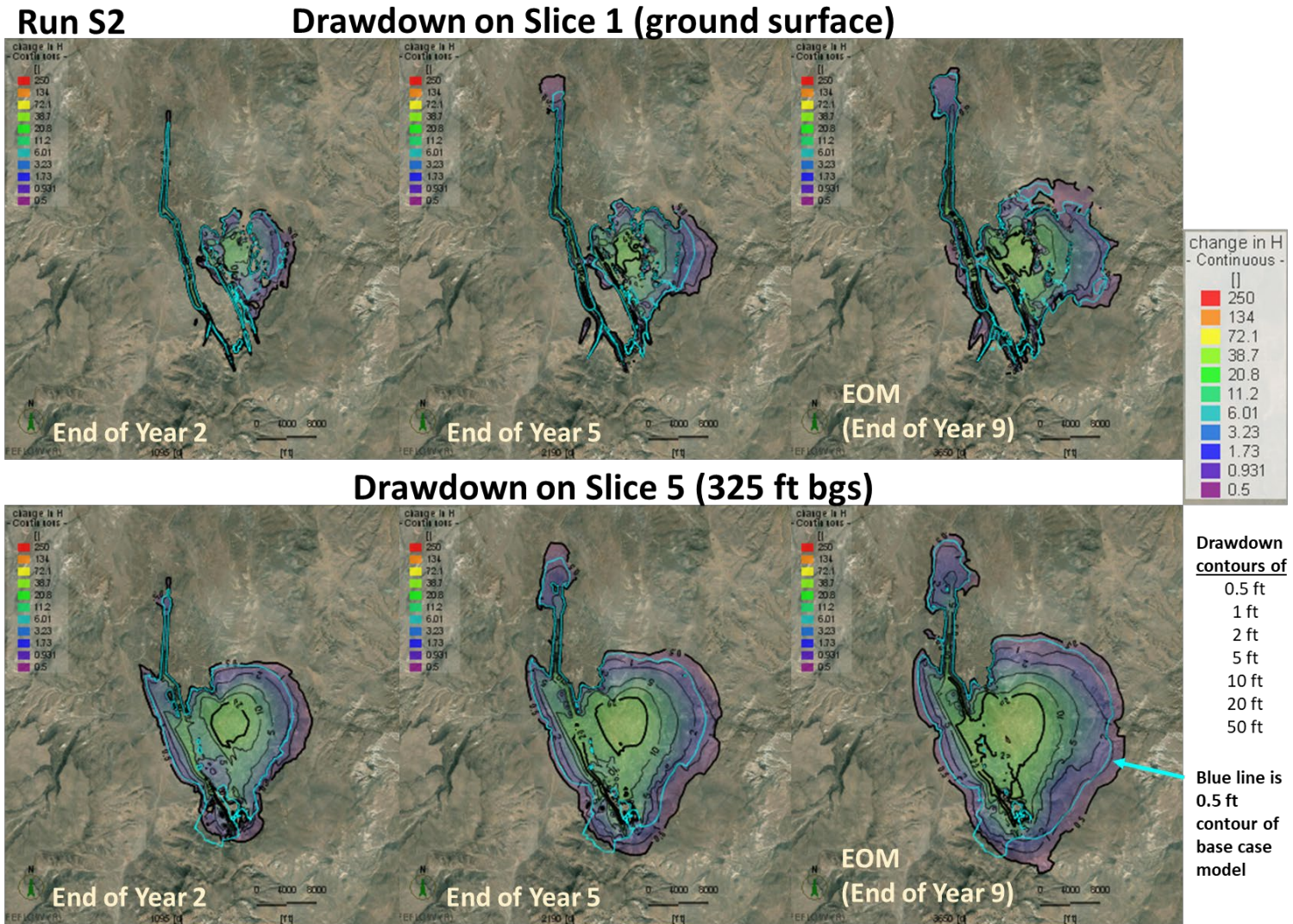


Figure II-7: Predicted Drawdown, Model Slices 1 and 5, End of Mine Years 2, 5 and 9, Sensitivity Run S2.

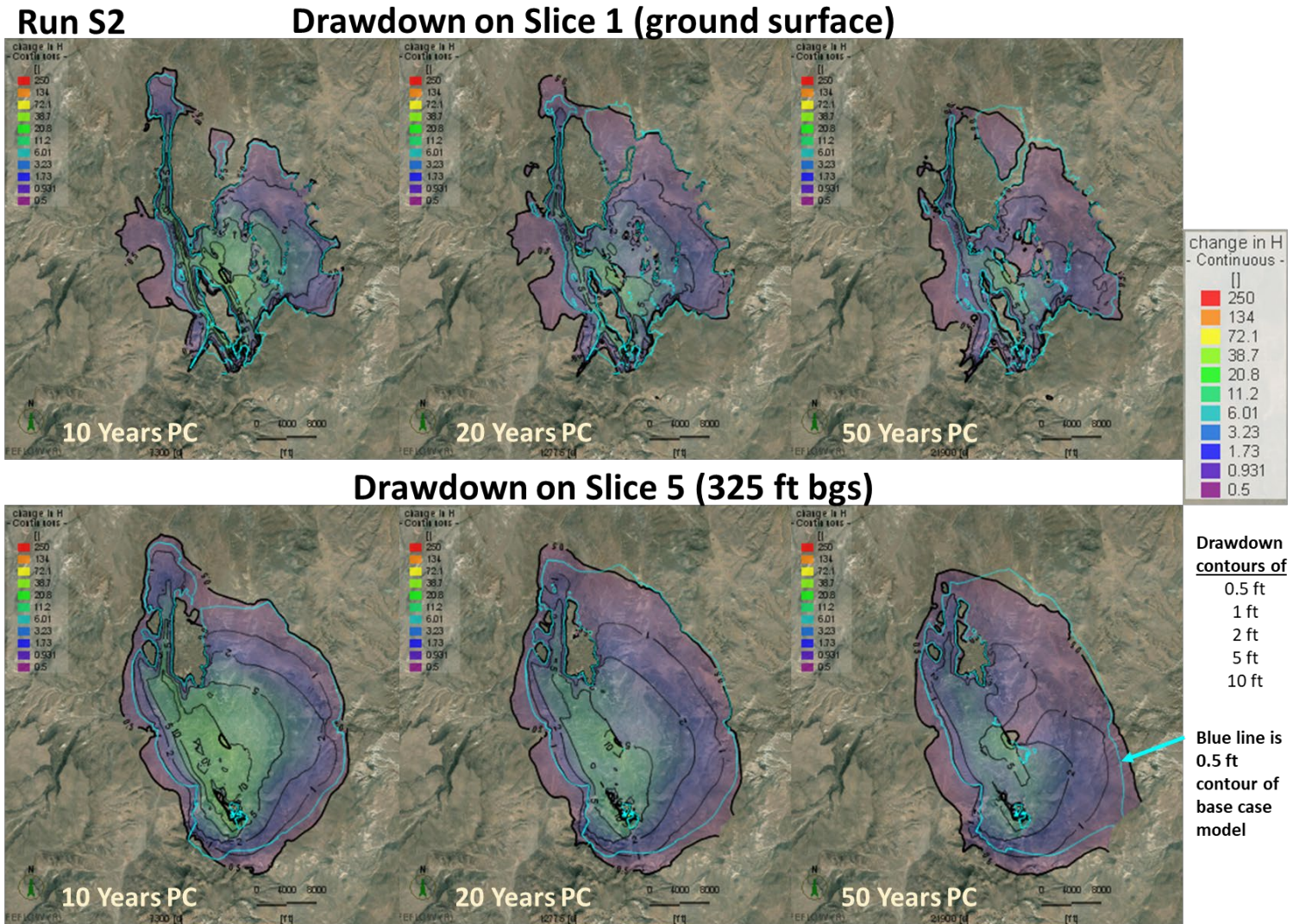
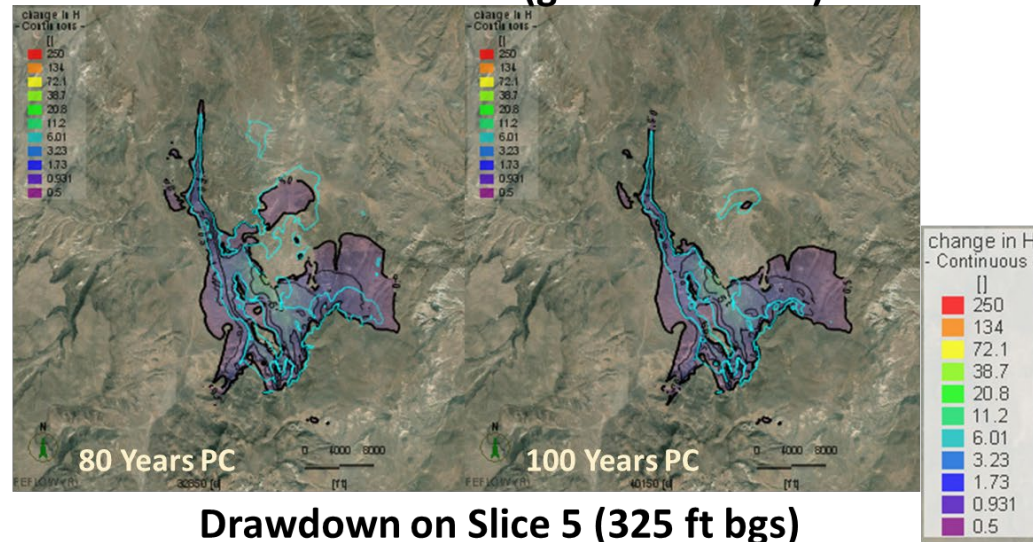


Figure II-8: Predicted Drawdown, Model Slices 1 and 5, 10, 20 and 50 Years After End of Mining, Sensitivity Run S2.

Run S2

Drawdown on Slice 1 (ground surface)



Drawdown on Slice 5 (325 ft bgs)

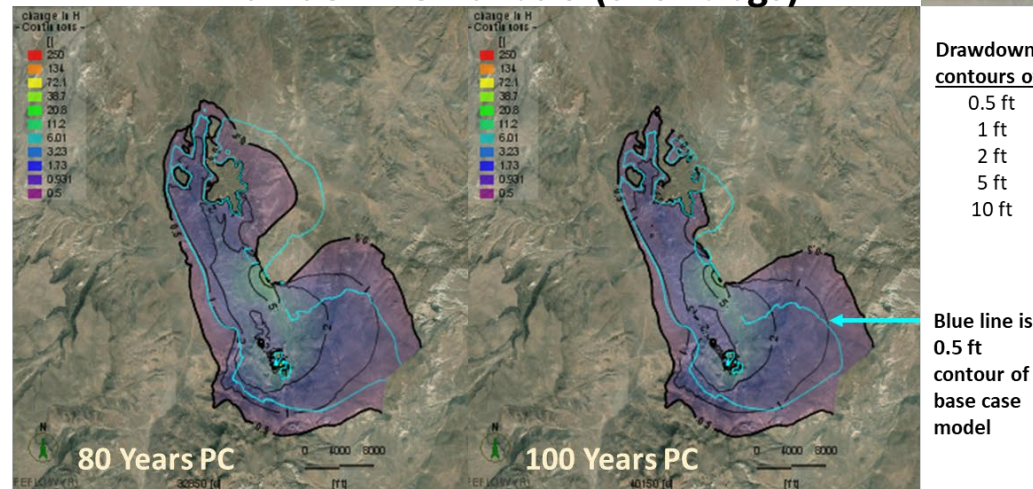


Figure II-9: Predicted Drawdown, Model Slices 1 and 5, 80 and 100 Years After End of Mining, Sensitivity Run S2.

Run S2

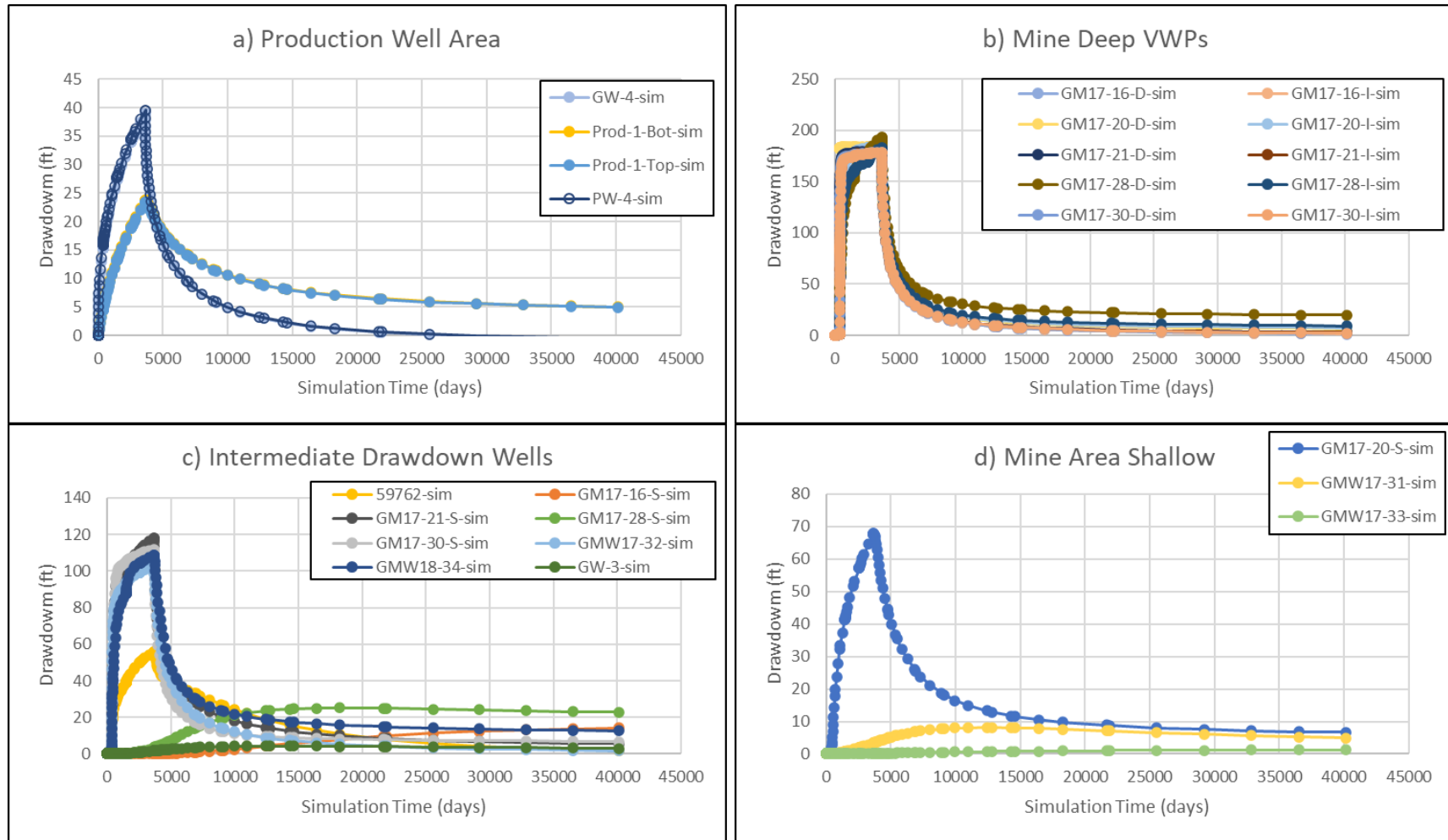


Figure II-10: Time-Series of Simulated Drawdown, Higher Drawdown Wells, Sensitivity Run S2.

Run S2

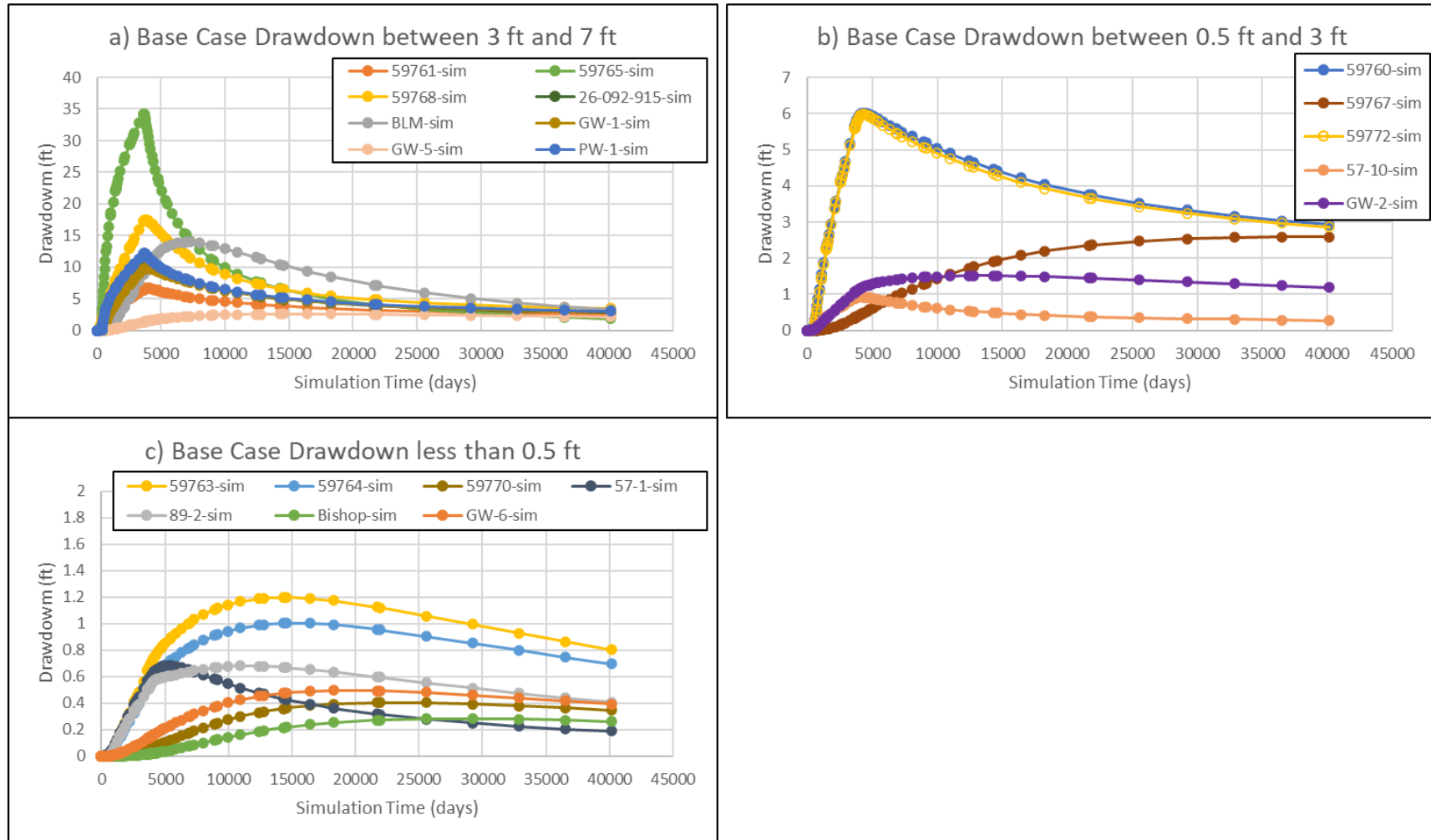


Figure II-11: Time-Series of Simulated Drawdown, Lower Drawdown Wells, Sensitivity Run S2.

Run S2

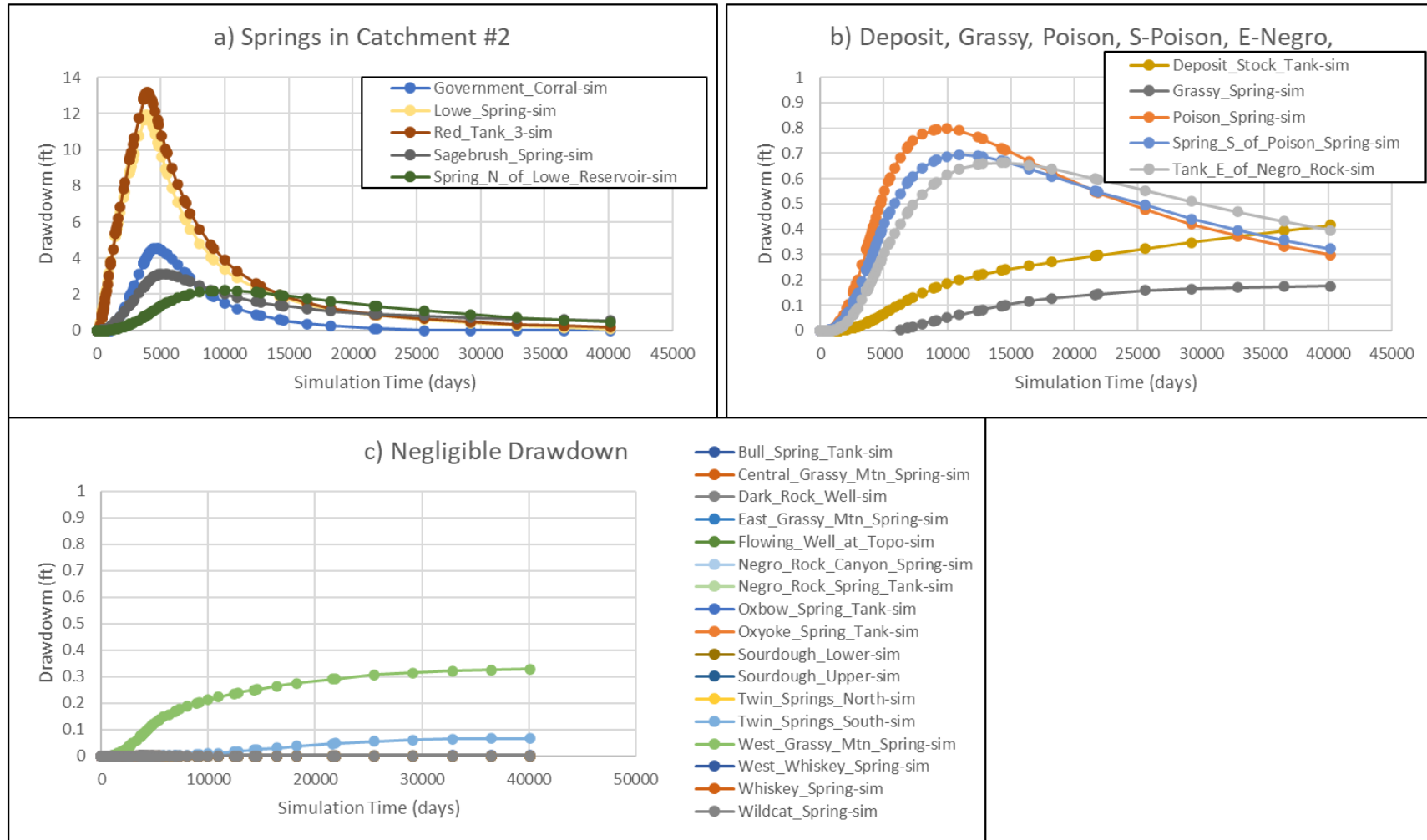


Figure II-12: Time-Series of Simulated Drawdown, Springs, Sensitivity Run S2.

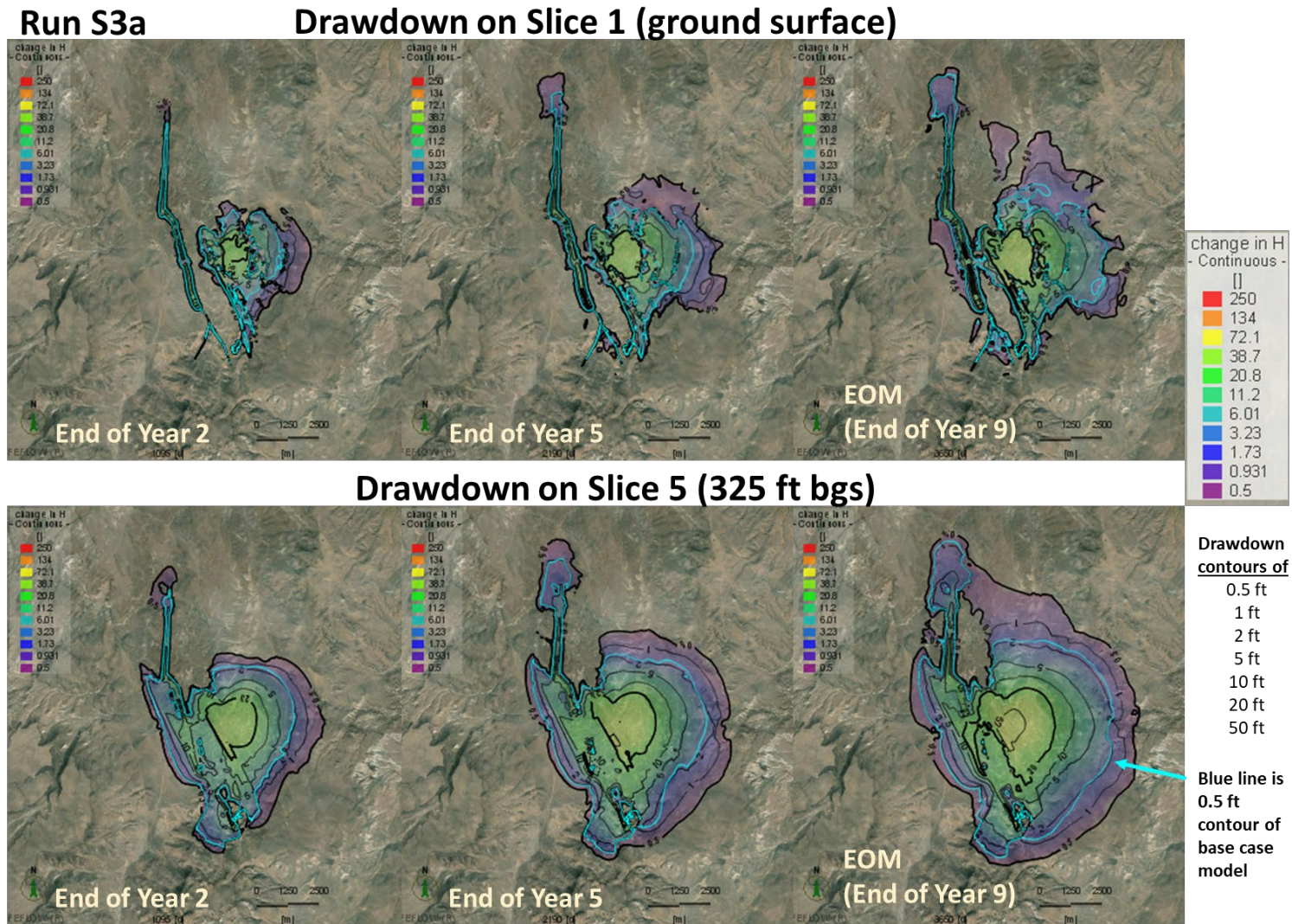


Figure II-13: Predicted Drawdown, Model Slices 1 and 5, End of Mine Years 2, 5 and 9, Sensitivity Run S3a.

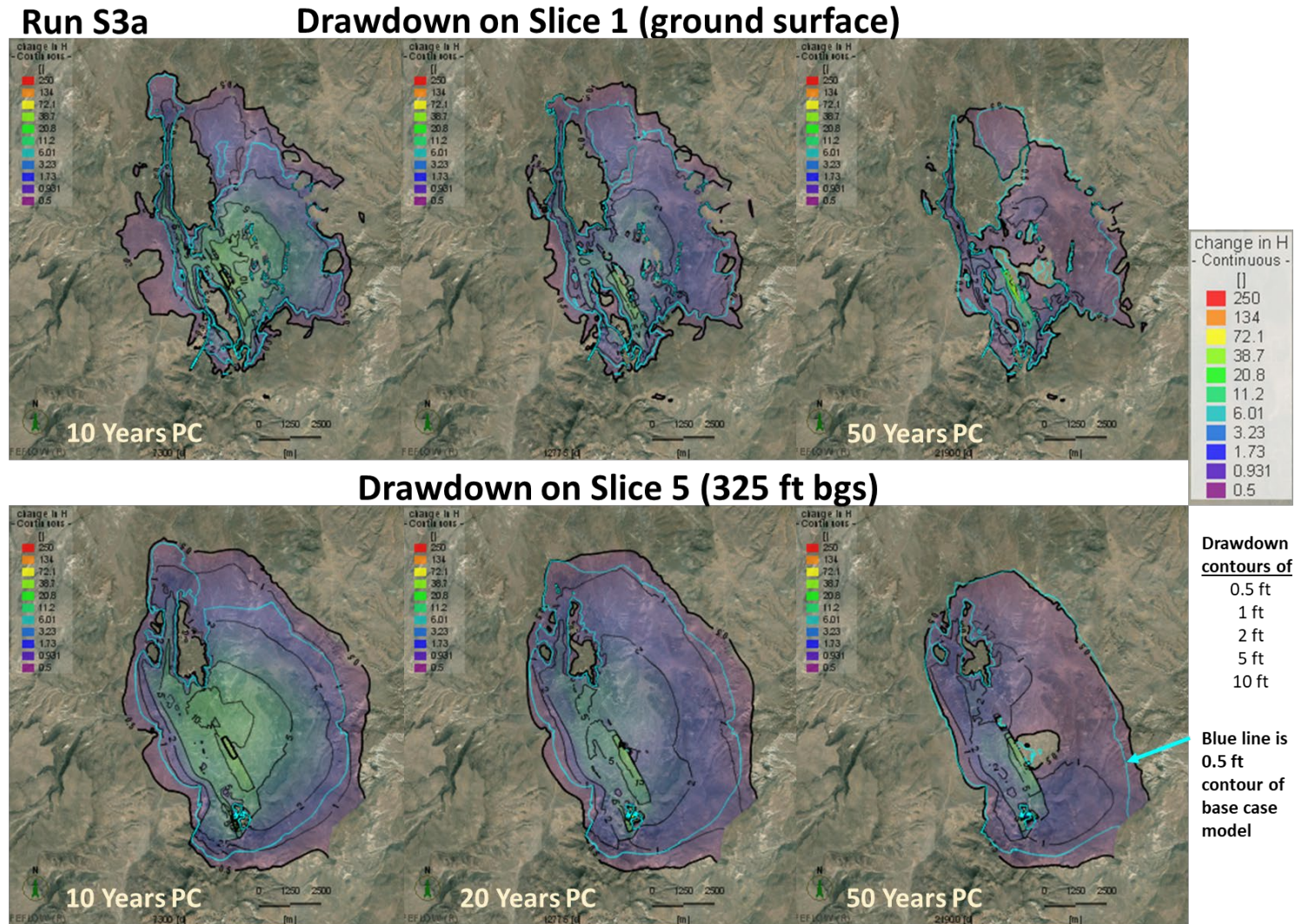
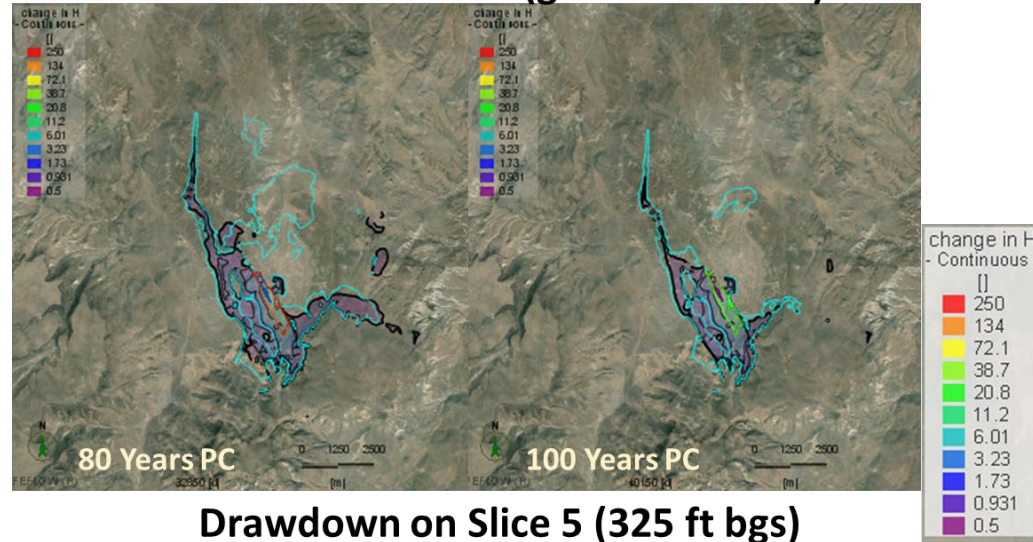


Figure II-14: Predicted Drawdown, Model Slices 1 and 5, 10, 20 and 50 Years After End of Mining, Sensitivity Run S3a.

Run S3a

Drawdown on Slice 1 (ground surface)



Drawdown on Slice 5 (325 ft bgs)

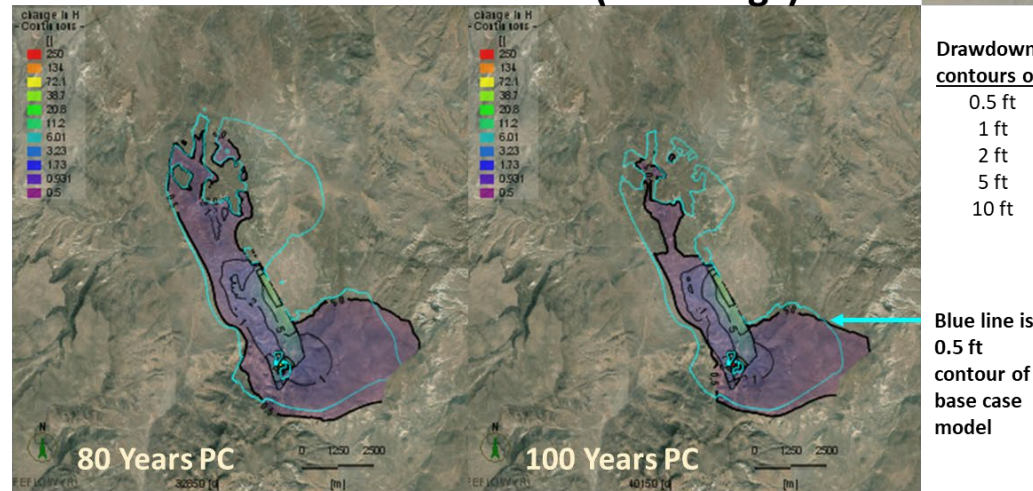


Figure II-15: Predicted Drawdown, Model Slices 1 and 5, 80 and 100 Years After End of Mining, Sensitivity Run S3a.

Run S3a

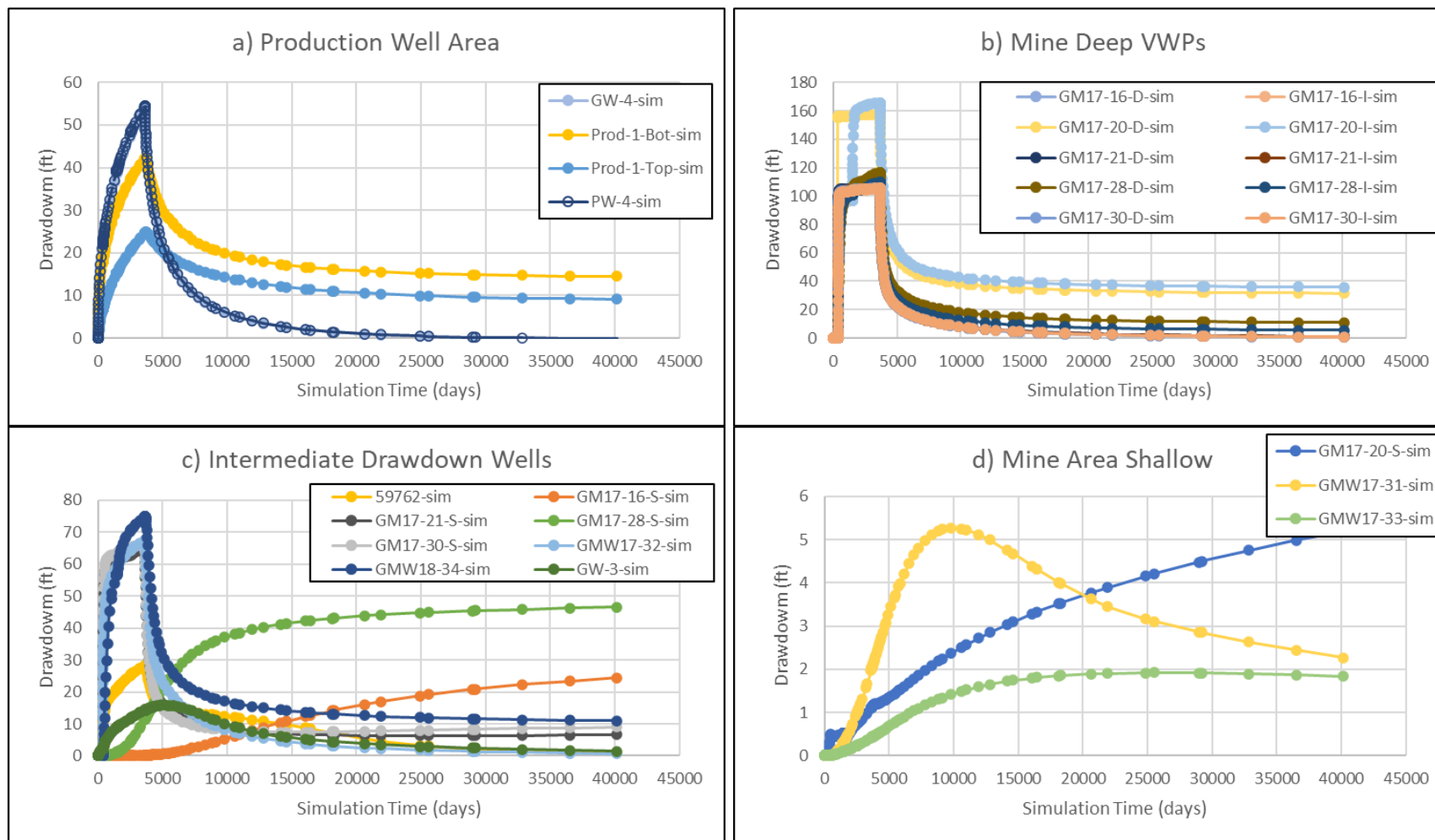


Figure II-16: Time-Series of Simulated Drawdown, Higher Drawdown Wells, Sensitivity Run S3a.

Run S3a

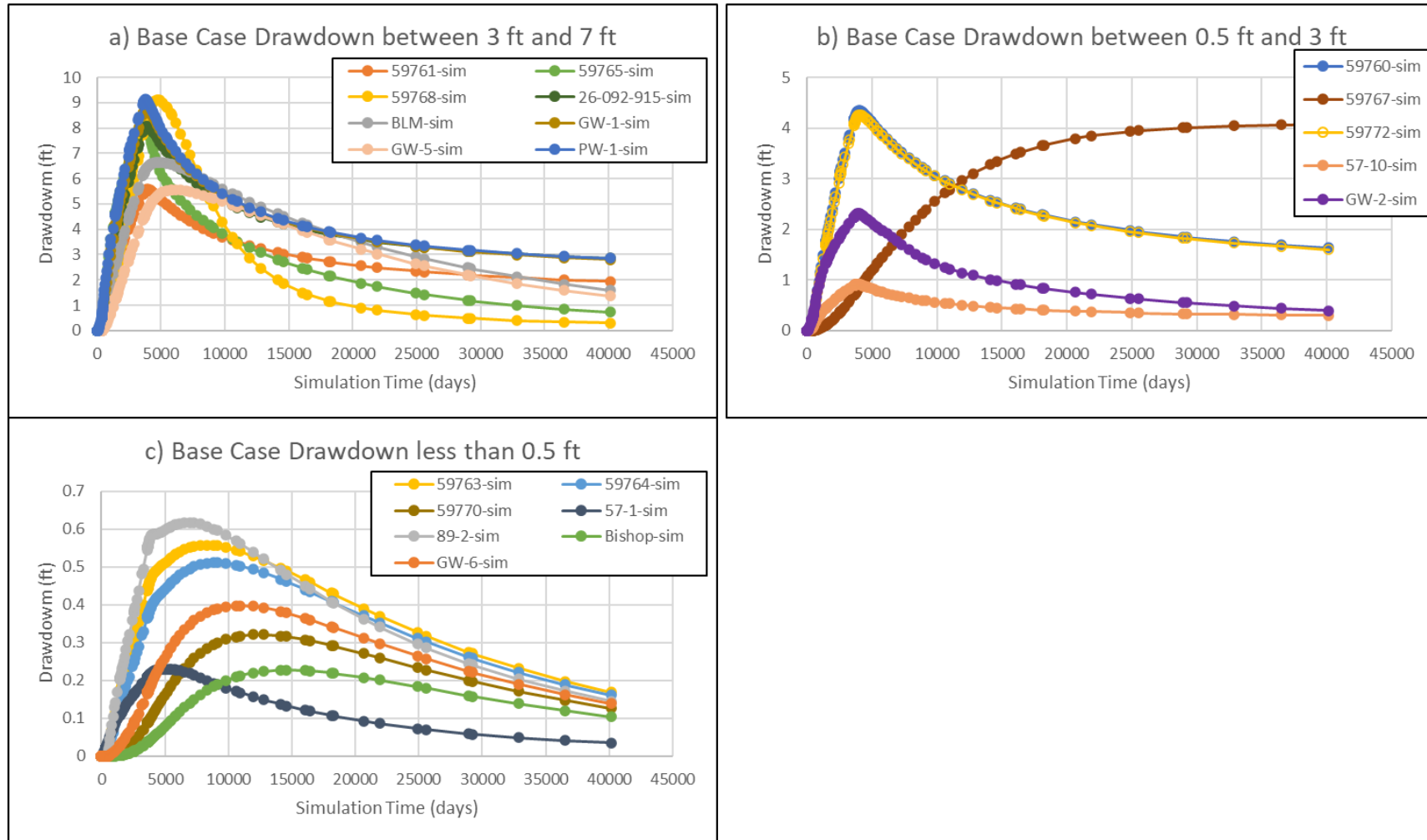


Figure II-17: Time-Series of Simulated Drawdown, Lower Drawdown Wells, Sensitivity Run S3a.

Run S3a

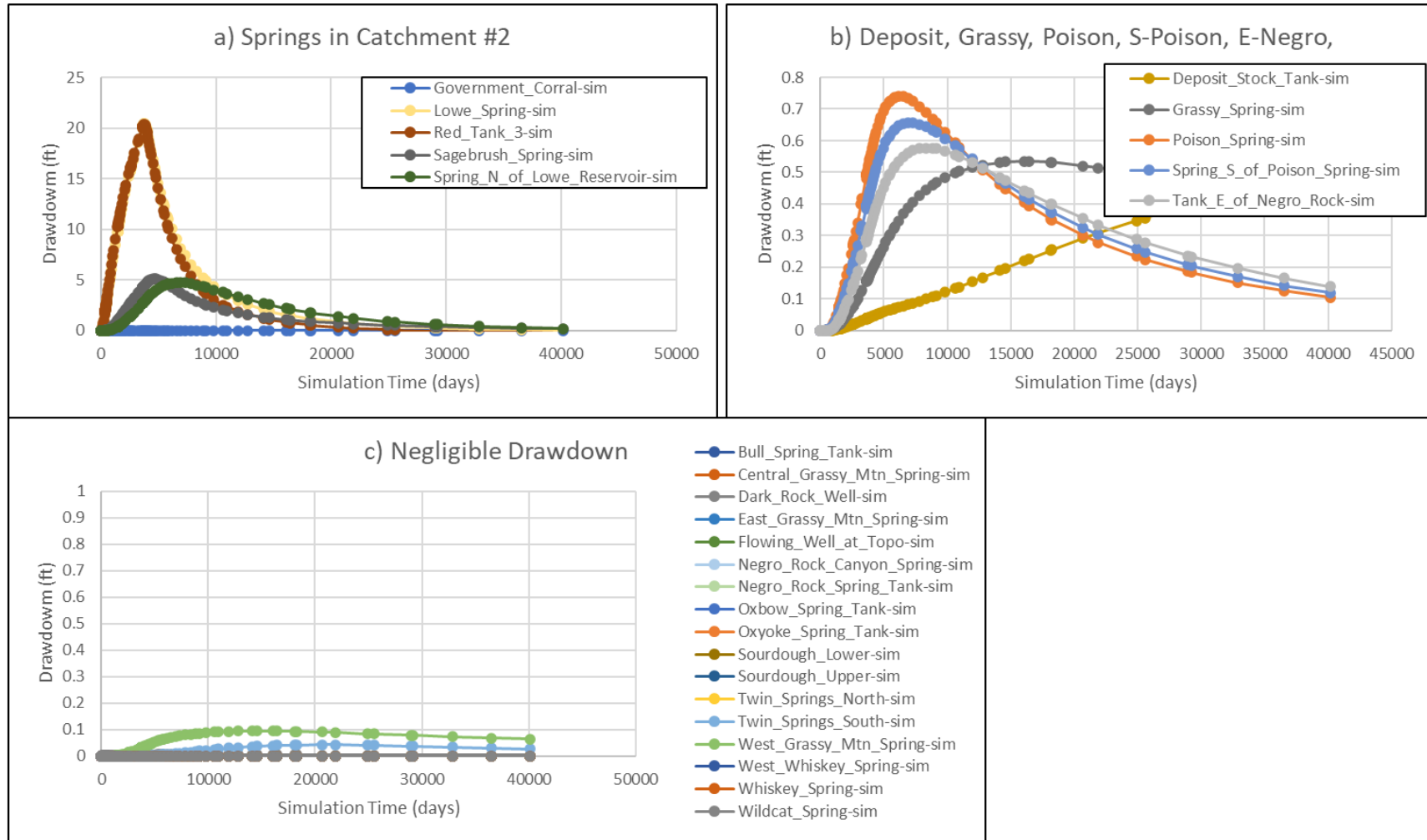


Figure II-18: Time-Series of Simulated Drawdown, Springs, Sensitivity Run S3a.

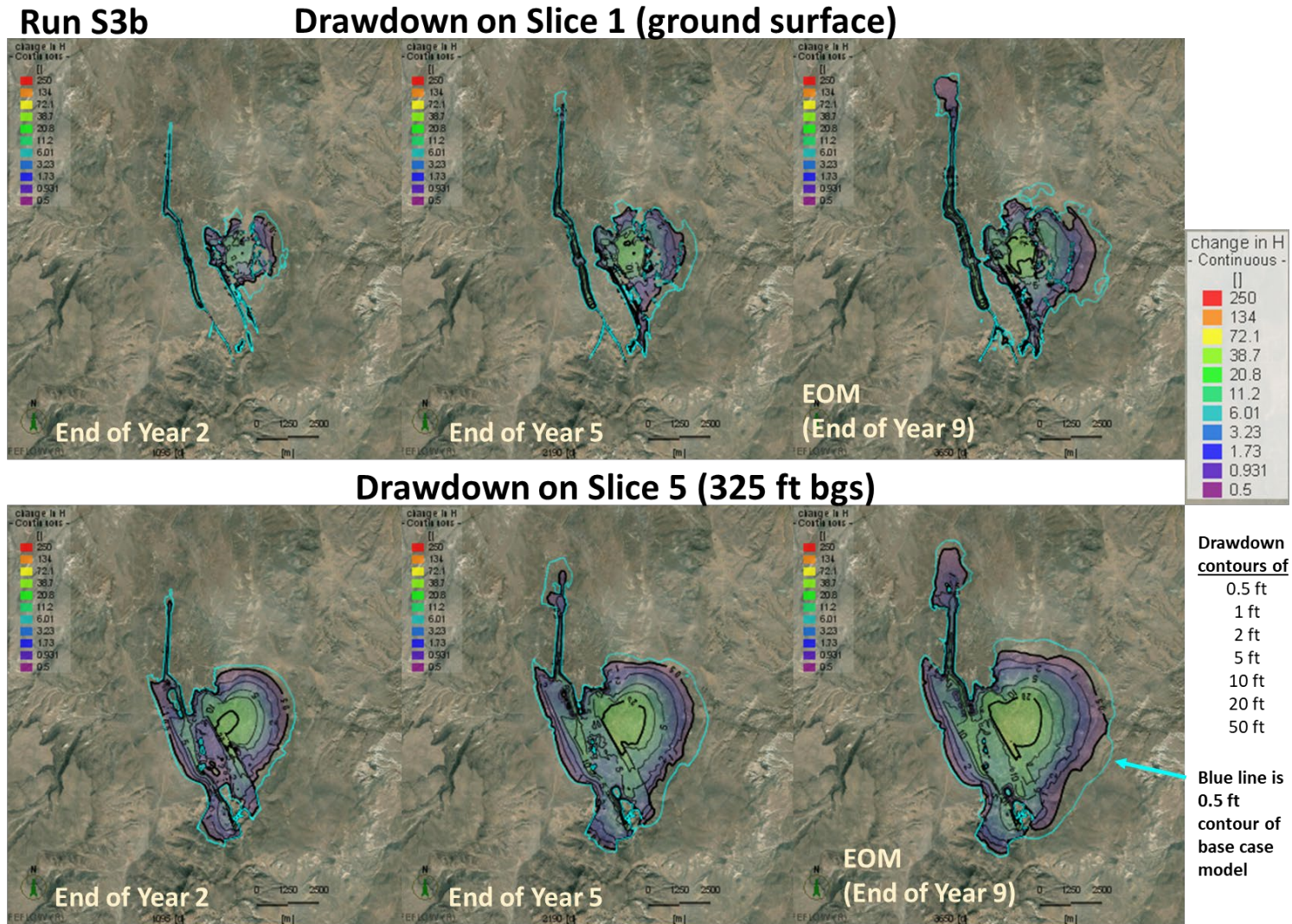


Figure II-19: Predicted Drawdown, Model Slices 1 and 5, End of Mine Years 2, 5 and 9, Sensitivity Run S3b.

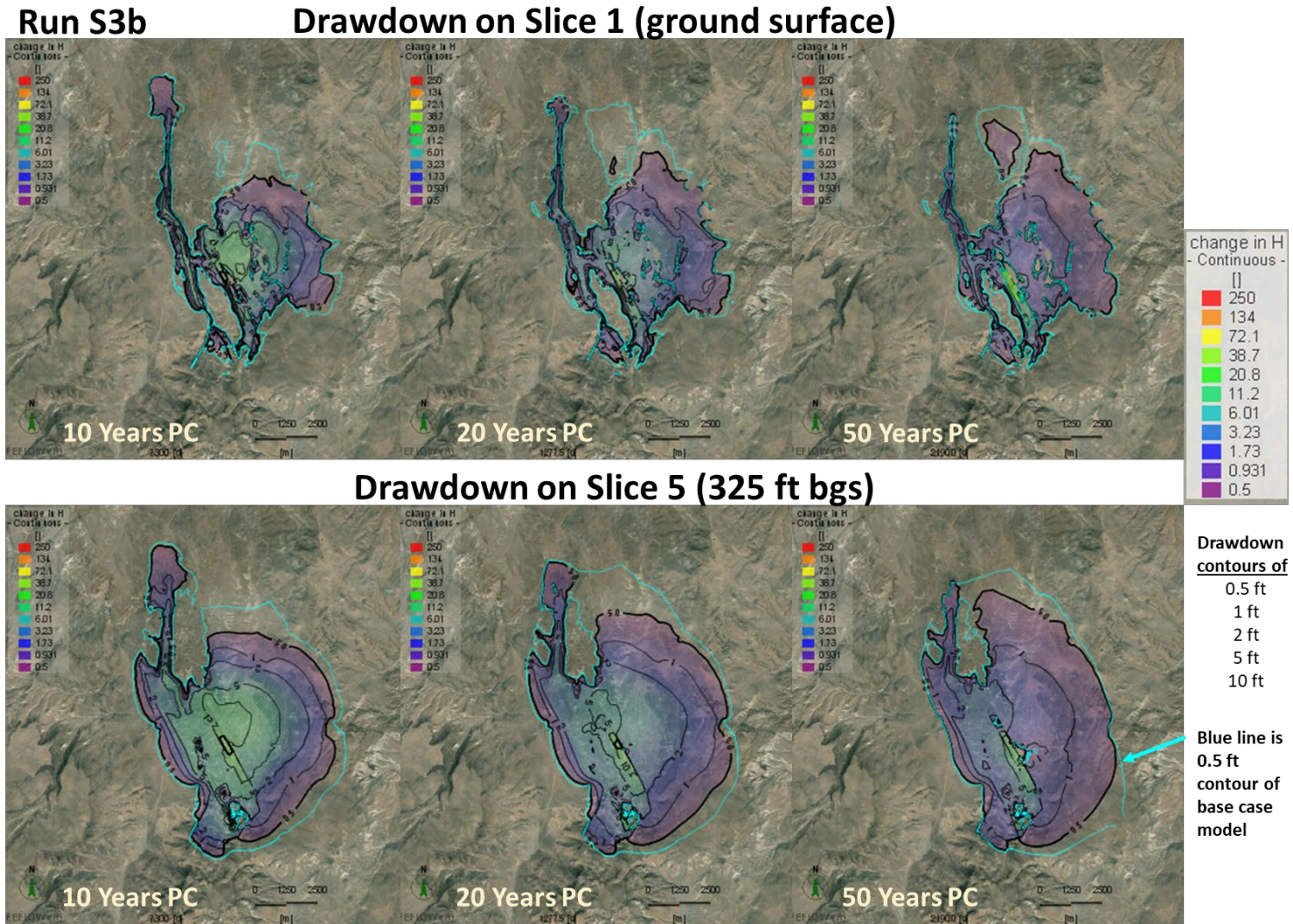
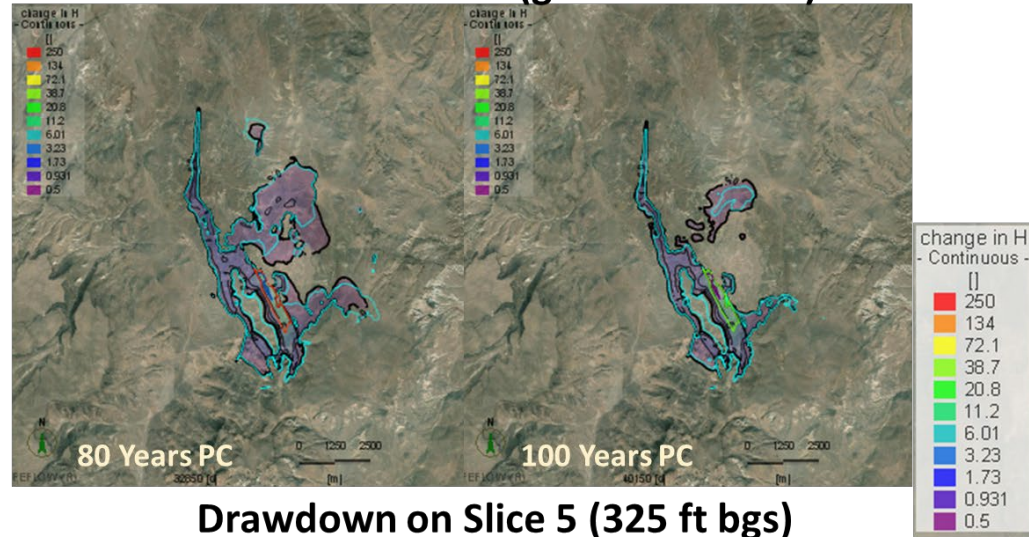


Figure II-20: Predicted Drawdown, Model Slices 1 and 5, 10, 20 and 50 Years After End of Mining, Sensitivity Run S3b.

Run S3b

Drawdown on Slice 1 (ground surface)



Drawdown on Slice 5 (325 ft bgs)

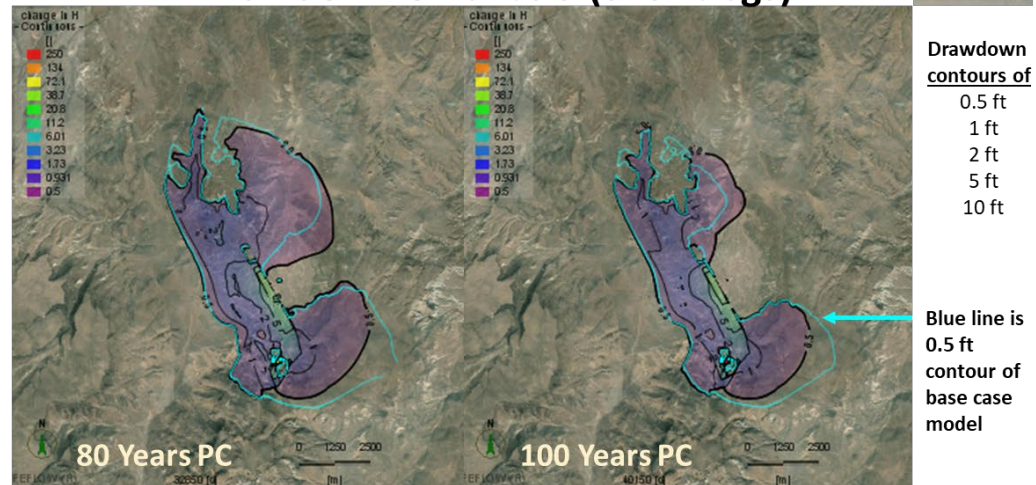


Figure II-21: Predicted Drawdown, Model Slices 1 and 5, 80 and 100 Years After End of Mining, Sensitivity Run S3b.

Run S3b

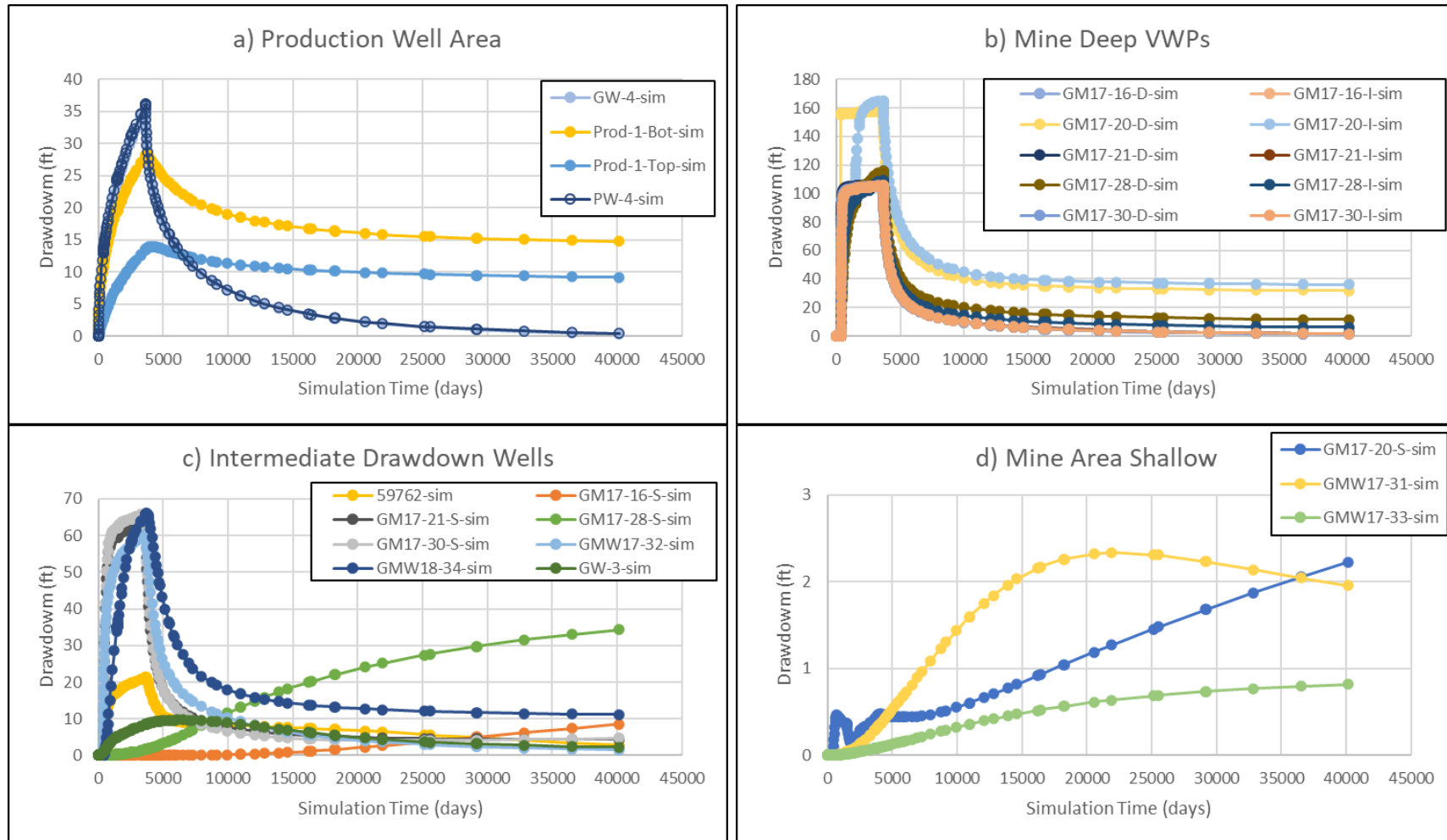


Figure II-22: Time-Series of Simulated Drawdown, Higher Drawdown Wells, Sensitivity Run S3b.

Run S3b

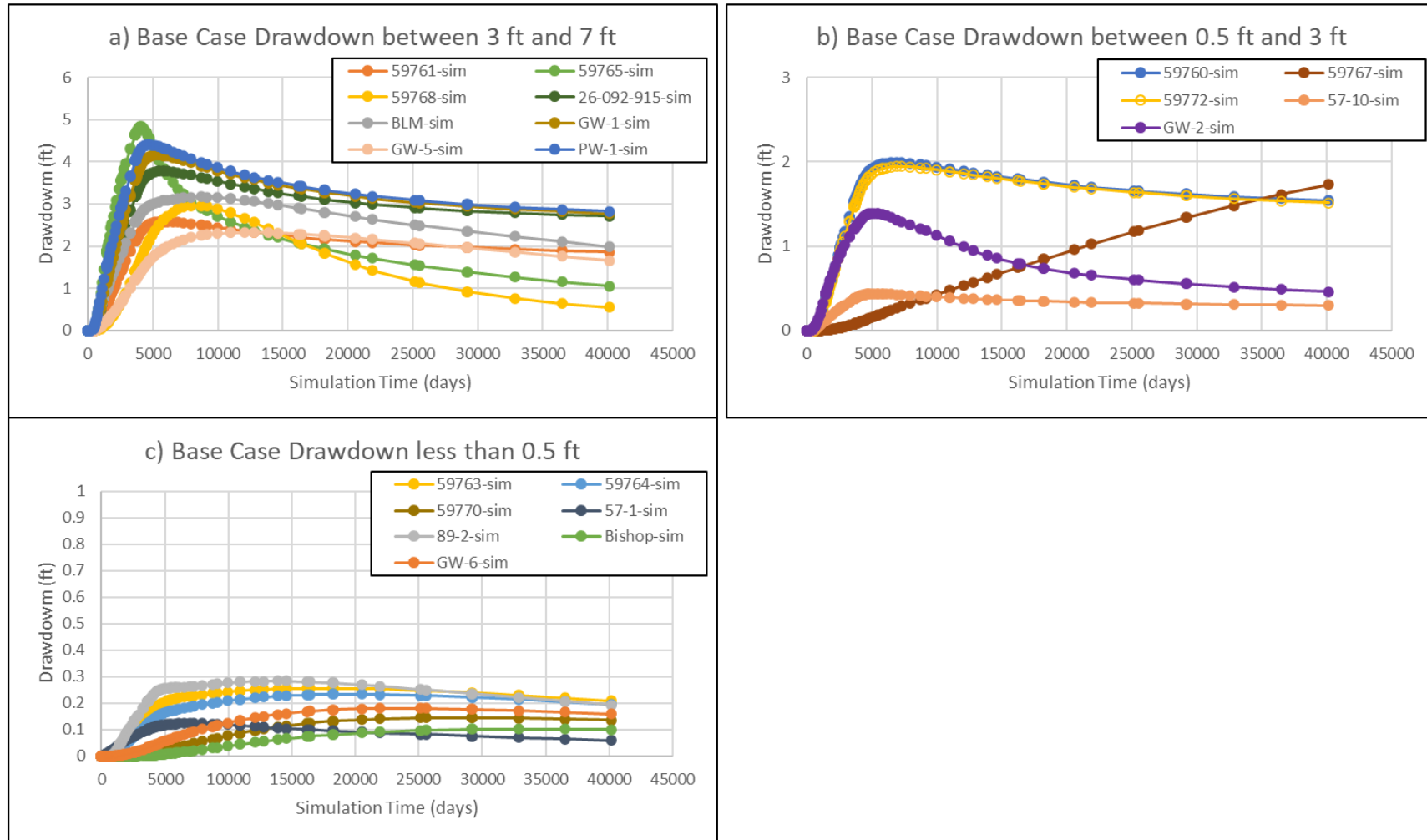


Figure II-23: Time-Series of Simulated Drawdown, Lower Drawdown Wells, Sensitivity Run S3b.

Run S3b

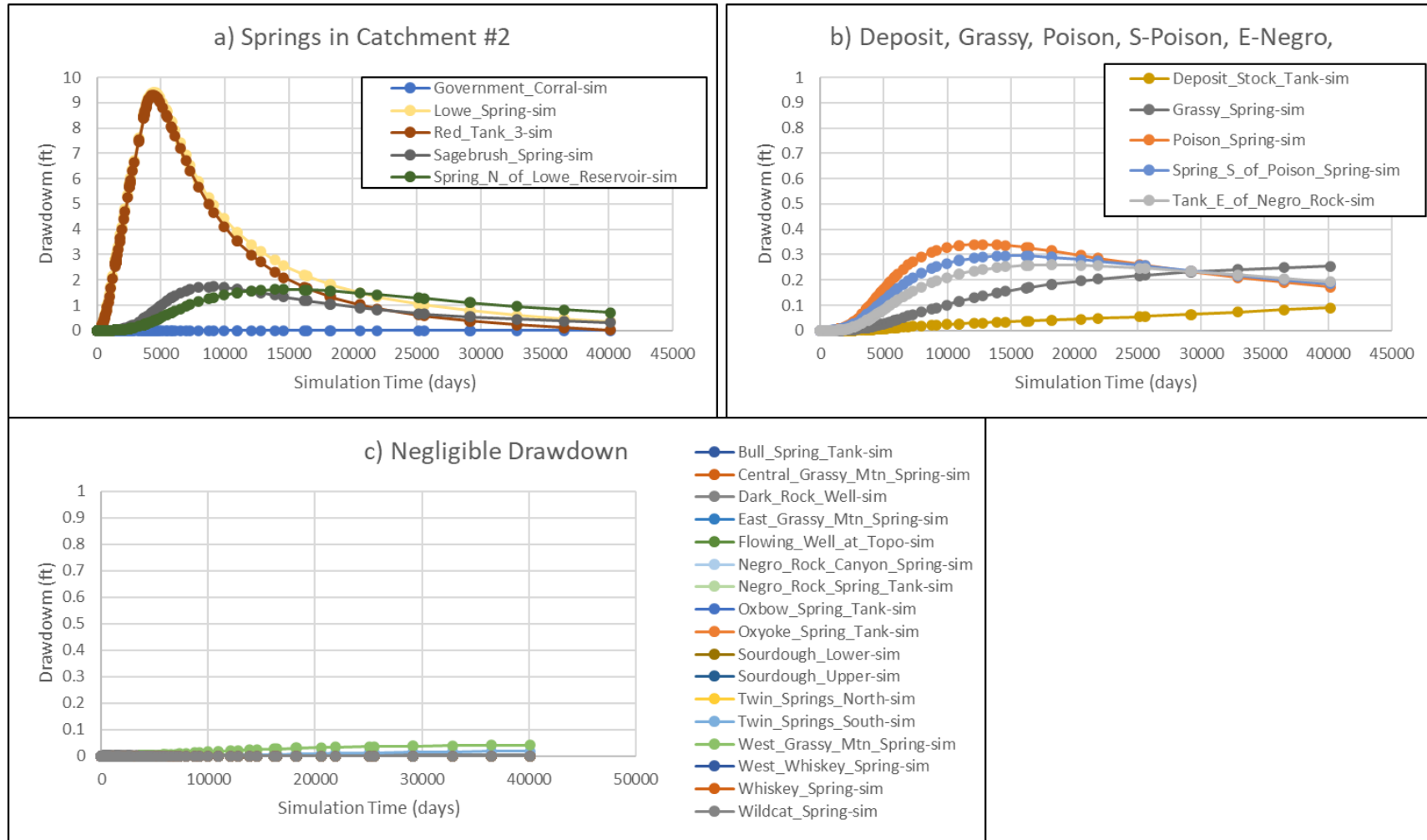


Figure II-24: Time-Series of Simulated Drawdown, Springs, Sensitivity Run S3b.

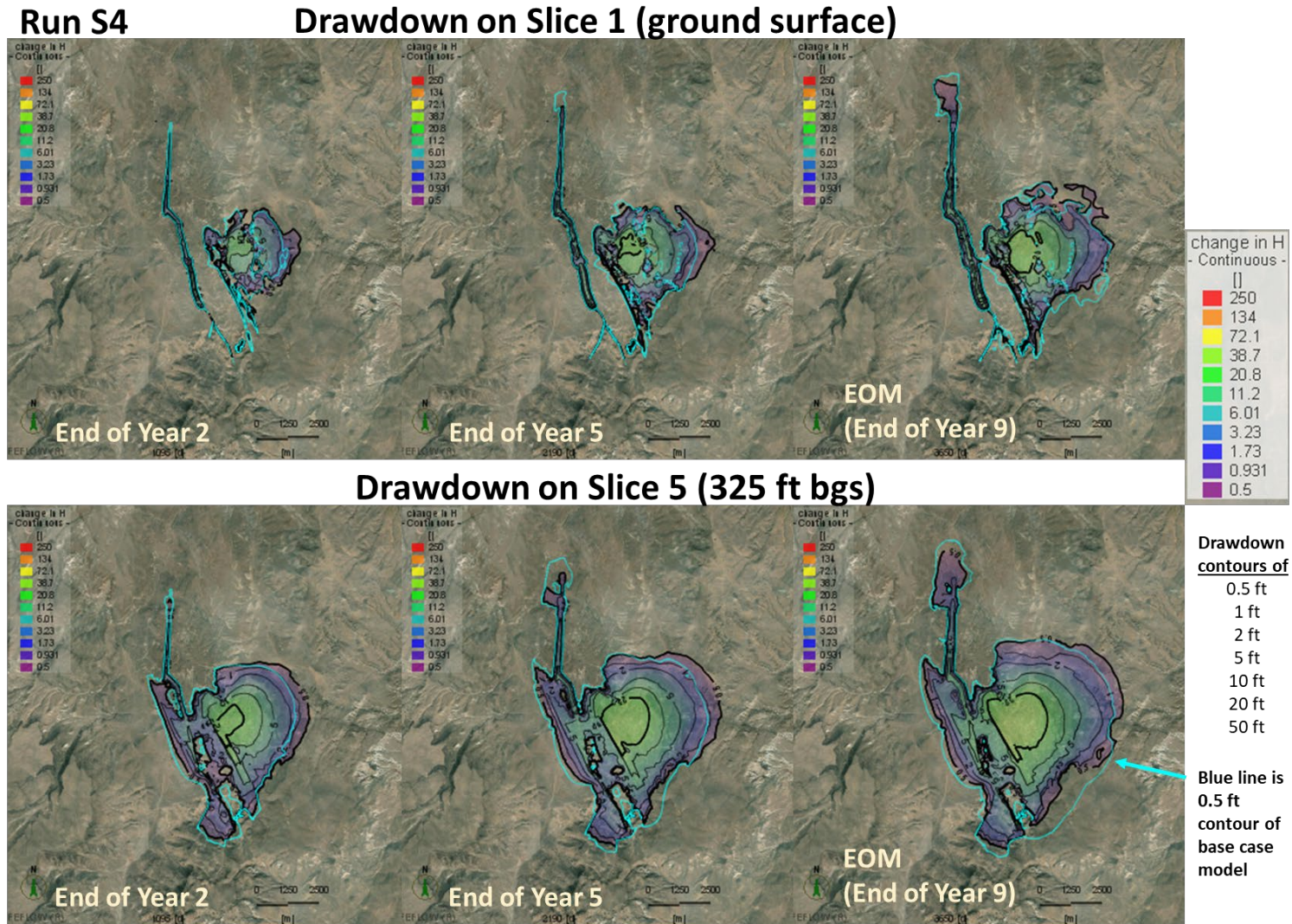


Figure II-25: Predicted Drawdown, Model Slices 1 and 5, End of Mine Years 2, 5 and 9, Sensitivity Run S4.

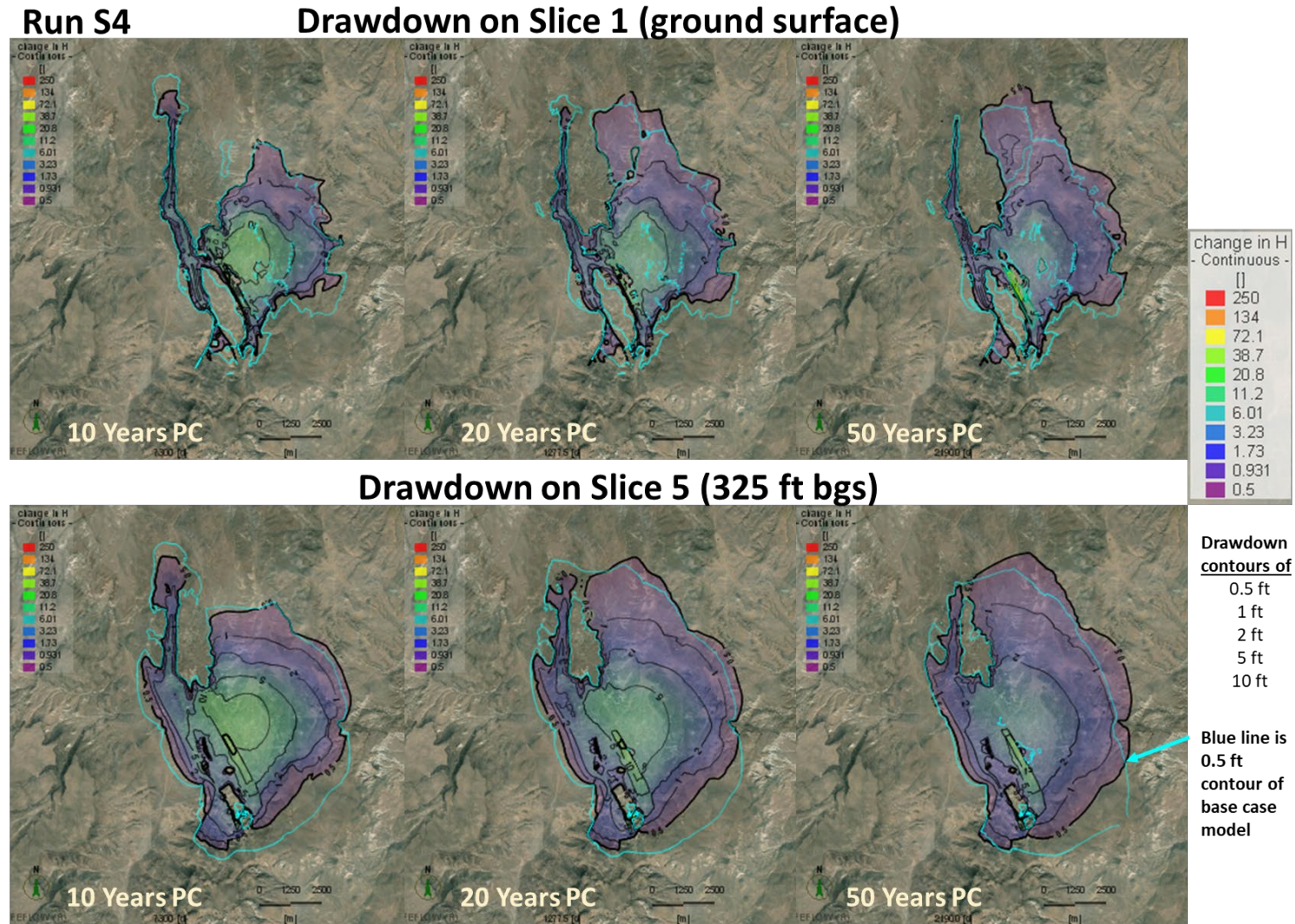
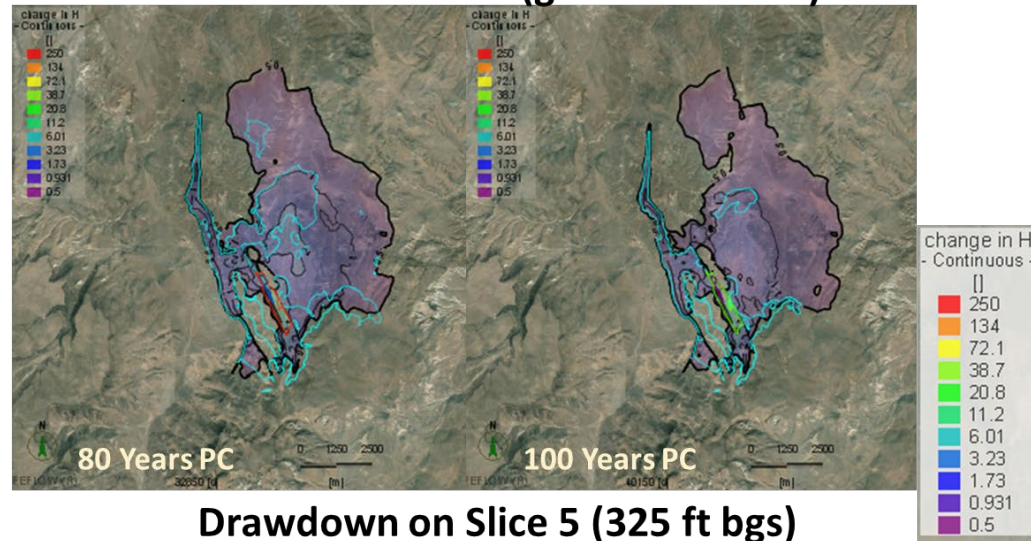


Figure II-26: Predicted Drawdown, Model Slices 1 and 5, 10, 20 and 50 Years After End of Mining, Sensitivity Run S4.

Run S4

Drawdown on Slice 1 (ground surface)



Drawdown on Slice 5 (325 ft bgs)

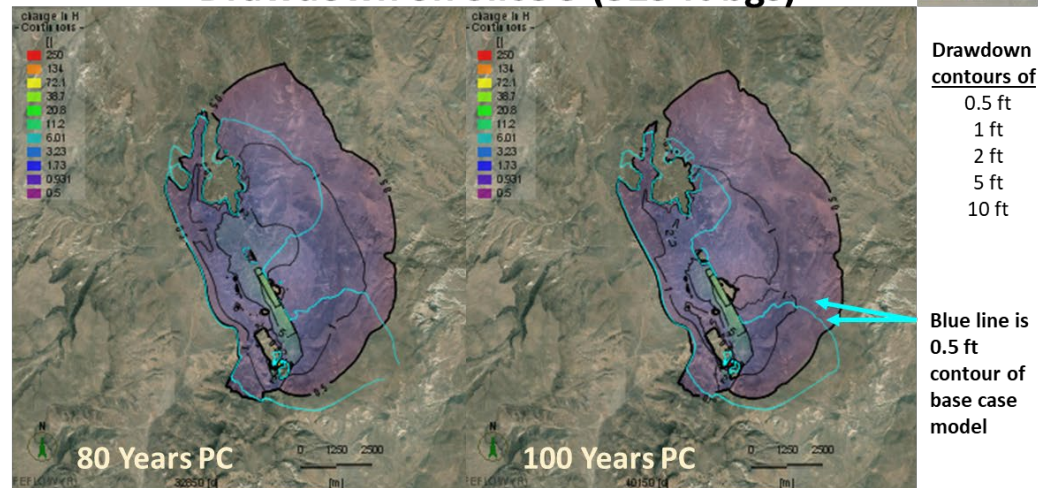


Figure II-27: Predicted Drawdown, Model Slices 1 and 5, 80 and 100 Years After End of Mining, Sensitivity Run S4.

Run S4

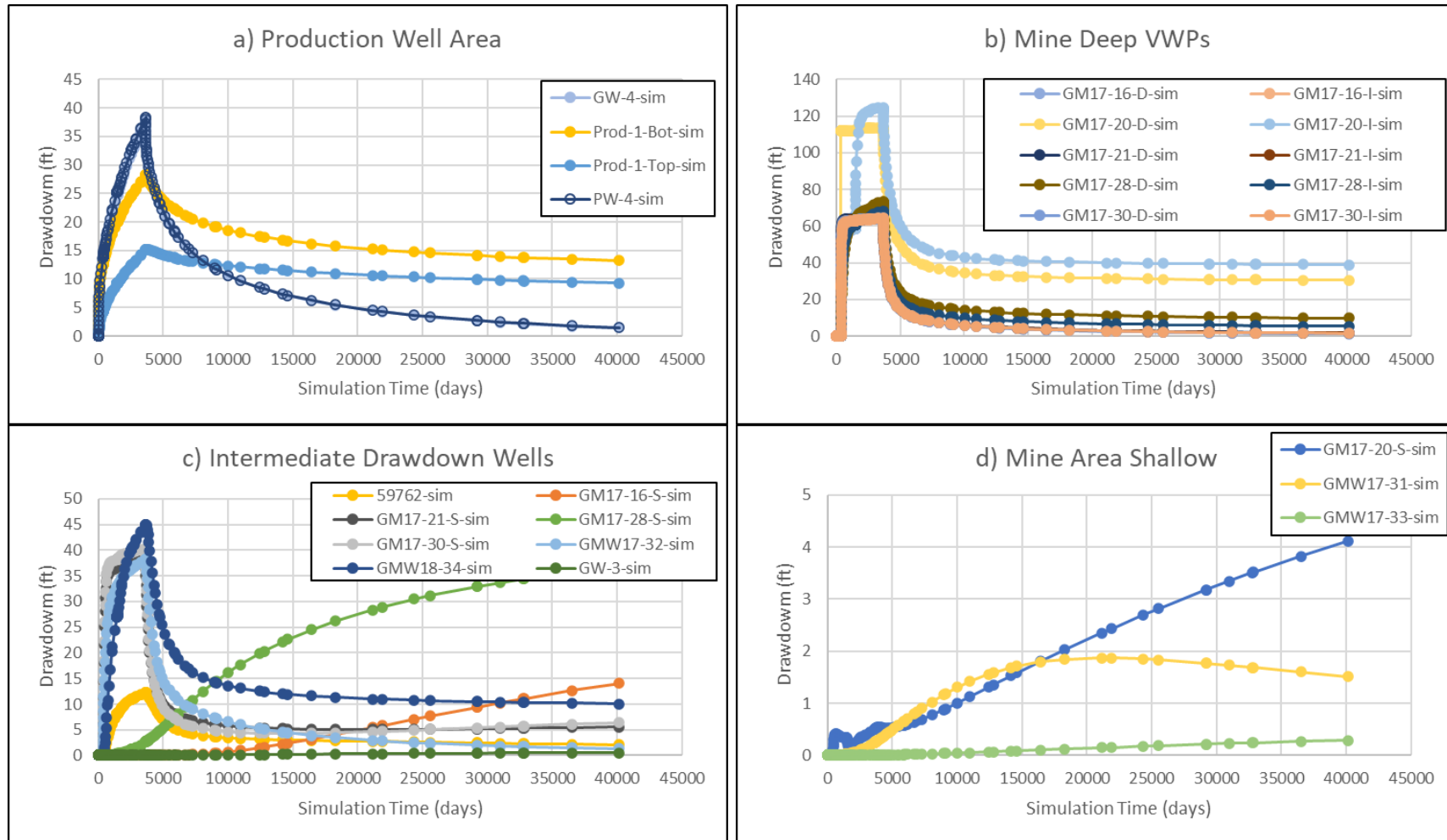


Figure II-28: Time-Series of Simulated Drawdown, Higher Drawdown Wells, Sensitivity Run S4.

Run S4

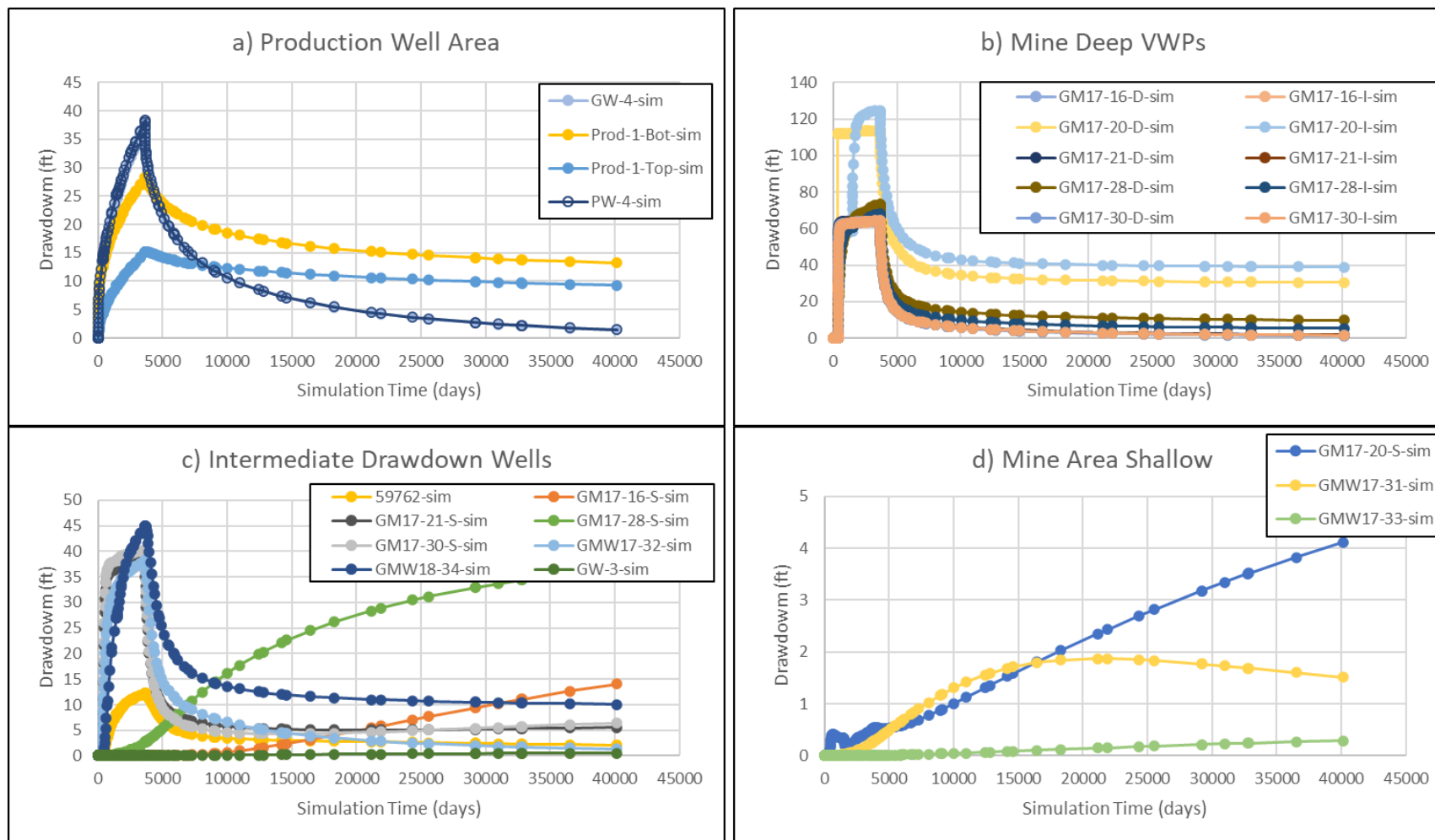


Figure II-29: Time-Series of Simulated Drawdown, Lower Drawdown Wells, Sensitivity Run S4b.

Run S4

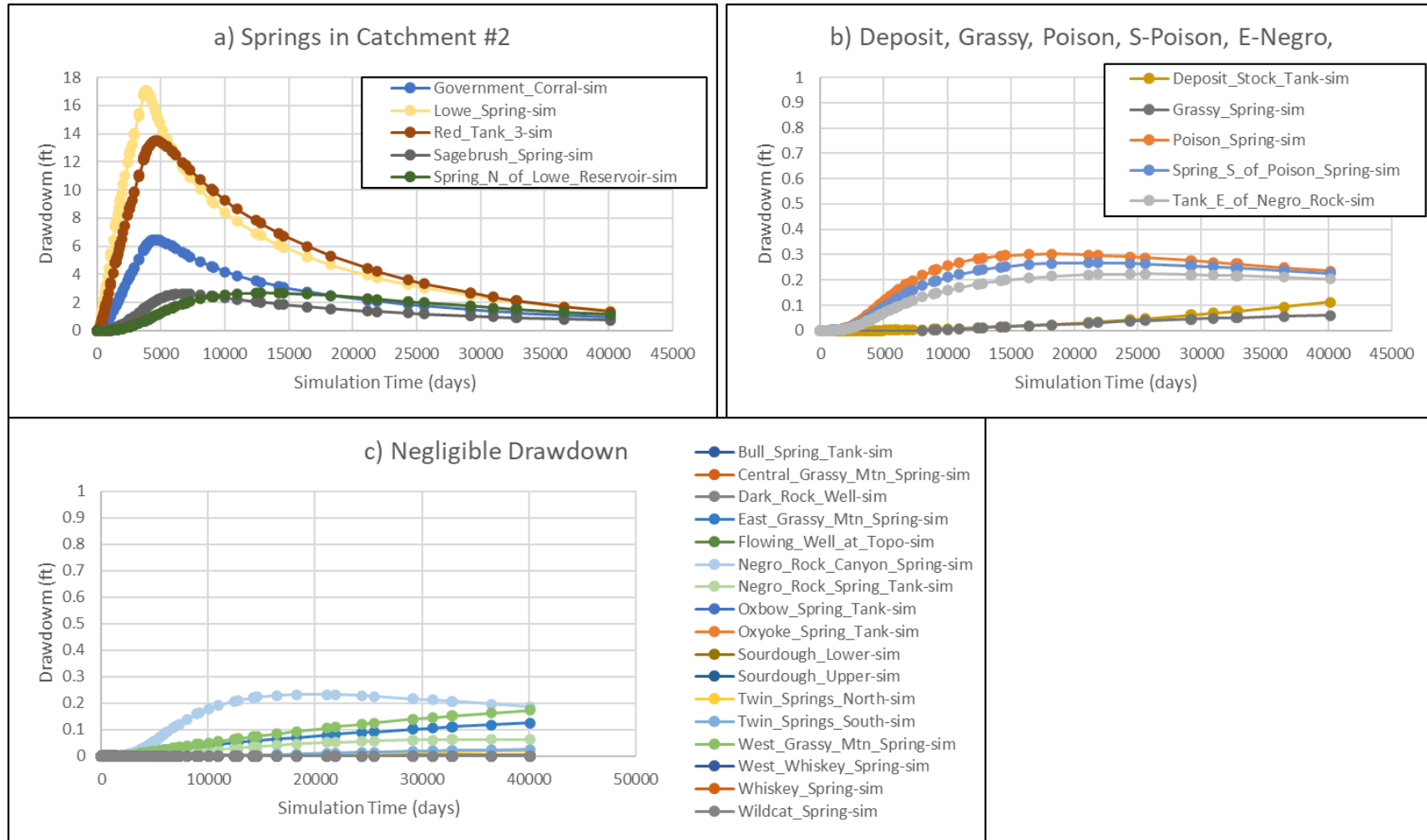


Figure II-30: Time-Series of Simulated Drawdown, Springs, Sensitivity Run S4.

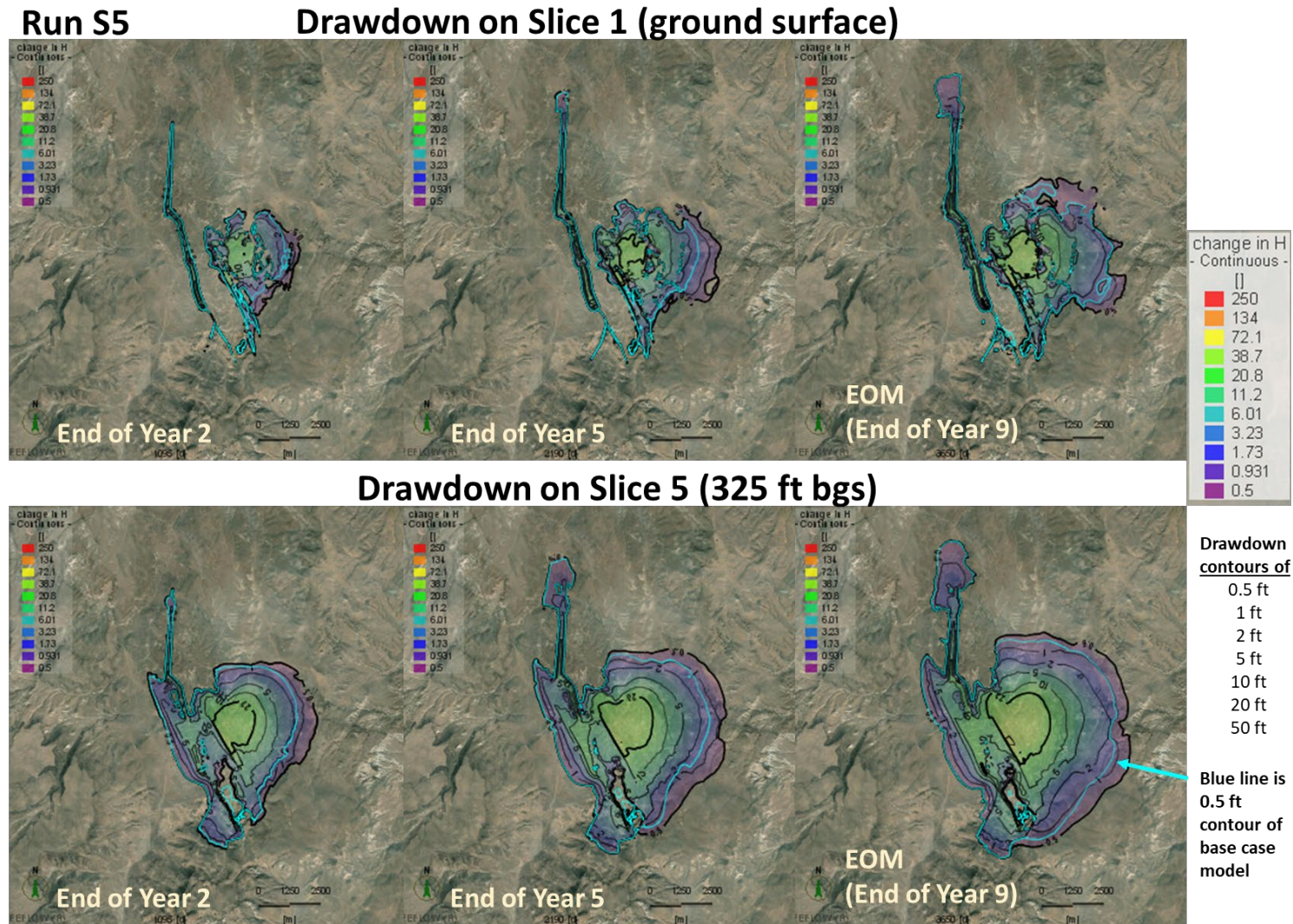


Figure II-31: Predicted Drawdown, Model Slices 1 and 5, End of Mine Years 2, 5 and 9, Sensitivity Run S5.

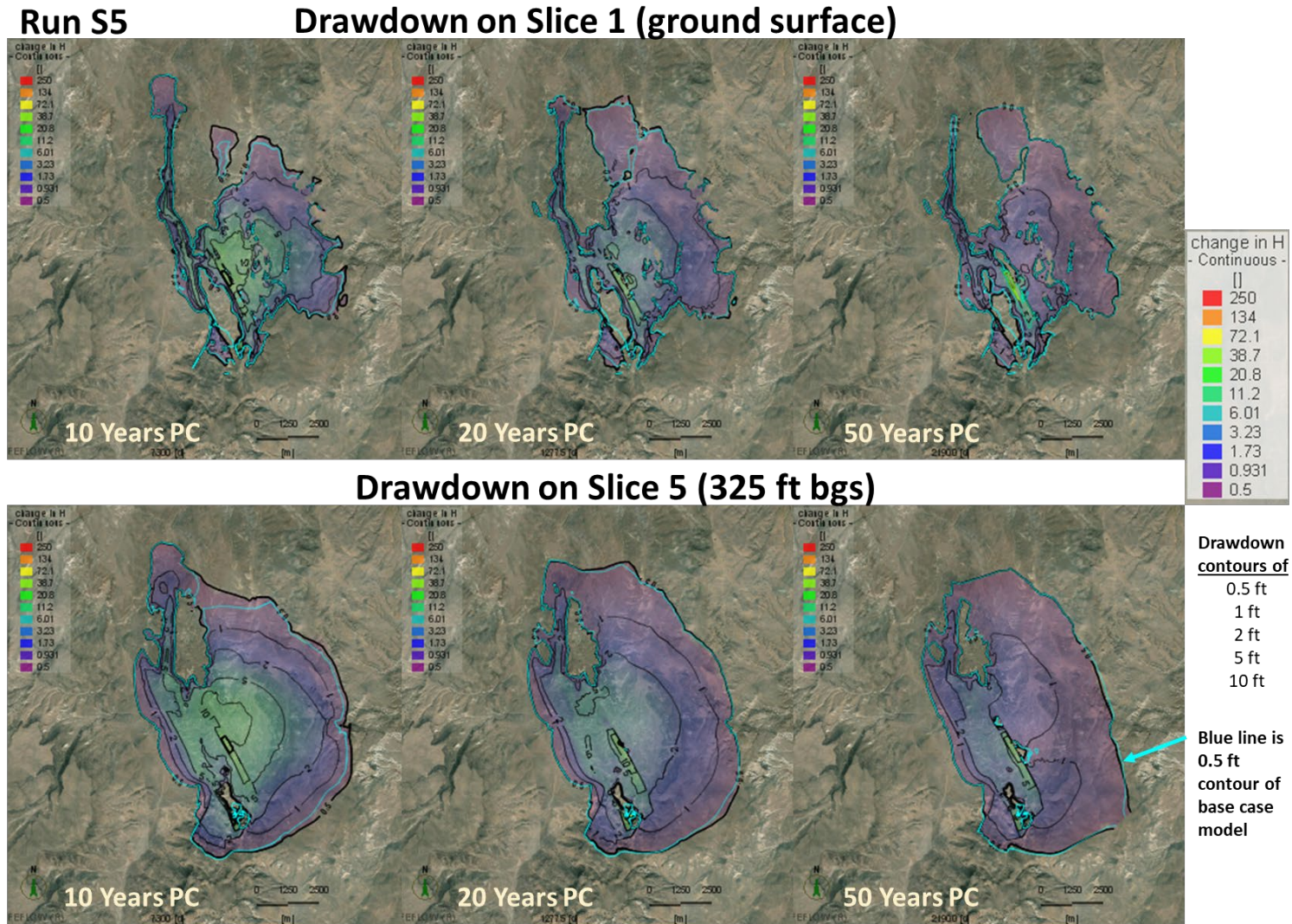
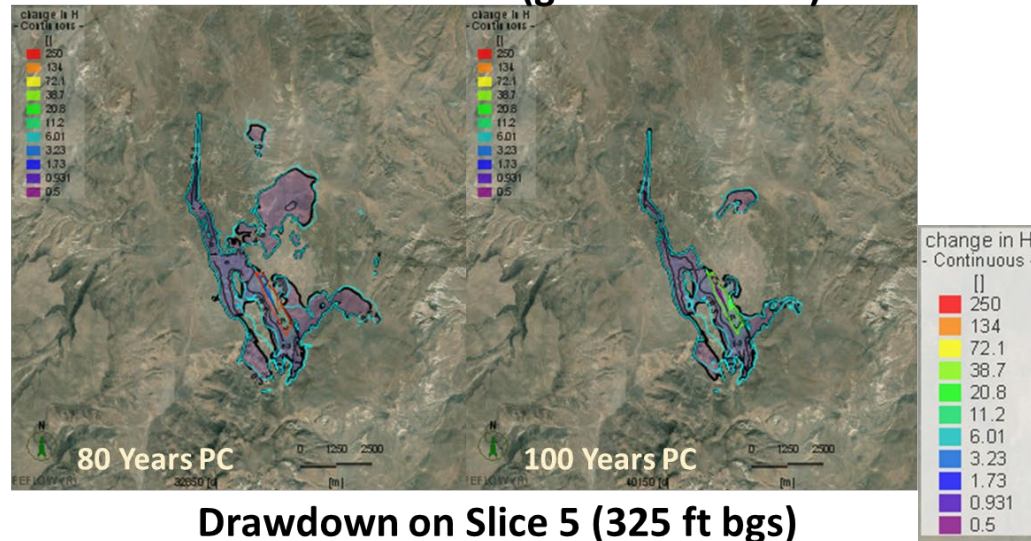


Figure II-32: Predicted Drawdown, Model Slices 1 and 5, 10, 20 and 50 Years After End of Mining, Sensitivity Run S5.

Run S5

Drawdown on Slice 1 (ground surface)



Drawdown on Slice 5 (325 ft bgs)

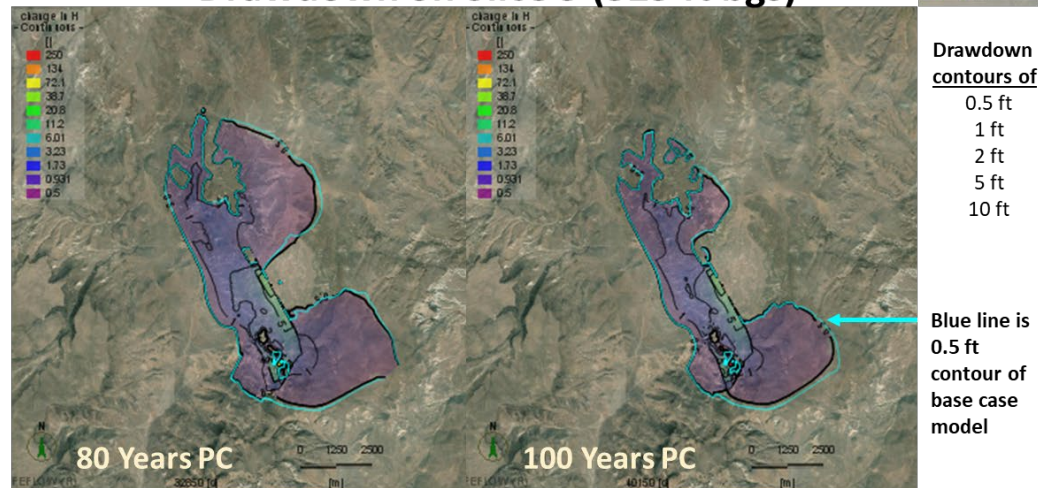


Figure II-33: Predicted Drawdown, Model Slices 1 and 5, 80 and 100 Years After End of Mining, Sensitivity Run S5.

Run S5

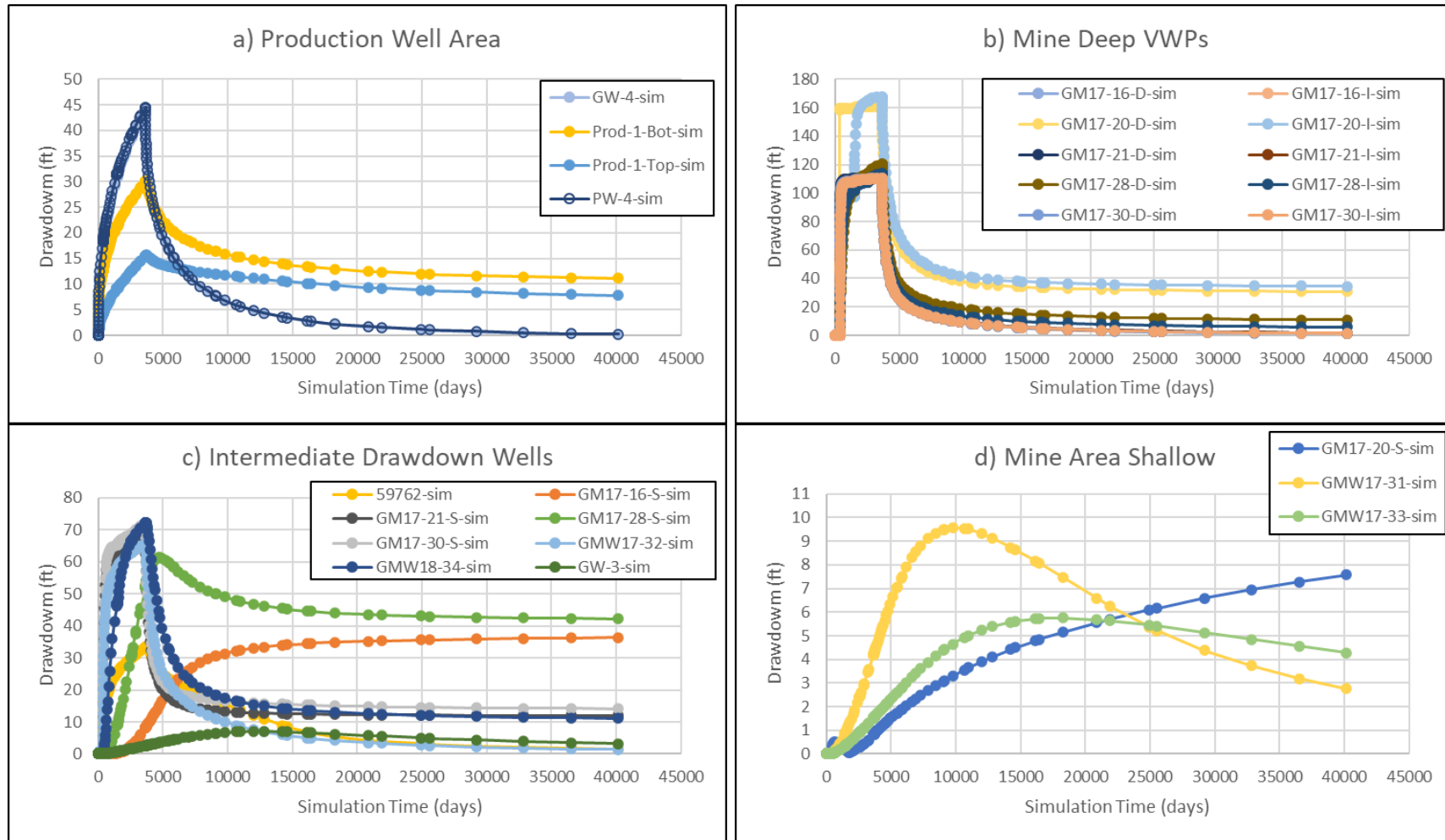


Figure II-34: Time-Series of Simulated Drawdown, Higher Drawdown Wells, Sensitivity Run S5.

Run S5

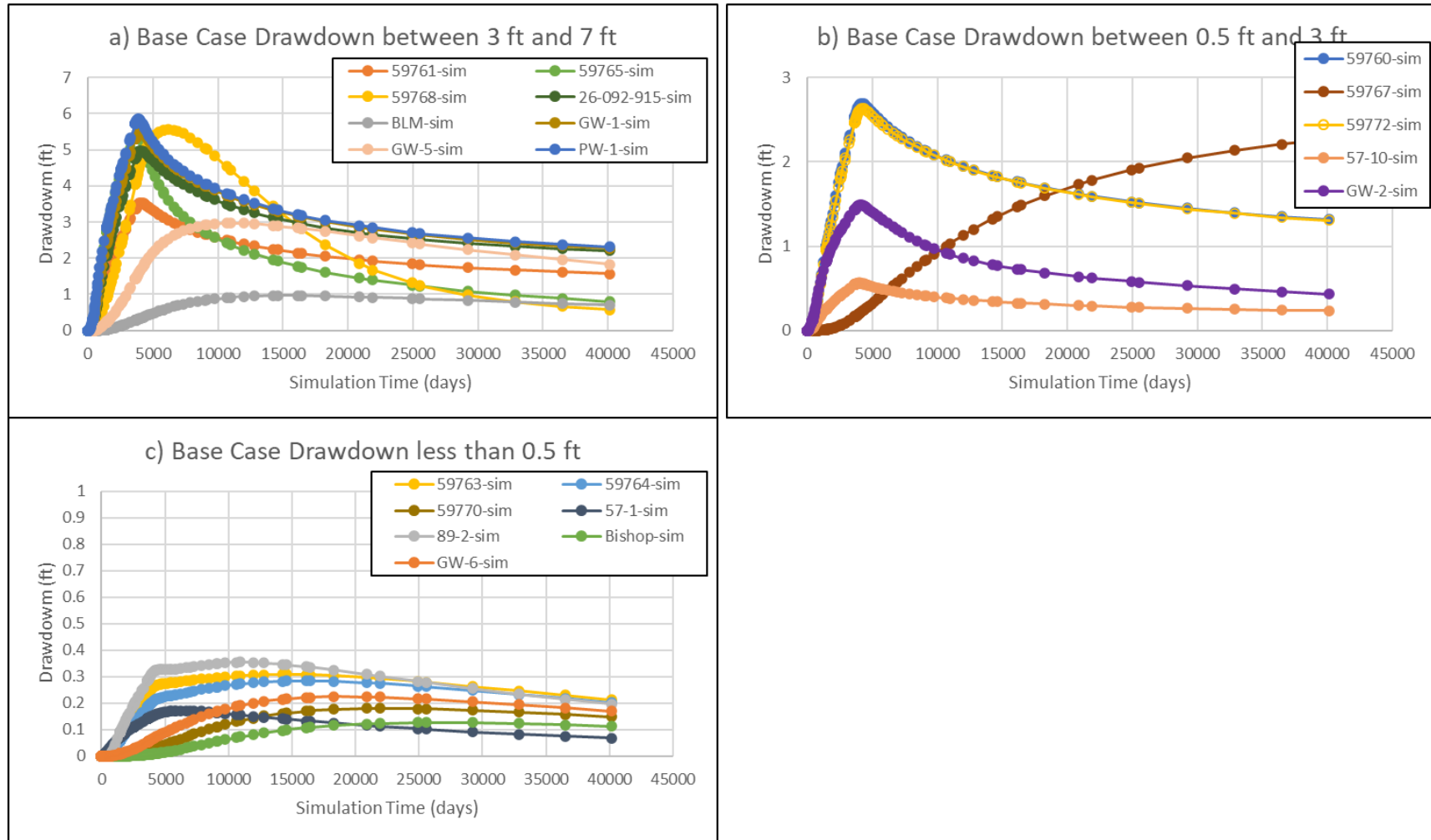


Figure II-35: Time-Series of Simulated Drawdown, Lower Drawdown Wells, Sensitivity Run S5.

Run S5

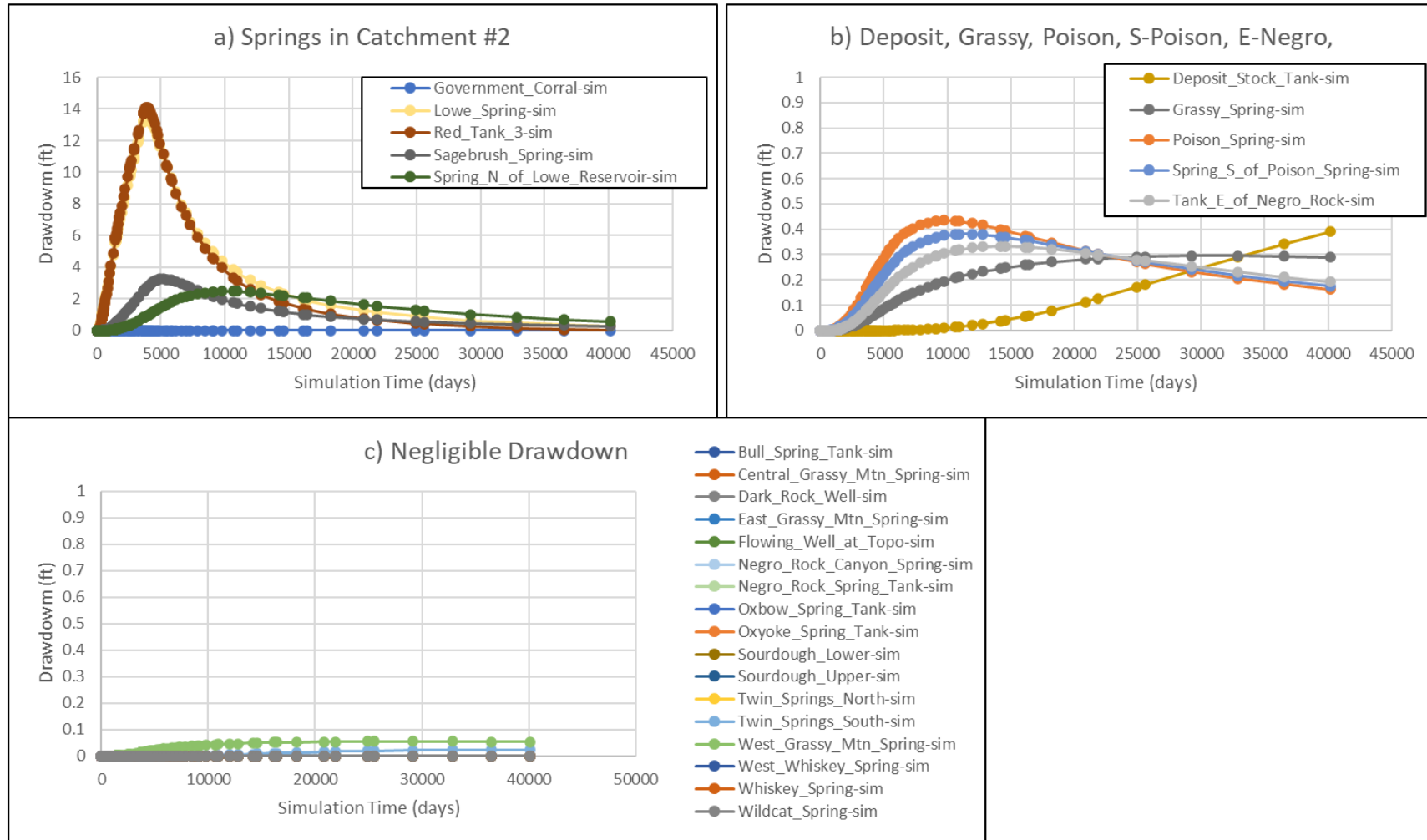


Figure II-36: Time-Series of Simulated Drawdown, Springs, Sensitivity Run S5.

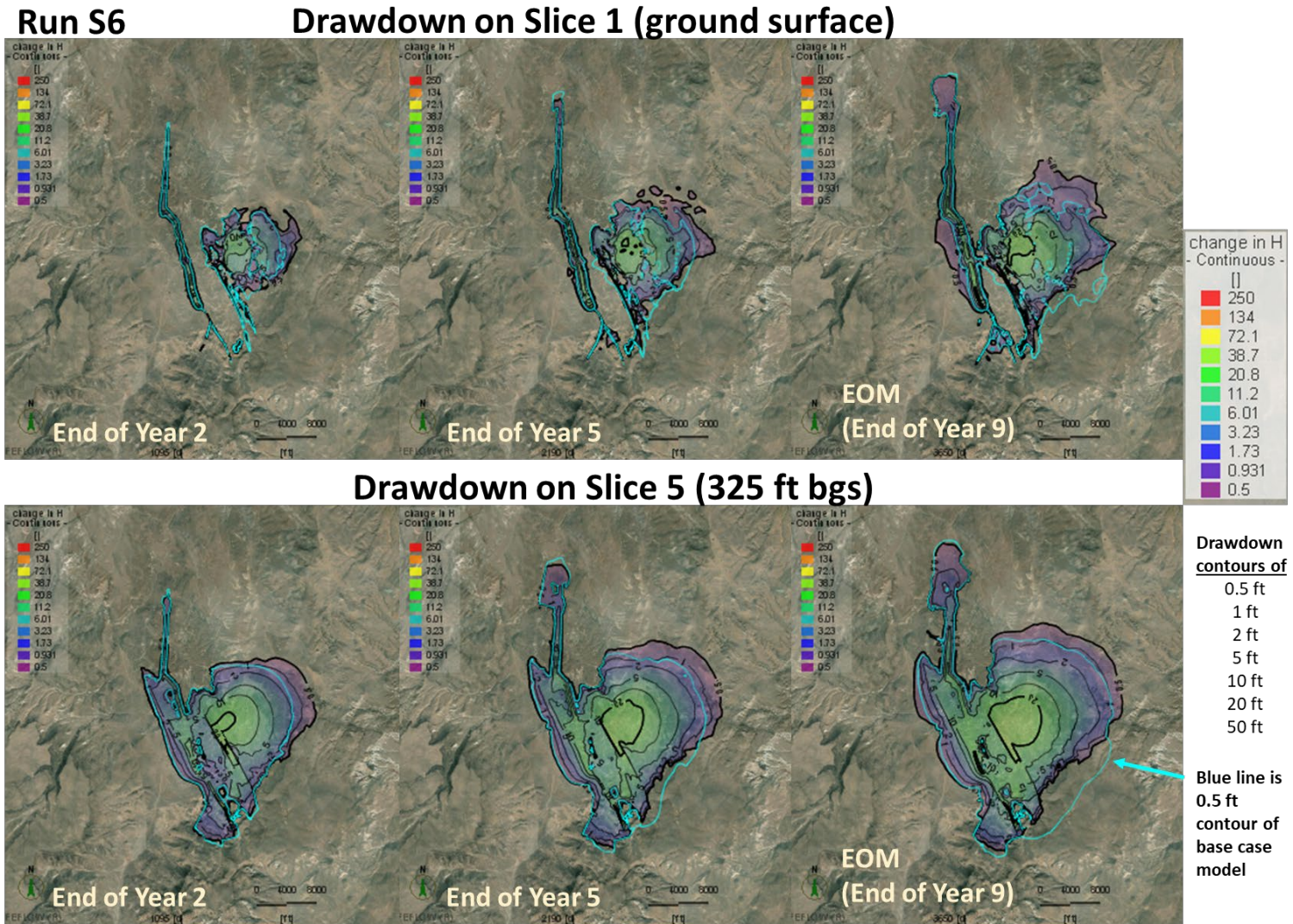


Figure II-37: Predicted Drawdown, Model Slices 1 and 5, End of Mine Years 2, 5 and 9, Sensitivity Run S6.

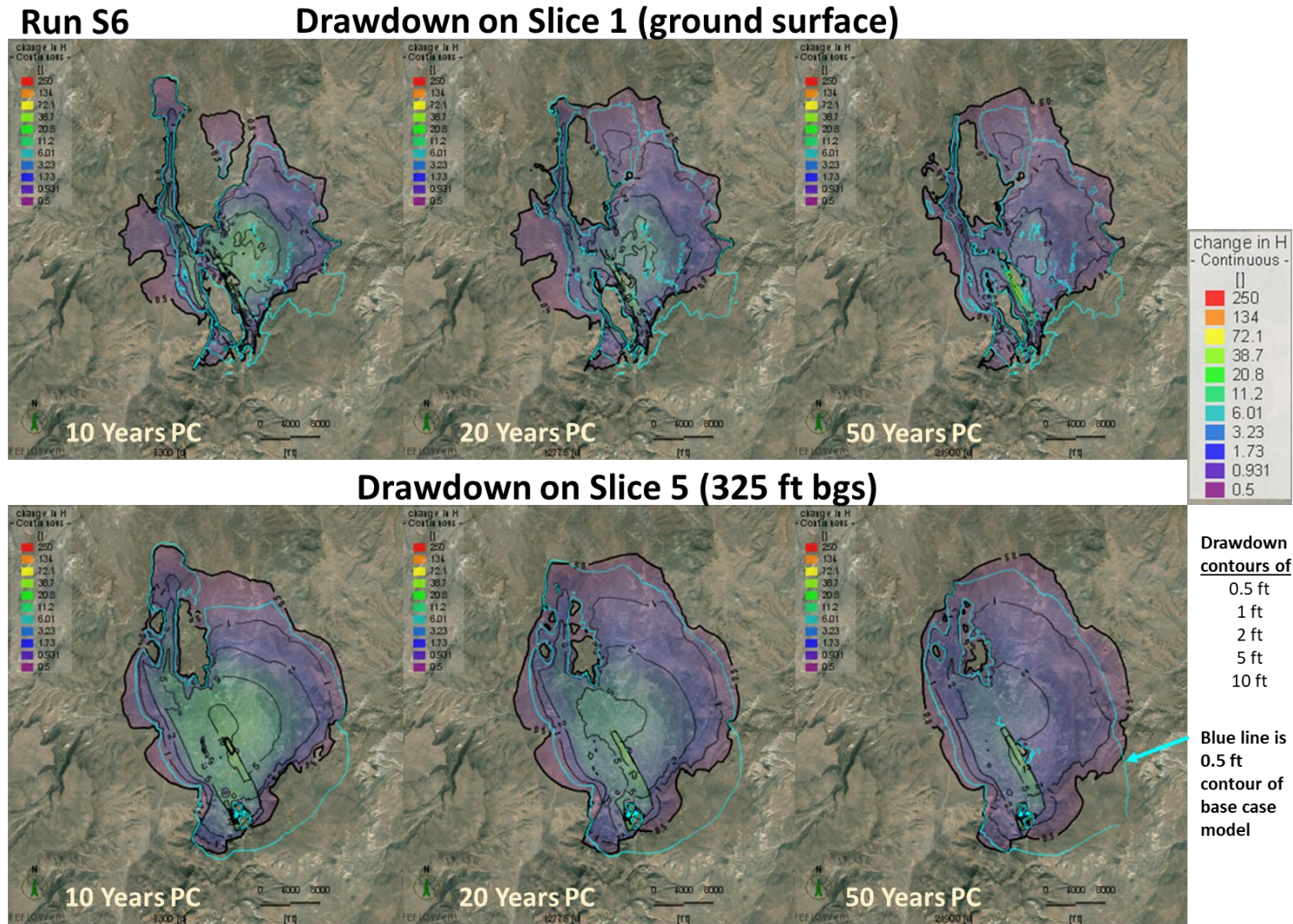
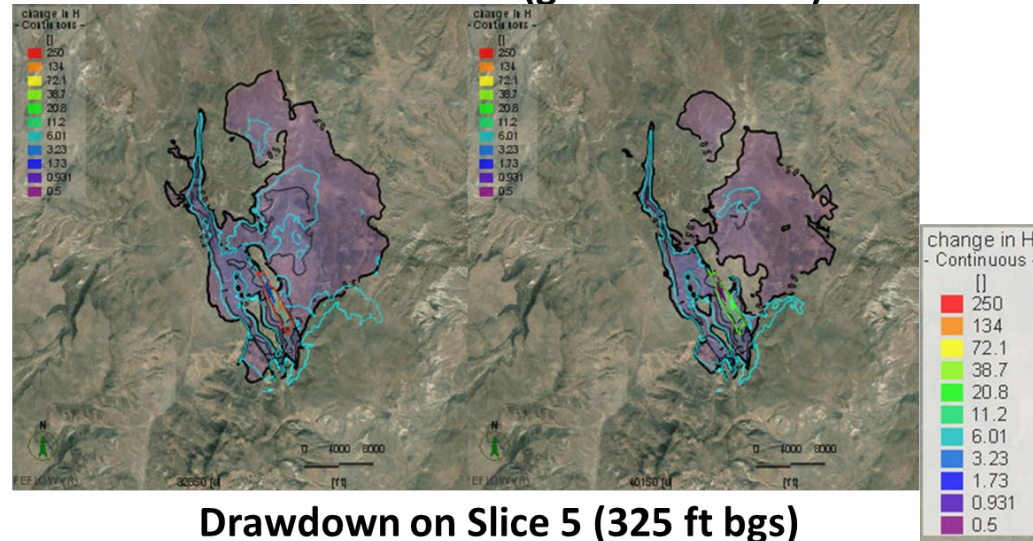


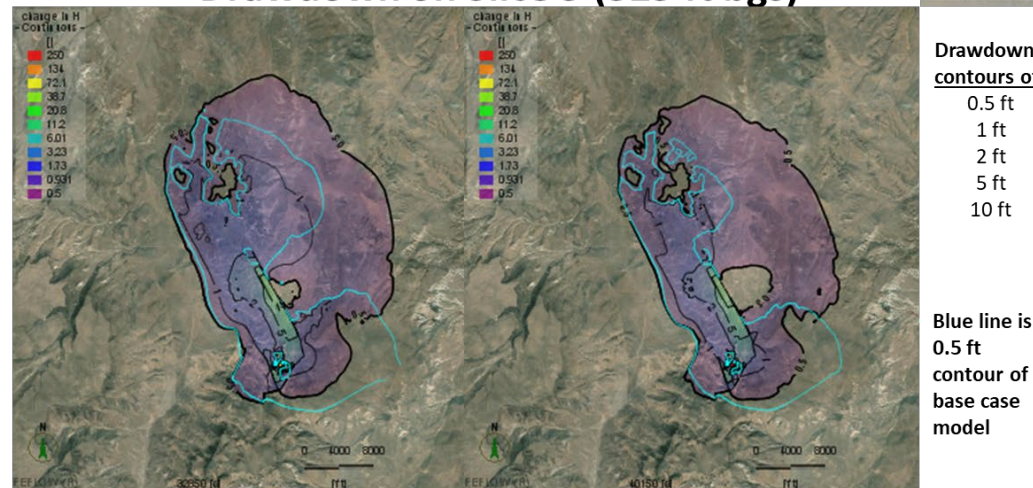
Figure II-38: Predicted Drawdown, Model Slices 1 and 5, 10, 20 and 50 Years After End of Mining, Sensitivity Run S6.

Run S6

Drawdown on Slice 1 (ground surface)



Drawdown on Slice 5 (325 ft bgs)



Drawdown contours of

0.5 ft
1 ft
2 ft
5 ft
10 ft

Blue line is
0.5 ft
contour of
base case
model

Figure II-39: Predicted Drawdown, Model Slices 1 and 5, 80 and 100 Years After End of Mining, Sensitivity Run S6.

Run S6

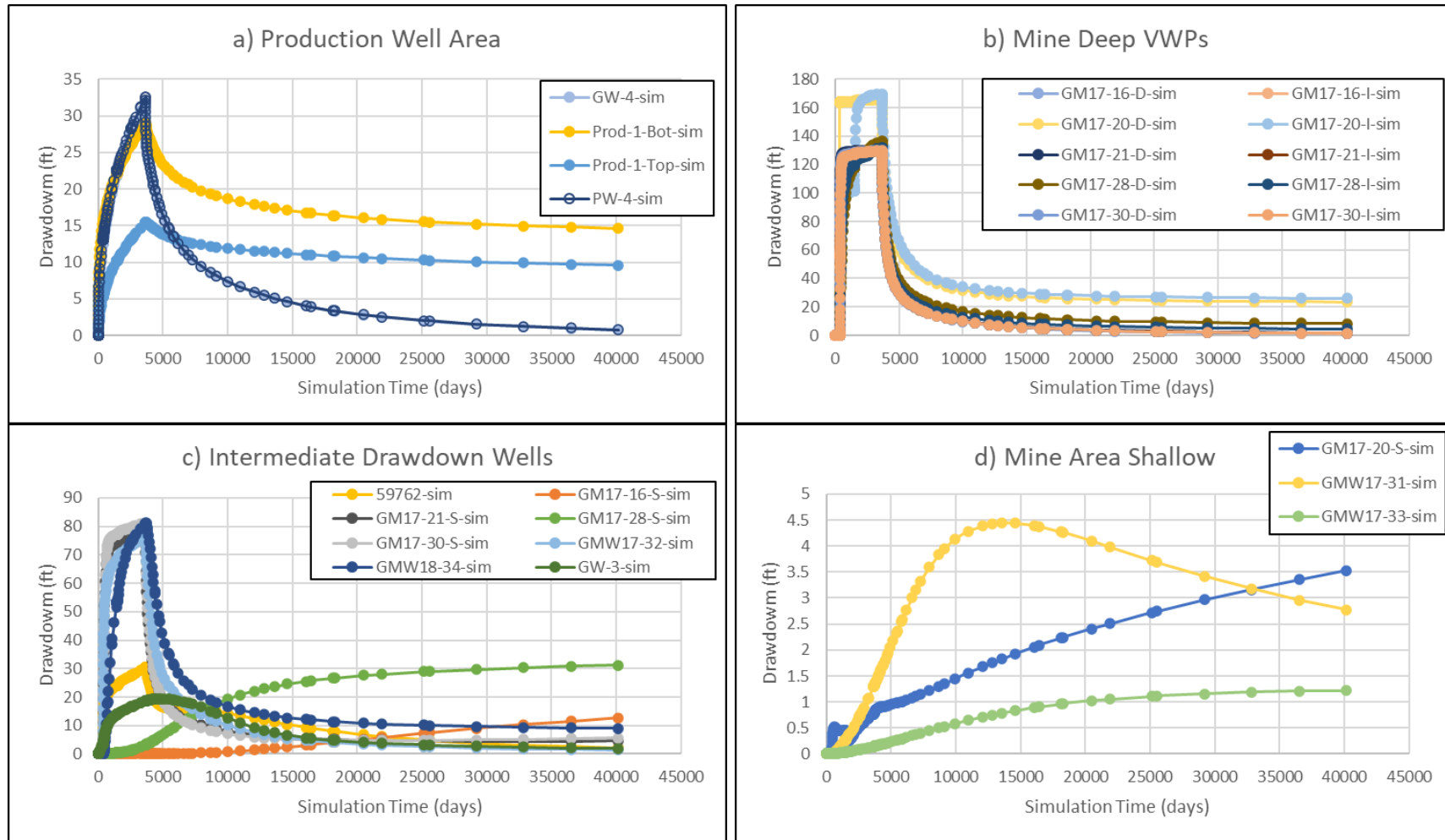


Figure II-40: Time-Series of Simulated Drawdown, Higher Drawdown Wells, Sensitivity Run S6.

Run S6

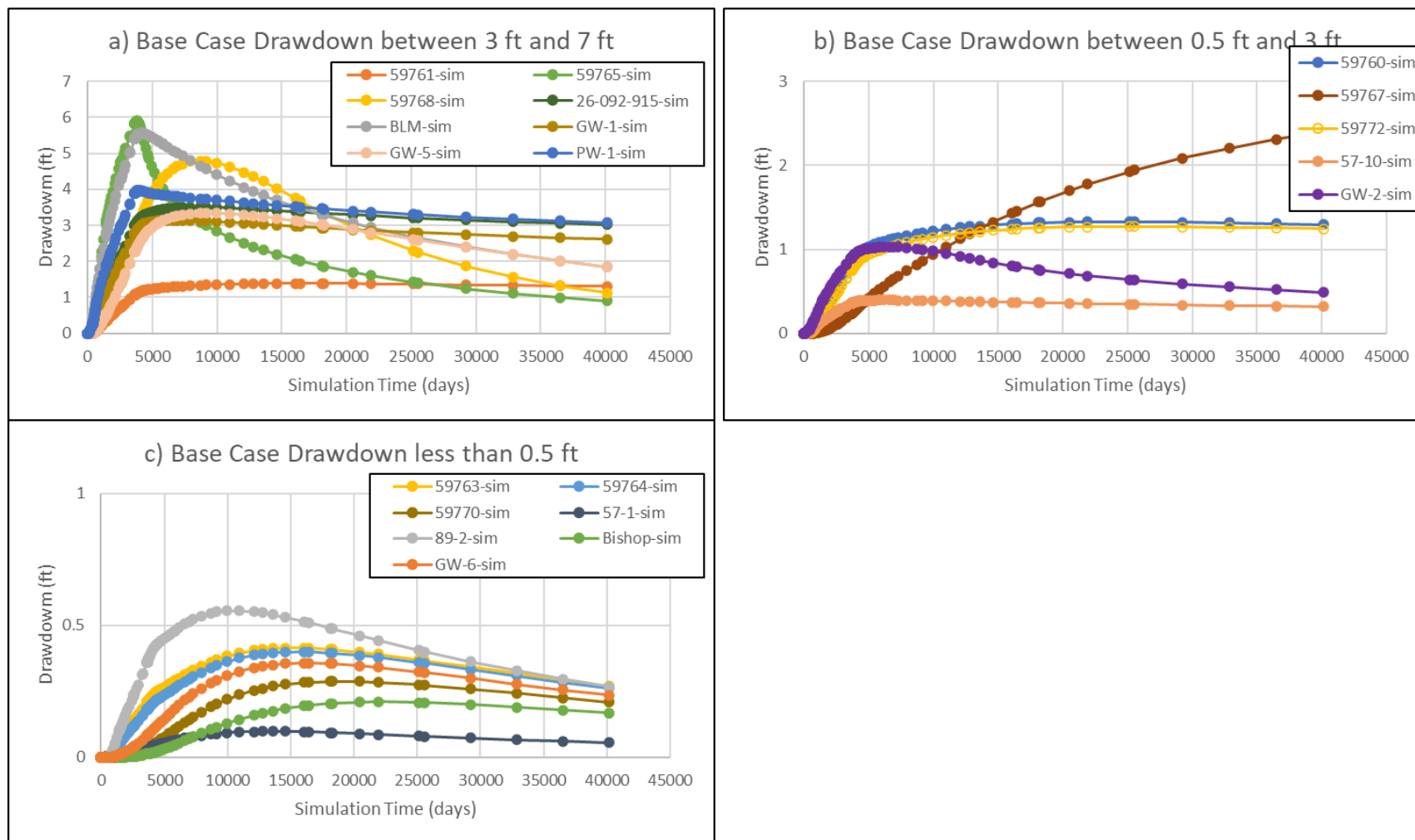


Figure II-41: Time-Series of Simulated Drawdown, Lower Drawdown Wells, Sensitivity Run S6.

Run S6

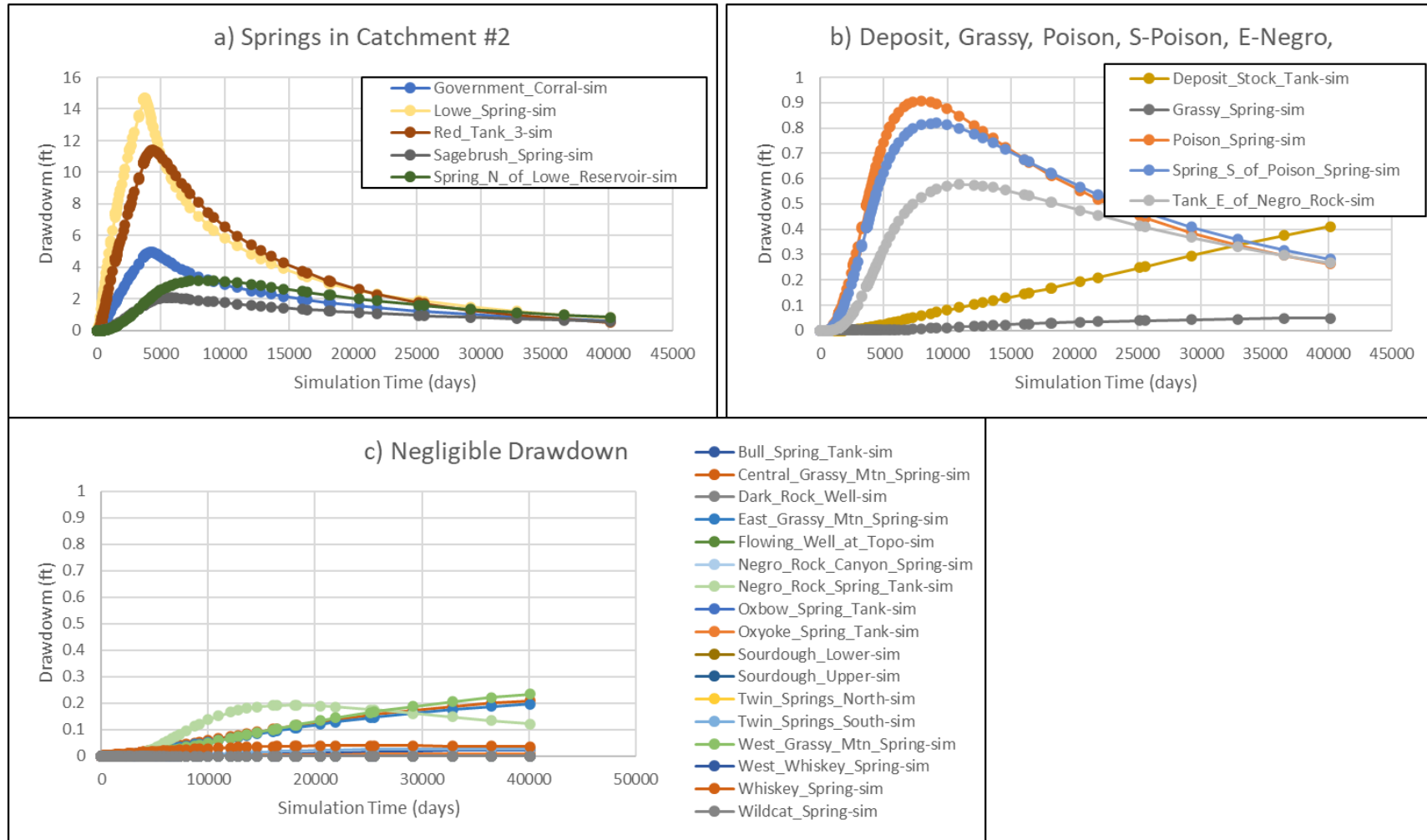


Figure II-42: Time-Series of Simulated Drawdown, Springs, Sensitivity Run S6.

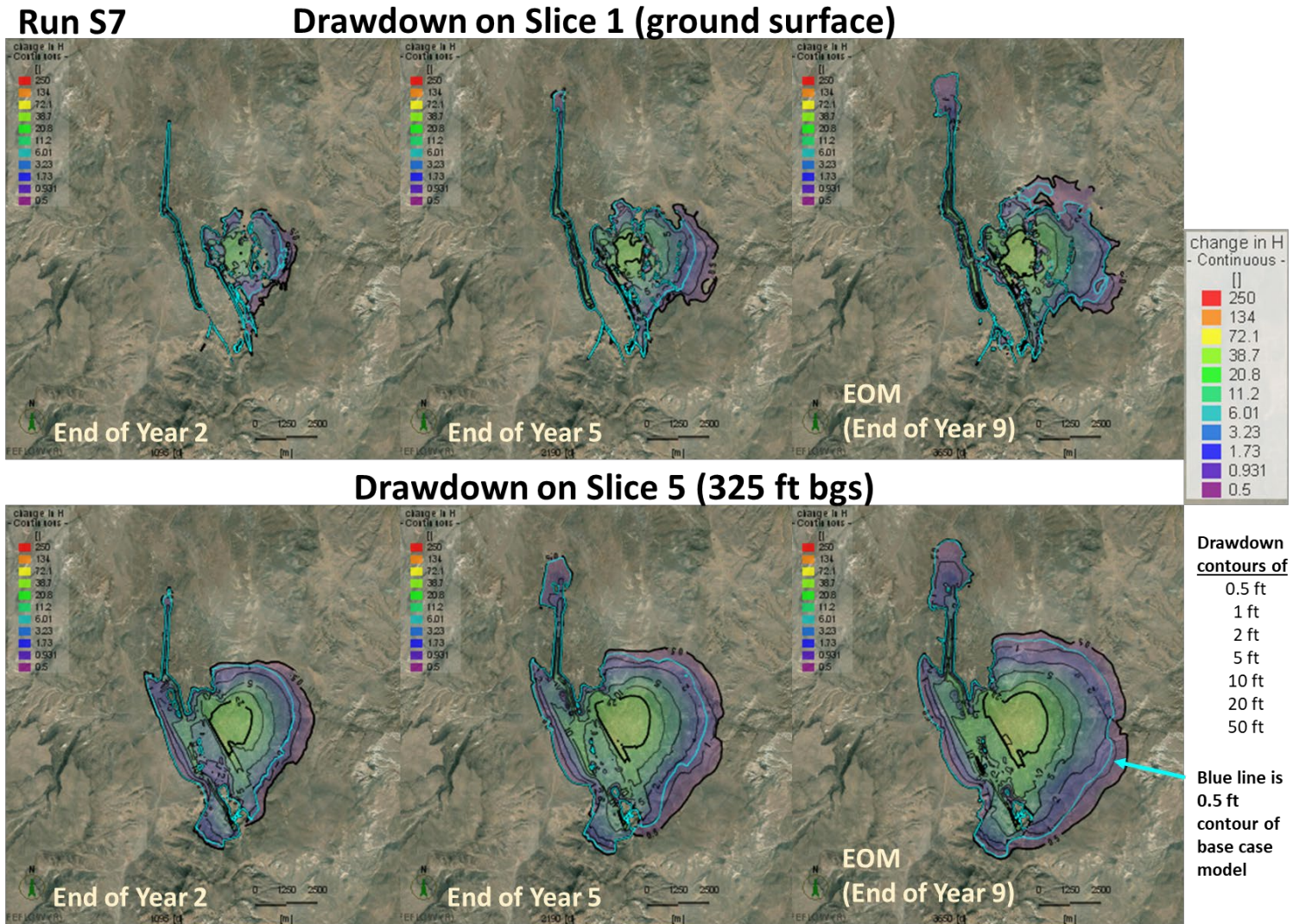


Figure II-43: Predicted Drawdown, Model Slices 1 and 5, End of Mine Years 2, 5 and 9, Sensitivity Run S7.

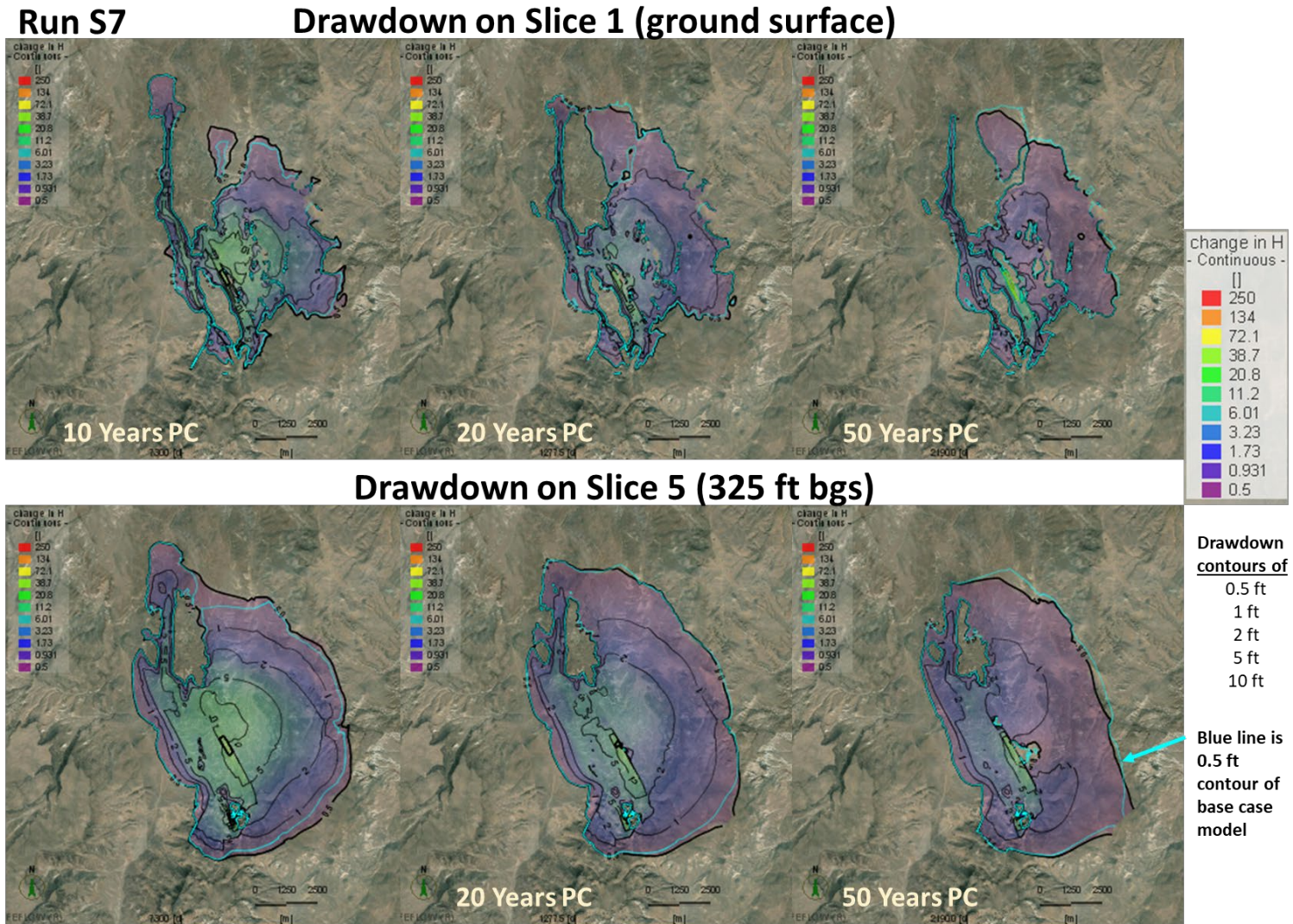
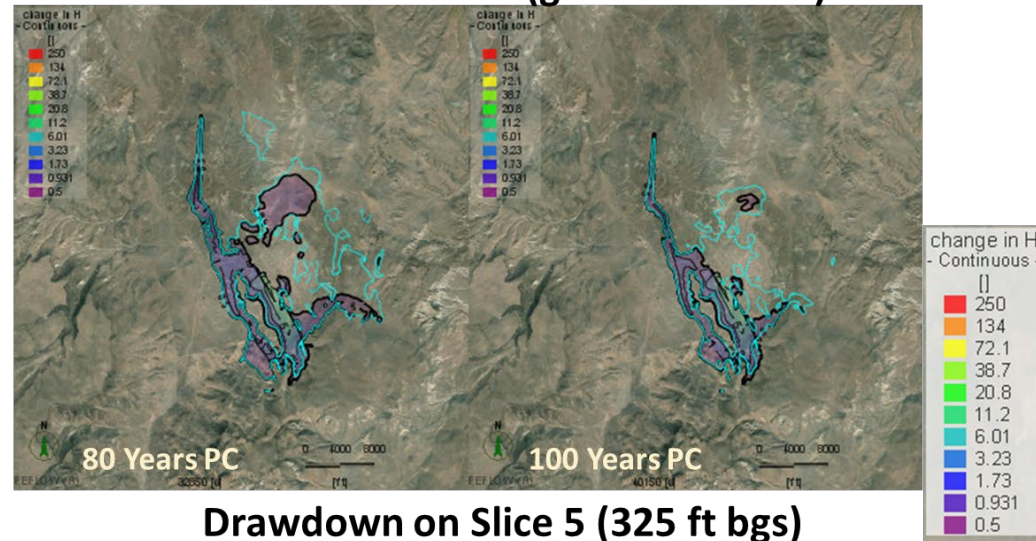


Figure II-44: Predicted Drawdown, Model Slices 1 and 5, 10, 20 and 50 Years After End of Mining, Sensitivity Run S7.

Run S7

Drawdown on Slice 1 (ground surface)



Drawdown on Slice 5 (325 ft bgs)

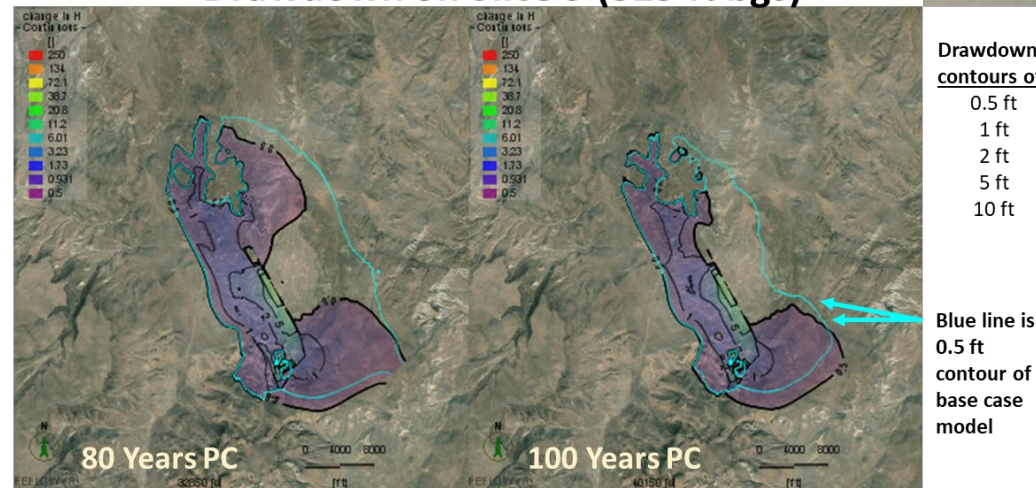


Figure II-45: Predicted Drawdown, Model Slices 1 and 5, 80 and 100 Years After End of Mining, Sensitivity Run S7.

Run S7

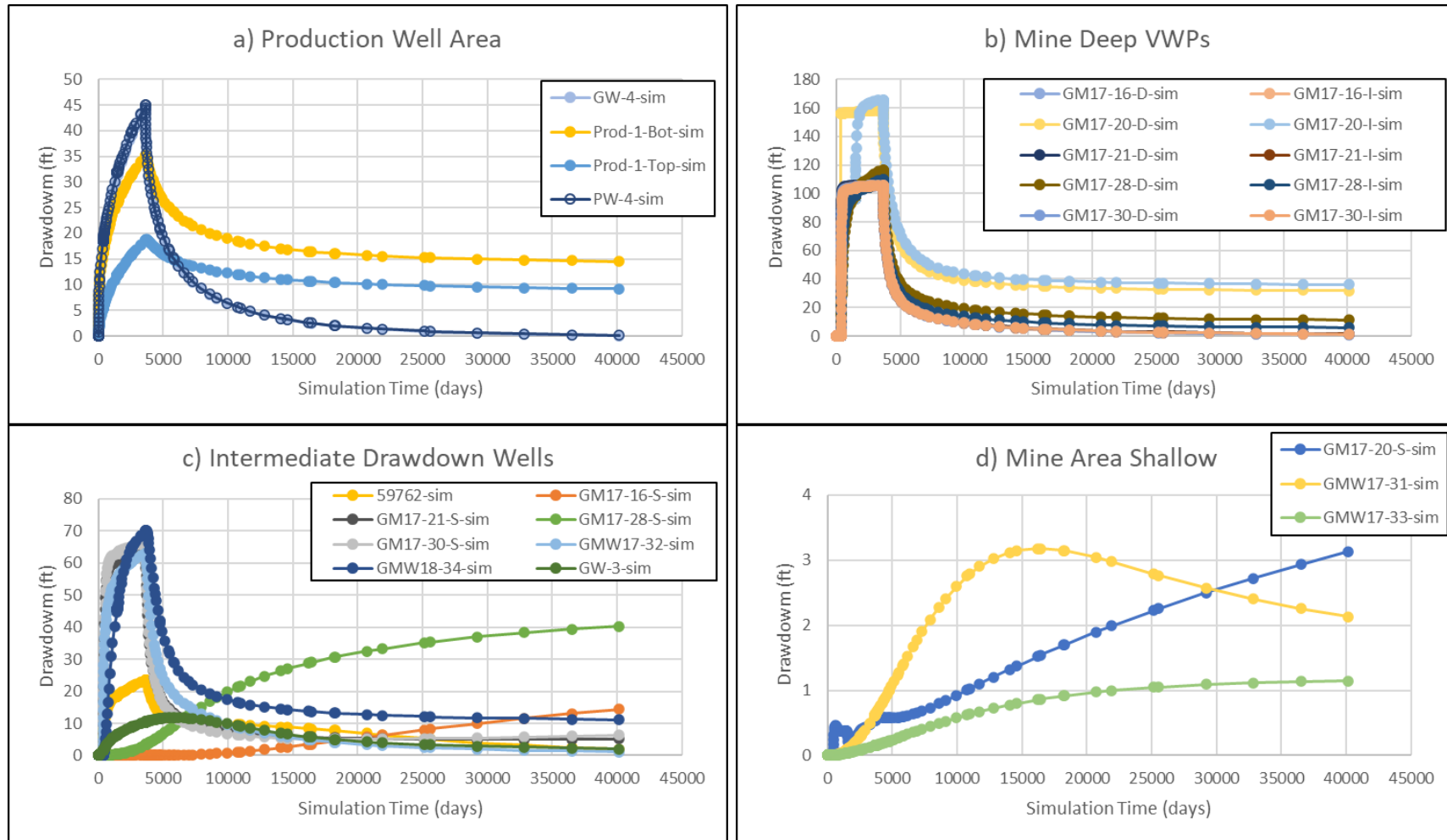


Figure II-46: Time-Series of Simulated Drawdown, Higher Drawdown Wells, Sensitivity Run S7.

Run S7

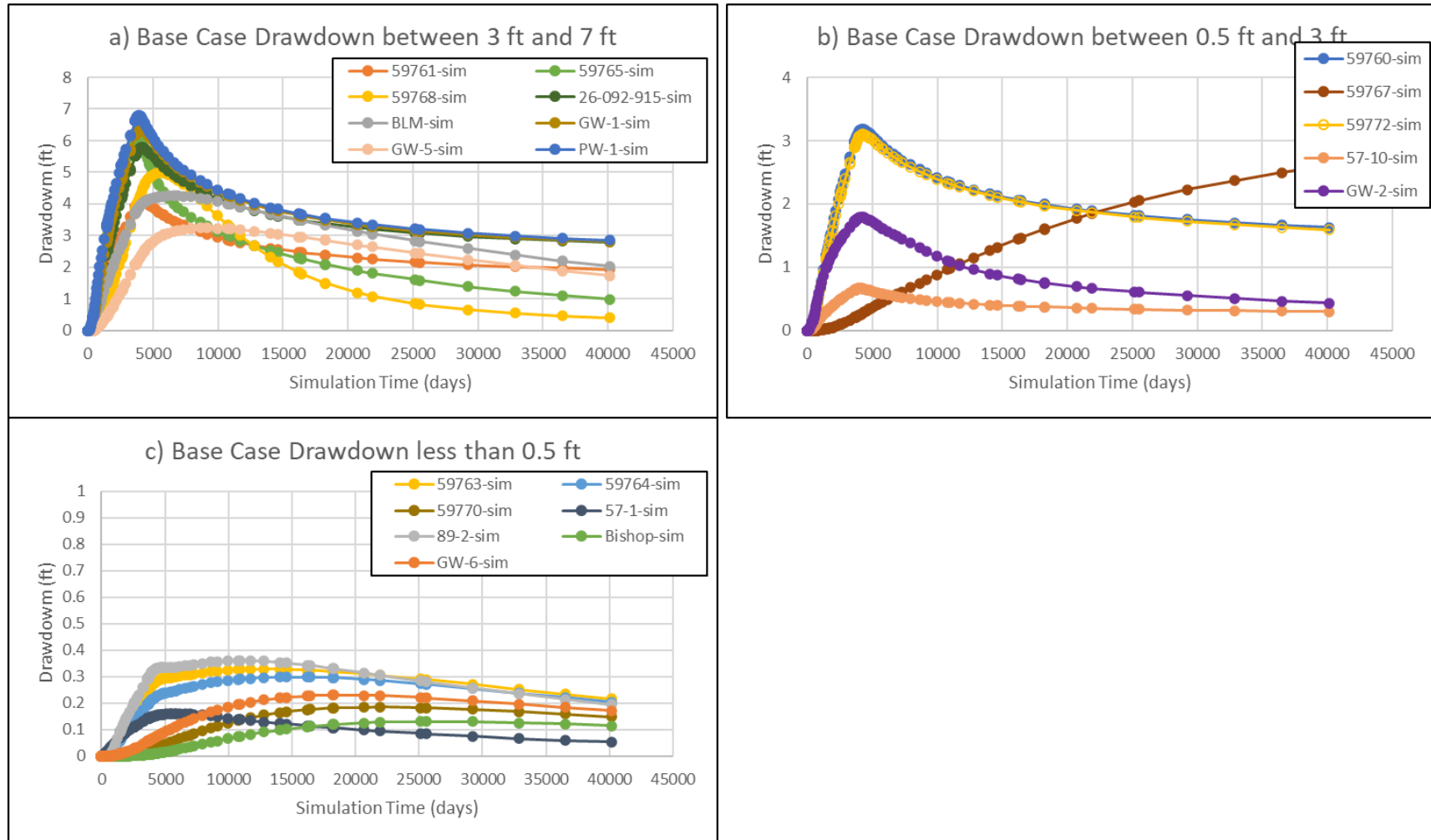


Figure II-47: Time-Series of Simulated Drawdown, Lower Drawdown Wells, Sensitivity Run S7.

Run S7

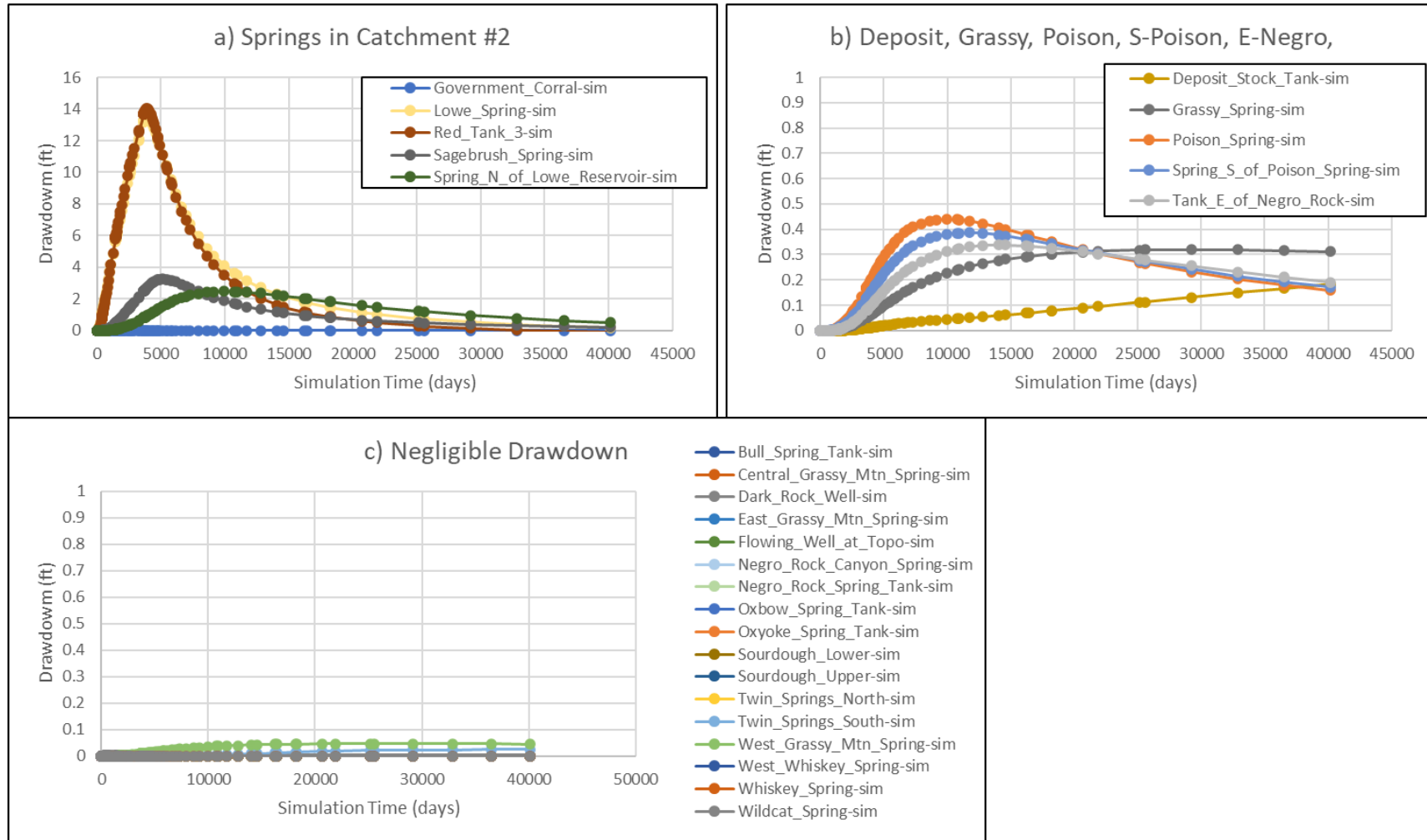


Figure II-48: Time-Series of Simulated Drawdown, Springs, Sensitivity Run S7.